UNIVERSITÀ DEGLI STUDI DI MILANO

Dipartimento di Chimica

PhD in Industrial Chemistry – XXIX Cycle

TiO_2 Photocatalysis for Improving the Air Quality: from Molecules, to Building Materials Development

SSD: CHIM/04 and ING-IND/25

Marta Stucchi, R10605
Tutor: Prof. Claudia L. Bianchi
Co-Tutor: Prof. Christos Argirusis

Coordinator: Prof. Maddalena Pizzoti

Doctorate thesis – A.Y. 2016-2017

Dedicated to
My Mother

Era tale l'entusiasmo generato in me dalla scoperta che ogni mio pensiero, di giorno e di notte, era fisso su questo fenomeno.

(Elogio dell'imperfezione, Rita L. Montalcini)

Table of contents

List of abbreviations

Advanced Oxidation Processes (AOP)
Band gap energy (E_{bg})
Brunauer–Emmett–Teller (BET)
Binding energy (BE or E_b)
Carbon monoxide (CO)
Classical impregnation method (CIM)
Conduction band (CB)
Contact angle (CA)
Continuous Stirred-Tank Reactor (CSTR)
Density functional theory (DFT)
Diffuse reflectance spectroscopy (DRS)
Energy Dispersive X-ray Spectrometry (EDS)
Energy Dispersive X-ray Analysis (EDX)
Electron volts (eV)
Electron-hole (e^-/h^+)
Electrons (e^-)
EU National Emission Ceilings (NEC)
European Environment Agency (EEA)
Fermi level (EF)
Flatband potential (EFB)
Gas controller unit (GCU)
Gas chromatography (GC)
Fourier Transform Infrared Spectroscopy (FTIR)
High-resolution Transmission Microscopy (HR-TEM)
Hydroxyl radicals (•OH)
Holes (h^+)
Infrared (IR)
International Agency for Research on Cancer (IARC)

Kinetic energy (E_K)
Liquid controller unit (LCU)
Long-term adverse effect level (LOAEL)
Metal (M)
Metal oxides (MO)
Minimal risk level (MRL)
Micro Gas Chromatograph (Micro-GC)
National Human Activity Pattern Survey (NHAPS)
Nanoparticles (NPs)
Nitrogen Oxides (NO_x)
No observed adverse effect level (NOAEL)
Organizzazione mondiale sanità (OMS)
Particulate matter (PM)
Polychlorinated biphenyls (PCB)
Proton Transfer Reaction Mass Spectrometry (PTR-MS)
Room temperature (RT)
Scanning Electron Microscopy (SEM)
Semi-volatile Organic Compound (SVOC)
Sick Building Syndrome (SBS)
Silver nanoparticles (AgNPs)
Specific Surface Area (SSA)
Titanium dioxide (TiO_2)
Trichloroethylene (TCE)
Ultrasound (US)
Ultraviolet (UV)
Valence band (VB)
Visible light activity (VLA)
Volatile organic compounds (VOC)
World Health Organization (WHO)

X-ray Diffraction (XRD)

X-ray photoelectron spectra (XPS)

General abstract

1. Introduction

During these last years, the innovation and development processes lead pollution to its highest level; the air pollution is one the most prominent and dangerous form of it. Causes are several, from fuel combustion to factories activity, which increase the level of organic molecules and nitrogen or sulfur oxides in atmosphere (WHO Global Urban Ambient Air Pollution Database, update 2016).

Unfortunately, effects are more than evident: from the global warming, to the acid rains, from the sudden climate changes, to the increase of diseases such as asthma and lung cancer (Ambient (outdoor) air quality and health, WHO).

Outdoor air pollution is the major environmental health problem affecting everyone in developed and developing countries alike, however, unlike one might usually think, indoor levels of organic pollutants are often higher than outdoor (Viegi et al., 2004). The problem is even more important because people live mainly indoors, constantly exposed to all the pollutants present in these close environments (Chen et al., 2016; Allen et al., 2016).

For this reason, demands to improve the air quality situation have been largely extended, finding new strategies for waste reduction or for the oxidation and degradation of pollutants (Ambient (outdoor) air quality and health, WHO).

Among several processes, considering that very important factors are saving energy and reducing emissions, photocatalysis has been exploited as very suitable technique to reduce pollution.

In a photocatalytic reaction (eq. 1), a semiconductor material, the photocatalyst, is activated by light and, thanks to the formation of some electron-hole couples between his valence and conduction bands, it is able to reduce or oxidize molecules that adsorb on his surface (J.M. Herrmann, 2005).

In heterogeneous photocatalysis, the reaction implies the previous formation of an interface between the semiconductor and the reactants of the reaction (K. Demeestere et al., 2007; M. Schiavello, 1997).

$$(Ox_1)_{ads} + (Red_2)_{ads} \xrightarrow[h\nu > E_{bg}]{\text{semiconductor}} Red_1 + Ox_2 \qquad (1)$$

Among a large variety of semiconductor materials, which are mainly metal oxides, only few of them are considered to be applicable photocatalysts, in relation with their specific photocatalytic properties. Titanium dioxide (TiO_2) induced photocatalysis is an example of AOP processes and it has been demonstrated its efficiency in the decomposition of various organic contaminants. TiO_2 is a very well known and well-researched material due to the stability of its chemical structure, biocompatibility, physical, optical, and electrical properties (M. Serpone et al., 1989).

The crystalline forms of TiO_2 are anatase, rutile and brookite (A. Linsebigler et al., 1995). In general, TiO_2 is preferred in anatase form because of its high photocatalytic activity, however the major drawbacks of TiO_2-based photocatalysts is related to the rapid charge recombination of the electron−hole pairs, and the wide band gap, which restricts light absorption to only ultraviolet region (wavelength <390 nm), restraining the practical applications of TiO_2-based photocatalysts under solar light or visible light.

TiO_2-based photocatalysts are used for a variety of applications such as degradation of volatile organic compounds (VOCs) and decomposition of nitrogen pollutants (NO_x) or also organic dyes, like Methylene Blue (K. Demeestere et al., 2007; P.K.J. Robertson et al., 2005).

When TiO_2 is irradiated with energies equal to or higher than its band gap (>3.0 eV), electrons are excited from the valence band into the conduction band, leading to excited electrons in the conduction band and positive holes in the valence band. This fundamental process can be expressed by the following reaction equations (eq. 2):

$$TiO_2 + h\nu \rightarrow e^- + h^+ \qquad (2)$$

As electrons have a reducing potential, holes can oxidize water and lead to the formation of more oxidant species such as hydroxyl radicals, able to oxidize organics.

As mentioned above, the field of practical applications of TiO_2-based photocatalysts becomes less expanded under solar light or visible light.

In this sense, different strategies have been developed (X. Li et al., 2011; S. Afzal et al., 2013; S. Wu et al., 2013; Y. Cho et al., 2001), starting from the chemical modification of TiO_2 lattice using non-metals, particularly carbon, nitrogen and sulfur (S. Khan et al., 2002; J. Gole et al., 2003; T. Umebayashi et al., 2003).

The presence of metal nanoparticles on TiO_2 surface can promote charge transfer process in the composite systems (N. Chandrasekharan et al., 2000; A. Dawson et al., 2001), because of the electron injection that occurs from the nanosurface to the conduction band of TiO_2 and the metal particle.

In recent years, formation of photocatalytic heterostructures based on TiO_2 with other semiconductor/noble metal has emerged as an

important strategy to increase the separation of charge carriers and suppress the recombination rate of photoinduced electron–hole pairs, resulting in improved photocatalytic efficiency (F.X. Xiao et al., 2012; B. Liu et al., 2011; V. Etacheri et al., 2013; V. Etacheri et al., 2010; V. Etacheri et al., 2012; Y. Wang et al., 2013).

Aims of the work

The aims of the work regard different points of the TiO_2 study and improvement. Starting from the choice of the best commercial powder of TiO_2 to replace the titanium oxide nano-powders, through its modification to make it useful in visible light, until the application on ceramic supports to prepare building materials appropriate for outdoor and indoor pollution abatement, to improve the air quality and the quality of our life as well.

The purposes of this research project can be therefore summarized as follows:

- Study in depth the real potential of a micrometer TiO_2, finding the best candidate among several commercial samples to obtain benefits such as economic saving, safety, ease in product handling in industry;
- Improve the use and application of micro-TiO_2 on building materials to optimize their performances in pollution abatement, with particular attention to realistic settings; in this sense, find innovative methods to test materials and assesses the photocatalytic potentials;
- Make micro-TiO_2 active under visible light, modifying it with noble metals and in particular combining the process with the use of high-energy ultrasound (US).

2. Experimental details

2.1 Commercial samples of TiO_2

In this work, the starting point was the study of different commercial powders of TiO_2.

Five commercial TiO_2 materials by Kronos, Hundsman, Sachtleben (two different powders) and Cristal (respectively quoted with the B–E letters) have been selected. They are all available in the market as pigmentary powders, and they have the following key features: pure anatase phase, uncoated surface, undoped material, not sold as photocatalytic material. P25 by Evonik is the nanometric commercial TiO_2 reference for photocatalytic applications, and it is the most used and studied. All commercial powders were used as received without any further treatment or activation process (C.L. Bianchi et al., 2015).

Table 1: Main features of the selected commercial TiO_2 powders

Sample	**Anatase:Rutile**	**Average crystallite size (nm)**	**SSA (m^2/g)**	**XPS**	**Band gap (eV)**
P25	75:25	26	50	Ti(IV)	3.21
1077 by Kronos (A)	100	110	12	Ti(IV)	3.15
B	100	95	11	Ti(IV)	3.25
C	100	40	23	Ti(IV)	3.28
D	100	Mix (micro-sized+ ultrafine)	11	Ti(IV)	3.25
E	100	180	11	Ti(IV)	3.17

The crystallographic phase composition have been valued by XRD patterns and all the samples are pure anatase, except for P25. Crystallite size of 1077 by Kronos endorses its micro-sized nature, always connects

to a low surface area. As expected, P25 is a nano-sized powder. Studying more thoroughly the morphological characteristics particularly by TEM analysis, it can be notice that the reference P25 powder is made up of well-crystallized particles of rather roundish shape, closely packed and with an average size of 20–30 nm. XPS results give information about the surface states of TiO_2 and there are not differences among all the present samples concerning binding energy (BE). Even the band gap values, evaluated by means of diffuse reflectance UV–Vis analysis, do not exhibit large differences among the various samples.

2.2 Selected pollutants

Photocatalysts, whether commercial as such or modified as explained in the next sections, have been tested on VOCs molecules referring to indoor pollution, and on nitrogen oxides (NO_x) in reference to outdoor pollution. Some reagents are liquid, other are gaseous and stored in cylinders under pressure. The following table reports the list of selected molecules and the relative details. All substances were used as purchased without any particular pre-treatments or purification.

Table 2: List of pollutants and general details

Molecule	Description	Form
Toluene	ACS Reagent, ≥99,5% - Sigma Aldrich	Liquid
Acetone	CHROMASOLV® Plus, ≥99,9% - Sigma Aldrich	Liquid
Ethanol	CHROMASOLV®, ≥99,8% - Sigma Aldrich	Liquid
Formaldehyde	• ACS Reagent 37%wt in H2O, 10-15% Methanol as stabilizer – Sigma Aldrich; • In water, Certified reference material – Sigma Aldrich	Liquid Liquid

Acetaldehyde	ACS Reagent, ≥99,5% - Sigma Aldrich	Liquid
Nitrogen Oxides (NOx)	SAPIO, cylinder 4ppm [NO_2+NO]	Gas
Aldehydes (Mixture)	Apel-Riemer Environmental, Inc. – Cylinder (2000psi), Multicomponent calibration mix	Gas
VOCs (Mixture)	Apel-Riemer Environmental, Inc. – Cylinder (2000psi), Multicomponent calibration mix	Gas

2.3 Photocatalytic reactors

VOCs degradation

Photocatalytic degradations were conducted in a Pyrex glass cylindrical reactor with diameter of 200 mm and effective volume of 5 L. The catalyst in powder form has been deposited on a flat glass sheet (100cm^2) as thin film, from a suspension in 2-propanol. The catalyst amount used in each tests was 0.05 g. The atmosphere in the reactor was obtained by mixing hot chromatographic air humidified at 40%, and a fixed amount of volatilized pollutant, in order to avoid condensation. Photon sources were provided by a 500 W iron halogenide lamp (Jelosil, model HG 500) emitting in the 315–400nm wavelength range (UV-A) at 30Wm^{-2}, or by a LED (MW mean well, 350 mA rated current, 9–48 V DC voltage range, 16.8 W rated power) with an emission between 400 and 700 nm. The actual concentrations of pollutant in the reactor were determined directly by micro-GC sampling or by Proton transfer reaction mass spectrometry (PTR-MS) (detailed description is reported in the next sections).

Nitrogen oxides degradation

- NO_x photocatalytic degradations were conducted in a Pyrex glass cylindrical reactor with an effective volume of 20 L in batch mode. The catalyst in the form of powder has been deposited

from 2-propanol suspension on a flat glass sheet (40cm^2), and the amount used in each tests was 0.05 g. The gaseous mixture in the reactor was obtained by mixing NO_x (mixture of NO and NO_2 in air) with air humidified at 40%. The initial concentrations of NO_x in the reactor were 1000 ppb in order to follow the same pollutant concentration requested by the ISO 22197-1 rules (www.iso.org) and 200 ppb that is very close to the alert threshold set by the EU Directive 2008/50/CE for NO_2 (http://eur-lex.europa.eu). Photon source was provided by a 500 W iron halogenide lamp (Jelosil, model HG 500) emitting in the 320–400 nm wavelength range (UV-A). The specific UV power on the surface of the samples was 10 Wm^{-2}. The concentration of pollutants in the reactor was determined directly by chemiluminescence (Teledyne, Mod. 200E).

- The continuous flow reactor has been used only for testing photocatalytic building materials; it has got walls of 10 mm in thickness, and an internal size of 625 × 625 × 115 mm^3, with four inlets and one opposite outlet and can house a sample of 600 × 600 × 10 mm^3. It is equipped with a thermo-hygrometer model HT- 3006A to measure the temperature and humidity during the tests. The relative humidity inside the reactor is maintained constant around a value between 40 and 50%. The experiments were carried out either using UV lamps (UV-A region, 20 Wm^{-2}) or using sunlight from July to September. The degradation was performed at different initial NO_x concentrations ranging from 100 ± 10 ppb to 200 ± 10 ppb, at room temperature and working with total gas flow rates of 140 and 180 NL h^{-1}. Even for these tests, the concentration values were chosen in order to work closely to the limit values reported on Directive 2008/50/EC, in

particular, 106 ppb (equal to 200 μg m^{-3}) and 213 ppb (400 μg m^{-3}, alert threshold). The duration of each continuous run was set at 6, 12 or 24 h. The final design of the reactor was selected among several possibilities by considering the good homogeneity of the reactant in the gas phase and a contact between the reactant and the photocatalytic material that effectively reproduce the real working conditions.

2.4 Samples characterization

The morphology of TiO_2 in form of powder, both commercial and synthesized or modified, was inspected by means of high-resolution transmission microscopy (HR-TEM) (Jeol JEM 3010 instrument, equipped with LaB6 filament and operating at 300 kV), and the surface area of all the catalysts was determined by conventional N_2 adsorption (BET) at 77 K using a Sorptometer (Costech Mod. 1042). XRD spectra were collected using a PW 3830/3020 X' Pert Diffractometer from PANalytical working Bragg-Brentano, using the Cu Kα1 radiation (k = 1.5406 Å). X-ray photoelectron spectra (XPS) were taken in an M-probe apparatus (Surface Science Instruments). Diffuse reflectance spectroscopy (DRS) of the ground powders was performed with a Thermo Scientific Evolution 600 spectrophotometer, equipped with a diffuse reflectance accessory Praying-Mantis sampling kit (Harrick Scientific Products, USA). A Spectralon1 disk was used as reference material, and the experimental absorption versus lambda plot was elaborated using the Kubelka–Munk function. Absorption/transmission IR spectra were obtained on a Perkin-Elmer FT-IR System 2000 spectrophotometer equipped with a Hg–Cd–Te cryo-detector. Particularly for metals-modified TiO_2, ICP/OES analysis has been performed using a Perkin Elmer Optima 8300 instrument. HR-SEM-EDX

analysis was performed particularly on photocatalytic building materials (tiles) (Field Emission Gun Electron Scanning Microscopy LEO 1525, metallization with Cr. Elemental composition was determined using Bruker Quantax EDS). The surface wettability was evaluated by static contact angle (CA) measurements performed with an OCA20 instrument (DataPhysics Co., Germany) equipped with a CCD camera and a 500μL-Hamilton syringe to dispense liquid droplets.

2.5 Metal NPs modified TiO_2: synthesis procedure

To obtain the surface modification of the commercial powder of TiO_2, in this work we performed a synthesis by means of high-energy US. Procedure steps are slightly different from a metal to another, but in general they follow the same scheme, described in the next lines. The precursor materials are organic or inorganic salts of different metals, selected in accordance with characteristics that will be detailed in the following chapters. For the US generation, we used A Bandelin SONOPLUS HD 3200 utilizing a 200W U/S generator and a sonication extension horn of 13mm diameter. Generally, the metal precursor and the commercial powder of TiO_2 have been put together in a 100 ml glass flask, and they have been solved with the preferred solvent (aqueous or organic). The solution is then sonicated at constant temperature with a specific amplitude and intensity (Wcm^{-2}). At the end the solution is centrifuged many times to remove all the solvent and the final powder is washed before evaporation and/or calcination steps.

2.6 Building materials production: ACTIVE® photocatalytic tiles (by GranitiFiandre S.p.A)

Airless spray classic preparation

Industrial porcelain grés tiles are manufactured under high pressure by

dry-pressing fine processed ceramic raw materials with large proportions of quartz, feldspar, and other fluxes and finally fired at high temperatures (1200–1300°C) in a kiln.

To obtain photoactive porcelain grés tiles, they were subsequently covered by airless spray with a mixture of micro-TiO_2 (specifically, 1077 by Kronos has been selected as best commercial powder) mixed with an aqueous suspension of a commercial SiO_2-based compound (process developed by GranitiFiandre S.p.A, patent n. EP2443076). At the end of the preparation procedure, tiles were fired at high temperature (min 680°C) for 80 min. Finally, the powder present at the sample surface and not completely stuck was brushed and removed.

Digital Printing technology: DigitaLife Project

The digital printing technology is based on suitably designed print heads using a tailored solvent-based ink, micro-sized TiO_2 and additives (process developed by GranitiFiandre S.p.A, DigitaLife project). Specific and more detailed information will be given in the various chapters dedicated.

3. Results and discussion

3.1 Characterization of the TiO_2 powders and materials

Among the starting selected commercial samples, 1077 by Kronos has been chosen as best micrometer candidate to replace the nanometric reference P25. For this reason, all the results that will be presented in this thesis refers to P25 or 1077 as commercial references, nano and micro-sized respectively, and, all the structural modification studies, synthesis, tests, have been performed using 1077 as TiO_2 support on which make changes.

Table 3: Samples list

Sample	**Main structural features**			
TiO_2 - Commercial	**Anatase:Rutile** (Chrystallographic phases composition)	**TiO_2 Average particles size (nm)**	**BET Surface Area (gm^{-2})**	**M-NPs Average particles size (nm)**
P25	75:25	26	50	--
1077	Anatase	110	12	--
TiO_2 – modified by metal NPs – NO US				
TiO_2 + Ag (1-10%wt)	Anatase	110		1-10
TiO_2 + Mn (5-20%wt)	Anatase	110		10-20
TiO_2 – modified by metal NPs – US assisted method				
TiO_2 + Ag (1-20%wt)	Anatase	110		10-20
TiO_2 + Cu (1-75%wt)	Anatase	110		5-20
TiO_2 + Mo	Anatase	110		--
TiO_2 + W	Anatase	110		--
TiO_2 + Re	Anatase	110		--
TiO_2 – ceramic grés tiles				
Z23_Airless spray deposition	Anatase	110		
S24_Digital Printing technology	Anatase	110		

HR-TEM images confirm the nanometric nature of P25 and the micrometric dimension of the TiO_2 particles of 1077 commercial sample. Results are absolutely completely in line with the results about the surface area (gm^{-2}), which is very low in case of bigger TiO_2 particles. From the same characterization analysis performed on the various modified samples, it is shown that this structure composition has not been changed by thermic treatments (calcination steps) or modification steps of the original sample with metals, or by classical impregnation methods either by using ultrasound as will be described in the dedicated chapters. XRD spectra give particularly information about the crystallographic phase composition. As presented in the table above, 1077 consists completely of anatase, which is a very good feature in term of photocatalytic activity. Any modification steps have not altered even this composition. All the samples presented in this work, except P25, consist of anatase. Useful in term of photocatalytic activity is also the distribution on the TiO_2surface of the OH groups, which are measurable in relation to the total oxygen (O_{TOT}), particularly by means of XPS analysis; 1077 by Kronos presents a higher OH/O_{TOT} ratio (0.14 and 0.32 for P25 and 1077 respectively) than P25, and this value, ascertainable even more accurately using the IR spectra, increases modifying 1077 TiO_2 by metals (see Fig. 1).

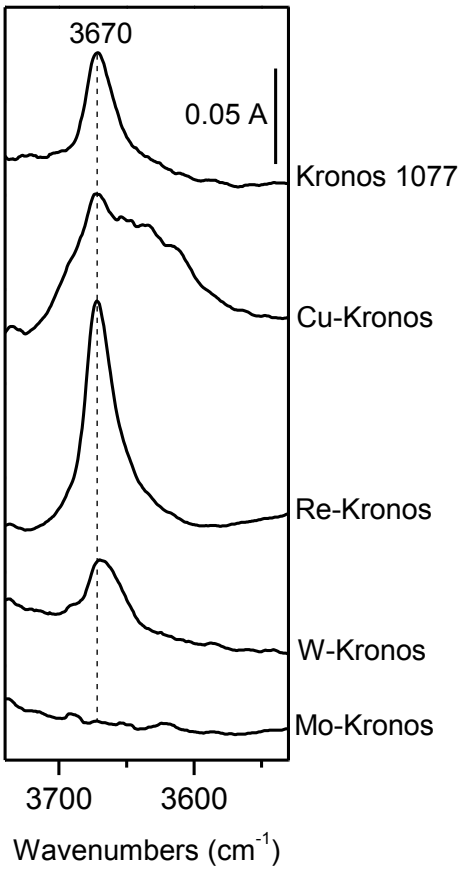

Fig. 1: Analysis of the surface hydroxyl groups (OH) collecting FT-IR spectra after prolonged outgassing at room temperature in order to remove physisorbed molecular water – Comparison between 1077 by Kronos and various samples decorated by metals.

When TiO_2 is decorated on surface with noble metal or metal-oxides nanoparticles (*for every modified-metals-TiO_2 sample presented in this work, we have usually a mixture of metal and metal-oxides NPs*) the UV-VIS

spectra show that the absorption shifts to the visible wavelengths, more or less depending on the metal species and its amount deposited on TiO_2 (Fig. 2). UV-VIS spectra collected on the references, P25 and 1077 respectively, confirm the slight absorption in the visible of P25, because of the presence of rutile, and the absence of absorption in visible of 1077 by Kronos, which can be activated only by UV irradiation, even because its band gap, typical of anatase TiO_2 (3.2 eV). Referring to the surface area, presented above for the references commercial powders, deposition of NPs on TiO_2 surface can have slights effects on the final surface area, which increases, even if the value is very small and almost negligible.

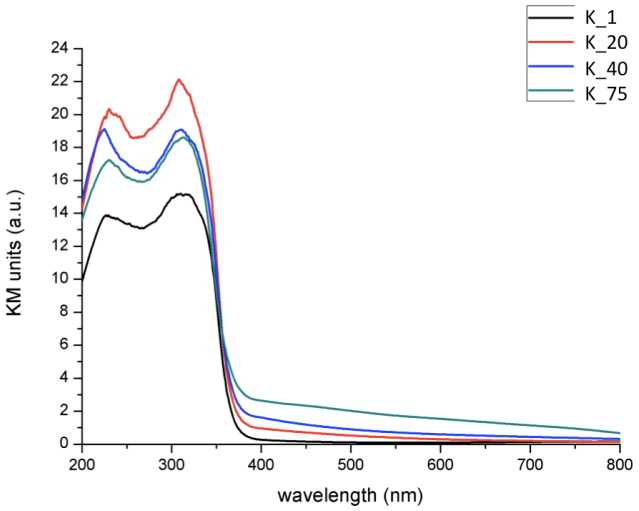

Fig. 2: Absorbance spectra in UV-VIS region of samples K_1, K_20, K_40, and K_75, with 1%,20%,40% amd 75% of Cu contain respectively.

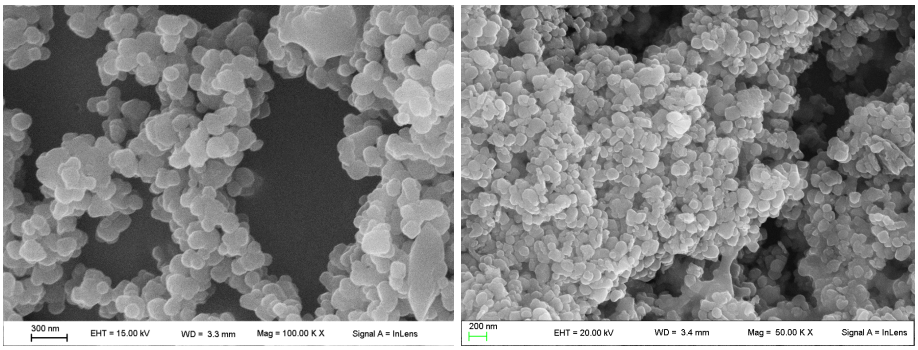

Fig. 3: SEM images of photoactive grés tiles prepared with two different methods: figure on the left refers to the classical spray deposition method; figures on the right refers to the new digital printing technology.

Finally, SEM characterization is very useful to study the ceramic surfaces when TiO_2 is deposited in them. In particular, the main points in case of the two photoactive grés ceramic tiles samples are a) the fact that 1077 TiO_2 does not change its nature so remains anatase and micrometer; b) changing the deposition method the distribution of the TiO_2 particles completely changes (Fig. 3).

3.2 Pollutants photodegradation: Nitrogen Oxides

Table 4: Photocatalytic activity in the degradation of NO_x (1000 ppb)

Sample	**Conv. NOx% after 30′**	**Conv. NOx% after 60′**	**Conv. NOx% after 120′**
P25	72	90	99
1077	79	89	92

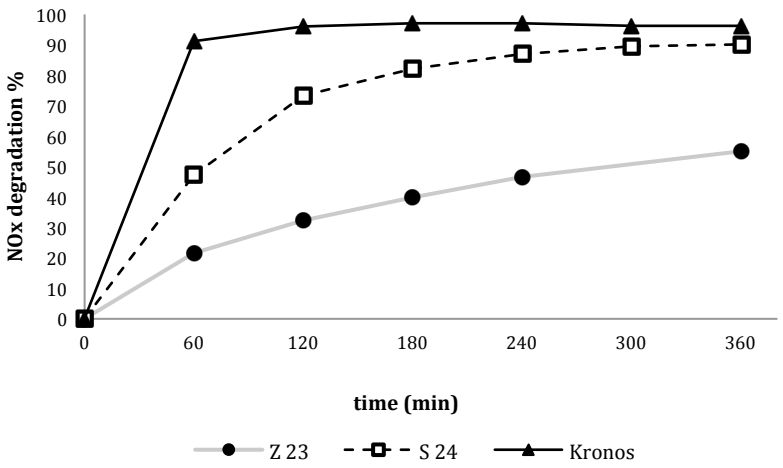

Fig. 4: Photocatalytic degradation % of NO_x(1000ppb) vs. time using a) 1077 by Kronos (black triangles); b) Photoactive tile Z23 (Airless spray classic deposition method) (black dots); c) Photoactive tile S24 (Digital Printing technology) (white squares); Irradiation by UV lamp.

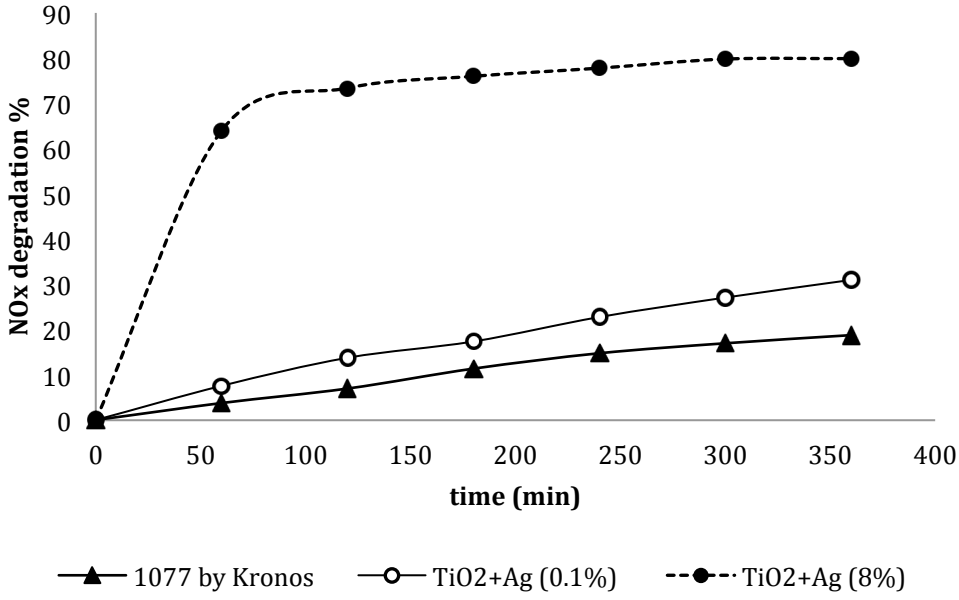

Fig. 5: Photocatalytic degradation % of NO_x(1000ppb) vs. time using a) 1077 by Kronos (black triangles); b) 1077 TiO_2 + Ag0.1%wt (classic impregnation)

(white dots); c) 1077 TiO_2 + Ag8%wt (classic impregnation) (white squares); irradiation by LED.

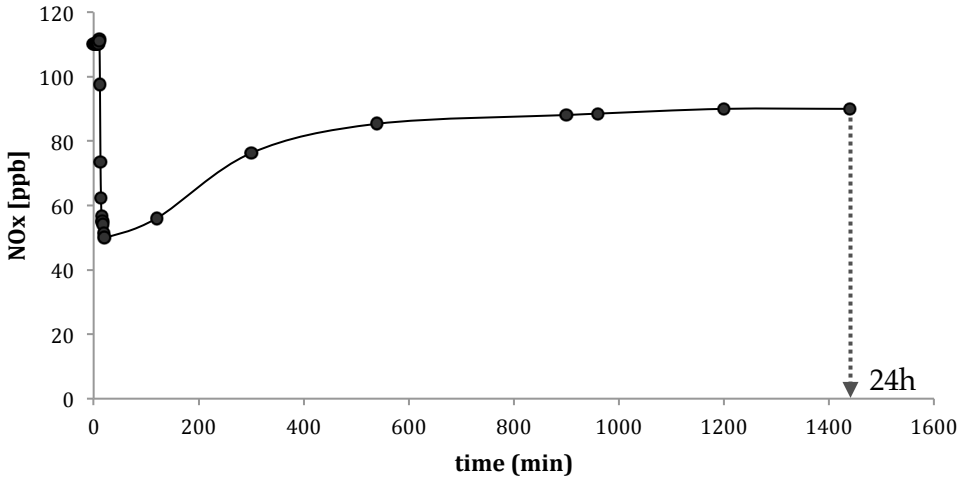

Fig. 6: Continuous flow reactor – Tile: S24 (Digital Printing) – size area: 3600cm^2 – continuous NO_x flow (set at 110 ppb) and UV irradiation from time 0 until 24h.

The use of a pigmentary powder of TiO_2 as 1077 by Kronos, consisting in micrometer particles with a lower surface area, is absolutely effective in case of NO_x abatement. The comparison between 1077 and P25 (as reported in Table 4) shows that the degradation percentage obtained after 120 minutes of photocatalytic reaction is very slight and almost negligible, if we consider the advantages in term of economic saving (2$/kg for P25 vs. 0.45$/Kg for 1077) and safety. The main reasons why 1077 shows to be a very good candidate between various pigmentary and commercial TiO_2 in photocatalysis, are firstly its phase composition, i.e. anatase, without rutile. Moreover we have to consider that 1077 surface present a wide population of OH groups, which both for the adsorption of pollutant molecules and for them degradation are crucial.

Therefore, especially for NO_x abatement, micro-TiO_2 as it is proves to be efficient. Thus, a modification of the material with metals, which increase the final cost, is unnecessary. 1077 however presents a very low activity if irradiated only by visible wavelengths, as confirmed by the UV-VIS spectra, which do not show absorption peaks after 400nm (visible spectrum from 400nm to 700nm). In this case, the surface modification of TiO_2 with metal NPs is a key factor to have effective samples in nitrogen oxides abatement. Preparation methods are different and they will be deeply described in the dedicated chapters. To summarize the most important results, as can be seen from the presented graphs (Fig. 4-6), the presence of silver nanoparticles clearly improve the photocatalytic activity of the sample, and the key factor related to a better NO_x degradation are particularly the metal-NPs amount and dimension. Finally, after showing that 1077 by Kronos is effective, it has been deposited on ceramic grés tiles as already mentioned. The borderline between samples Z23 and S24 is the method with which the deposition is obtained. Digital printing technology leads to a better and more uniform distribution of the TiO_2 powder, as well as to a lower loss of it during the process, with the final results clear presented in the kinetics graphs (see Fig. 4).

3.3 Pollutants degradation: VOCs

	Acetone (400 ppm)	**Ethanol (400 ppm)**	**Toluene (400 ppm) (after 6h)**	**Acetaldehyde (400 ppm)**	**Formaldehyde (500 ppb)**
P25	100% in 70 min.	100% in 30 min.	52%	100% in 60 min.	90% in 30 min.
1077	100% in 90 min.	100% in 60 min.	46%	100% in 70 min.	70% in 30 min.

Table 5: Photocatalytic degradation % of VOCs (C.L. Bianchi et al., 2014)

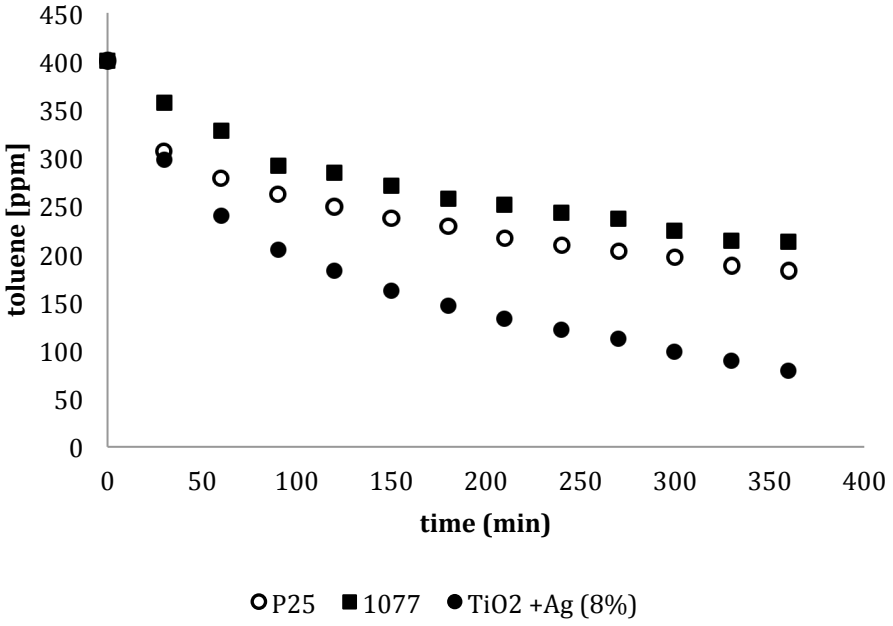

Fig. 7: Toluene photodegradation reaction – UV irradiation – toluene concentration vs. time and comparison between nano-P25 (white dots) or micro-1077 (black squares) with 1077 TiO_2 modified by Ag, 8%wt, obtained by classic impregnation method.

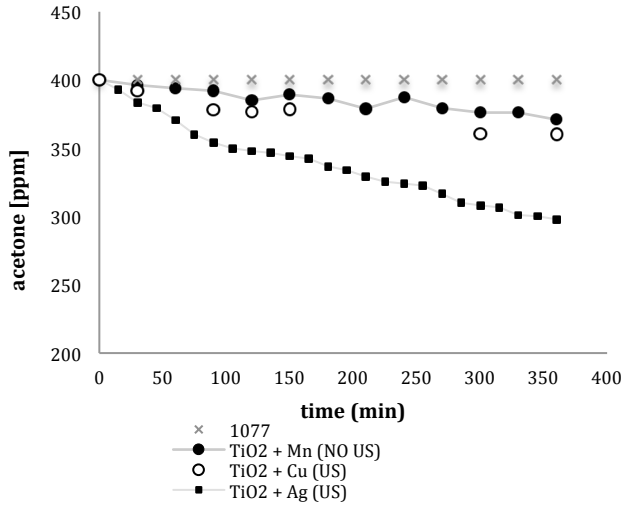

Fig. 8: Acetone photodegradation reaction – LED irradiation – acetone concentration vs. time and comparison between 1077 (grey crosses) and 1077 TiO_2 modified by Ag (black squares), Mn (black dots) and Cu (white dots) respectively.

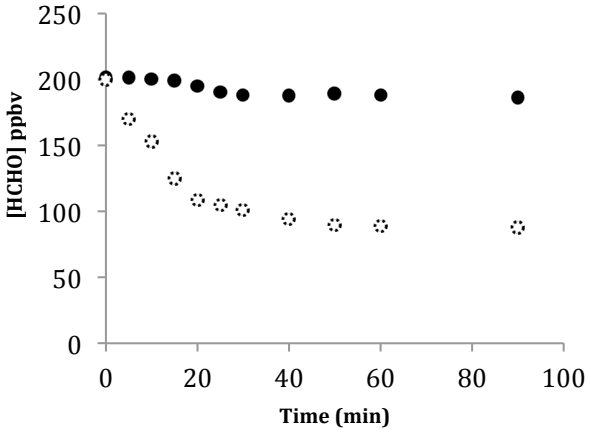

Fig. 9: Formaldehyde concentration (ppbv) over time; Photodegradation by photoactive grés tile prepared with the classical airless spray deposition method (black dots), and by digital printing tiles (white dashed points).

Commercial powders of TiO_2 have been already exploited in VOCs photodegradation (C.L. Bianchi et al., 2014; S.B. Kim et al., 2002; G.M. Zuo et al., 2006), showing very good results against various molecules (see tab.5). However, and it is more evidently than in nitrogen oxides photodegradation, 1077 by Kronos is slightly less effective mainly due to its lower surface area. Moreover, the oxidation of more complex molecules, as in case of toluene that is an aromatic compound, both P25 or 1077 are not able to reach the complete degradation of it after 6 hours of UV irradiation. For this reason, even for this kind of application, the modification and improvement of the TiO_2 photocatalyst is necessary. The presence of metals and metal oxides on the TiO_2 influences the electrons-holes separation, the number of available electrons, the band gap value and the organic molecule adsorption respectively (V.E. Henrich, 1994; H. Al-Abadleh and Grassian, 2003). Among different metals, with properties that will be deeply explained in the dedicated chapters, silver seems to be the best in term of organics oxidation, showing a consistent improvement in the degradation reaction of toluene as reported in fig. 7. Metals-surface decoration is essential under visible light. Anatase-TiO_2 with a band gap of 3.2 eV (C. Dette et al., 2014) is not photocatalytically active. Thus, the presence of metals on its surface is needful. The most important factors that influence the final result are i) metal species and the nature of the species deposited on the TiO_2 surface; ii) metal amount; iii) metal NPs average dimension; iv) metal NPs distribution. In this sense, the synthesis method is very important because can change these latter parameters, and the use of US during the TiO_2 decoration step as reported in (M. Stucchi et al., 2016; M. Stucchi et al., 2014) are very important. US do not change the morphology of TiO_2, but they are crucial for the formation of metal and metal oxides nanoparticles as well as for their good distribution on the

semiconductor surface, as well as, particularly in case of silver, to obtain bigger spherical particles. The number of silver nanoparticles distributed onto TiO_2 surface affects the final photoactivity, and finally a higher number of NPs leads to a better caption of the visible light electrons.

4. Conclusion

As a conclusion to this work, some final remarks can be claimed:

- Comparing the photocatalytic performances of various commercial TiO_2 powders with those of the reference P25 system, in the degradation of different VOCs, such as acetone, toluene, or ethanol, or NO_x, different performances have been achieved. The different performances achieved by the various materials are representative of the different physico-chemical features of them. With the main aim to replace the nanosized P25 with a micrometer powder of TiO_2, 1077 by Kronos shows the best performances. Thus, the present research indicates first that also micro-sized TiO_2 powders, of commercial origin and normally employed as pigments, are very promising materials to be used in the photocatalytic degradation of VOCs and NO_x, which would help limiting the risks for human health deriving from the use of nanoparticles.
- Then, comparing specifically the photocatalytic performance of P25 and 1077 by Kronos, it is shown that: the adsorption of the pollutant molecule at the semiconductor surface is important to promote the photocatalytic reaction, and in this sense, FTIR analysis of the OH stretching region demonstrated the presence

of a good amount of Ti-OH-Ti bridged species on the surface of the micro-sized TiO_2, which plays a key role in driving the photocatalytic activity.

- Through the innovations introduced by sonochemistry, it was possible to obtain a new type of surface decoration of the pigmentary micro-TiO_2, proving that this modification method can improve the photocatalytic activity of the material, in particular under the visible light, where pure TiO_2 is not an effective photocatalyst. Indeed, when TiO_2 is irradiated by visible wavelengths only, the photocatalytic activity is completely lost and particularly, the deposition of both metal or metal oxides nanoparticles, can positively affect its activation under visible light.
- In this research project, the features of Ag, Cu and Mn, have been respectively studied, in particular focusing the attention of the preparation method and the metal amount deposited on the TiO_2 surface. It is possible to summarize that: i) high energy US is a facile and fast method to obtain the surface decoration, even when the support is commercial and micrometric; US do not change the morphology of TiO_2, but they are crucial for the formation of metal and metal oxides nanoparticles as well as for their good distribution on the semiconductor surface; ii) copper proves to be a good candidate, and its amount is crucial, because as a higher amount of copper both increases the absorption of the visible light and improves the electron-hole separation, over a certain amount of metal the performance decreases, because of the excessive coverage of the active sites of TiO_2; iii) Ag shows even better properties in term of TiO_2 activation under visible light. Even in this case US do not change the morphology of the

micrometric support, and they are important to obtain bigger spherical particles of silver as well. Moreover, the number of silver nanoparticles distributed onto TiO_2 surface affects the final photoactivity, and the correlation is linear, because an higher number of NPs leads to a better caption of the visible light electrons first, as well as they reduce the electron-hole recombination, acting as electron traps.

Suggestions for the continuation of the work concern the development of production processes to apply the new metal-modified TiO_2 powders on ceramic materials, to obtains building products active and effective particularly in indoor environment. Secondly, concerning the use of ultrasound in metal NPs synthesis and their application on TiO_2, study further its effects in the pollutants degradation kinetics, as well as in the photocatalytic reactors rheology. Finally, investigate further the degradation of organic molecules with different effects from air pollution: ethylene is harmless for human health, but it is the fruit-ripening hormone. Thus TiO_2-materials can be studied for applications regarding food storage and preservation.

References

Afzal S., Daoud W.A., Langford S. J., "Photostable Self-Cleaning Cotton by a Copper(II) Porphyrin/TiO_2 Visible-Light Photocatalytic System", ACS Appl. Mater. Interfaces, **2013**, 5, 4753−4759.

Al-Abadleh H. and Grassian, "Oxide surfaces as environmental interfaces", Surface Science Reports, **2003**, 52 (3;4), 63–161.

Allen N.D.C, Brewer P.J., Brown R.J.C., Lipscombe R.P., Woods P.T., "International comparison of key volatile organic components in indoor air", Measurement, **2016**, 82, 476–481.

Bianchi C.L., Gatto S., Pirola C., Naldoni A., Di Michele A., Cerrato G., Crocellà V., Capucci V., "Photocatalytic degradation of acetone, acetaldehyde and toluene in gas-phase: Comparison between nano and

micro-sized TiO_2", Appl. Cat. B: Env., **2014**, 146, 123–130.
Bianchi C.L., Pirola C., Galli F., Stucchi M., Morandi S., Cerrato G., Capucci V., "Nano and micro-TiO_2 for the photodegradation of ethanol: experimental data and kinetic modeling", RSC Adv., **2015**, 5, 53419.
Chandrasekharan N., Kamat P. V., "Improving the Photo- electrochemical Performance of Nanostructured TiO_2 Films by Adsorption of Gold Nanoparticles", J. Phys. Chem. B, **2000**, 104, 10851−10857.
Chen A., Cao Q., Zhou J., Yang B., Chang V.W.C., Nazaroff W.W., "Indoor and outdoor particles in an air-conditioned building during and after the 2013 haze in Singapore", Build. Environ., **2016**, 99, 73-81.
Cho Y., Choi W., Lee C.H., Hyeon T., Lee H.I., "Visible Light-Induced Degradation of Carbon Tetrachloride on Dye-Sensitized TiO_2", Environ. Sci. Technol., **2001**, 35, 966−970.
Dawson A., Kamat P. V., "Semiconductor−Metal Nano- composites. Photoinduced Fusion and Photocatalysis of Gold-Capped TiO_2 (TiO_2/Gold) Nanoparticles", J. Phys. Chem. B, **2001**, 105, 960− 966.
Demeestere K., Dewolf J., Van Langenhove H., "Heterogeneous photocatalysis as an advanced oxidation process for the abatement of chlorinated, monocyclic aromatic and sulfurous volatile organic compounds in air: State of the art", Crit. Rev. Env. Sci. Technol., **2007**, 37(6), 489-538.
Dette C., Pérez-Osorio M.A., Kley C.S., Punke P., Patrick C.E., Jacobson P., Giustino F., ì Jung S.J., Kern K., "TiO_2 Anatase with a Bandgap in the Visible Region", Nano Lett., **2014**, 14(11), 6533–6538.
Etacheri V., Michlits G., Seery M. K., Hinder S. J., Pillai S. C., "A Highly Efficient TiO_2−xCx Nano-heterojunction Photocatalyst for Visible Light Induced Antibacterial Applications", ACS Appl. Mater. Interfaces, **2013**, 5, 1663−1672.
Etacheri V., Seery M. K., Hinder S. J., Pillai S. C., "Highly Visible Light Active TiO_2−xNx Heterojunction Photocatalysts", Chem. Mater., **2010**, 22, 3843−3853.
Etacheri V., Seery M. K., Hinder S. J., Pillai S. C., "Nanostructured Ti1−xSxO_2−yNy Heterojunctions for Efficient Visible- Light-Induced Photocatalysis", Inorg. Chem., **2012**, 51, 7164−7173.
Gole J. L., Stout J. D., Burda C., Lou Y., Chen X., "Highly Efficient Formation of Visible Light Tunable TiO_2−xNx Photocatalysts and Their Transformation at the Nanoscale", J. Phys. Chem. B, **2003**, 108, 1230−1240.
Henrich V.E., "The Surface Science of Metal Oxides", New York: Cambridge University Press., **1994**, pp. 14–61.
Herrmann J.M., "Heterogeneous photocatalysis: state of the art and present applications", Top. Catal., **2005**, 34, 49-65.
Khan S. U. M., Al-Shahry M., Ingler W. B., "Efficient Photochemical Water Splitting by a Chemically Modified n-TiO_2", Science, **2002**, 297, 2243−2245.
Kim S.B., Hwang H.T., Hong S.C., "Photocatalytic degradation of volatile organic compounds at the gas-solid interface of a TiO_2 photocatalyst", Chemosphere, **2002**, 48(4), 437-44.
Li X., Liu L., Kang S.Z., Mu J., Li G., "Differences Between Zn- Porphyrin-Coupled Titanate Nanotubes with Various Anchoring Modes: Thermostability, Spectroscopic, Photocatalytic and Photo- electronic

Properties", Appl. Surf. Sci., **2011**, 257, 5950−5956.
Linsebigler A.L., Lu G., Yates Jr. J.T., "Photocatalysis on TiO_2 surfaces — Principles, mechanisms, and selected results", Chem. Rev., **1995**, 95, 735–758.
Liu B., Khare A., Aydil E. S., "TiO_2−B/Anatase Core−Shell Heterojunction Nanowires for Photocatalysis", ACS Appl. Mater. Interfaces, **2011**, 3, 4444−4450.
Robertson P.K.J., Bahnemann D.W., Robertson J.M.C., Wood F., "Photocatalytic detoxification of water and air", Handbook of Environmental Chemistry (**2005**), Vol. 2, Part M, 367-423. Publisher: Springer, Berlin, Germany.
Schiavello M., "Heterogeneous photocatalysis", Wiley Series in Photoscience and Photoengineering, **1997**, Vol. 3. John Wiley & Sons Ltd.
Serpone M., Pelizzetti E., "Photocatalysis: Fundamentals and applications", **1989**, John Wiley & Sons, Inc.
Stucchi M., Bianchi C.L., Pirola C., Cerrato G., Morandi S., Argirusis S., Sourkouni G., Naldoni A., Capucci V., "Copper NPs decorated titania: A novel synthesis by high energy US with a study of the photocatalytic activity under visible light", Ultrason. Sonochem., **2016**, 31, 295–301.
Stucchi M., Bianchi C.L., Pirola C., Vitali S., Cerrato G., Morandi S., Argirusis C., Sourkouni G., Sakkas P.M., Capucci V., "Surface decoration of commercial micro-sized TiO_2 by means of high energy ultrasound: a way to enhance its photocatalytic activity under visible light", Appl. Catal. B Env., **2014**.
Umebayashi T., Yamaki T., Tanaka S., Asai K., "Visible Light- Induced Degradation of Methylene Blue on S-doped TiO_2", Chem. Lett., **2003**, 32, 330−331.
Viegi G., Simoni M., Scognamiglio A., "Indoor air pollution and airway disease", Int J. Tuberc Lug Dis, **2004**, 8, 1401-15.
Wang Y., Liu L., Xu L., Meng C., Zhu W., "Ag/TiO_2 Nanofiber Heterostructures: Highly Enhanced Photocatalysts under Visible Light", J. Appl. Phys., **2013**, 113, 174311.
WHO Global Urban Ambient Air Pollution Database, update **2016**.
WHO, "Guidelines for indoor air quality: selected pollutants", **2016**.
Wu S.H., Wu J.L., Jia S.Y., Chang Q.W., Ren H.T., Liu Y., "Cobalt(II) Phthalocyanine-Sensitized Hollow Fe_3O_4@SiO_2@TiO_2 Hierarchical Nanostructures: Fabrication and Enhanced Photocatalytic Properties", Appl. Surf. Sci., **2013**, 287, 389−396.
Xiao F.X., "Construction of Highly Ordered ZnO−TiO_2 Nanotube Arrays (ZnO/TNTs) Heterostructure for Photocatalytic Application", ACS Appl. Mater. Interfaces, **2012**, 4, 7055−7063.
Zuo G.M., Cheng Z.X., Chen H., Li G.W., Miao T., "Study on photocatalytic degradation of several volatile organic compounds", J. Hazar. Mater., 2006, 128(2;3), **2006**, 158–163.

CHAPTER 1:
GENERAL INTRODUCTION

1.1 Pollution: a global problem

Pollution is a word that each of us hears every day, particularly nowadays.
Pollution occurs when pollutants contaminate the natural or artificial environment, causing changes that affect the human population lifestyle in a negative manner, and by disturbing the ecosystem and the environmental equilibrium.
Today, the innovation and development processes lead pollution to its highest level.
Air pollution is the most prominent and dangerous form of pollution. The causes are several and various: from fuel combustion, to factories activity, the release of chemical substances in air, as well the presence of nitrogen and sulfur oxides is huge.
The effects are more than evident: from the global warming, to the acid rains, from the sudden climate changes, to the increase of diseases such as asthma and lung cancer.

More than 80% of people living in urban areas that monitor air pollution are exposed to air quality levels that exceed the World Health Organization (WHO) limits.
As urban air quality declines, the risk of stroke, heart disease, lung cancer, and chronic and acute respiratory diseases, including asthma, increases for the people who live in them (WHO Global Urban Ambient Air Pollution Database, update 2016).
There are many natural and anthropogenic sources of air pollution, which contribute to outdoor air quality (Lu et al., 2016). Pollutants in the atmosphere can farther settle into water systems, soil or onto the surfaces of plants, and thus the outdoor air quality may impact on food

production and livelihoods. Several ambient air pollutants are governed by standards, and the list includes ozone, carbon monoxide, sulphur dioxide, nitrogen oxides, lead and particulates. In addition, there are numerous other outdoor air pollutants, including volatile and semi-volatile organic compounds such as benzene, polycyclic aromatic hydrocarbons and pesticides (Forbes et al., 2016).

Actually, outdoor air pollution is a major environmental health problem affecting everyone in developed and developing countries alike. An assessment by WHO's International Agency for Research on Cancer (IARC) concluded that outdoor air pollution is carcinogenic to humans, with the particulate matter component of air pollution most closely associated with increased cancer incidence, especially cancer of the lung (Ambient (outdoor) air quality and health, WHO).

Ambient (outdoor air pollution) in both cities and rural areas was estimated to cause 3.7 million premature deaths worldwide per year in 2012. The "WHO Air quality guidelines" offer global guidance on thresholds and limits for key air pollutants that pose health risks. The Guidelines indicate that by reducing particulate matter (PM10) pollution from 70 to 20 micrograms per cubic meter ($\mu g/m^3$), we can cut air pollution-related deaths by around 15%.

The Guidelines apply worldwide and are based on expert evaluation of current scientific evidence for:

- Particulate matter (PM)
- Ozone (O_3)
- Nitrogen dioxide (NO_2)
- Sulfur dioxide (SO_2)

The particulate matter (PM) contents are sulfate, nitrates, ammonia, sodium chloride, black carbon, mineral dust and water, both solid and liquid particles of organic and inorganic substances suspended in the

air. Air quality measurements are typically reported in terms of daily or annual mean concentrations of PM10 particles per cubic meter of air volume (m^3).

The relationship between exposure to high concentrations of small particulates (PM10 and PM2.5) and increased mortality is very narrow. Small particulate pollution have health impacts even at low concentrations, indeed no threshold has been identified below which no damage to health is observed.

Guideline values		
PM2.5	10 µg/m^3 annual mean	25 µg/m^3 24-hour mean
PM10	20 µg/m^3 annual mean	50 µg/m^3 24-hour mean

Table 1: Guideline values for PM2.5 and PM10

There are serious risks to health not only from exposure to PM, but also from exposure to ozone (O_3), nitrogen dioxide (NO_2) and sulfur dioxide (SO_2). Ozone is the main cause in asthma, while nitrogen dioxide and sulfur dioxide can cause, besides asthma, bronchial symptoms and lung inflammation.

Guideline values		
NO_2	40 µg/m^3 annual mean	200 µg/m^3 1-hour mean

Table 2: Guideline values for NO_2

NO_2 is the main source of nitrate aerosols, which form an important fraction of PM2.5 and ozone, in the presence of UV light (Jiang et al., 2016).

Their principal sources are the combustion processes (heating, power generation, and engines in vehicles and ships).

Demands to improve the air quality situation have been largely extended: from the use of clean technologies for industries, to the quest of some cleaner modes of power generation for transport, until to the improving of the energy efficiency of buildings and making cities energy efficient. The increase of the use of low-emissions fuels and renewable power sources is also crucial, as finding new strategies for waste reduction or for the oxidation and degradation of pollutants (Ambient (outdoor) air quality and health, WHO).

A one-hour indoor nitrogen dioxide guideline of 200 $\mu g/m^3$ and an annual average indoor nitrogen dioxide guideline of 40 $\mu g/m^3$ is recommended by WHO air quality guideline. At about twice this level, asthmatics exhibit small pulmonary function decrements. It was assumed that having a gas stove was equivalent to an increased average indoor level of 28 $\mu g/m^3$, which was associated with a 20% increased risk of lower respiratory illness in children (Selected pollutants, WHO).

From a scientific point of view, the indoor air research community was created in 1978 during the first international conference on indoor environments, which was attended by 194 scientists. The first scientific journal "Indoor Air" was published in 1991. Since that moment, the unhealthy environments have been considered not only for the health concern, but also for the materials and the modern techniques that could be the source of the problem.

People live mainly indoors, that means public environments such as schools, hospitals, cinema and gyms, professional environments like offices and industries, and the private houses (Marbury et al., 1991). Thus, we are constantly exposed to all the pollutants present in these close environments (Chen et al., 2016; Allen et al., 2016). There are two different types of harmful effects caused by the exposure to pollutants: milder effects caused by short exposures at high pollutants

concentration, or the effects that are caused by a continuous and prolonged exposure at lower concentrations (IEH, 2001).

While in the first case the symptoms are clear and evident, such as irritation of skin, mucous and respiratory track, in the second case, the constant exposure to an unhealthy environment leads to respiratory diseases, or neurological diseases or even cardiovascular diseases, until the development or even more serious diseases such as cancer (Logue et al., 2010).

General average	**16 hours and 10 minutes/day (67%)**
25% of world population	> 83%
Women	17 hours/day (71%)
Men	15 hours/day (63%)
< 5 years old ; > 60 years old	17 hours/day

Table 3: Time spent indoor, summary of some data.

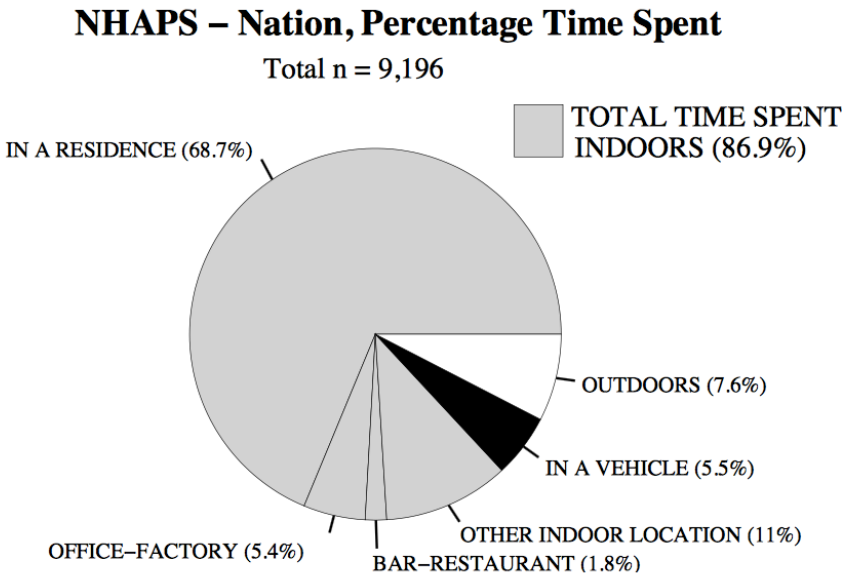

Figure 1: Pie chart showing the mean percentage of time the NHAPS respondents spent in six different locations on the diary day (weighted) (Klepeis et al., NHAPS).

About some of these dangerous substances and their health effects, precise regulations have already been established: tobacco smoke, asbestos, radon and benzene, for instance, have been classified as carcinogen.

Volatile organic compounds (VOC) and aldehydes are, in the most part of cases, the cause of eye irritation and respiratory irritation. Some of them, such as benzene and formaldehyde, have been already classified as carcinogen by the International Agency for Research on Cancer (IARC), while others, such as pesticides, phthalates and chlorinated compounds, are associated to neurotoxic effects.

The Sick Building Syndrome (SBS) is defined as an excess of non-specific symptoms, such as headaches, skin irritation or eye irritation, which appear in people who spend a long time in a close and non-industrial environment (Viegi et al., 2004). The origin of SBS is multifactorial, and it is related to the presence of VOC, contaminants, insufficient light and poor ventilation (OMS, 2007).

Indoor pollution is confined in a delimited space, thus the study of its composition is much less complex than the external air, where the emission sources are several, pollutants are very different from each other, their concentration is not constant and the people exposed are very heterogeneous. Moreover, climate conditions are very influential. Anyhow, both outdoor and indoor pollution are a global problem (Chi et al., 2016).

The diseases caused by unhealthy substances that are present indoor and outdoor affecting more than 30% of the population of industrial countries (Jantuneri et al., 2011). Every year from 12 to 40 billions of dollars are spent on health, and the impact of air pollution is very high.

Sources of pollution	Pollutants
Daily activities	VOC and SVOC (semi-volatile organic compounds), such as ethanol, acetone, polycyclic aromatic hydrocarbons; NO_2, CO and bacteria.
Environment and materials	VOC such as aldehydes, alkanes, alcohols, ketones, olefins, phthalates, chlorinated compounds and paraffin.
Heating and refrigeration systems	CO, NO_2, VOC.
Secondary pollution	From the interaction between O_3 and organic compounds; formaldehyde, benzaldehyde and other aldehydes.

Table 4: Source of pollution and related pollutants.

1.1.1 Chemical pollutants: which of them affect our life?

Clean air is a basic requirement of life. The quality of air inside homes, offices, schools, day care centers, public buildings, health care facilities or other private and public buildings where people spend a large part of their life is an essential determinant of healthy life and people's well-being.

Carbon monoxide (CO), and the most part of VOC, SVOC and aldehydes come from sources related to human activities, from construction products and products for decoration, and from combustion reactions. Volatile organic compounds consist of carbon, hydrogen, oxygen and other elements like halogens. Their ebullition point is between 50°C and 100°C, and they are often used for the fabrication of several materials, such as paintings, glues, adhesives, or in cleaning products and fabrics.

- **Benzene**

Originated from internal sources, such as combustion processes, or vehicles; the highest concentrations occur at service stations and in close

proximity of industries. It is carcinogen (Group 1). Benzene is present in both outdoor and indoor air, with the indoor concentrations that are generally higher than those in outdoor air. Benzene is a genotoxic carcinogen in humans and no safe level of exposure can be recommended. The geometric mean of the range of the estimates of the excess lifetime risk of leukemia at an air concentration of 1 $\mu g/m^3$ is 6×10^{-6}. The concentrations of airborne benzene associated with an excess lifetime risk of 1/10 000, 1/100 000 and 1/1000 000 are 17, 1.7 and 0.17 $\mu g/m^3$, respectively.

There is no known exposure threshold for the risks of benzene exposure, thus, it is expedient to reduce indoor exposure levels to as low as possible (Selected pollutants, WHO).

- **Formaldehyde**

Emitted from the most part of construction materials and several objects of common use, such as furnishings, craft products and cosmetics. Present in tobacco smoke, chimney smoke, auxiliary heating, and vehicles. It is also generated from the reaction of other pollutants, in particular ozone and unsaturated organic compounds. Classified as carcinogenic from 2004 (IARC). The lowest concentration reported to cause sensory irritation of the eyes in humans is 0.36 mg/m^3 for four hours. Increases in eye blink frequency and conjunctival redness appear at 0.6 mg/m^3, which is the no observed adverse effect level (NOAEL).

The perception of odor may result in some individuals reporting subjective sensory irritation, and individuals may perceive formaldehyde at concentrations below 0.1 mg/m^3. The NOAEL of 0.6 mg/m^3 for the eye blink response is adjusted using an assessment factor of 5 derived from the standard deviation of nasal pungency (sensory irritation) thresholds, leading to a value of 0.12 mg/m^3, which has been

rounded down to 0.1 mg/m^3. This value is thus considered valid for short-term (30-minute) duration, and this threshold should not be exceeded at any 30-minute interval during a day.

Thus, a short-term (30-minute) guideline of 0.1 mg/m^3 is recommended as preventing sensory irritation in the general population.

Evaluations of long-term effects, including cancer, based on a NOAEL produce similar results, with values of approximately 0.2 mg/m^3. The use of the short-term (30-minute) guideline of 0.1 mg/m^3 will also prevent long-term health effects, including cancer (Selected pollutants, WHO).

- **Semi-volatile organic compounds**

Present in air both in gaseous form and condensed and deposited on surfaces in the domestic environments. They are phthalates, pesticides, and flame-retardants, alkylphenols and polychlorinated biphenyls (PCB), or polycyclic aromatic hydrocarbons. Concern in this type of compounds is growing in the last years because they easily permeate in tissues, so that they are present in blood and urine. Phthalates in particular are very dangerous for their toxic effects and their persistence in the environment.

- **Trichloroethylene**

There are different interpretations of trichloroethylene (TCE) toxicity and divergent estimates of human cancer risk. Anyway, the carcinogenicity in animals and the probability of a human cancer risk leads to the recommendation of a non-threshold approach with a risk estimate rather than a safe level.

The unit risk estimate of 4.3×10^{-7} $(\mu g/m^3)^{-1}$ is proposed as the indoor air quality guideline. This was also the conclusion of WHO in 2000, the

European Union in 2004 and the French Agency for Environmental and Occupational Health in 2009.
The concentrations of airborne TCE associated with an excess lifetime cancer risk of 1/10.000, 1/100.000 and 1/1.000.000 are respectively 230, 23 and 2.3 $\mu g/m^3$ (Selected pollutants, WHO).

- **Tetrachloroethylene**

On the basis of a long-term LOAEL of 102 mg/m^3, a guideline value of 0.25 mg/m^3 has been calculated. A chronic inhalation minimal risk level (MRL) of 0.28 mg/m^3 (0.04 ppm) has been derived by the Agency for Toxic Substances and Disease Registry.
Establishing a long-term value is more protective of human health, and the recommended guideline for year-long exposure is 0.25 mg/m^3 (Selected pollutants, WHO).

1.2 Advanced Oxidation Processes: Photocatalysis and its application

Oxidation is described as the transfer of electrons from an electron donor (reductant) to an electron acceptor (oxidant), which has a higher affinity for electrons. The electron transfers result in a chemical transformation of both the oxidant and the reductant, producing chemical species with an odd number of valence electrons, known as radicals. These latter are highly unstable and highly reactive because one of their electrons is unpaired. Oxidation reactions that produce radicals are usually followed by additional oxidation reactions between the radical oxidants and other reactants (both organic and inorganic) until thermodynamically stable oxidation products are formed. The ability of an oxidant to start chemical reactions is measured in terms of

its oxidation potential. Among the most powerful oxidants there are the hydroxyl radicals (•OH), ozone, and chlorine with oxidation potentials of 2.70 electron volts (eV) (Dorfman and Adams, 1973). The end products of complete oxidation (i.e., mineralization) of organic compounds are carbon dioxide (CO_2) and water (H_2O).

Advanced Oxidation Processes (AOPs) include each highly competitive treatment technology, based on chemical oxidation, for the removal of organic persistent pollutants in both gas and liquid phase (Oller et al., 2011).

AOPs involve two stages of oxidation mentioned above: a) the formation of strong oxidants (e.g., hydroxyl radicals) and b) the reaction of these oxidants with organic contaminants in water. However, the term advanced oxidation processes refers specifically to processes in which oxidation of organic contaminants occurs primarily through reactions with hydroxyl radicals (Glaze et al., 1987). In water treatment applications, AOPs usually refer to a specific subset of processes that involve O_3, H_2O_2, and/or UV light. Nevertheless, AOPs refer to a more general group of processes that also involve TiO_2 catalysis, E-beam irradiation, Fenton's reaction, and cavitation.

AOPs can be divided into established and emerging technologies.

Established technologies are:

- Hydrogen Peroxide/Ozone (H_2O_2/O_3)
- Ozone/Ultraviolet Irradiation (O_3/U_v)
- Hydrogen Peroxide/ Ultraviolet Irradiation (H_2O_2/UV)

Emerging technologies are:

- High Energy Electron Beam Irradiation (E-beam)
- Cavitation (Sonication & Hydrodynamic)
- TiO_2-catalyzed UV Oxidation
- Fenton's Reaction

Overall, AOPs rely on generation of reactive radical species, i.e. •OH. Reactions that take place on the illuminated surface of semiconductor metal oxides have the most attention. These compounds are semiconductors with a restrained energy band-gap (see tab. 5), and they are the main actors of the process normally called photocatalysis, described in detail below.

Semiconductors	**Band-gap energy (eV)**	**Semiconductors**	**Band-gap energy (eV)**
Diamond	5.4	WO_3	2.76
CdS	2.42	Si	1.17
ZnS	3.6	Ge	0.744
ZnO	3.436	Fe_2O_3	2.3
TiO_2	3.03	PbS	0.286
SnO_2	3.54	PbSe	0.165
Cu_2O	2.172	ZrO_2	5-6

Tab. 5: Band-gap energies for some common semiconductor materials at 0K (Kabra et al., 2004; Kawai et al., 1979; Sato et al., 1980).

1.2.1 Photocatalysis: general definition

A catalyst is a substance able to accelerate a chemical reaction without being consumed as reactant, and which lowers the free activation enthalpy of the reaction (M. Castellote and N. Bengtsson, in Y. Ohama and D. Van Gemert, 2011). Photocatalysis can be described as the acceleration of a photoreaction by the presence of a particular catalyst, which usually is a semiconductor material (J.M. Herrmann, 2005). However, there is no accord in the scientific community about a proper definition of photocatalysis, and in general the term is used to describe a process in which light activate a substance, i.e. the photocatalyst, which modifies the rate of a reaction, without being involved itself in the chemical transformation (Dimitris I. Kondarides, Photocatalysis). Thus, the main difference between a conventional thermal catalyst and a

photocatalyst is that the former is activated by heat whereas the latter is activated by photons of appropriate energy.

In heterogeneous photocatalysis, the reaction implies the previous formation of an interface between the semiconductor and the reactants of the reaction (K. Demeestere et al., 2007; M. Schiavello, 1997). Therefore, the term "heterogeneous photocatalysis" is mainly used in cases where a light-absorbing semiconductor photocatalyst is utilized, which is in contact with either a liquid or a gas phase (J.M. Herrmann, 2005).

Heterogeneous photocatalysis is the most intensively studied, in particular because of its environmental and energy-related applications, or in organic syntheses (M. Gratzel, 1983).

When the light is adsorbed by the catalyst (C), the system represents a sensitized photoreaction, which may occur through two different ways:

1. Via energy transfer, by forming an activated state of the reactant of interest, S, which is more easily oxidized than their ground state;
2. Via electron transfer, by acting either as an electron donor or acceptor.

Particularly, in semiconductor photocatalysis, the absorption of a photon leads to the excitation of an electron from the valence band to the conduction band. However, the photon energy must be equal or higher than the band-gap energy of the semiconductor.

Eq. 1.1 describes the general scheme of a semiconductor-mediated photocatalytic reaction:

$$(Ox_1)_{ads} + (Red_2)_{ads} \xrightarrow[h\nu > E_{bg}]{\text{semiconductor}} Red_1 + Ox_2 \qquad (1.1)$$

Among a large variety of semiconductor materials, which are mainly metal oxides, only few of them are considered to be applicable

photocatalysts, in relation with their specific photocatalytic properties. Wide-band gap semiconductor, such as TiO_2, show to be better photocatalysts than low-band gap metal oxides, in particular because of the low chemical and photochemical stability of these latter (M. Serpone et al., 1989).

1.2.2 Fundamental concepts and properties of semiconductors

Materials are classified as conductors, semiconductors or insulators, according to the band theory. Bands with different energy are formed by the energy levels of the huge numbers of atoms that interact in a solid material, and electrons occupy them from the lowest energy to the highest. The highest energy band is the valence band (VB), while the next higher band is called conduction band (CB). The band gap energy (E_{bg}) is the energy gap that separates the VB and the CB. In particular, a semiconductor is characterized by a specific band gap, generally lower than 4 eV, which the electrons can overpass if stimulate by heat or light. Normally, the most part of the electrons are in the VB.
When a valence band electron (e^-) is excited into the CB, leaves behind an unoccupied state in the valence band, called hole (h^+). Electrons and holes flow in opposite directions in the presence of an electric field but contribute to current in the same direction since they are oppositely charged. In this way, they created intrinsic charge carriers.
Another important parameter in the band theory is the Fermi level (EF). Electrons are distributed in available energy states following the Fermi-Dirac statistics, and in this sense the Fermi energy level is described as the energy at which the probability of occupancy is equal to 0.5, in relation to the number of electrons in the system.

The Fermi level of a semiconductor is located between CB and the VB and it exemplifies the equal statistical probability of finding a charge carrier in either of these two energy bands.

1.2.3 Photocatalytic oxidation of organic molecules

The most important photocatalytic reaction, especially related to environmental applications, is the oxidation of organic molecules (K. Demeestere et al., 2007; P.K.J. Robertson et al., 2005).
The position of the semiconductor valence band, and the redox potential of the organic substrate respectively, regulate the redox potential needed for the oxidation.
More specifically, it occurs when the redox level of the photogenerated hole is higher than the organic substrate redox potential, or, more frequently, when hydroxyl radicals (•OH) are formed.

1.3 TiO_2

1.3.1 A brief historical background

The commercial production of TiO_2 began in the early twentieth century, and from that this semiconductor has been widely used for many applications, mostly as pigment (G. Pfaff et al., 1999), in sunscreens [A. Salvador et al., 2000). In 1972, Fujishima and Honda discovered the phenomenon of photocatalytic splitting of water on a TiO_2 electrode under ultraviolet (UV) light (A. Fujishima et al., 1972; A. Fujishima et al., 2000; D. Tryk et al., 2000). After that, the research on TiO_2 constantly increased, particularly for the several promising applications in areas ranging from photovoltaics and photocatalysis to

photo/electrochromics and sensors (M. Graetzel et al., 2001; A. Hagfeldt et al., 1995; A. Linsebigler et al., 1995; A. Millis et al., 1997). As the most promising photocatalyst, TiO_2 materials are expected to play an important role in helping solve any serious environmental and pollution challenges (M.R. Hoffmann et al., 1995).

When several papers published by Ollis established that TiO_2 could be used for degrading organic compounds present in water or air steam (S. CRAIG et al., 1990), practical applications of TiO_2 photocatalysis have been employed (A. Fujishima et al., 1999) and scientists started to conduct further studies to understanding the fundamental processes occurring in photocatalysis.

1.3.2 Structural properties of TiO_2 materials

Among different semiconductor the good properties of TiO2 makes it very interesting, in particular in the field of photocatalysis.

TiO_2 has got mainly three different crystal structures, rutile (tetragonal), anatase (tetragonal), and brookite (orthorhombic) (A. Linsebigler et al., 1995).

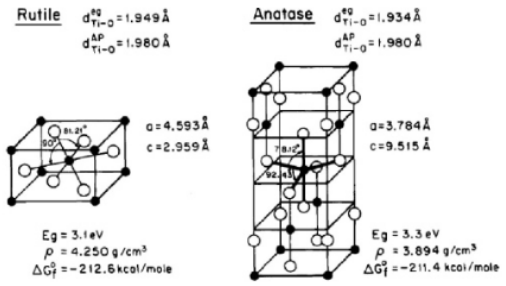

Fig. 2: Lattice structure of rutile and anatase TiO_2. (A. Linsebigler et al., 1995).

The first two, i.e. anatase and rutile, can be described in terms of chains of TiO_6 octahedra, where each Ti^{4+} ion is surrounded by an octahedron of six O^{2-} ions. The two crystal structures differ in the distortion of each octahedron, because in rutile, the octahedron shows a slight orthorhombic distortion, while in anatase, the octahedron is significantly distorted so that its symmetry is lower than orthorhombic.
The different Ti-Ti and Ti-O distances in anatase and rutile respectively, and the different numbers of octahedrons in contact, lead to different mass densities and electronic band structures between the two forms of TiO_2.
While rutile is the most stable form, anatase and brookite are metastable and are easily transformed to rutile at high temperatures (A. Di Paola et al., 2013).
The theoretical density of TiO_2 ranges from 3895 kg/m^3 for anatase to 4250 kg/m^3 for rutile (Kirk-Othmer Encyclopedia of Chemical Technology, Wiley). The melting point of rutile is between 1830°C and 1850°C, while the anatase transition to rutile occurs abroad a temperature range between 500°C and 900°C.
Brookite has an orthorhombic crystalline structure (L. Pauling et al., 1928). The structure is composed of octahedra, in which the titanium atom is in the center and the oxygen atoms are in the corners (Figure 2).

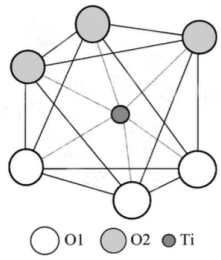

Fig 2: Octahedron of the crystalline structure of brookite.

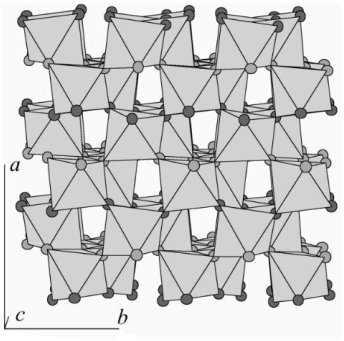

Fig 3: Crystalline structure of brookite.

X-ray diffraction (XRD) analysis is usually used to evaluate the presence of the different crystallographic phases. Brookite in the XRD patterns is evidenced from the presence of the (121) peak at 2θ = 30.81°, while the main (101) diffraction peak of anatase is at 2θ = 25.28°.

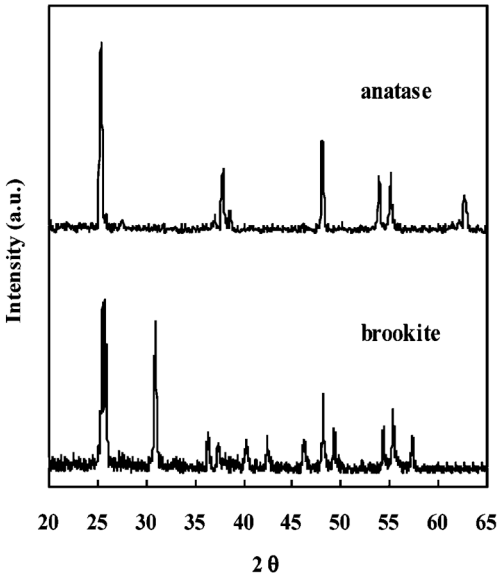

Fig. 4: X-ray diffraction (XRD) analysis patterns of anatase and brookite (A. Di Paola et al., 2013).

The electronic band structure of the TiO_2 polymorphs is related to the photocatalytic behaviour of the pure phases or their mixtures. In 1985, Grätzel and Rotzinger (M.Grätzel et al., 1985) estimate the band gap value, of brookite as 3.14 eV. Afterwards, the band gap values were corrected, starting from most modern techniques and calculations, and the specific values for brookite, rutile and anatase were defined 3.26 eV, 2.98 eV and 3.05 eV respectively (fig 5) (M. Landmann et al., 2012).

The band gap was usually determined by diffuse reflectance measurements, from the tangent lines to the plots of the modified Kubelka-Munk function (Y.I. Kim et al., 1993).

The flatband potential (EFB) of a semiconductor is a fundamental property for the thermodynamics of the interfacial electron transfer steps. For an n-type semiconductor as TiO_2 it can be assumed that the positions of the flatband potential and the quasi-Fermi level (*Ef) are the same and very close to the lower edge of the conduction band (D. Dung et al., 1982).

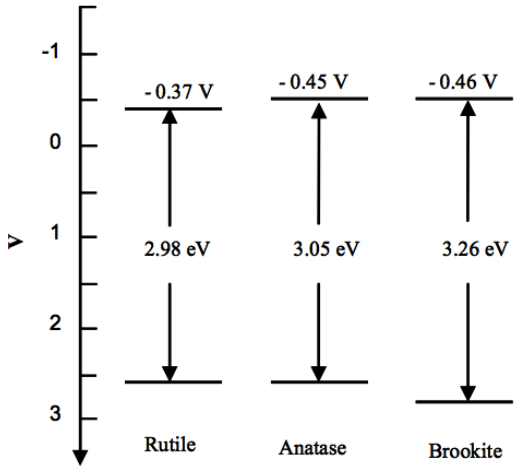

Fig. 5: Electrochemical potentials of the band edges of anatase, brookite, and rutile at pH = 7 (A. Di Paola et al., 2009).

1.3.3 Photo induced electron-hole properties

When TiO_2 is irradiated with energies equal to or higher than its band gap (>3.0 eV), electrons are excited from the valence band into the conduction band, leading to excited electrons in the conduction band and positive holes in the valence band. These charge carriers can recombine or get trapped and react with electron donors or acceptors adsorbed on the surface of the photocatalyst. This fundamental process can be expressed by the following reaction equations (2-10.1):

$$TiO_2 + h\nu \rightarrow e^- + h^+ \quad (2.1)$$

$$e^- + Ti(IV)O—H \rightarrow Ti(III)O—H^-(X) \quad (3.1)$$

$$h^+ + Ti(IV)O—H \rightarrow Ti(IV)O\bullet —H^+(Y) \quad (4.1)$$

$$h^+ + \tfrac{1}{2} O^{2-} \rightarrow \tfrac{1}{4} O_2(g) + \text{vacancy} \quad (5.1)$$

$$e^- + O_2 \rightarrow O^{2-} \quad (6.1)$$

$$O_2^- + H^+ \rightarrow HO_2 \quad (7.1)$$

$$h^+ + Ti(III)O—H^- \rightarrow Ti(IV)O—H \quad (8.1)$$

$$e^- + Ti(IV)O\bullet —H^+ \rightarrow Ti(IV)O—H \quad (9.1)$$

$$O_2 + Ti(IV)O\bullet\text{—}H^+ \rightarrow Ti(IV)O\text{—}H + O_2 \quad (10.1)$$

Eq. (2-9): 2) photon absorption process; (3-7) photocatalytic redox pathways; (8-10) recombination channels; (4,5) competition pathways for holes, leading to bound OH radicals and O vacancies, respectively. (S.H. Szczepankiewicz et al., 2000).

1.3.4 Crystallographic phases of TiO_2 and photocatalytic activity

The triangular arrangement of the oxygen ions position on the exposed crystal surface of anatase is suitable for a good absorption of organic molecules. Instead, rutile does not present this structural layout. This latter is one of the crucial reasons because of the higher photocatalytic activity of anatase compared to rutile (T. Weng, 1993).
However, a mixture of anatase and rutile often leads to a better photocatalytic efficiency, because the presence of rutile phase introduces mesoporosity and a wider pore size distribution (R.I. Bickley et al., 1991; R.R. Beska, J. Kiwi, 1998).

1.3.5 TiO_2 particles size distribution and photocatalytic activity

Particles size of TiO_2 influences the photocatalytic activity. The matter has been deeply investigated and in literature there are some several papers that report the optimal particle size for a given reaction (A.J. Maira et al., 2000; Z. Zhang et al., 1998; C.B. Almquist et al., 2002). Overall, the photocatalytic activity increases when the particles size decreases.

The high surface area brought about by small particle size is beneficial to many TiO_2-based devices, as it facilitates reaction/interaction between the devices and the interacting media, which mainly occurs on the surface or at the interface and strongly depends on the surface area of the material. Thus, the performance of TiO_2-based devices is largely influenced by the sizes of the TiO_2 building units, apparently at the nanometer scale.

1.4 TiO_2 and visible light photocatalysis

The major drawbacks of TiO_2-based photocatalysts is related to the rapid charge recombination of the electron−hole pairs, and the wide band gap, which restricts light absorption to only ultraviolet region (wavelength <390 nm), restraining the practical applications of TiO_2-based photocatalysts under solar light or visible light.

Different strategies, including dye sensitization (X. Li et al., 2011; S. Afzal et al., 2013; S. Wu et al., 2013; Y. Cho et al., 2001), metal (B. Qi et al., 2012; N. Serpone et al., 1994; S.N.R. Inturi et al., 2014; J. Xu et al., 2008; L. Devi et al., 2012) or nonmetal doping (C. Han et al., 2011; P. Periyat et al., 2008; M.V. Dozzi et al., 2013) have been developed to improve the visible light activity (VLA) of TiO_2 in order to use the solar irradiation or interior lighting efficiently.

The first approaches began around 1986 with the chemical modification of TiO_2 lattice using non-metals, particularly carbon, nitrogen and sulfur (S. Khan et al., 2002; J. Gole et al., 2003; T. Umebayashi et al., 2003). As reported by Asahi et.al, nitrogen-doped TiO_2 exhibited a good enhancement in visible light photocatalysis (R. Asahi et al., 2001), thus following this work various scientists started to work in visible-light-active-N-doped-TiO_2 photocatalysts (M. Pelaez et al., 2013; N.T. Nolan et

al., 2012), finding that in general doping TiO_2 by non-metal ions shifts the absorption band of the semiconductor towards the visible region. Reasons are numerous, principally, the presence of defects associated with oxygen vacancies in doped TiO_2 can be responsible for their visible light activity (Serpone et al., 2006), as the Density functional theory (DFT) predicted that the doped atoms could occupy substitutional or interstitial sites in the TiO_2 lattice and generate localized energy levels in the band gap (C. Di Valentin et al., 2005; C. Di Valentin et al., 2007).
Overall, the visible light response in doped materials is thought to arise from the presence of localized energy levels of the dopant lying above the valence band or oxygen vacancies as demonstrated in Figure 6.

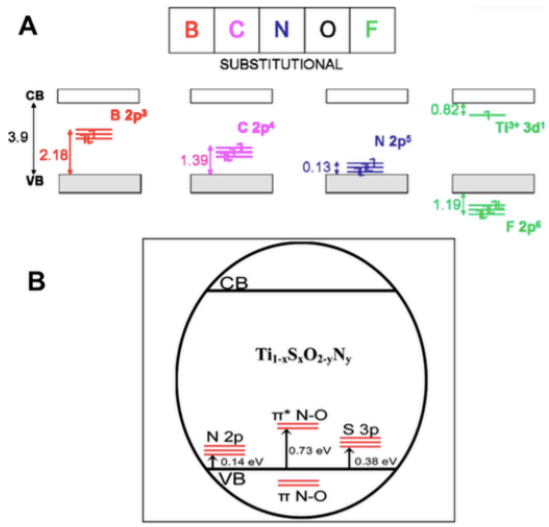

Fig. 6: Localized impurity energy states for the substitutionally doped TiO_2.

The improving of the visible-light activity and of the photocatalytic efficiency can be also obtained inhibiting the charge recombination, through the co-doping of TiO_2 with two or more nonmetals such as S–N

(J.H. Xu et al., 2008), B−N (G. Liu et al., 2008), C−N (G. Liu et al., 2013) or N−F (A. Katsanaki et al., 2013).

Another interesting approach was the TiO_2 chemical modifications with 3d transition metal ions, such as lanthanides, and noble metals (A. Di Paola et al., 2002; M.K. Seery et al., 2007; I. Arabatzis et al., 2003). Specifically, among different noble metals, the addition of increased amounts of Ag up to 5 mol % facilitates visible light absorbance (I. Arabatzis et al., 2003; N.T. Nolan et al., 2010). The main reasons related to the enhancement of the visible light activity also in this case include band gap narrowing, the formation of impurity energy levels within the band gap of TiO_2, and the formation of intrinsic defects, such as oxygen vacancies.

Finally, the presence of metal nanoparticles on TiO_2 surface can promote charge transfer process in the composite systems (N. Chandrasekharan et al., 2000; A. Dawson et al., 2001), because of the electron injection that occurs from the nanosurface to the conduction band of TiO_2 and the metal particle.

In recent years, formation of photocatalytic heterostructures based on TiO_2 with other semiconductor/noble metal has emerged as an important strategy to increase the separation of charge carriers and suppress the recombination rate of photoinduced electron−hole pair, resulting in improved photocatalytic efficiency (F.X. Xiao et al., 2012; B. Liu et al., 2011; V. Etacheri et al., 2013; V. Etacheri et al., 2010; V. Etacheri et al., 2012; Y. Wang et al., 2013). Additionally, the synergistic effects induced by the components in the heterostructure also result in an increased photostability and photocatalytic efficiency.

1.5 From powders to materials

1.5.1 Photocatalytic ceramic tiles

Porcelain grés are manufactured under high pressure, by dry-pressing fine processed ceramic raw materials, which contain for the most part quartz, feldspar and other fluxes (R. Casasola et al., 2012). After this first process, the body of the material is fired at high temperature ranging from 1200°C and 1300°C in particular long roller kilns, in which temperature is carefully monitored. The porcelain grés tiles obtained shows lack of porosity, durability, high breaking, wear resistance properties and a complete frost resistance. Moreover, it is characterized by a very low water absorption rate (C.L. Bianchi et al., 2012). The high resistance and the lack of porosity, however, do not always go together with an aesthetic beauty. While at the beginning of the production the production the porcelain grés tiles have been considered just a technical material, in the last years much more attention is given also to their aesthetic features.

Actually, in particular thanks to new industrial production methods, both technical properties and aesthetic features can be obtained, completely answering to the market requests (C.L. Bianchi et al., 2012).

Moreover, beside these noteworthy architectural features, new surface properties have been introduced in the last generation of these materials.

TiO_2 is one of the most used and efficient photocatalytic material and, especially in the field of construction and building materials, it is the most widely used (S. de Niederha˜usern and M. Bondi, 2013). It has been widely used in many researches and practical applications, including self-cleaning and anti-bacterial effect, as cement mortar, in exterior tiles,

paving blocks, glass, PVC fabric, and to protect the Cultural Heritage surfaces (M.V. Diamanti et al., 2008; X.J. Zhao et al., 2008; E. Quagliarini et al., 2012). In a recent work, F. Bondioli et al. reported the possibility of tile surface functionalization using a sol-gel technique to improve both wear resistance and cleanability of unglazed surfaces (F. Bondioli et al., 2009).

Ceramic tile is one of the most widely used materials in construction, and in the last years the demand for environmentally responsible construction and the ever more restrictive environmental requirements derived from the legislation are increased in the functional tiles (D.B. María et al., 2010).

Substituting antimicrobial tiles for other surfaces support is important to have a healthier environment, and in this sense it is essential to improve ability to control and destroy microorganisms to many organizations and industries, such as healthcare, food and drink, water treatment and military industries (M. Archana et al., 2012).

There are several approaches to obtain a multifunctional surface for ceramic tiles using both soluble salt solutions and sol-gel technology have been studied. In particular, TiO_2 improves the surface cleanability properties and it is widely utilized as a self-cleaning and self-disinfecting material for surface coating in many applications. These properties have been applied in removing bacteria and harmful organic materials from water and air, as well as in self-cleaning or self-sterilizing surfaces for places such as medical centers (C. McCullagh et al., 2007). Overall, TiO_2 is the most widely used material in the field of construction and building materials (F. Bondioli et al., 2013). As well-known, TiO_2 activity is influenced by a variety of factors, such as crystal structure, surface area, nanoparticles size distribution, porosity and a

number and density of hydroxyl groups on the TiO_2 surface (S. Kwon et al., 2008).

Thus, starting from the point that TiO_2 deposition in ceramic tiles, their preparation and characterization is at the base of a new kind of fired tiles able to reduce polluting molecules present in air thanks to its new photocatalytic properties. However, if until today almost all the techniques and procedure involve the use of the classical nanometric TiO_2, a novel approach is the surface deposition of microsized TiO_2 instead of nano.

Indeed, the nanoparticles exhibit potential risks, in particular in terms of dispersability, ecotoxicity and bioaccumulation. Human health danger related to nanopowders of TiO_2 include both inhalation and exposure (V. Vishwakarma et al., 2010), because they leads to various toxic effects, from genotoxicity to diseases such as inflammations or lung diseases, although TiO_2 is chemically inert (E. Bermudez et al., 2004; G. Oberdörster et al., 2005; N. Sharma et al., 2007; C.M. Sayes et al., 2005; B. Trouiller et al., 2009).

The possibility to use microsized TiO_2 in a commercial manufactured product, such as tiles, opens a new generation of building materials intrinsically safer than the traditional photocatalytic products for both workers in the factories and public safety (C.L. Bianchi et al., 2012).

1.6 Aims of the work

The aims of this work are all aiming to achieve a general common goal: the improvement of air quality and the corresponding pollution abatement. Thus, the single objectives can be summarized as follows:

- Building materials development: the target is the pollution abatement in contexts of daily life, thus this research presents the

development and the improvement of TiO_2-based photocatalytic building materials, starting from the choice of a commercial, micrometer, and relative inexpensive powder of TiO_2. Then, specifically, we presents the study about a new technology of TiO_2 deposition of ceramic tiles, i.e. Digital Printing, which leads to many advantages in term of photoactivity and materials performance, money saving and energy consumption. Reference pollutant molecules are NO_x and many different VOCs for outdoor and indoor pollution respectively.

- Real conditions: the most part of TiO_2 photocatalytic building materials have been tested in conditions very far from reality, from the reactors dimension to the concentration levels of pollutants. In this work the TiO_2-photoactive tiles have been tested on large-scale, and new kind of reactors have been presented and described.
- Indoor pollution: indoor environments present two key factors that can not be ignored, they are i) the lighting system, now almost completely achieved by LEDs, which emit light only in the visible wavelengths; ii) the presence of several and different organic molecules simultaneously; thus, we studied in depth the TiO_2 modification in order to make it active under visible light first. Particularly, in this work, a new synthesis by means of high energy US is presented, to produce Ag, Mn, or Cu respectively – decorated TiO_2. Moreover, synthesized samples have been tested through new and non-conventional methods, that provide for the possibility to follow the kinetics of degradation of many organic pollutants simultaneously.

References

Afzal S., Daoud W.A., Langford S. J., "Photostable Self-Cleaning Cotton by a Copper(II) Porphyrin/TiO_2 Visible-Light Photocatalytic System", ACS Appl. Mater. Interfaces, **2013**, 5, 4753−4759.

Allen N.D.C, Brewer P.J., Brown R.J.C., Lipscombe R.P., Woods P.T., "International comparison of key volatile organic components in indoor air", Measurement, **2016**, 82, 476–481.

Almquist C.B., Biswas P., "Role of synthesis method and particle size of nanostructured TiO_2 on its photoactivity", J. Catal., **2002**, 212(2), 145-156.

Arabatzis I. M., Stergiopoulos T., Bernard M. C., Labou D., Neophytides S. G., Falaras P., "Silver-Modified Titanium Dioxide Thin Films for Efficient Photodegradation of Methyl Orange", Appl. Catal., B, **2003**, 42, 187−201.

Archana M., Pratima C., Amita M., Abhay K. P., "Surface Functionalization of TiO_2 with Plant Extracts and their Combined Antimicrobial Activities Against E. faecalis and E. Coli", J. Res. Updates Polymer Sci., **2012**, 1, 43-51.

Asahi R., Morikawa T., Ohwaki T., Aoki K., Taga Y., "Visible- Light Photocatalysis in Nitrogen-Doped Titanium Oxides", Science, **2001**, 293, 269−271.

Bermudez E., Mangum J., Wong B., Asgharian B., Hext P., Warheit D., "Pulmonary responses of mice, rats, and hamsters to subchronic inhalation of ultrafine titanium dioxide particles", Toxicol. Sci., **2004**, 77, 347–357.

Beska R.R., Kiwi J., App. Catal. B: Environ., **1998**, 16, 19.

Bianchi C.L., Pirola C., Gatto S., Nucci S., Minguzzi A., Cerrato G., Biella S., Capucci V., "New Surface Properties in Porcelain Gres Tiles with a Look to Human and Environmental Safety", Adv. Mater. Sci. Eng., **2012**, 2012, 1-8.

Bianchi C.L., Pirola C., Gatto S., Nucci S., Capucci V., "Porcelain gres tiles with photocatalytic properties for a better environment", 7th International Conference on Environmental Catalysis, **2012**.

Bickley R.I., Gonzalez-Carreno T., Lees J.S., Palmisano L., Tilley R.J.D., "A structural investigation of titanium dioxide photocatalysts", J. Solid State Chem., **1991**, 92(1), 178-190.

Bondioli F., De Niederhãusern S., Bondi M., "Self-Cleaning and Antibacteric Ceramic Tile Surface", Int. J. App. Ceramic Technol., **2013**, 10(6), 949–956.

Bondioli F., Taurino R., Ferrari A.M., "Functionalization of Ceramic Tile Surface by Sol-Gel Technique", J. Colloid Interface Sci., **2009**, 334(2), 195–201.

Casasola R., Rinco´n J. M., Romero M., "Glass-ceramic glazes for ceramic tiles: a review", J. Mater. Sci., **2012**, 47(2), 553–582.

Castellote M., Bengtsson N., Chapter 2: "Principles of TiO_2 Photocatalysis, in the book Application of titanium dioxide photocatalysis to construction materials, State-of-the-art", Report of the RILEM Technical Committee, Ohama Y., Van Gemert D., **2011**, XII, 48pp – retrieved from http://www.springer.com/978-94-007-1296-6.

Chandrasekharan N., Kamat P. V., "Improving the Photo- electrochemical Performance of Nanostructured TiO_2 Films by Adsorption of Gold Nanoparticles", J. Phys. Chem. B, **2000**, 104, 10851−10857.

Chen A., Cao Q., Zhou J., Yang B., Chang V.W.C., Nazaroff W.W., "Indoor and outdoor particles in an air-conditioned building during and after the 2013 haze in Singapore", Build. Environ., **2016**, 99, 73-81.
Chi C., Chen W., Guo M., Weng M., Yan G., Shen X., "Law and features of TVOC and Formaldehyde pollution in urban indoor air", Atmos. Environ., **2016**, 132, 85-90.
Cho Y., Choi W., Lee C.H., Hyeon T., Lee H.I., "Visible Light-Induced Degradation of Carbon Tetrachloride on Dye-Sensitized TiO_2", Environ. Sci. Technol., **2001**, 35, 966−970.
Craig S., Turchi D., Ollis F., "Photocatalytic Degradation of Organic Water Contaminants: Mechanisms Involving Hydroxyl Radical Attack", J. Catal., **1990**, 122, 178-192.
Dawson A., Kamat P. V., "Semiconductor−Metal Nano- composites. Photoinduced Fusion and Photocatalysis of Gold-Capped TiO_2 (TiO_2/Gold) Nanoparticles", J. Phys. Chem. B, **2001**, 105, 960− 966.
Demeestere K., Dewolf J., Van Langenhove H., "Heterogeneous photocatalysis as an advanced oxidation process for the abatement of chlorinated, monocyclic aromatic and sulfurous volatile organic compounds in air: State of the art", Crit. Rev. Env. Sci. Technol., **2007**, 37(6), 489-538.
De Niederhausern S., Bondi M., "Self-Cleaning and Antibacteric Ceramic Tile Surface", Int. J. Appl. Ceram. Technol., **2013**, 10(6), 949–956.
Devi L. G., Kumar S. G., "Exploring the Critical Dependence of Adsorption of Various Dyes on the Degradation Rate Using Ln^{3+}−TiO_2 Surface under UV/Solar Light", Appl. Surf. Sci., **2012**, 261, 137− 146.
Diamanti M. V., Ormellese M., Pedeferri M., "Characterization of Photocatalytic and Superhydrophilic Properties of Mortars Containing Titanium Dioxide", Cem. Concr. Res., **2008**, 38(11), 1349–1353.
Di Paola A., Bellardita M., Palmisano L., "Brookite, the Least Known TiO_2 Photocatalyst", Catalysts, **2013**, 3, 36-73.
Di Paola A., Bellardita M., Ceccato R., Palmisano L., Parrino F., "Highly active photocatalytic TiO_2 powders obtained by thermohydrolysis of $TiCl_4$ in water", J. Phys. Chem. C, **2009**, 113, 15166–15174.
DiPaola A., García-Lopez E., Ikeda S., Marcí G., Ohtani B., Palmisano L., "Photocatalytic Degradation of Organic Compounds in Aqueous Systems by Transition Metal Doped Polycrystalline TiO2", Catal. Today, **2002**, 75, 87−93.
Di Valentin C., Finazzi E., Pacchioni G., Selloni A., Livraghi S., Paganini M.C., Giamello E., "N-dopedTiO2:Theoryand Experiment", Chem. Phys., **2007**, 339, 44−56.
Di Valentin C., Pacchioni G., Selloni A., Livraghi S., Giamello E., "Characterization of Paramagnetic Species in N-Doped TiO_2 Powders by EPR Spectroscopy and DFT Calculations", J. Phys. Chem. B, **2005**, 109, 11414−11419.
Dozzi M. V., Selli E., "Doping TiO_2 with p-Block Elements: Effects on Photocatalytic Activity", J. Photochem. Photobiol. C, **2013**, 14, 13−28.
Dorfman L. M. and Adams G. E., "Reactivity of the Hydroxyl Radical", National Bureau of Standards, Report No. NSRDS-NBS-46, **1973**.

Dung D., Ramsden J., Grätzel M., "Dynamics of interfacial electron-transfer processes in colloidal semiconductor systems", J. Am. Chem. Soc., **1982**, 104, 2977–2985.
Etacheri V., Michlits G., Seery M. K., Hinder S. J., Pillai S. C., "A Highly Efficient TiO_2−xCx Nano-heterojunction Photocatalyst for Visible Light Induced Antibacterial Applications", ACS Appl. Mater. Interfaces, **2013**, 5, 1663−1672.
Etacheri V., Seery M. K., Hinder S. J., Pillai S. C., "Highly Visible Light Active TiO_2−xNx Heterojunction Photocatalysts", Chem. Mater., **2010**, 22, 3843−3853.
Etacheri V., Seery M. K., Hinder S. J., Pillai S. C., "Nanostructured Ti1−xSxO_2−yNy Heterojunctions for Efficient Visible- Light-Induced Photocatalysis", Inorg. Chem., **2012**, 51, 7164−7173.
Forbes P.B.C., Garland R.M., "Outdoor air pollution", Comp. Anal. Chem., **2016**, 73, doi:10.1016/bs.coac.2016.02.004.
Fujishima A., Hashimoto K., Watanabe T., "TiO_2 Photocatalysis: Fundamentals and Applications", **1999**, (BKC, Tokyo).
Fujishima A., Honda K., "Electrochemical Photolysis of Water at a Semiconductor Electrode", Nature, **1972**, 238, 37-38.
Fujishima A., Rao T.N., Tryk D.A., "Titanium dioxide photocatalysis", J. Photochem. Photobiol. C, **2000**, 1, 1-21.
Glaze W.H., Kang J.W., Chapin D.H. "The Chemistry of Water Treatment Processes Involving Ozone, Hydrogen Peroxide, and Ultraviolet Radiation", Ozone Sci. Eng., **1987**,9, 335-352.
Gole J. L., Stout J. D., Burda C., Lou Y., Chen X., "Highly Efficient Formation of Visible Light Tunable TiO_2−xNx Photocatalysts and Their Transformation at the Nanoscale", J. Phys. Chem. B, **2003**, 108, 1230−1240.
Graetzel M., "Photoelectrochemical cells", Nature, **2001**, 414, 338-344.
Grätzel M., Rotzinger F.P., "The influence of the crystal lattice structure on the conduction band energy of oxides of titanium(IV)", Chem. Phys. Lett., **1985**, 118, 474–477.
Hagfeldt A., Gratzel M., "Light-induced redox reactions in nanocrystalline systems", Chem. Rev., **1995**, 95, 49-68.
Han C., Pelaez M., Likodimos V., Kontos A. G., Falaras P., O'Shea K., Dionysiou D. D., "Innovative Visible Light-Activated Sulfur Doped TiO_2 Films for Water Treatment", Appl. Catal. B, **2011**, 107, 77−87.
Herrmann J.M., "Heterogeneous photocatalysis: state of the art and present applications", Top. Catal., **2005**, 34, 49-65.
Hoffmann M.R., Martin S.T., Choi W., Bahnemann D.W., "Environmental Applications of Semiconductor Photocatalysis", Chem. ReV., **1995**, 95, 69-96.
Inturi S. N. R., Boningari T., Suidan M., Smirniotis P. G., "Visible-Light-Induced Photodegradation of Gas Phase Acetonitrile Using Aerosol-Made Transition Metal (V, Cr, Fe, Co, Mn, Mo, Ni, Cu, Y, Ce, and Zr) Doped TiO_2", Appl. Catal. B, **2014**, 144, 333−342.
Jantuneri M., Oliveira F.E., Carrer P., Kephalopoulos S., "Promoting action for healthy indoor air (IAIAQ)", European commission directorate general for health and consumers, **2011**, Luxembourg, 52p.

Jiang J., Zhang J., Zhang Y., Zhang C., Tian G., "Estimating nitrogen oxides emissions at city scale in China with a nightlight remote sensing model", Sci. Total Environ., **2016**, 544, 1119–1127.
Kabra K., Chaudhary R., Sawhney R.L., "Treatment of hazardous organic and inorganic compounds through aqueous-phase photocatalysis: a review", Ind. Eng. Chem. Res., **2004**, 43, 7683-7696.
Katsanaki A. V., Kontos A. G., Maggos T., Pelaez M., Likodimos V., Pavlatou E. A., Dionysiou D. D., Falaras P., "Photocatalytic Oxidation of Nitrogen Oxides on N-F-Doped Titania Thin Films", Appl. Catal. B, **2013**, 140, 619–625.
Kawai T., Sakata T., "Hydrogen evolution from water using solid carbon and light energy", Nature, **1979**, 282, 283-284.
Khan S. U. M., Al-Shahry M., Ingler W. B., "Efficient Photochemical Water Splitting by a Chemically Modified n-TiO_2", Science, **2002**, 297, 2243–2245.
Kim Y.I., Atherton S.J., Brigham E.S., Mallouk T.E., "Sensitized layered metal oxide semiconductor particles for photochemical hydrogen evolution from nonsacrificial electron donors", J. Phys. Chem., **1993**, 97, 11802–11810.
Kirk-othmer, "Encyclopedia of chemical technology, titanium compounds, inorganic", in Wiley, **2000**,1-58.
Klepeis N.E., Nelson W.C., R.O Wayne, Robinson J.P., Tsang A.M., Switzer P., Behar J.V., Hern S.C., Engelmann W.H., "A Resource for Assessing Exposure to Environmental Pollutants", The National Human Activity Pattern Survey (NHAPS).
Kondarides D.I., "Photocatalysis", in Catalysis, ed. Gabriele Centi.
Kwon, S., Fan M., Cooper A.T., Yang H., "Photocatalytic applications of micro- and nano-TiO_2 in environmental engineering", Crit. Rev. Env. Sci. Tec., **2008**, 38, 197-226.
Landmann M., Rauls, E., Schmidt W.G., "The electronic structure and optical response of rutile, anatase and brookite TiO_2", J. Phys., **2012**, 24(19).
Li X., Liu L., Kang S.Z., Mu J., Li G., "Differences Between Zn- Porphyrin-Coupled Titanate Nanotubes with Various Anchoring Modes: Thermostability, Spectroscopic, Photocatalytic and Photo- electronic Properties", Appl. Surf. Sci., **2011**, 257, 5950–5956.
Linsebigler A.L., Lu G., Yates Jr. J.T., "Photocatalysis on TiO_2 surfaces — Principles, mechanisms, and selected results", Chem. Rev., **1995**, 95, 735–758.
Liu G., Han C., Pelaez M., Zhu D., Liao S., Likodimos V., Kontos A. G., Falaras P., Dionysiou D. D., "Enhanced Visible Light Photocatalytic Activity of C-N-Codoped TiO_2Films for the Degradation of Microcystin-LR", J. Mol. Catal. A: Chem., **2013**, 372, 58–65.
Liu B., Khare A., Aydil E. S., "TiO_2–B/Anatase Core–Shell Heterojunction Nanowires for Photocatalysis", ACS Appl. Mater. Interfaces, **2011**, 3, 4444–4450.
Liu G., Zhao Y., Sun C., Li F., Lu G. Q., Cheng H.M., "Synergistic Effects of B/N Doping on the Visible-Light Photocatalytic Activity of Mesoporous TiO_2", Angew. Chem., Int. Ed. **2008**, 47, 4516– 4520.
Logue J.M., McKone T.E., Sherman M.H., "Hazard assessment of chemical air contaminants measured in residences", Indoor Air, **2011**,21(2), 92-109.

Lu C., Deng Q., Li Y., Sundell J., Norbäck D., "Outdoor air pollution, meteorological conditions and indoor factors in dwellings in relation to sick building syndrome (SBS) among adults in China", Sci. Total Environ., **2016**, 560–561, 186–196.
Maira, A.J., Yeung, K.L., Lee, C.Y., Yeu, P.L. and Chan, C.K., "Size effects in gas-phase photo-oxidation of trichloroethylene using nanometer-sized TiO_2 catalysts", J. Catal., **2000**, 192(1), 185-196.
Marbury M., Krieger R., in Samet R., Sprengler J., Indoor air pollution, The Johns Hopkins University press, Baltimore, **1991**, pp. 223-251.
María D.B., Elena D.A., Antonio G., Francisco J.C., Julio S., "Environmental performance of ceramic tiles: Improvement proposals Materials and Design", **2010**, 31(2010), pp. 35–41.
McCullagh C., Robertson J. M. C., Bahnemann D. W., Robertson P. K.J ., "The application of TiO_2 photocatalysis for disinfection of water contaminated with pathogenic micro-organisms: A review", Res. Chem. Intermediat., **2007**, 3, 359–375.
Millis A., Le Hunte S.J., "An Review of Semiconductor Photocatalysis", Photochem. Photobiol. A, **1997**, 108, 1-35.
Nolan N. T., Seery M. K., Hinder S. J., Healy L. F., Pillai S. C., "A Systematic Study of the Effect of Silver on the Chelation of Formic Acid to a Titanium Precursor and the Resulting Effect on the Anatase to Rutile Transformation of TiO_2", J. Phys. Chem. C, **2010**, 114, 13026−13034.
Nolan N. T., Synnott D. W., Seery M. K., Hinder S. J., Van Wassenhoven A., Pillai S. C., "Effect of N-Doping on the Photo- catalytic Activity of Sol-Gel TiO_2", J. Hazard. Mater., **2012**, 211, 88−94.
Oberdörster G., Oberdörster E., Oberdörster J., "Nanotoxicology: an emerging discipline evolving from studies of ultrafine particles", Env. Health Pers., **2005**, 113(7), 823-839.
Oller I., Malato S., Sanchez-Perez J.A., "Combination of advanced oxidation processes and biological treatments for wastewater decontamination: a review", Sci. Tot. Environ., **2011**, 409, 4141-4166.
Pauling L., Sturdivant J.H., "The crystal structure of brookite", Z. Kristall., **1928**, 68, 239–256.
Pelaez M., Baruwati B., Varma R. S., Luque R., Dionysiou D. D., "Microcystin-LR Removal from Aqueous Solutions Using a Magnetically Separable N-Doped TiO_2 Nanocomposite under Visible Light Irradiation", Chem. Commun., **2013**, 49, 10118−10120.
Periyat P., Pillai S. C., McCormack D. E., Colreavy J., Hinder S. J., "Improved High-Temperature Stability and Sun-Light-Driven Photocatalytic Activity of Sulfur-Doped Anatase TiO_2", J. Phys. Chem. C, **2008**, 112, 7644−7652.
Pfaff G., Reynders P., "Angle-Dependent Optical Effects Deriving from Submicron Structures of Films and Pigments", P. Chem. Rev., **1999**, 99, 1963.
Qi B., Yu Y., He X., Wu L., Duan X., Zhi J., "Series of Transition Metal-Doped TiO_2 Transparent Aqueous Sols with Visible-Light Response", Mater. Chem. Phys., **2012**, 135, 549−553.

Quagliarini E., Bondioli F., Goffredo G. B., Licciulli A., Munafo P.,"Smart Surfaces for Architectural Heritage: Preliminary Results About the Application of TiO_2-Based Coatings on Travertine", J. Cult. Herit., **2012**, 13(2), 204–209.
Robertson P.K.J., Bahnemann D.W., Robertson J.M.C., Wood F., "Photocatalytic detoxification of water and air", Handbook of Environmental Chemistry (**2005**), Vol. 2, Part M, 367-423. Publisher: Springer, Berlin, Germany.
Sato S., White J.M., "Photodecomposition of water over Pt/TiO_2 catalyst", Chem. Phys. Lett., **1980**, 72, 83-86.
Sayes C.M., Gobin A.M., Ausman K.D., Mendez J., West J.L., Colvin V.L., "Nano-C60 cytotoxicity is due to lipid peroxidation", **2005**, Biomater., 26(36), 7587-7595.
Schiavello M., "Heterogeneous photocatalysis", Wiley Series in Photoscience and Photoengineering, **1997**, Vol. 3. John Wiley & Sons Ltd.
Seery M. K., George R., Floris P., Pillai S. C., "Silver Doped Titanium Dioxide Nanomaterials for Enhanced Visible Light Photo- catalysis", J. Photochem. Photobiol. A, **2007**, 189, 258−26.
Serpone N., "Is the Band Gap of Pristine TiO_2 Narrowed by Anion- and Cation-Doping of Titanium Dioxide in Second-Generation Photocatalysts?", J. Phys. Chem. B, **2006**, 110, 24287−24293.
Serpone N., Lawless D., Disdier J., Herrmann J.M., "Spectroscopic, Photoconductivity, and Photocatalytic Studies of TiO_2 Colloids: Naked and with the Lattice Doped with Cr^{3+}, Fe^{3+}, and V^{5+} Cations", Langmuir, **1994**, 10, 643−652.
Serpone M., Pelizzetti E., "Photocatalysis: Fundamentals and applications", John Wiley & Sons, Inc.
Sharma N., Kalra K.L., Oberoi H.S., Bansal S., "Optimization of fermentation parameters for production of ethanol from kinnow waste and banana peels by simultaneous saccharification and fermentation", Indian J. Microb., **2007**, 47(4), 310-316.
Short S., "The issues and implications of setting and applying indoor air quality guidelines", IEH Institute for Environmental & Health.
Szczepankiewicz S. H., Colussi A. J., Hoffmann M. R. J., Phys. Chem. B, **2000**, 104, 9842.
Trouiller A., Reliene R., Westbrook A., Solaimani P., Schiestl R.H., "Titanium dioxide nanoparticles induce DNA damage and genetic instability in vivo in mice," Cancer Res., **2009**, 69(22), 8784–8789.
Tryk D.A., Fujishima A., Honda K., "Recent topics in photoelectrochemistry: achievements and future prospects", Electrochim. Acta, **2000**, 45, 2363-2376.
Umebayashi T., Yamaki T., Tanaka S., Asai K., "Visible Light- Induced Degradation of Methylene Blue on S-doped TiO_2", Chem. Lett., **2003**, 32, 330−331.
Viegi G., Simoni M., Scognamiglio A., "Indoor air pollution and airway disease", Int J. Tuberc Lug Dis, **2004**, 8, 1401-15.
Vishwakarma V., Samal S.S., Manoharan N., "Safety and Risk Associated with Nanoparticles: A Review", J. Min. Mater. Char. Eng., **2010**, 9(5), 455-459.

Wang Y., Liu L., Xu L., Meng C., Zhu W., "Ag/TiO_2 Nanofiber Heterostructures: Highly Enhanced Photocatalysts under Visible Light", J. Appl. Phys., **2013**, 113, 174311.
WHO, "Ambient (outdoor) air quality and health", retrieved from http://www.who.int/mediacentre/factsheets/fs313/en.
WHO, Global Urban Ambient Air Pollution Database, **2016**.
WHO, "Guidelines for indoor air quality: selected pollutants", **2016**.
WHO, " Indoor air pollution: National burden of disease estimates", **2007**.
Wu S.H., Wu J.L., Jia S.Y., Chang Q.W., Ren H.T., Liu Y., "Cobalt(II) Phthalocyanine-Sensitized Hollow Fe_3O_4@SiO_2@TiO_2 Hierarchical Nanostructures: Fabrication and Enhanced Photocatalytic Properties", Appl. Surf. Sci., **2013**, 287, 389−396.
Xiao F.X., "Construction of Highly Ordered ZnO−TiO_2 Nanotube Arrays (ZnO/TNTs) Heterostructure for Photocatalytic Application", ACS Appl. Mater. Interfaces, **2012**, 4, 7055−7063.
Xu J., Ao Y., Fu D., Yuan C., "A Simple Route for the Preparation of Eu, N-Codoped TiO_2 Nanoparticles with Enhanced Visible Light-Induced Photocatalytic Activity", J. Colloid Interface Sci., **2008**, 328, 447−451.
Xu J.H., Li J., Dai W.L., Cao Y., Li H., Fan K., "Simple Fabrication of Twist-Like Helix N,S-Codoped Titania Photocatalyst with Visible-Light Response", Appl. Catal. B, **2008**, 79, 72−80.
Yuan S.A., Chen W.H., Hu S.S., "Fabrication of TiO_2 nanoparticles/surfactant polymer complex film on glassy carbon electrode and its application to sensing trace dopamine", Mater. Sci. Eng. C, **2005**, 25, 479-485.
Zhao X. J., "Development of Multifunctional Photoactive Self- Cleaning Glasses," J. Non-Cryst. Solids, **2008**, 354(12–13), 1424–1430.
Zhang Z., Wang C.C., Zakaria R., Ying J.Y., "Role of Particle Size in Nanocrystalline TiO_2-Based Photocatalysts", J. Phys. Chem. B, **1998**, 102(52), 10871–10878.

CHAPTER 2:
GENERAL EXPERIMENTAL PART

2.1 Catalysts

Among different commercial TiO_2 powders and after some previous tests, performed in preceding works, P25 and 1077 by Kronos have been selected as basic references, nanometric and micrometric respectively.
Afterwards, samples prepared starting from 1077 modified with metal atoms will be presented and deeply described.
Finally, samples obtained from 1077 deposition on grés ceramic tiles are explained in this section.

2.1.1 Commercial TiO_2 powders

During the three years of Ph.D. the commercial catalysts studied, tested and evaluated were different. However, it was decided to focus attention only on one nanometric powder as reference, i.e. P25, and one pigmentary and micrometer, i.e. 1077 by Kronos. In general, the main target to choose the commercial samples was based on their crystallographic phase composition and particles size average distribution.

2.1.1.1 P25

In the field of photocatalysis, P25 (Degussa) is the standard material. It is well-known that anatase particles with a large surface area are efficient for the decomposition of pollutants in air and water (M.V. Rao et al., 1980; S. Nishimoto et al., 1985). However, P25 consists in both anatase and rutile phases: Bickley et al. (R.I. Bickely et al., 1991) published the first work with a correlation between its photoactivity and structure. Shortly after Datye et al. (A.K. Datye et al., 1995) showed that

anatase and rutile single crystalline particles exist separately in P25 powder. The presence of both anatase and rutile phases can be crucial for some photocatalytic reactions; indeed pure-phase rutile is inactive because of the rapid rates of e^-/h^+ recombination, while, in mixed-phase TiO_2, charges produces on rutile are stabilized through electron transfer to lower energy anatase lattice trapping sites (A.G. Agrios et al., 2003).
P25 powder is manufactured by the Aerosil process, by which Titanium tetrachloride ($TiCl_4$) is hydrolyzed in vapor phase at high temperature (R.I. Bickely et al., 1991). In particular, it is shown that anatase and rutile particles grow on different nuclei (T. Ohno et al., 2001).

P25 summarized physical features are presented in table 2.1:

Name	Anatase:rutile	Average crystallite size (nm)	SSA (m^2/g)	XPS	Band gap (eV)
P25	75:25	26	50	Ti(IV)	3.21

Table 2.1: summary of the main features of P25 (C.L. Bianchi et al., 2014)

Characterization analysis conducted on P25 commercial TiO_2 powder show the following results. P25 exhibits the well-known phase composition 75:25 in anatase/rutile ratio that is indicated particularly by the XRD spectrum (Fig. 2.1). The main diffraction peak at about 2θ = 25.5° related to the planes (101) has been employed to calculate the average crystallite sizes (Table 2.1, third column) (C.L. Bianchi et al., 2014).

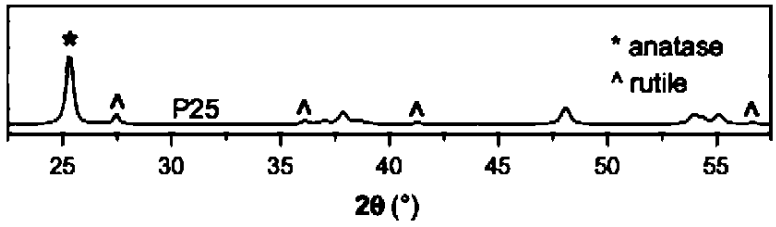

Fig. 2.1: XRD patter of P25

As expected, P25 is a nano-sized powder, being the crystallite size lower than 30 nm, and it is made up of well-crystallized particles of rather roundish shape, closely packed and with an average size of 20–30 nm. Particularly, by TEM images (see Fig. 2.2), it can be evidenced that the most exposed crystal planes belong to the (101) family of the anatase polymorph (ICDD Anatase file No. 21-1272).

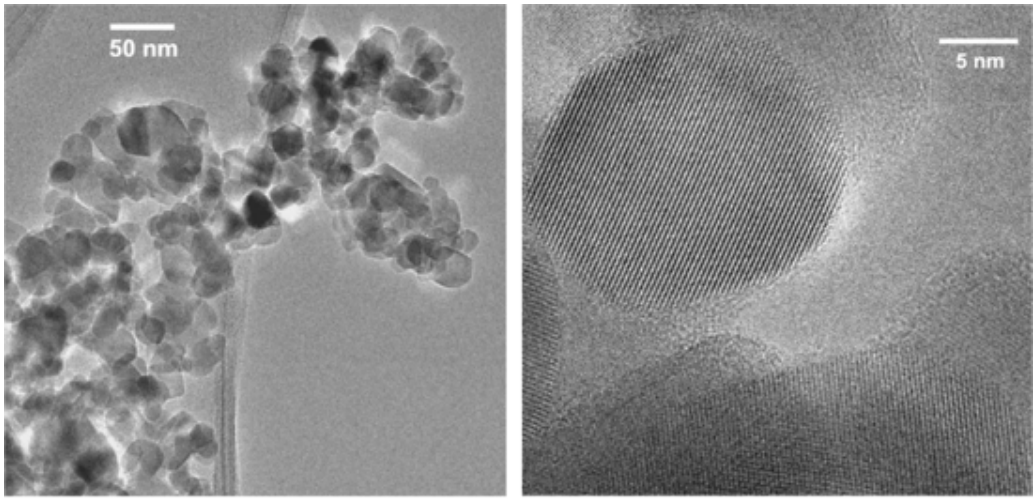

Fig. 2.2: TEM images of the reference P25 at different magnifications.

The surface states of the TiO_2 particles were analyzed by XPS. The peak of Ti $2p_{3/2}$ is regular and the BE at about 458.5 ± 0.1 eV compares well with the data for Ti(IV) in TiO_2 materials (G. Cappelletti et al., 2006). Diffuse reflectance UV–Vis spectra were collected on a UV-Vis scanning spectrophotometer and data were elaborated using the Kubelka-Munk function reported below (G. Kortüm, 1969).

$$F(R) = (1-R)^2 / 2R \qquad \text{eq. 2.1}$$

R is the reflactance of the powder. Then, the band-gap values (reported in sixth column of table 2.1) was determined by performing the first derivative of the Kubalka-Munk function:

$$dF(R) / d\lambda \qquad \text{eq. 2.2}$$

where λ is the wavelenght of the incident radiation.

Figure 2.3 reports the FTIR spectrum of P25. The material exhibits two complex absorption bands, respectively located in the 3000–3450 cm^{-1} range and at $\nu \geq 3600$ cm^{-1}. On the basis of the spectral behavior and of literature data (C.L. Bianchi et al. 2014), the former envelope can be ascribed to the stretching mode of all H-bonded OH groups present at the surface of the various solids, whereas the latter corresponds to the stretching mode of all Ti–OH species free from hydrogen bonding interactions (L.H. Little et al., 1966; C. Morterra et al., 1988; C. Morterra et al., 1989; A.L. Linsebigler et al. 1995).

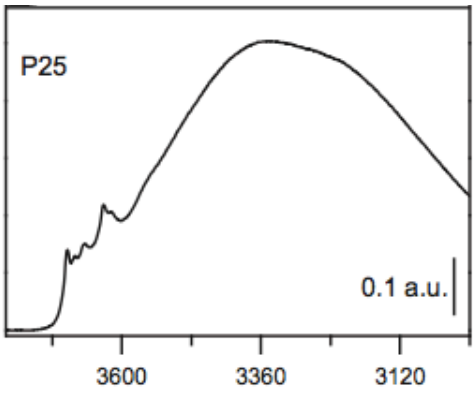

Fig. 2.3: FT-IR spectra of P25 sample in air

2.1.1.2 1077 by Kronos

1077 is a pigmentary powder of TiO_2 produced by Kronos Company. The main and typical structural feature that makes it more interesting than others commercial TiO_2, is that it consist completely of anatase, as presented and well described through the characterization analysis.
The synthesis route presented in literature in order to prepare TiO_2 lead to nano-powders, because of the higher photocatalytic efficiency (S.M. Gupta et al., 2012; X. Wang et al., 2009; D.P. Macwan et al., 2011). As already mentioned in the introduction section, this run does not take into account the possibility that nano-sized materials could be dangerous for the human health. Thus, a very important point is if it is necessary the use of nano-sized particles in an exclusive way.
Among the commercial titania-based pigmentary products having some specific features, 1077 pure anatase polymorph consists of particle size over 100 nm (micro-sized), it is devoid of ultrafine particles, it is not subject to specific post-treatments to stabilize it after the preparation, and it is dopants-free (C.L. Bianchi et al., 2014).

1077 sample physical features are presented below:

Name	**Anatase:rutile**	**Average crystallite size (nm)**	**SSA (m^2/g)**	**XPS**	**Band gap (eV)**
1077	Anatase	130	12	Ti(IV)	3.15

Table 2.2: summary of the main features of 1077 (C.L. Bianchi et al., 2014)

Anatase is the unique polymorph (Fig. 2.4) and the crystallographic reflex (101) has been employed to calculate the average crystallites size and the sample 1077 is characterized by a value of 130 nm, as reported in table 2.2 (third column). This structure reflects in the BET surface

area, which is much lower compared to the nano-sized P25 presented in the previous paragraph.

The morphological feature exhibited by the micro-size TiO_2 was investigated by TEM (Fig. 2.5), which confirms the above average crystallites size extrapolated by XRD analysis also excluding the presence of ultrafine particles.

The surface state of the TiO_2 particles was analyzed by XPS (see fig. 2.7, which presents a comparison between P25 and 1077). The survey shows traces of K for 1077 (3.3 at%) due to the starting reactants of the industrial process. However, no significant differences can be appreciated in the Ti 2p region concerning the binding energies (BE) and the full width at half-maximum (FWHM) values. The peak Ti $2p_{3/2}$ is always regular and the BE compares well with the data for Ti(IV) in TiO_2 materials (G. Cappelletti et al., 2006). The analysis of the oxygen peaks exhibits the presence of more than one component, which can be attributed to lattice oxygen in TiO_2 (529.9 eV) and to surface OH species (>531.5 eV) respectively (S. Ardizzone et al., 2007).

Starting from the XPS analysis, it is possible to evaluate the OH/O_{tot} surface ratio, which refers to a quantitative measure of the hydrophilicity/hydrophobicity of the TiO_2 surface (A. Naldoni et al., 2013). The micro-sized 1077 sample presents a higher atomic concentration of OH groups in comparison with P25, pointing out a higher hydrophilic character of their surface. This feature is very important, because the hydrophilicity/hydrophobicity character of photocatalysts surface plays a crucial role in determining the adsorption step and thus the photocatalytic activity (S. Ardizzone etal., 2008; A. Naldoni et al., 2013).

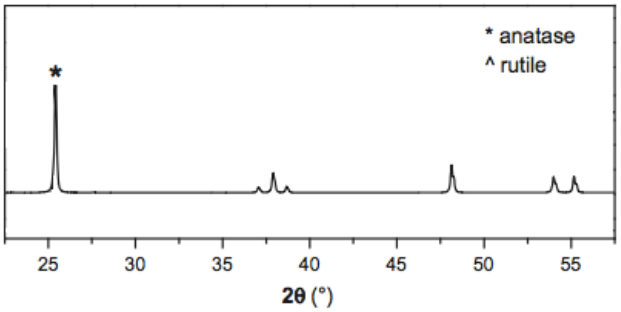

Fig. 2.4: XRD pattern of 1077 by Kronos.

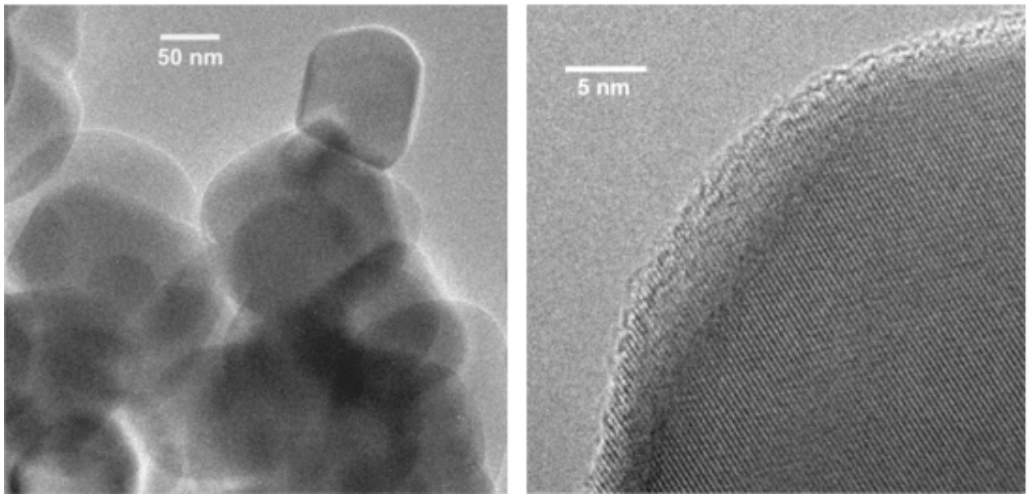

Fig. 2.5: TEM images of 1077 at different magnifications.

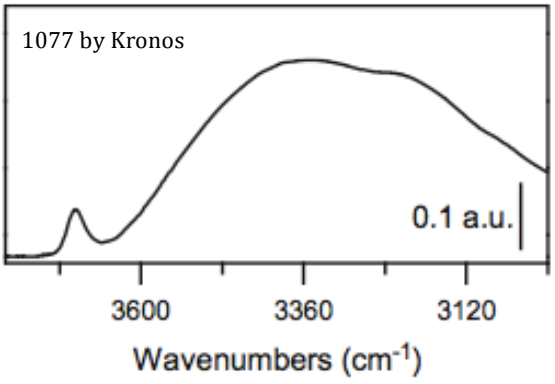

Fig. 2.6: FT-IR spectra of 1077 sample in air.

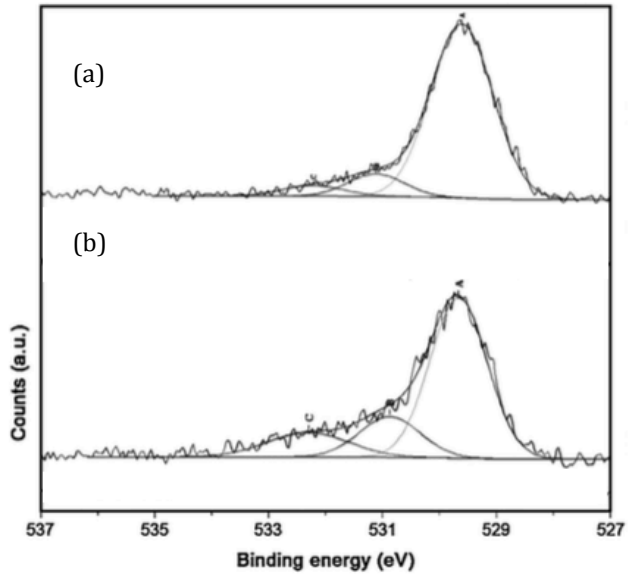

Fig 2.7: O1s XPS spectra for a) p25 and b) 1077.

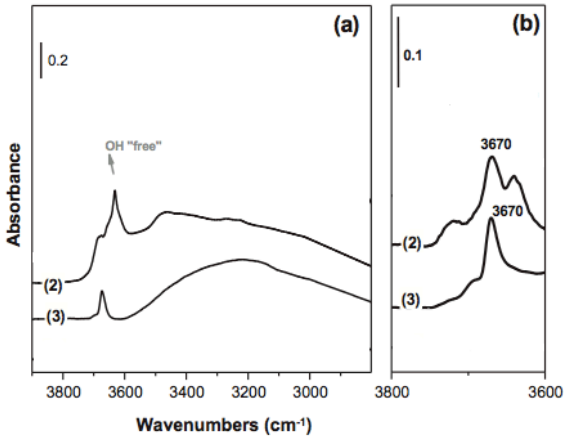

Fig. 2.8: Absorbance IR spectra, mass-normalized to the weight of the heaviest sample, relative to the O-H stretching spectral region of samples outgassed at RT for 60 min (section a) and activated (in presence of O2) at 300°C for 60 min (section b): P25 (2); 1077 (3).

The study of the surface OH species has been performed by means of in situ FTIR spectroscopy. Section (a) of Fig. 2.8 reports the spectra of P25

and 1077 respectively, after prolonged outgassing at room temperature (RT). Both materials exhibit two complex absorption bands, respectively located in the 3000–3450 cm^{-1} range and at $\nu \geq 3600$ cm^{-1}.

On the basis of literature data, the first envelope can be ascribed to the ν_{OH} of all H-bonded OH groups present at the surface of the solid (L.H. Little et al., 1966; C. Morterra, 1988; C. Morterra et al., 1989). Then, to identify the different spectral components present at higher ν, all samples have been activated at 300°C (fig. 2.8, section b). This thermal treatment is able to remove the interference between the ν_{OH} signals of adsorbed water and the surface OH groups, as it should only remove the signals of adsorbed water leaving virtually unchanged the distribution of surface "free" OH species (M. Minella et al., 2010).

The bands observed at $\nu \geq 3680$ cm^{-1} can be ascribed to linear (terminal) Ti-OH species, whereas the bands at lower frequencies can be related to Ti-OH-Ti bridged species.

Comparing nano and micro-sized spectra, it is possible to see that P25 is characterized by a higher amount of terminal Ti-OH species, even if 1077 presents a rather intense peak that can explain better its photoactivity.

2.1.2 Decorated-TiO_2 samples: synthesis by means of high energy US

The surface deposition of metal or metal oxide nano-particles (NPs) modifies the TiO_2 surface makes it active even to the visible wavelengths. Metals species enhance the electron transfer or the charge separation and improve the formation of the free hydroxyl radicals. (H. Park et al., 2013; D.M. Tobaldi et al., 2013).

The principle on which this effect is based is that the free electrons in the metal particles can be excited by light and in this way metals act as an

electron sink promoting in particular the charge separation. Decoration of M- or MO-NPs is commonly implemented by means of ultra-sounds (US) in aqueous or organic solutions where ceramics or polymer substrate powders are dispersed (A. Gedanken et al., 2007). Thus, in this work we applied the same method using 1077 by Kronos as substrate, depositing on its surface different metal species.
First samples that will be presented are prepared with tungsten, rhenium, molybdenum and copper respectively (M. Stucchi et al., 2015).
The sono-chemical method described here has been already used by Sakkas et.al, for the decoration of anode materials for Solid Oxide Fuel Cells (SOFC) (P.M. Sakkas et al. 2014).

2.1.2.1 First group: Molybdenum, Tungsten, and Rhenium modified-TiO_2

For the sonochemical method, the precursor materials are purchased and used without supplementary purification. A Bandelin SONOPLUS HD 3200 utilizing a 200W U/S generator and a sonication extension horn of 13mm diameter has been used to obtain sonication.
Precursor molecules are reported in table 2.3.

$Mo(CO)_6$	**≥99,9% Sigma Aldrich**
$Re_2(CO)_{10}$	98% Aldrich
$W(CO)_6$	99,99% Sigma Aldrich

Table 2.3: Precursor molecules used for US deposition on TiO_2.

0.25 g of the selected precursor molecule and 1 or 2 g (depending of the metal species with which is decorated) of 1077 by Kronos have been mixed together in a 100 ml glass flask, using diphenylmethane as

solvent (100 ml). The solution is then sonicated at constant temperature of 80°C for 3 hours, setting US at 33.0% amplitude and 50 Wcm^{-2} intensity. And the end of the US application, the solution has been centrifuged many times to remove solvent. Then, it has been washed by n-pentane, for the first three washings, centrifuged again, and finally re-washed with pentane.
Samples have been dried at 100°C over night, and conclusively calcined at 480°C for 40 h to completely remove the organic scents.
Three TiO_2 decorated powders have been obtained, and they are listed in the table 2.4, reported below.

Sample name	**Precursor molecules**	**Average metal percentage ($\%_{w/w}$) content**
TiO_2_Mo$_{(US)}$	1077 + $Mo(CO)_6$	10-12$\%_{w/w}$
TiO_2_W$_{(US)}$	1077 + $W(CO)_6$	10-12$\%_{w/w}$
TiO_2_Re$_{(US)}$	1077 + $Re_2(CO)_{10}$	20-25$\%_{w/w}$

Table 2.4: TiO_2-decorated samples by means of US – first group.

2.1.2.2 Second group: copper-modified TiO_2

The study of copper ions is recently further developed because, comparing it with other metals, such as silver or gold, it is firstly cheaper and rather abundant (L.F. Chiang et al., 2014). Moreover, it has been proved that Cu, as other metallic species, decreases the electron-hole recombination and improves the photocatalytic activity of TiO_2 (B. Xina et al., 2008). This property does not only concern copper in its metal form, but also in the Cu(I) and Cu(II) species (including Cu_2O and CuO), which can serve as electron mediator extending the adsorption to the long wavelength region. This happens specifically because of the

formation of a heterojunction between copper and TiO_2, able to promote the charge separation (L.F. Chiang et al., 2014).

The precursor compound for copper is $CuCl_2$*$2H_2O$ (99% Sigma Aldrich), which was purchased and used without further purification, as all the other reagents.

The experimental procedure was based on the work of Tao et al. (X. Tao et al., 2011), and details about the synthesis used to obtain 1077 by Kronos decorated with copper is here reported. A first solution, which contained 3 g of L-ascorbic acid, 5g of CTAB, 72 ml of H_2O and 2 g the TiO_2 support, has been prepared. Then we prepared a second solution, containing 0.02-1.5 g of $CuCl_2$•$2H_2O$, 6 ml of NH_3 and 15 ml of H_2O. The solution obtained mixing them is sonicated at a set temperature of 62°C for 2.5 h, with a 55,0% amplitude and a 100 Wcm^{-2}. The final obtained sample has been centrifuged and washed with water. After washing, the powder is calcined at 480°C for 40 h. L-ascorbic acid acts as reducing agent, while CTAB, which acts as surfactant, plays a crucial role on the morphology and size of the final product.

Samples of Cu-M and MO decorated titania have been prepared by means of high energy US, with a copper amounts in the range 1–75 wt.%. Samples list is reported in table 2.5.

Sample name	**Precursor molecules**		**TiO_2 : $CuCl_2$•$2H_2O$ (g)**
TiO_2_$Cu_{(US)}$_1	1077 $CuCl_2$•$2H_2O$	+	2 g : 0.02 g
TiO_2_$Cu_{(US)}$_5	1077 $CuCl_2$•$2H_2O$	+	2 g : 0.1 g
TiO_2_$Cu_{(US)}$_10	1077 $CuCl_2$•$2H_2O$	+	2 g : 0.2 g
TiO_2_$Cu_{(US)}$_20	1077 $CuCl_2$•$2H_2O$	+	2 g : 0.4 g
TiO_2_$Cu_{(US)}$_40	1077 $CuCl_2$•$2H_2O$	+	2 g : 0.8 g

TiO_2_$Cu_{(US)}$_75	1077	+	2 g : 1.5 g
	$CuCl_2 \cdot 2H_2O$		

Table 2.5: TiO_2-decorated samples by means of US – second group (Cu).

2.1.2.3 Third group: silver-modified TiO_2

The plasmonic noble metal nanostructures, such as silver nanoparticles (AgNPs), promote charge separation and enhance light absorption because of the plasmon resonance (SPR) phenomena (S.A. Ansari et al., 2015; C. Su et al., 2012). In particular, AgNPs can interact with the radiation in the visible range, improving the photocatalytic responses obtained for metal-metal oxide photocatalytic materials, as well as nanoparticles on the TiO_2 surface slow down the recombination of excited electron-hole pairs (S.A. Ansari et al., 2013).

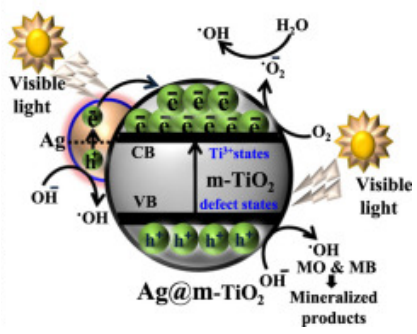

Fig. 2.9: Mechanism of visible light activation of TiO_2 decorated with silver nanoparticles onto surface (S.A. Ansari et al., 2015).

The preparation of many metal nanoparticles as the specific synthesis of silver nanoparticles can be carry out by various methods, deeply described in literature (M. Darroudi et al., 2011; Y. Liu et al., 2009; C.

Dong et al., 2014; I.K. Shim et al., 2008; Z. Khan et al., 2011). The most important problem is that several of them are toxic (K. Tahira et al., 2015). As for copper, here the TiO_2 surface decoration by AgNPs is described.

The metal precursor compound is silver nitrate ($AgNO_3$) (ACS Reagent, ≥99%,), polyvinylpyrrolidone (PVP40) (average mol wt. 40,000) and sodium borohydride ($NaBH_4$) (≥99%), purchased and used without further treatments. Goharshadi et al. have already described ultrasound-assisted synthesis of silver colloid nanoparticles, and we performed the TiO_2 surface decoration assisted by US on the basis of this procedure.

Silver NPs were synthesized during the process according to the reduction of silver nitrate because of the presence of $NaBH_4$, as reported in equation 2.3.

$$AgNO_3 + NaBH_4 + 3H_2O \rightarrow Ag + H_3BO_3 + NaNO_3 + 7/2H_2 \quad (2.3)$$

Two solutions have been prepared first. Solution A contains $AgNO_3$, PVP, 1077 TiO_2 and water respectively, while solution B is a $NaBH_4$ aqueous solution. The PVP content has been calculated according to the constant ratio mol ($AgNO_3$):g(PVP)/1:40.

After 10 minutes of US applied only to solution A, the reducing solution B has been added. Sonication has been continuing for 60 minutes (US power set at 30 Wcm^{-2} for samples indicated with "a", or 50 Wcm^{-2}, for samples "b"). The reaction temperature was controlled for 30±1 °C.

Finally, at the end of the US treatment, the powder has been washed and centrifuged with distilled water, then dried at 100°C overnight, and finally calcined at 400°C for 2 hours.

AgNPs-TiO_2 samples have been synthesized changing the silver nitrate percentage content referring to the weight of the TiO_2 powder used in each preparation, as reported in table 2.6.

Sample name	1077 TiO_2 (g)	$AgNO_3$ (g)
K-Ag(1a)	2	0.02
K-Ag(1b)	2	0.02
K-Ag(5a)	2	0.1
K-Ag(5b)	2	0.1
K-Ag(10a)	2	0.2
K-Ag(20a)	2	0.4

Tab. 2.6: TiO_2-decorated samples by means of US – second group (Ag).

2.1.3 Decorated-TiO_2 by classical impregnation method

The surface modification of TiO_2 can be obtained even by simple modification (Park et al., 2013), which can easily alter the mechanism and accelerate the photocatalytic reaction kinetics (P.V. Kamat et al., 2002; W. Choi et al., 2003). The most frequently employed modification method is to load nano-sized metals at TiO_2 surface via photo-deposition (E. Bae et al., 2003) and impregnation (J.S. Jang et al., 2008; C.S. Mei et al., 2005).

2.1.3.1 Silver (Ag) modified TiO_2

Classical impregnation method (CIM) with $AgNO_3$

A precise amount of 1077 TiO_2, usually 1 g, has been weighted in a 100 ml glass flask. The powder is wetted with a small amount of acetone (CHROMASOLV® Plus, for HPLC, ≥99.9%) and then an aqueous solution of $AgNO_3$ is added. Silver nitrate aqueous solution has been prepared with the minimum of water to have the complete dissolution

of the salt, the weight of which is determined depending on the ratio between TiO_2 and silver to be achieved. The solution is maintained under stirring for 24h by means of a rotavapor, at a constant temperature of 40°C. After 24h temperature has been raised up to 80°C, maintaining the solution under stirring for other two hours. The not evaporated solvent is removed at 100°C overnight, then the samples in form of dry powder has been calcined at 400°C for 2 hours.
Different samples with different TiO_2:Ag ratio have been prepared. The selected are reported in table 2.7.

Classical impregnation method (CIM) with AgNPs obtained by electrochemical synthesis.

Reagents used for this synthesis procedure are KNO_3, $AgNO_3$, and poly(N-vinylpyrrolidone) (PVP) (BASF) respectively, purchased and used without further purification. Classical electrochemical synthesis for silver nanoparticles is performed on the basis on the B. Yin et al. previous work (B. Yin et al., 2003), using platinum sheets as cathode and anode. Particularly, PVPK30 served as the main stabilizer for silver nanoparticles, but we reduced the molar ratio between PVP and Ag, in order to obtain bigger metal nanoparticles, as better explained in Results and discussion section. The electrolysis was carried out in the potentiostatic manner at room temperature (~22 °C) under mechanical stirring. A starting cyclic voltammetry is applied in order to calculate the correct reduction potential value (usually around 0,21 V). Then, this potential has been applying for 10 minutes, until the complete reduction of $AgNO_3$ to Ag^0. Through this simple process, an aqueous solution of PVP-stabilized silver NPs have been obtained. This solution is used for the impregnation of TiO_2 support, adding NH_3 up to a pH value of 12.5.

Impregnation has been conducted following the same steps described in the forgoing paragraph.

Different samples containing different $Ag\%_{wt}$. have been prepared. Complete list is reported in table 2.7.

Sample name	Ag (%wt.)
TiO_2-Ag_1	1%
TiO_2-Ag_8	8%
TiO_2-Ag_8(NH_3)	8%

Table 2.7: TiO_2-decorated samples by CIM – (Ag).

2.1.3.2 Manganese (Mn) modified TiO_2 (at different pH)

As already explained, loading titania with different transition metal elements was found to have significant influences on many properties of TiO_2 based catalysts. It is clear that the photocatalytic activity of samples strongly depended on the metal dopant used. For this reason in this work also the Mn properties have been studied, even on the basis of works previously published in literature (O. Kerkez-Kuyumcu et al., 2015).

It is explained in literature that the presence of transition metals might introduce new intra band gap states, giving the TiO_2 the capacity to absorb light at lower energy levels, thus, promoting the absorption on the visible part of the spectrum (J.F. Zhu et al., 2006; S. Klosek et al., 2001). In literature we found many contributions about manganese and its good properties in visible light absorption (Q.R. Deng et al., 2011; X.H. Xia et al., 2012; L. Wang et al., 2015).

1077 TiO_2 has been decorated with Mn atoms, starting from $Mn(NO_3)_2$ as precursor. The procedure follows the CIM and steps in detail, with slight differences between a sample and the other, are described below.
The first procedure (A) provides the preparation of an aqueous solution of manganese nitrate tetrahydrate first; then 1077 by Kronos is added and the suspension has been kept under stirring for 4 hours at a constant temperature of 80°C, using a rotavapor. At the end, suspension has been placed in the oven at 110°C for the next 24 h to have the complete evaporation of the solvent. The raw powder is finally calcined at 550°C for 6 h.
In the second version of synthesis (B), 1077 powder has been weighted and placed in a becker, with pure acetone. $Mn(NO_3)_2$ is dissolved in the minimum amount of water, and the solution is then mixed with the powder of TiO_2. As expected, suspension is kept under stirring using a rotavapor for 24 h at 40°C. Temperature is then raised up to 75°C and suspension is maintained continuously stirred for other two hours. Samples is placed in the oven at 110°C for 48 h, and the collected powder is calcined at two different temperatures, that are 300°C for 2 h or 600°C for 2 h respectively.
In table 2.8 the list of Mn-TiO_2 decorated TiO_2 different samples is reported.

Sample name	**Mn %wt.**	**Procedure**	**Calcination T°C**
TiO_2-Mn_5	5%	A	550°C
TiO_2-Mn_20$_{(300)}$	20%	B	300°C
TiO_2-Mn_20$_{(600)}$	20%	B	600°C
TiO_2-Mn_30	30%	B	300°C

Table 2.8: TiO_2-decorated samples by CIM – (Mn)

2.1.4 TiO_2 deposition on ceramic building materials: photoactive grés tiles

The materials coating with TiO_2 powders confers to the surfaces all the properties of TiO_2 as semiconductor (Taurino et al., 2016). Over the years, the purposes of its application have been many (Graziani et al., 2014; Chen et al., 2009; Fujishima, Honda, 1972; Zhao et al., 2003; Diamanti et al., 2013).

Different techniques can be employed to prepare and coat TiO_2 on solid supports, and particularly, to improve both adhesion and hydrophilicity, silica can be added as a suspension. Among the several kind of supports to obtain TiO_2-coated materials, porcelain grés tiles are very attractive: they are characterized by a very low water absorption rate (less than 0.5%) and are manufactured under high pressure by dry-pressing fine processed ceramic raw materials with large proportions of quartz, feldspar, and other fluxes. Afterwards, the body of these materials is fired at very high temperatures (1200–1300°C) in kilns (Casasola et al., 2012). The final material is thus characterized by lack of porosity, complete waterproofing, durability, hardness, wear resistance properties and a complete frost resistance. The deposition of anatase TiO_2 makes the traditional ceramic into a photocatalytic eco-active material able to reduce polluting molecules present in both air and water, to eliminate bacteria and to reduce the surface dirt thanks to the self-cleaning property (Bianchi et al., 2013b).

The industrial preparation of a photoactive porcelain grés tile, coated by spray method with the micro-sized TiO_2 (White Ground Active), or by the novel Digital Printing method is here presented.

2.1.4.1 Photoactive porcelain grés ceramic tiles: traditional spray TiO_2 deposition

Industrial porcelain grés tiles are manufactured under high pressure by dry-pressing fine processed ceramic raw materials with large proportions of quartz, feldspar, and other fluxes and finally fired at high temperatures (1200–1300°C) in a kiln.
They are the support to obtain photoactive porcelain grés tiles, by covering their surface with a mixture of micro-TiO_2 (1077 by Kronos) mixed with an aqueous suspension of a commercial SiO_2-based compound (process developed by GranitiFiandre S.p.A, patent n. EP2443076). Method used, namely Airless spray, is based on the use of nozzles, of appropriate dimensions and suitably studied to obtain the best dispersion of the product on the surface. After the deposition step, and after a first light-drying at room temperature, tiles were fired at high temperature (min 680°C) for 80 min. Some of the TiO_2 powder usually does not completely stuck, thus each tile surface has been brushed to remove it.

2.1.4.2 Photoactive porcelain grés ceramic tiles: Digital Printing technology

The digital printing technology is based on suitably designed print heads using a tailored solvent-based ink, micro-sized TiO_2 and additives (process developed by GranitiFiandre S.p.A, DigitaLife project). In a different way from the classical airless spray deposition just described, TiO_2 powder is already present in the ink solution that is usually used for coloring or decorating tiles. Indeed, deposition has been performed

by means of a classic digital printer, in which nozzles have been specially designed for this type of application.
Tiles were then treated at high temperature (680°C), and brushed at the end at the same way of the previous described process. However, Digital Printing process leads to many advantages, which concern first of all in a lower loss of TiO_2 powder, as of water, and secondly but almost most important, it is possible to reach an improved TiO_2 distribution on the surface, which is directly related to the photocatalytic activity of the material, as will be deeply explained in the results and discussion section.
Table 2.9 shows tiles samples names with a summary of the main physical features.

Sample tile name	**Deposition method**	**TiO_2**	**Chrystallographic TiO_2 phase at the surface**	**Temperature treatment**
Z23	Airless spray	1077 by Kronos	Anatase	680°C
S24	Digital printing	1077 by Kronos	Anatase	680°C

Table 2.9: Ceramic grés photoactive tiles list.

2.2 Characterization of the catalysts

2.2.1 Crystallographic phase composition of TiO_2

TiO_2 occurs in nature ad three distinct crystallographic phases that are anatase, rutile and brookite. The different octahedral arrangement for

each polymorph leads to different physical and electronic properties, which are also reflected on the final photocatalytic activity. In particular, the energy values of their band gaps vary from 3.0 eV (λ=413 nm) in rutile to 3.2 eV (λ=387 nm) in anatase. If the pure phases are specifically evaluated, it is reported that anatase is the polymorph that shows the highest activity in photocatalytic processes. The reason is mainly the higher conduction band edge of anatase responsible for photoexcited electrons. However, it is shown that a synergistic effect between anatase and rutile leads to an enhanced photocatalytic activity, that is the specific case of P25, because of the effective separation of the photogenerated charge carriers induced by the injunction between different crystalline phases (D.D. Dionysiou et al., RCS Energy and Environment Series).

X-ray powder diffraction (XRD) is the analytical technique used for TiO_2 phase identification and can even provide information on unit cell dimensions. Principle is based on the Max von Laue's scientific discovery, in 1912, i.e. that crystalline substances act as three-dimensional diffraction gratings for X-ray wavelengths similar to the spacing of planes in a crystal lattice (B.L. Dutrow et al., retrieved form http://serc.carleton.edu/research_education/geochemsheets/techniques/XRD.html).

X-ray diffraction relies on the constructive interference of monochromatic X-rays and a crystalline sample. The interaction between them produces constructive interference (and a diffracted ray) when conditions satisfy Bragg's Law ($n\lambda=2d \sin \theta$). By scanning the sample through a range of 2θ angles, all possible diffraction directions of the lattice are attained. Because of the unique d-spacings of each mineral, the conversion of the diffraction peaks to d-spacings permits the identification of the mineral.

In more detail, X-rays are generated in a cathode ray tube by heating a filament to produce electrons, accelerating the electrons toward a target by applying a voltage, and bombarding the target material with them. When electrons have sufficient energy to remove the inner shell electrons of the target material, characteristic X-ray spectra are produced. Copper is the most common target material for single-crystal diffraction, with CuKα radiation = 1.5418 Å (D.L. Bish and J.E. Post, 1989; B.D. Cullity, 1978; H.P. Klug and L.E. Alexander, 1974; D.M. Moore and R.C. Reynolds, 1997).
Additionally, XRD identifies the presence of any metal species or metal oxides in the sample, and it has been used in this regard for the specific characterization of the TiO_2-modified samples presented in the previous section.

Experimental: X- ray diffraction (XRD) spectra were obtained by means of a PW3050/60 X'Pert PRO MPD diffractometer from PAN analytical working Bragg-Brentano, using as source the high power ceramic tube PW3373/10 LFF with a Cu anode equipped with Ni filter to attenuate Kβ. A RTMS (Real Time Multiple Strip) X'celerator detector has been used to collect the scattered photons. The calculation of the crystallite size is given by the Scherrer equation (eq. 2.4), as it is usually done.

$$t = 0.9\,\lambda/(\beta_{hkl} \times \cos\theta_{hkl}) \qquad (2.4)$$

t is the crystallite size, λ is the X-ray wavelength of radiation for CuKβ, β_{hkl} is the full width at half maximum (FWHM) at (*h k l*) peak and θ_{hkl} is the diffraction angle.

2.2.2 Morphology of TiO_2 powders and ceramic photoactive tiles surface

As phase composition, particles size of TiO_2 is an important parameter that influences physical properties of the material, usually related to photocatalytic properties as well. In general, a lower particles dimension is directly connected to a higher surface area (K. Suttiponparnit et al., 2011). Because of the importance of the molecules adsorption on TiO_2 surface, in case of reactions of oxidation or reduction, usually a higher surface area leads to better adsorption, more active sites, higher photocatalytic activity (J. Nowotny et al., 2006). However, specifically in this research work, one of the main targets is to confirm the micrometric nature of a commercial TiO_2 powder. Indeed, because of the dangerousness related to the use of nano-powders of TiO_2, we need to confirm that a sample is micrometer and remains micrometer, even after some physical or chemical treatments.
The specific particles size determination can be based on the direct observation of TiO_2 particles, by means of Transmission Electron Microscopy (TEM) or Scanning electron Microscope technique (SEM) (K. Thamaphat et al., 2008).

2.2.2.1 Scanning electron microscopy (SEM)

Scanning electron microscope (SEM) produces the images of a sample by scanning it with a focused beam of electrons, which interact with atoms producing various signals particularly about the sample's surface topography and composition.
Manfred von Ardenne invented the first true microscope with high magnification in 1937 (M. von Ardenne, 1937), and he further discussed

the various detection modes, possibilities and theory of SEM (M. von Ardenne, 1938).
In more detail, in SEM the signals result from interactions of the electron beam with atoms at various depths within the sample. In the most common or standard detection mode, secondary electron imaging or SEI, the secondary electrons are emitted from very close to the specimen surface. Consequently, SEM can produce very high-resolution images of a sample surface, revealing details less than 1 nm in size. Thus, SEM micrographs are among the most useful techniques for understanding the surface structure of a sample. Wide range of magnifications is possible, from about 10 times (about equivalent to that of a powerful hand-lens) to more than 500,000 times, about 250 times the magnification limit of the best light microscopes.

2.2.2.2 Energy Dispersive X-ray Spectrometry (EDS)

EDS or EDX (Energy Dispersive X-ray Analysis) is an instrumental analytical method that is based on the X-ray emissions, generated by an accelerate electron bean. It is normally associated to SEM (and for this reason it is usually indicated as SEM/EDS). The electrons source is usually a tungsten or lanthanum hexa-boride filament. The electron bean is generated in vacuum by thermionic effect and it is accelerated and deflected, up to collapse on the sample. In particular, the EDS detector consists in a single silicon (or germanium) crystal doped by lithium, coated with a gold conductive layer.

2.2.2.3 High-Resolution Transmission Electron Microscopy (HR-TEM)

Transmission electron microscopy (TEM) is a microscopy technique in which a beam of electrons is transmitted through an ultra-thin specimen, interacting with the specimen as it passes through it (D.A. Skoog et al., 2006). An image is formed from the interaction of the electrons transmitted through the specimen; the image is magnified and focused onto an imaging device, such as a fluorescent screen, on a layer of photographic film, or to be detected by a sensor such as a charge-coupled device.

TEM was used to further examine the particle size, crystallinity and morphology of samples, and TiO_2 is one of the most investigated by this technique. Indeed, TEMs are capable of imaging at a significantly higher resolution than light microscopes, owing to the small de Broglie wavelength of electrons (S. J. Pennycook et al.).

TEM images give principally information about the particle size of TiO_2. Indeed, it is possible to clear distinguish a single TiO_2 particle, which can be easily measured. However, information even about the crystallographic phase composition can be extrapolated, particularly because rutile and anatase present slight differences in the morphology. TiO_2 powders in rutile phase consist of both spherical and rod shapes, while the particle of anatase phase are mostly spherical morphology. Max Knoll and Ernst Ruska in 1931 developed the first TEM.

Experimental: SEM analysis has been made in collaboration with University of Perugia (Dr. Di Michele). Exactly, the electron microscopy Philips XL-30CP with RBS detector of back-scattered electrons has been use to gather the SEM images, and an EDS analyzer was used to describe the surface and elemental composition of catalysts.

HR-TEM analysis has been made in collaboration with the University of Turin (Prof.ssa Cerrato, Dr.ssa Crocellà, Dr.ssa Morandi). The specific instrument use for the images acquisition is a JEOL 3010-UHR instrument (acceleration potential: 300 kV; LaBs filament). Samples were "dry" dispersed on lacey carbon Cu grids.

2.2.3 Samples surface area

The photocatalytic properties are influenced by physicochemical variables and surface area is one on the most important (K. J.A. Raj et al., 2009). Researchers usually use Langmuir-Hinshelwood kinetic expression to model photocatalytic reaction data, showing the importance of substrate absorption and thus surface area. Many studies support the dependence of surface area and photocatalytic activity of TiO_2 (A. Sclafani et al., 1990; C. Turchi et al., 1990), as well as Anpo et al. (M. Anpo et al., 1987) reported that for anatase photocatalytic activity increases with decreasing size. Considering the characteristics affecting photocatalytic activity is necessary to make efficient use of existing catalysts and to find the best methods to prepare new catalysts.

2.2.3.1 Brunauer Emmett Teller (BET) technique

According to Nelsen et al. (F.M. Nelsen et al., 1958) the most widely used method for determining surface area involves measuring the amount of gas (usually nitrogen) adsorbed on a solid surface at a temperature close to the boiling point of the gas. Adsorption methods provide different information, from the simple total surface area of the catalyst, to the more specific surface area of the phase carrying the active sites, or moreover, even the number and type of active sites. Specifically,

it is possible to exploit two different kind of interaction between the adsorbate and the adsorbent, namely the chemical absorption (chemisorption) or the physical absoprtion (physisorption). Specifically BET method is based on physical adsorption (J. Haber J. et al., 1995), and its name refers particularly to the authors that defined the equation, on which the calculation of the solids superficial specific area (SSA) is based on.

They are Brunauer, Emmett and Teller respectively, and their work is reported in Brunauer et al., 1938. SSA refers to the specific relationship between the catalyst total surface and its weight, and it is normally expressed in m^2g^{-1}.

To estimate the amount of the inert adsorbed gas, BET technique evaluates the proportion between the nitrogen partial pressure and its vapor pressure, changing temperature.

The concept of the theory is an extension of the Langmuir theory, based on the hypotheses that (i) gas molecules physically adsorb on a solid in infinite layers, ii) there is no interaction between each adsorption layer, and iii) the Langmuir theory can be applied to each layer. The resulting BET equation (eq. 2.5) is the following:

$$\frac{V}{V_m} = \frac{c\frac{p}{p^\circ}}{\left[1-\left(\frac{p}{p^\circ}\right)\right]\left[1+(c-1)\frac{p}{p^\circ}\right]} \qquad (2.5)$$

Where V is the volume of adsorbed gas at pressure P, p° refers to the gas saturation pressure at temperature T, p/p° is the relative pressure and finally C is the BET constant, which can be written by eq. 2.6:

$C = \exp((q_1-q_L)/RT)$ (2.6)

Where in detail, we have q_1 that is the heat of adsorption of the first layer, and q_L that is the heat of adsorption of the second and higher layers.

The linearization of eq. 2.3 leads to the V_m calculation, for which it was shown that a linearity is maintained only in the range of $0.05 < P/P^0 < 0.35$.

Equation reported below (eq. 2.7) is the adsorption isotherm that can be plotted as a straight line with $1/V[(P°/P)–1]$ on the y-axis and P/P^0 on the x-axis.

$$\frac{\frac{p}{p^\circ}}{V\left[1-\left(\frac{p}{p^\circ}\right)\right]} = \frac{1}{CV_m} + \frac{(c-1)\frac{p}{p^\circ}}{cV_m} \quad (2.7)$$

From the Vm value it is possible to calculate the specific surface area (SSA), as follows:

$$S.A. = \frac{V_m . N_{AV} . A_{mol}}{V_{mol}} \quad (2.8)$$

where N_{AV} is the Avogadro's number, and A_{mol} and V_{mol} are the adsorption cross section (for N_2 = 16.2 Å^2) and the molar volume of gas (22414 ml/mol), respectively.

Experimental: A Costech Sorptometer 1042 "KELVIN" have been used to investigate the BET surface area of the TiO_2, using liquid nitrogen. The procedure requires that, before the analysis, the catalyst is put in oven

(T = 110°C for 16 h) to remove the adsorbed water. Subsequently, the set quantity is analyzed in the instrument. The sample is pre-treated for 2 h at T = 200°C in a N_2 flow to remove all the impurity, then a check with helium is made to calibrate the interspatial volume.

2.2.4 Study of TiO_2 surface

2.2.4.1 X-ray photoelectron spectroscopy (XPS)

The deeper study of the TiO_2 surface particularly refers to its atomic composition, the chemical environment and the electronic state of the existent elements, can be performed by means of the X-ray photoelectron spectroscopy (XPS). This quantitative technique in based on the irradiation of the sample with a monochromatic beam of X-rays, which lead to an emission of electrons from the core or the atoms. The kinetic energy (E_K) and the number of the electrons are simultaneously measured. From this point, the binding energy (E_b) can be calculated as follows:

$$E_b = h\nu - (E_K + \Phi) \qquad (2.9)$$

$h\nu$ is the energy of the incident X-ray photons, E_K is the kinetic energy of photoelectrons emitted from the sample and Φ is the work function of the spectrophotometer.
XPS, also known as ESCA, an abbreviation for Electron Spectroscopy for Chemical Analysis, requires ultra-high vacuum (UHV) conditions and detects all elements with an atomic number (Z) between those of lithium (Z=3) and lawrencium (Z=103), with a limitation that thus regards the detection of hydrogen (Z=1) and helium (Z=2). Therefore, XPS is usually

used to measure elemental composition of the surface (1–10 nm), empirical formula of pure materials, elements that contaminate a surface, chemical or electronic state of each element in the surface. Indeed, it has been widely used in catalyst research to provide general qualitative analyses, to investigate the depth profile distribution of active species, to obtain estimates of dispersion, clustering and other morphological variations, to study metal-metal and metal-support interactions and to examine the chemical states of additives, poisons and transition metal ions in zeolites (J.L. Lemaitre et al., 1984; C.H. Bartholomew In: Z. Paal et al., 1988). Starting from a suitable calibration procedure, the surface concentration of the various elements can be measured with accuracy of the order of 20%. Moreover, one of the major interests focuses on the observation of the "chemical shift" effects, which reflect the oxidation state, and the chemical environment of the emitter.

XPS spectra are obtained by recording the quantity of photoelectrons emitted as a function of the binding energy. The different peaks that make the spectra are specific and different from atom to atom. Their position depends especially on the chemical environment, i.e. the number of valence electrons and the specific bonds with the neighboring atoms. For this reason it is possible to discern not only different elements, but also, different oxidation states.

Experimental: XPS measurements were performed in a M-Probe Instrument (SSI) equipped with a monochromatic Al Ka source (1486.6 eV) with a spot size of 200mm - 750 mm, pass energy is 25 eV, and the resolution provided is 0.74 eV. The accuracy of the reported binding energies (BE) can be estimated to be 0.2 eV. The quantitative data were

checked accurately and reproduced several times (at least 10 times for each sample).

2.2.4.2 FT-IR analysis

Infrared spectroscopy is obviously focused on the infrared region of the electromagnetic spectrum. The infrared portion of the electromagnetic spectrum is divided into three regions that precisely are the near-, mid- and far-infrared, named for their relation to the visible spectrum (P. Griffiths et al., 2007). More specifically, the far-infrared, approximately 400-10 cm^{-1} (1000–30 μm), lying adjacent to the microwave region, is the one having a lower energy and for this reason it is suitable for rotational spectroscopy. The mid-infrared, approximately 4000-400 cm^{-1} (30–1.4 μm) is instead suitable for studying the fundamental vibrations and associated rotational-vibrational structure. Finally, the higher energy near-IR, approximately 14000-4000 cm^{-1} (1.4–0.8 μm) can excite overtone or harmonic vibrations (D.R. Smith et al., 1968). In general, infrared spectroscopy can be used to identify compounds or investigate sample composition. In detail, IR spectroscopy exploits the fact that molecules have specific frequencies at which they rotate or vibrate corresponding to discrete energy levels and these resonant frequencies are determined by the shape of the molecular potential energy surfaces, the masses of the atoms and by the associated vibronic coupling (J. Connes et al., 1966). A vibrational mode in a molecule is IR active if it is associated to changes in the permanent dipole. In particular, according to the Born-Oppenheimer and harmonic approximations, exactly it happens when the molecular Hamiltonian, which corresponds to the electronic ground state, can be approximated in the neighborhood of the molecular geometry equilibrium, by a harmonic oscillator. The resonant

frequencies are determined by the normal modes corresponding to the molecular electronic ground state potential energy surface, and they can be in a first approach related to the strength of the bond, and the mass of the atoms at either end of it. Thus, the frequency of the vibrations can be associated with a particular bond type.

Molecules that are more complex have many bonds and vibrations can be conjugated, leading to infrared absorptions at characteristic frequencies that may be related to chemical groups.

From the examination of the transmitted light it is possible to evaluate the amount of the absorbed energy at each wavelengths. Particularly, it is possible to use a monochromatic beam, changing wavelength over time, or a Fourier transform instrument to measure all wavelengths at once. The transmittance of absorbance spectrum is then produced. Spectrum shows exactly at which IR wavelengths the sample absorbs, and the analysis of the absorption reveals details about the molecular structure of the sample (P.R. Griffiths et al., 2002). This vibrational spectroscopy is used for characterization of high area supported or unsupported catalysts, including zeolites. Information is available, either directly or by study of "probe" adsorbates, on the chemistry of surface groups (particularly on oxides). Problems include low transmission at high metal loadings and strong oxide scattering. Absorption at lower wavenumbers often prevents observation of modes such as adsorbate-metal stretching. Principal advantages of Fourier Transform (FIIR) spectrometers are the higher energy throughput and faster data acquisition or higher signal-to-noise ratio. Moreover, the data processing is easy. These features are significant when examining very strongly absorbing and scattering solids and when following dynamic processes.

Experimental: Absorption/transmission IR spectra have been acquired using a Perkin-Elmer FT-IR System 2000 spectrophotometer equipped with a Hg- Cd-Te cryo-detector, working in the range of wavenumbers 7200-580 cm^{-1} at a resolution of 2 cm^{-1} (number of scans ~20). The TiO_2 powder catalysts have to be compressed in self-supporting disc (of about 10 mg cm^{-2}) and placed in a homemade quartz cell, equipped with KBr windows, and connected to a conventional high-vacuum line (UHV). Spectra were recorded at room temperature (RT) on the samples in air and after prolonged outgassing at RT.

2.2.4.3 Surface wettability

Wetting is the ability of a liquid to stay in contact with a solid surface, resulting from intermolecular interactions. Wettability is evaluated by the degree of wetting, which is exactly determined by a force balance between adhesive and cohesive forces (O. Dezellus, and N. Eustathopoulos, 2010). More precisely, the contact angle (θ) is the angle at which the liquid–vapor interface meets the solid–liquid interface. As the tendency of a drop to spread out over a flat solid surface increases, the contact angle decreases. Thus, the contact angle provides an inverse measure of wettability (E. Sharfrin et al., 1960). As summarized in table 2.10, a contact angle less than 90° (low contact angle) usually indicates that wetting of the surface is very favorable, and the fluid will spread over a large area of the surface. Contact angles greater than 90° (high contact angle) generally mean that wetting of the surface is unfavorable, so the fluid will minimize contact with the surface and form a compact liquid droplet. Referring particularly to water molecules, a wettable surface is described as hydrophilic, on the contrary a non-wettable surface is hydrophobic. Superhydrophobic surfaces have contact angles

greater than 150°, showing almost no contact between the liquid drop and the surface (N. Eustathopoulos et al., 1999).

Contact angle	Degree of wetting
$\theta = 0$	Perfect wetting
$0 < \theta < 90°$	High wettability
$90° \leq \theta < 180°$	Low wettability
$\theta = 180°$	Perfect non-wetting

Table 2.10: contact angles and their corresponding solid/liquid and liquid/liquid interactions.

The main characteristic of superhydrophobic surfaces is a high roughness. The latter usually implies low adhesion forces between contaminating particles and the surface. On the contrary, TiO_2 is able to confer superhydrophilic properties to surfaces, based on the wettability conversion on TiO_2. A UV light illuminated TiO_2 single-crystal surface exhibited a 0° contact angle for water, indicative of a highly amphiphilic surface against its native hydrophobic surface (Jesus et al., 2015). This effect depends on the photo-reduction of surface Ti^{4+} to Ti^{3+} at definite sites, leading to preferential adsorption of dissociative water on top. However, a long-term storage of the highly amphiphilic surface resulted in reconversion of the surface wettability, and specifically the amphiphilic-to-hydrophobic reconversion is due to the replacement of the adsorbed hydroxyl groups by oxygen, which returns the surface geometric and electronic structures similar to the native TiO_2 surface (R. Wang et al., 1999; S.Y. Lien et al., 2013; M. Järn et al., 2010).

Experimental: The water contact angle (CA) (FM40Mk2 EasyDrop, KRUSS GmbH) was determined through a DSA1 program, which offers the possibility to evaluate mathematically the drop image. Starting from the estimation of the exact baseline of the CA, the correct angle value is

calculated by means of the Conic Section method, which completes profile of a sessile drop, giving a general conic equation. Specifically for small angles, it is possible to adopt the Young-Laplace and Circle Fitting methods (CA inferior than 60° and 30°). The first one determines the CA fitting it to a polynomial function. The second one is particularly suitable for small CA (<30°C). In that case, the drop shape is adapted mathematically to a circular segment shape, by evaluating the whole drop outline and not just the area of intersection with the baseline.

2.2.5 Study of the TiO_2 absorption in UV-VIS spectrum

The TiO_2 light absorption at different wavelengths is exactly the matter on which depends its photocatalytic activity thus is crucial. From a general point of view, this is also its problem. Indeed TiO_2 absorbs light only in the ultraviolet wavelengths. Study a TiO_2 sample and its absorption spectrum in the UV-VIS wavelengths is the starting point to collect information about its absorption capacity and its band gap and then about the effects of the modifications eventually done. This happens because modifications of TiO_2 shift the absorption in the visible.

2.2.5.1 Diffuse Reflectance Spectroscopy (DRS)

Diffuse Reflectance Spectroscopy (DRS) is the spectroscopic techniques to obtain the absorption spectrum of a liquid or solid sample, such as TiO_2. Ultraviolet–visible spectroscopy or ultraviolet-visible spectrophotometry (UV-Vis or UV/Vis) refers to absorption spectroscopy or reflectance spectroscopy in the ultraviolet-visible spectral region. Molecules containing π-electrons or non-bonding electrons (n-electrons) can absorb the energy in the form of ultraviolet or

visible light to excite these electrons to higher anti-bonding molecular orbitals. The more easily excited the electrons (i.e. lower energy gap between the HOMO and the LUMO), the longer the wavelength of light it can absorb (F. Jentoft, 2004).

Materials contain components that scattered and absorb light. Kubelka-Munk theory must be capable of predicting the fraction of light reflected from a surface expose to a radiation from all directions (J.H. Nobbs, 1985). The interaction between sample and light depends on incident light and transmitted light, from which it is possible to evaluate the absorption. The Lambert-Beer law is the empiric relation that correlates the absorbed light quantity to the physical and chemical properties of the medium. Particularly, the transmittance (T) is defined as the ratio between transmitted and incident light, and it is directly related to the absorbance (A) through the relation reported in eq. 2.10.

$$T = I_1 / I_0 = e^{-A} \qquad (2.10)$$

Starting from the absorption and scattering of light, Kubelka-Munk function is usually used to extract the absorption properties of the sample. It is possible to calculate the absorbance as a function of transmittance or reflectance and plot the experimental absorption versus lambda (λ), i.e. the irradiation wavelength (A. Naldoni et al., 2013).

Diffuse reflectance spectra can be specifically used even to calculate the band gap of TiO_2 powders. Data have to be elaborated using again the Kubelka-Munk function (G. Kortüm, 1969), according to the equation reported below.

$$F(R) = (1-R)^2 / 2R \qquad (2.11)$$

In equation 2.11 R is the reflectance of the powder; the band-gap values have been determined by performing the first derivative of the Kubelka-Munk function according with:

$dF(R)/d\lambda$

where λ is the wavelength of the incident radiation. The energy of the radiation at which the first derivative $dF(R)/d\lambda$ shows the maximum was taken as an estimation of the band-gap values (C.L. Bianchi et al., 2015).

Experimental: Diffuse reflectance spectroscopy (DRS) of the ground powders was performed with a Thermo Scientific Evolution 600 spectrophotometer, equipped with a diffuse reflectance accessory Praying-Mantis sampling kit (Harrick Scientific Products, USA), with the reference material was a Spectralon1 disk, or using a UV–Vis scanning spectrophotometer PerkinElmer (Lambda 35), which was equipped with a diffuse reflectance accessory as well, with a ''total white'' PerkinElmer reference material used as reference.

2.3 Reactors

In this section all the reactors used to perform the various tests on TiO_2 samples will be presented and described. Their main features and relative differences depend particularly on the kind of molecules analyzed, on the kind of analysis method, and on the fact that the reaction is performed in continuous or in batch.

2.3.1 Photocatalytic tests on VOCs: reactors and setup

Photocatalytic tests on TiO_2 samples, in order to investigate their activity for the degradation of organics, have been usually performed in batch. In particular two different sampling methods have been exploited to follow the pollutant molecule concentration trend over time, mainly depending on the kind of molecule. For higher concentrations and standard VOC molecules, such as ethanol, toluene or acetone, the study of the reaction kinetic was performed through a chromatographic analysis of the components inside the reactor. For lower concentrations, particularly for formaldehyde or more complex mixture of organics, Proton Transfer Reaction (PTR) Mass Spectrometry (MS) have been exploited as a novel and advanced technique for photocatalytic applications and studies.

2.3.1.1 Gas-chromatography analysis configuration

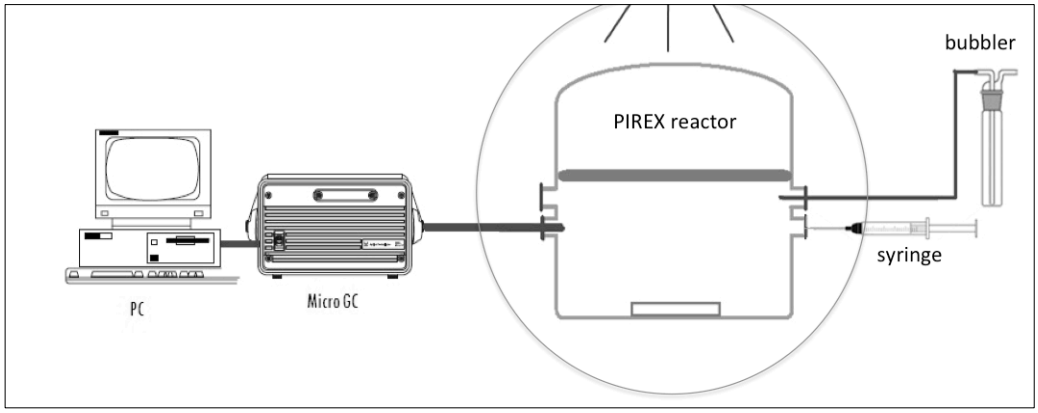

Fig. 2.10: Setup used for the VOCs photocatalytic degradation tests; analysis by standard gas chromatograph.

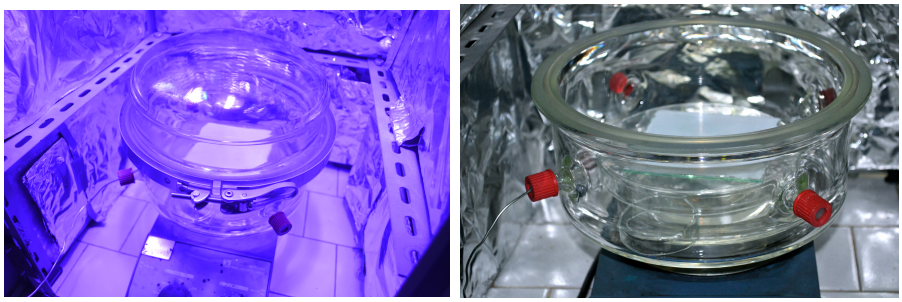

Fig. 2.11: VOCs reactor pictures

The reactor used for the tests on VOC molecules is a batch cylindrical glass reactor (diameter = 200mm and volume = 5L). It is provided with four vents, closed with plugs fitted with rubber septa, with 3-4 mm thickness. As schematically presented in fig. 2.10, photon sources are placed above the reactor, at a set distance. They were provided by a 500 W UV lamp (Jelosil model HG 500) emitting in the 315–400 nm wavelength range (UV-A) at 30 Wm^{-2} on the sample surface (placed as described in the next lines), or, to work only in the visible wavelengths, by a a LED (MW mean well, 350 mA rated current, 9–48 V DC voltage range, 16.8 W rated power) with an emission between 400 and 700 nm. In this case, the amount of emitted light depended on the distance and it has been measured in Lux. Lux is the SI unit of illuminance and luminous emittance per unit area. It is equal to lumen per square meter. We measured the emitted light at difference distances, finding approximately 15000 lux for 20 cm, 2000 lux for 40 cm and 1100 lux for 60 cm (SI Derived Units, National Institute of Standards and Technology). The VOC molecule concentration, as the concentration of the carbon dioxide produced at the end of the oxidation process, was constantly monitored using on-stream gas chromatography (Agilent 3000 A micro-GC), directly connected with the reactor by one of the vent. The others are kept closed during the photodegradation test. Pollutant molecule is loaded in the reactor through one of the rubber

septa, using a syringe (fig. 2.10). More precisely, the gaseous mixture in the reactor was obtained by mixing hot chromatographic air, humidified at 40%, and the fixed amount of volatilized pollutant to have the set concentration, usually calculated in ppmv.

This reactor is suitable and it has been used both for TiO_2 in form of powder or directly for photoactive ceramic tiles. For TiO_2 powders, the amount of catalyst used in each test was 0.05 g and it was deposited on a glass support as a thin film, using 2-propanol as inert solvent (fig. 2.12).

Fig. 2.12: TiO_2 deposited on glass as thin film, after the complete evaporation of 2-propanol.

Photoactive ceramic tiles (size = 10 cm^2) have been directly deposited on the bottom of reactor. They surface area is the same in case of glass with TiO_2 film or tile, even if the effective TiO2 amount is lower in case of tiles, because of the loss during the preparation and even because of the different TiO_2 distribution on different supports.

2.3.1.2 PTR-MS analysis configuration

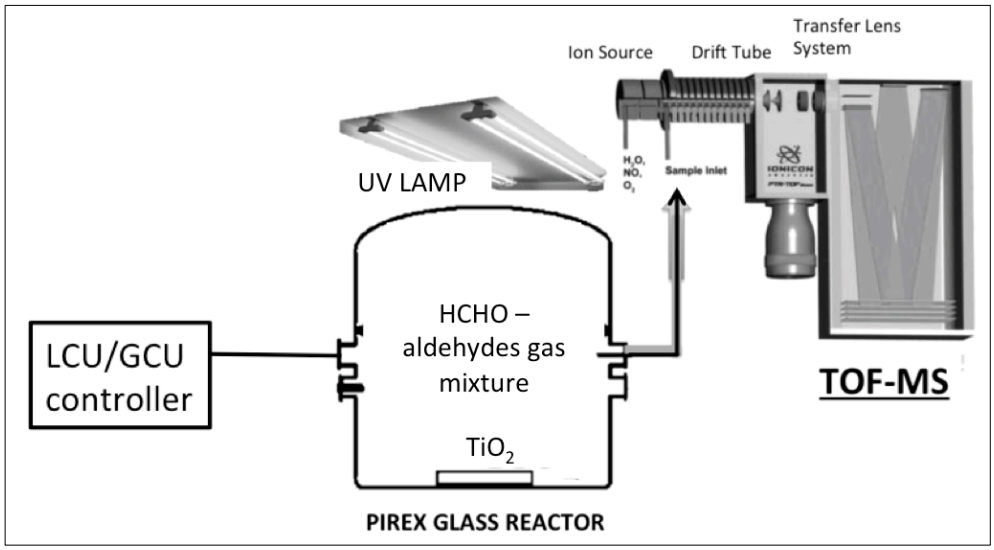

Fig. 2.13: Setup used for the VOCs photocatalytic degradation tests; analysis with PTR-MS instrument.

Fig. 2.14: A picture of the PTR-MS instrument (IONICON).

The Pyrex glass reactor is the same described in the previous paragraph as the irradiation is provided with the same configuration, both in case of UV or LED lamp, using the same equipment (see par. 2.3.1.1). For this configuration, the reactor loading is different, as there are different connection between the reactor and the analyzer instrument. In detail, by means of a liquid controller unit (LCU) or a gas controller unit (GCU) the pollutant, in liquid or in gas phase respectively, has been mixed with air to obtain a gaseous flow with fixed and constant concentration. The gaseous flow passes through the reactor until a constant concentration is reached. This is the reactor loading process, which requires a specific time depending on the flow rate. The gas flows continuously into the reactor until a constant concentration is reached. Tests have been conducted in batch, thus, before starting the photocatalytic reaction, all the reactor outputs have been closed, and the incoming pollutant flow has been stopped. As schematically presented in fig. 2.13, PTR-MS instrument is directly connected to the reactor using one of the rubber septum entries. Details about the analytical techniques will be presented in the next sections.

2.3.2 Photocatalytic tests on NO_x

The performance of the various TiO_2 samples have been investigated even for the NO_x degradation, considering that they are the main responsible for outdoor pollution. NO_x (NO_2 + NO) have been loaded in the reactors as gaseous mixture (diluted with chromatographic air or atmospheric air) and photodegradation reactions have been performed both in batch and in continuous. The specifications of the different reactors used will be now described.

2.3.2.1 NO_x photodegradation in batch mode

The photocatalytic activity of the TiO_2 samples was tested in NO_x degradation firstly operating in static condition. Photocatalytic degradations were conducted in a Pyrex glass cylindrical reactor with an effective volume of 20 L (fig. 2.15).

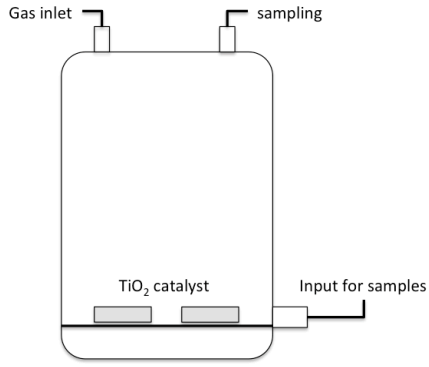

Fig. 2.15: NO_x batch reactor, 20 L volume.

Light source is placed above the reactor, with the same configuration presented for VOCs. The specific distance, both in case of UV light or LED, is set and modified depending on the irradiation power set for each test. TiO_2 samples have been placed at the bottom of reactor, both in case of powders and in case of tiles. TiO_2 powders have been deposited as thin film exactly using the same method described before (see par. 2.3.1.1), solving TiO_2 in isopropanol. Photoactive grés ceramic tiles of adequate size (2x20 cm^2) can be directly entered into reactor through the sample inlet located at the bottom (fig. 2.15).
The NO_x sampling over time has been performed by means of a chemiluminescence (Teledyne, Mod. 200E), which specifically revealed the NO, NO_2 and consequently their sum, i.e. NO_x concentrations in ppbv (S. Ardizzone et al., 2008; C.L. Bianchi et al., 2012).

2.3.2.2 NO_x photodegradation in continuous mode

CSTR (Continuous Stirred-Tank Reactor) (UNI 11484, 2013)

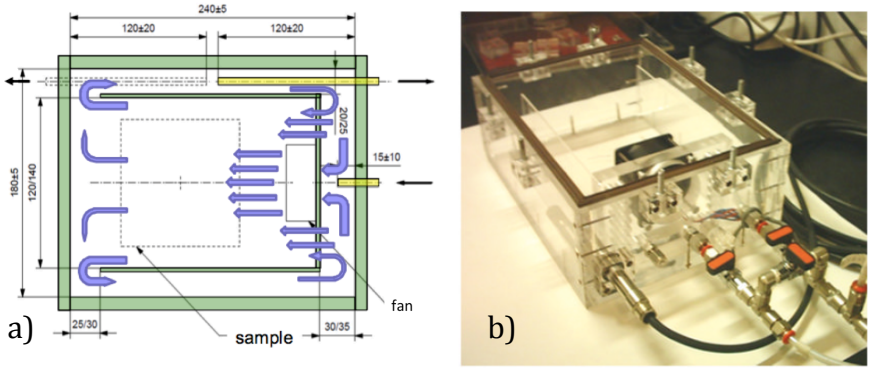

Fig. 2.16: CSTR (UNI 11484), a) reactor scheme and b) picture of the real reactor

Equation 2.12 reports the standard equation related to CSTR reaction kinetic.

$$V_R \, d/dt \, C_f(t) = F \, (C_0 - C_f(t)) - k_R \, S \, C_f(t) \qquad (2.12)$$

V_R is the volume of the reactor, C_0 and C_f are the starting and final concentrations respectively, F is the gas flow, k_R is the kinetic constant and S is the specimen area.
Particularly for the steady state, the following relation holds:

$$C_{\infty} = C_0 \, (F \, / \, F + K_R \, S) \qquad (2.13)$$

Conversion (η) can be calculated as $[(C_0 - C_{out})/C_0]$ and,

$$\eta_{\infty} = K_R S \, / \, (F + K_R S) \qquad (2.14)$$

thus, as reported in eq. 2.14, the conversion depends on F and on the specimen area (S). for this reason, conversion is a good parameter for evaluation of the sample performance, depending on the reaction conditions.

The first typology of continuous reactor used for NO_x photodegradation tests is presented in fig. 2.16. This kind of reactor is specific for TiO_2 samples with a surface area of 10x10 cm^2, and it is suitable both for TiO_2 in form of powders or tiles (sized as required). Reactor is provided with a gas inlet and a gas outlet, in order to have the continuous NOx flow inside the reactor, and a fan on the inside, with adjustable power. This is important because, changing the fan power, it is possible to evaluate the influence of the flow on the reaction kinetic (directly dependent on the range of Reynolds number, from turbulent to steady flow) (C. Minero, 1999; C. Minero and D. Vione, 2006).

Continuous flow reactor specific for large TiO_2 ceramic slabs (60x60 cm^2)

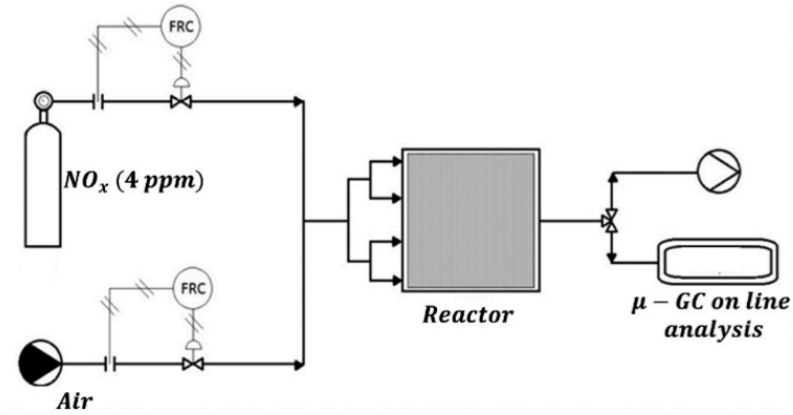

Fig. 2.17: Scheme of the experimental setup

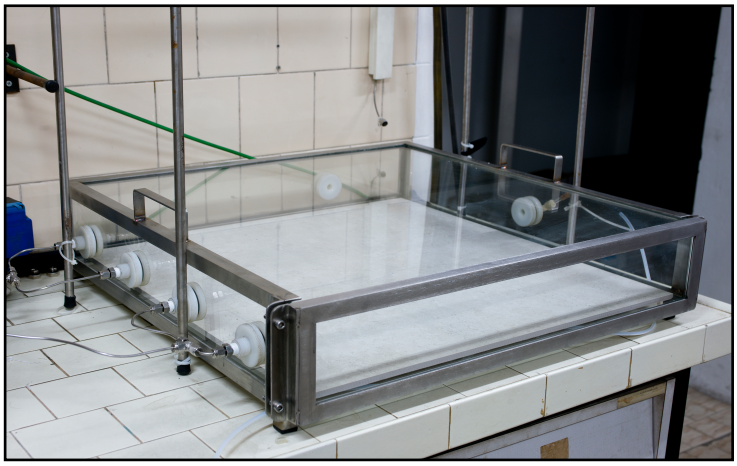

Fig. 2.18: Reactor containing the large TiO_2 ceramic tile (60x60 cm^2)

The reactor (Fig. 2.18) presents walls of 10 mm in thickness, and an internal size of 625 × 625 × 115 mm^3. It is provided with four inlets and one opposite outlet and can house a sample of 600 × 600 × 10 mm^3. Moreover, it is equipped with a thermo-hygrometer model HT-3006A to measure the temperature and humidity during the tests. The humidity inside the reactor is maintained constant at a relative humidity (RH) value between 40 and 50%. The experiments were carried out either using UV lamps, placed above the reactor at a set distance to have the required irradiation intensity, or even using sunlight.

In particular, irradiation source consists in two iron halogenide lamps (Jelosil, model HG 500) positioned at a 770 mm centre-to-centre distance. As in the configurations presented above, the light intensity in the UV-A region is measured using a Delta Ohm radiometer and regulated at the set value by adjusting the distance of the lamp from the reactor.

Reactor is directly connected with the cylinder containing the NO_x mixture. The output concentration of the pollutant [NO_x] outlet is measured by a chemiluminescence, directly connected with the output flow. The final design of the reactor was selected among several

possibilities by considering the results of the corresponding simulation studies, presented in the next paragraph. The size and the inlet/outlet position assure good homogeneity of the reactant in the gas phase and a contact between the reactant and the photocatalytic tiles that effectively reproduce the real working conditions.

2.3.2.1.1 Simulations

In order to study the best configuration for this large reactor, two sets of simulations with two different aims, i.e. fluid dynamics simulations and kinetic simulations, have been performed. The fluid dynamics simulations were performed using COMSOL Multiphysics® 4.0a to study the reactor configuration under flowing conditions, coupling the laminar flow with the transport of diluted species physics in a 3D space with each geometry resembling the relevant reactor dimensions and considering steady state conditions. These simulations were performed in order to verify the homogeneous distribution of the gas flow over the tile surface and to visualize the concentration gradients that build up during the NO_x treatment under steady state conditions.
The MatLab version R2015a software by The MathWorks, Inc. was used for the integration of the differential equation, adopting the ODE 15s algorithm, for the kinetic simulation assuming a uniform activity of the tile. Moreover, we also simulated the reaction using COMSOL, which considers the 3D geometry of the reactor and the local concentration upon the tile. In any case, the kinetic constants were considered proportional to the UV light intensity. Details about values and specific calculations will be presented in the related sections, in the results and discussion part.

2.4 Reaction conditions

Reaction conditions regard firstly the selected pollutant. For VOCs molecules, starting from the selected pollutant the relative conditions, i.e. starting concentration, relative humidity, irradiation, duration of the photodegradation and lamp, have been defined. For NO_x, the work conditions were quite similar even when the sample changed. Details will be now described.

2.4.1 VOCs photodegradation reaction conditions

2.4.1.1 Molecules

The VOC molecules selected and studied during this PhD research are:

- Acetone;
- Ethanol;
- Toluene;
- Formaldehyde;
- Acetaldehyde;
- Gaseous mixture of aldehydes;
- Gaseous mixture of different Volatile organic compounds.

Acetone, acetaldehyde, toluene and ethanol are all Fluka products at high purity grade (99.9%). Two different solutions of formaldehyde were purchased from Sigma-Aldrich: i) formaldehyde 37% in water containing 10-15% methanol as stabilizer; ii) formaldehyde (diluted in water and methanol free). The polymerization of the un-stabilized

aldehyde was avoided lowering the concentration of the molecule by dilution.

A gas cylinder containing a gaseous mixture of aldehydes was purchased from Apel-Riemer Environmental, Inc. Atmospheric Chemistry/Specialty gases. Standards are gravimetrically prepared in high-pressure aluminum cylinders that are cleaned and treated to eliminate contamination and ensure inertness. The specific list of aldehydes contained in the mixture is reported in Table 2.11.

Aldehyde	Concentration (ppb)
Formaldehyde	1119 ±5%
Acetaldehyde	1100 ±5%
Acrolein	933 ±5%
Propanal	986 ±5%
Butanal	1023 ±5%
Crotonaldehyde	1022 ±5%
Pentanal	968 ±5%
Hexanal	923 ±5%
Heptanal	952 ±5%
Octanal	965 ±5%
Nonanal	721 ±5%
Decanal	815 ±5%

Table 2.11: Aldehydes list and their concentration (ppb).

The gas cylinder containing the gaseous mixture of VOCs has been even purchased from Apel-Riemer Environmental, Inc., and it is named as "Cylinder (2000psi), Multicomponent calibration mix". List of VOC molecules contained in the mixture are listed in table 2.12 here reported.

Compound	**Volume mixing ratio / ppmV**	**Uncertainty *I* %**
Formaldehyde	1.10	± 7
Methanol	1.05	± 5
Acetonitrile	1.06	± 6
Acetaldehyde	1.04	± 5
Ethanol	1.10	± 5
Acrolein	0.91	± 5

Acetone	0.99	± 6
Isoprene	0.94	± 5
Crotonaldehyde	0.92	± 5
2-Butanone	0.97	± 5
Benzene	0.99	± 5
Toluene	0.93	± 5
o-Xylene	0.97	± 6
Chlorobenzene	0.98	± 6
a-Pinene	0.97	± 5
1,2-Dichlorobenzene	1.04	± 6
1,2,4-Trichlorobenzene	1.00	± 7

Tab. 2.12: List of VOCs and relative concentrations.

2.4.1.2 Analytical techniques

To determine the VOC molecules concentration inside the reactor during the photodegradation reaction, analytical techniques used in this work have been basically two, i.e. Gas-chromatography (GC) and Proton transfer reaction mass spectrometry (PTR-MS).

2.4.1.2.1 Gas chromatography

Gas chromatography (GC) is one of the most common and used technique used in analytical chemistry for separating and analyzing compounds (L. Donald et al., 2006).
The mobile phase consists in an inert gas, which in more than 90% of cases is helium (He), while the stationary phase is a liquid layer or a polymer placed on an inert solid support, inside a piece of glass or metal tubing, i.e. the chromatographic column. From the interactions between the compounds contained in the mobile phase and the stationary phase, each compound has a different elution time that controls its retention time. The chemical analysis instrument is the gas chromatograph. According to the basic principle described in the previous lines, the

chemicals exit the end of the column at different times, and they are detected and identified electronically.

2.4.1.2.2 Proton Transfer Reaction Mass Spectrometry

Proton-transfer reaction mass spectrometry (PTR-MS) is a technique developed almost exclusively for the detection of gaseous organic compounds in air. The crucial disadvantages of GC that can be solved using this technique are firstly the temporal resolution, and secondly the complication in the quantification of individual species, particularly when they are several and in mixture.
PTR-MS makes use of positive ions and, in particular, a proton donor to transfer protons to gaseous organic compounds. The modus operandi of PTR-MS is the chemical ionization, by proton transfer, of a gas sample inside a drift tube. The proton source is normally H_3O^+. The fixed length of the drift tube provides a fixed reaction time for the ions as they pass along the tube. Because the proton donor concentration is unchanged, after the addition of an analyte sample the measurement of the (proton donor)/(protonated acceptor) ion signal ratio allows the absolute concentration of the acceptor molecules, which can be calculated from a simple kinetic analysis. Consequently, by combining reaction kinetics with mass spectrometry, it is possible to both identify and quantify individual organic gases on a relatively short time scale and with a sensitivity that can reach well into the pptv mixing regime (R. S. Blake et al., 2009).

PTR-ToF-MS
Proton Transfer Reaction-Time of Flight-Mass Spectrometer (PTR-ToF-MS 8000, Ionicon Analytik , Innsbruck, Austria), worked in its standard

configuration (V mode). $H3O^+$ ions are generated in the hollow cathode discharge source from pure water vapor originating from pure water, and the ions produced are then transferred thanks to an applied voltage gradient into the drift tube, where they react with the analytes coming from an inlet line (W. Lindinger et al., 1998). The ions are then separated on the base of their mass-to-charge (m/z) ratio in the ToF-MS. Specifically, an E/N value of 130 Td (1 Td=$1\times10^{-21}Vm^2$) was used in the present study. The headspace of the samples was then analyzed by direct injection in the instrument via a heated (110 °C) PEEK inlet for 30 s (A. Fabris et al., 2010). The flow rate was set at 50 sccm (flow unit), and the headspace extracted during the analysis was continuously replaced with clean air, to avoid a pressure decrease. The external calibration is automatically done by the acquisition program (L. Cappellin et al., 2010). The selective reagent ions (SRI) used as reference are $H3O^+$ (mass 21,022), NO^+ (mass 29,997) and $C_6H_5I^+$ (mass 203,943), respectively. More specifically, formaldehyde was detected using PTR-ToF-MS by monitoring the mass spectral signal of $H{\cdot}HCHO^+$ at m/z 31.0184. Thermodynamically, this reaction is only slightly favorable since the proton affinity (PA) of HCHO (170.4 kcal/mol) is close to that of water (165.2 kcal/mol) (A. Vlasenko et al., 2010), making the concentration quantification humidity dependent (A. Jordan et al., 2009). For this reason, both temperature and humidity were monitored, as well confirming our tests are performed in stable conditions.

2.4.1.3 VOCs concentration

Acetone, toluene, ethanol and acetaldehyde have been detected by a Micro-GC, directly connected to the VOCs reactor (Fig.2.11) and that

automatically monitors the inner pollutants concentration. Basically, two different concentrations have been defined for the photodegradation kinetics of VOCs using TiO_2 catalysts and GC, and they are exactly 200ppm and 400ppm.

Reasons are mainly i) the instrument sensitivity, which it is not able to achieve a good accuracy under too low concentration values, ii) the possibility to observe and follow the formation of any photodegradation by-products, the concentration of which is detectable starting from higher pollutant molecule concentration, iii) the necessity to stress the materials at extreme condition, because, especially when the TiO_2 powders have been applied to ceramic material, a performance lowering is a constant; thus, TiO_2 powder samples need to be tested for the degradation of higher concentration of VOCs.

Formaldehyde, and the two gaseous mixtures of aldehydes and VOCs listed in Tab. 2.11 and Tab. 2.12 have been monitored, during the photodegradation studies, by means of the PTR-MS. Thus, starting concentrations of this kind of tests are slightly different. Both formaldehyde and the gaseous mixtures were loaded by means of LCU (Liquid Calibration Unit, IONICON Analytik GmbH, Austria) or GCU (Gas Calibration Unit, IONICON Analytik GmbH, Austria) in case of liquid or gaseous standards respectively. For pure formaldehyde, we operated at 500 ppb or 5000 ppb, which correspond approximately ten or hundred times over a typical indoor concentration. Indeed, we used these high concentrations to test in particular TiO_2 in form of powders, normally more effective than building materials. To study the performance of TiO_2 active tiles, the selected starting concentrations are obviously lower, with the final aim to reach conditions nearer to reality. Particularly, tests for the comparison between two kind of TiO_2-tiles (classical TiO2 deposition method, or Digital Printing) have been

performed at 200 ppbv as starting formaldehyde concentration. The reference value is 110 ppb (corresponding to 0.1 ppm), which agrees with the average concentration of formaldehyde measured in most environments. The Threshold Limit Value (TLV) is actually set at 0.3 ppm (0.37 mg/m^3), however a European proposal (SCOEL) aims to lower it to 0.2 ppm at least.
The mixture of aldehydes and VOCs was used at the concentrations provided by the supplier and listed in Tables (2.11 and 2.12).

2.4.1.4 Source of irradiation and photoatalytic tests duration

Ultraviolet irradiation
Ultraviolet (UV) is the electromagnetic radiation with a wavelength from 100 nm to 400 nm, which is shorter than that of visible light. UV radiation was discovered in 1801 by the German physicist Johann Wilhelm Ritter, by the observation of an oxidation effect on silver chloride-soaked paper. He called them "oxidizing rays" to emphasize chemical reactivity and to distinguish them from "heat rays", discovered the previous year at the other end of the visible spectrum. Afterwards, in 1893 Victor Schumann discovered the ultraviolet radiation below 200 nm, named vacuum ultraviolet because it is strongly absorbed by air (T. Lyman, 1914; S. Beeson and J.W. Mayer, James W., New York: Springer).
In this work, to conduct each photocatalytic phase under UV light, a UV lamp (Jelosil – Model HG-500, 500 W, λ = 315-400 nm) have been used.

Visible light irradiation
The visible spectrum is the portion of the electromagnetic spectrum with the electromagnetic radiation in the range of wavelengths from about 390 to 700 nm (C. Starr, 2005). The concept of the visible spectrum

became more definite in the early 19th century, when even the light outside the visible range was discovered and characterized by William Herschel (infrared) and Johann Wilhelm Ritter (ultraviolet) (M.J. Nye, 2003), and Young measured the wavelengths of different colors of light (J.C.D. Brand, 1995). Colors that can be produced by visible light of a narrow band of wavelengths (monochromatic light) are called pure spectral colors (Tab. 2.13).

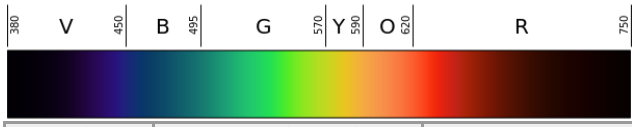

Color	Wavelength	Frequency	Photon energy
violet	380–450 nm	668–789 THz	2.75–3.26 eV
blue	450–495 nm	606–668 THz	2.50–2.75 eV
green	495–570 nm	526–606 THz	2.17–2.50 eV
yellow	570–590 nm	508–526 THz	2.10–2.17 eV
orange	590–620 nm	484–508 THz	2.00–2.10 eV
red	620–750 nm	400–484 THz	1.65–2.00 eV

Tab. 2.13: Colors and relative wavelengths, with frequencies (third column) and specific photon energy (fourth column).

A LED (MW mean well, 350 mA rated current, 9–48 V DC voltage range, 16.8 W rated power) with an emission between 400 and 700 nm have been used to perform the photocatalytic test on TiO_2 under visible light, without any presence of UV irradiation.

Tests duration

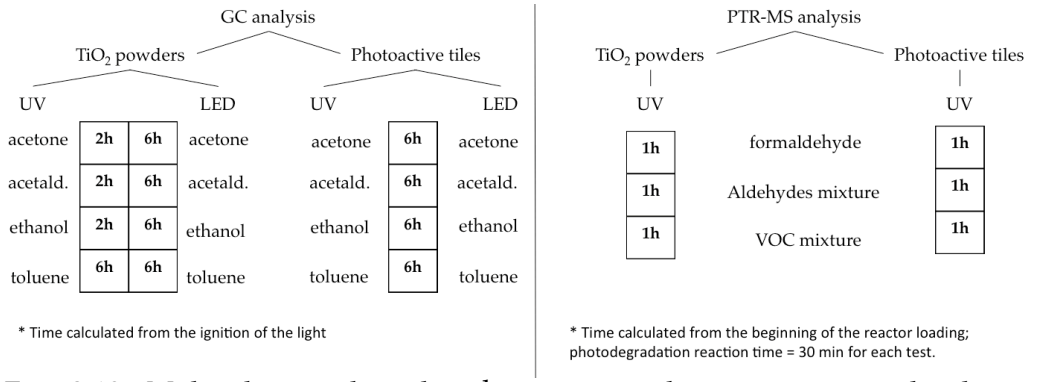

Fig. 2.19: Molecules, analytical techniques, irradiation source and relative duration of photocatalytic kinetics.

The overall reaction times were different as presented in the summary diagram above. Reasons are many and they were now explained. Tests on TiO_2 powders have a shorter duration than photodegration kinetics performed using tiles. Primary reason is that TiO_2 samples in form of powders are in general more photocatalytically efficient than building material. Indeed, in this case the TiO_2 powder is in direct contact with the pollution, and there are no other factors that could affect the absorption of the organic molecules on its surface, as well as there are no any components that could limit or cover the TiO_2 active sites, normally distributed on the surface. Testing TiO_2 powders first is useful to understand the behavior of different samples, to study their photocatalytic performances for specific applications, such as purification plants or particular reactions, and even to evaluate the possibility of different samples of TiO_2 in extreme or very hard conditions. However, even the molecule was crucial to set up the best reaction time. Kinetics performed on toluene last always 6 hours. Indeed, toluene has got a more articulated oxidation path, with the formation of many by-products. In general, molecules more cumbersome or organics with double bonds are more difficult to

degrade, thus it is necessary to use longer time duration to better evaluate the TiO_2 performances.
The source of irradiation has a strong influence on the degradation reaction. UV light is able to activated both naked TiO_2 and metal-modified samples of TiO_2, with higher energy. Thus, reactions under UV light are faster and require shorter times. Photocatalytic studies conducted using the PTR-MS technology to follow the molecules degradation have been set otherwise. The reaction duration never changes and it was fixed to 1 hour overall, which precisely consists in 30 minutes for the reactor loading and 30 minutes of effective irradiation to start the photocatalytic reaction. This decision have been made as first step of a project that will be developed, starting from the vast possibilities of the analysis tool.

2.4.2 NO_x photodegradation reaction conditions

Tests on TiO_2 samples to evaluate their photoatalytic behavior in the NO_x degradation the reaction conditions have been set particularly depending on the type of reactor and the catalyst form, i.e. TiO_2 powder or deposited on tiles. Indeed, TiO_2 samples have been tested with different NO_x starting concentration, different durations, and with different irradiation sources. Details will be now described.

2.4.2.1 NO_x gaseous mixture composition and dilution

The gaseous mixture in the reactors was obtained by mixing NO_2 (0.6% in nitrogen) with air humidified at 40% for tests conducted in batch. For tests in continuous, the NO_x starting concentration was obtained by diluting the steam of NO_x from a different cylinder (4 ppm). Dilution

with air was obtained using two different mass flow meters, which was adjustable to obtain the various starting NO_x concentrations. NO_x mixture consists of NO and NO_2, however, even when we started from an inlet gas of pure NO_2 pulsed into the reactor, as soon as it comes into contact in the air already present, reaches the chemical equilibrium between NO and NO_2. Thus, all the photocatalytic tests have been made using a mixture of NO and NO_2 in air.

2.4.2.2 Analytical technique: measurement principles of the chemiluminescence method

The chemiluminescence instrument exploits a very simple principle to detect NO_x. In general, NO is a rather non-stable molecule and it oxidizes to NO_2 in presence of O_3. This reaction produces a certain amount of light (i.e. chemiluminescence) for each NO molecule reacted, which can be measured by a photomultiplier tube. Controlling the gas volume and the relative volume of O_3, the light intensity is proportional to the NO concentration.

Reaction is the following:

$$NO + NO_3 \rightarrow NO_2 + O_2 + h\nu$$

Entering more in detail, when the sample is a mixture of NO_x (i.e. NO + NO_2), it has been passed through a heated catalyst that reduces all the molecules to NO. In this way it is possible to reveal the total amount of nitrogen oxides. This happens inside the instrument before the reaction chamber. Moreover, the instrument can perform the automatic

switching of the catalyst on and out of the sample path and in this way the resulting signals can be compared to measure indirectly even NO_2.
The specific instrument model used in this work is the chemiluminescence Serinus 40 Oxides of Nitrogen Analyzer.

2.4.2.3 Concentrations of NO_x

Static condition
The photocatalytic reactions conducted in batch mode have been performed selecting two different initial concentrations of NO_x: 1000 ppb in order to follow the same pollutant concentration requested by the ISO 22197-1 rules (www.iso.org) and 200 ppb that is very close to the alert threshold set by the EU Directive 2008/50/CE for NO_2 (http://eur-lex.europa.eu/LexUriServ/LexUriServ.do?uri=OJ:L:2008:152:0001:0044:EN:PDF).

Continuous mode
The NO_x degradation reactions conducted in the continuous flow reactor were performed at a NO_x concentration in the range from 100 ± 10 ppb to 200 ± 10 ppb, at room temperature and working with total gas flow rates of 140 and 180 NL h^{-1}. The concentration values were chosen in order to work closely to the limit values reported on Directive 2008/50/EC, in particular, 106 ppb (equal to 200 μg m^{-3}, a value not to exceed more than 18 times in a calendar year) and 213 ppb (400 μg m^{-3}, alert threshold). On the other hand, all the runs under direct sunlight were performed with a pollutant con- centration of 100 ± 10 ppb.

2.4.2.4 Source of irradiation and tests duration

For reactions conducted in static conditions, photon sources were provided by a 500 W iron halogenide lamp (Jelosil, model HG 500) emitting in the 320–400 nm wavelength range (UV-A). The specific UV power on the surface of the samples was 10 W m^{-2}. The NO_x photocatalytic tests were performed at 30 °C and lasted for 4 h. Other additional kinetics were carried out by irradiating the reactor without samples of titanium dioxide inside, to evaluate the effect of the simple photolysis action. Moreover dark experiments (i.e. with the catalyst inside the reactor but without UV irradiation) were conducted in order to obtain a proper estimation of the NO_x adsorption on the different catalytic samples.

Tests in the continuous flow reactor have been conducted particular on tiles. For this reason the kinetics duration is usually longer than the tests in batch. Moreover, the reactor contains tiles with a dimension of 600 × 600 × 10 mm^3, thus the lighting has been obtained with much larger UV lamps. In general, the experiments were carried out either using UV lamps or using sunlight from July to September 2014.

Specifically the irradiation was emitted by two iron halogenide lamps (Jelosil, model HG 500) positioned at a 770 mm centre-to-centre distance. The light intensity incident on the sample surface in the UV-A region was measured using a Delta Ohm radiometer and regulated in this configuration at 20 W m^{-2} by adjusting the distance of the lamp from the reactor. The duration of each continuous run was set at 6, 12 or 24 h, as has been mentioned before, with longer time because of the samples tested (i.e. large building materials) and the conditions as much as possible close to reality.

References

Anpo M., Shima T., Kodama S., Kubukawa Y., "Photocatalytic hydrogenation of propyne with water on small-particle titania: size quantization effects and reaction intermediates", J. Phys. Chem., **1987**, 91, 4305.

Ansari S.A., Khan M.M., Ansari M.O., Cho M.H., "Silver nanoparticles and defect-induced visible light photocatalytic and photoelectrochemical performance of Ag@m-TiO_2 nanocomposite", Sol. Energy Mater. Sol. Cells, **2015**, 141, 162–170.

Ansari S.A., Khan M.M., Ansari M.O., Lee J., Cho M.H., "Biogenic synthesis, photocatalytic, and photoelectrochemical performance of Ag−ZnO nanocomposite", J. Phys. Chem. C, **2013**, 117, 27023–27030.

Ardizzone S., Bianchi C.L., Cappelletti G., Gialanella S., Pirola C., Ragaini V., "Tailored anatase/brookite nanocrystalline TiO_2. The optimal particle features for liquidand gas-phase photocatalytic reactions", J. Phys. Chem. C, **2007**, 111, 13222–13231.

Ardizzone S., Bianchi C.L., Cappelletti G., Naldoni A., Pirola C., "Photocatalytic degradation of toluene in the gas phase. Relationship between the surface species and the catalyst features", Environ. Sci. Technol., **2008**, 42, 6671–6676.

Bae E., Choi W., "Highly enhanced photoreductive degradation of perchlorinated compounds on dye-sensitized metal/TiO_2 under visible light", Environ. Sci. Technol., **2003**, 37, 147–152.

Bartholomew C.H. In: Paal, Z. and Menon, P.G., "Hydrogen Effects in Catalysis", Marcel Dekker Inc., New York and Basel, **1988**.

Beeson S., Mayer J.W., "12.2.2 Discoveries beyond the visible", in Patterns of light: chasing the spectrum from Aristotle to LEDs, New York: Springer. p. 149.

Bianchi C.L., Gatto S., Pirola C., Naldoni A., Di Michele A., Cerrato G., Crocellà V., Capucci V., "Photocatalytic degradation of acetone, acetaldehyde and toluene in gas-phase: comparison between nano and micro-sized TiO_2", Appl. Catal. B: Environ., **2014**, 146, 123–130.

Bianchi C.L., Gatto S., Nucci S., Cerrato G., Capucci V., "Self-cleaning measurements on tiles manufactured with micro-sized photoactive TiO_2", Adv. Mater. Res., Int. J., **2013**, 2, 65-75.

Bianchi C.L., Pirola C., Galli F., Cerrato G., Morandi S., Capucci V., "Pigmentary TiO_2: A challenge for its use as photocatalyst in NOx air purification", Chem. Eng. J., **2015**, 261, 76-82.

Bianchi C.L., Pirola C., Selli E., Biella S., "Photocatalytic NOx abatement: the role of the material supporting the TiO_2 active layer", J. Hazard. Mater., **2012**, 211(212), 203–207.

Bickely R.I., Gonales-Carreno T., Lees J.S., Palmisano L., Tilley R.D., "A structural investigation of titanium-dioxide photocatalysts", J. Solid State Chem., **1992**, 92, 178-190.

Bish D.L., Post J.E., "Modern Powder Diffraction. Reviews in Mienralogy", Mineral. Soc. Am., **1989**, 20.

Blake R.S , Monks P.S., Ellis A.M., "Proton-Transfer Reaction Mass Spectrometry", Chem. Rev., **2009**, 109, 861–896.

Brand J.C.D., “Lines of light: the sources of dispersive spectroscopy, 1800–1930”, CRC Press. pp. 30–32, **1995**.
Brunauer S., Emmett P.H., Teller E., “Adsorption of gases in multimolecular layers”, J. Am. Chem. Soc., **1938**, 60, 309-319.
Cappelletti G., Bianchi C.L., Ardizzone S., “XPS study of the surfactant film adsorbed onto growing titania nanoparticles”, Appl. Surf. Sci., **2006**, 253, 519–524.
Cappellin L., Biasioli F., Fabris A., Schuhfried E., Soukoulis C., Märk T.D., Gasperi F., “Improved mass accuracy in PTR-TOF-MS: Another step towards better compound identification in PTR-MS”, Int. J. Mass Spectrom., **2010**, 290, 60–63.
Casasola R., Rinco´n J. M., Romero M., “Glass-ceramic glazes for ceramic tiles: a review”, J. Mater. Sci., **2012**, 47(2), 553–582.
Chen J., Poon C.S., “Photocatalytic construction and building materials: from fundamentals to applications”, Build. Environ., **2009**, 44, 1899–1906.
Chiang L.F., Doong R., “Cu–TiO_2 nanorods with enhanced ultraviolet and visible-light photoactivity for bisphenol A degradation”, J. Hazard. Mater., **2014**, 277, 84–92.
Choi W., Lee J., Kim S., Hwang S., Lee M.C., Lee T.K., “Nano Pt particles on TiO_2 and their effects on photocatalytic reactivity”, J. Ind. Eng. Chem., **2003**, 9, 96–101.
Connes, J., Connes, P., "Near-Infrared Planetary Spectra by Fourier Spectroscopy. (I) Instruments and Results", J. Opt. Soc. Am., **1966**, 56(7), 896–910.
Cullity B.D., “Elements of X-ray diffraction”, Reading, Mass, **1978**, Addison-Wesley 2nd edition.
Darroudi M., Ahmad M.B., Zamiri R., Abdullah A.H., Ibrahim N.A., Shameli K., Husin M.S., “Preparation and characterization of gelatin mediated silver nanoparticles by laser ablation”, J. Alloys Compd., **2011**, 509, 1301–1304.
Datye A.K., Riegel G., Bolton J.R., Huang M., Prairie M.R., "Microstructural characterization of a Fumed Titanium Dioxide Photocatalyst", J. Solid Chem., **1995**, 115, 236.
Deng Q.R., Xia X.H., Guo M.L., Gao Y., Shao G., “Mn-doped TiO_2 nanopowders with remarkable visible light photocatalytic activity”, Mater. Lett., **2011**, 65, 2051–2054.
Diamanti M.V., Del Curto B., Ormellese M., Pedeferri M.P., “Photo-catalytic and self-cleaning activity of colored mortars containing TiO_2”, Construc. Build. Mater., **2013**, 46, 167–174.
Dezellus O., Eustathopoulos N., "Fundamental issues of reactive wetting by liquid metals", J. Mat. Sci., **2010**, 45(16), 4256-4264.
Dionysiou D.D., Li Puma G., Ye J., Schneider J., Bahnemann D., “Photocatalysis: applications”, RSC Energy Env. Series, No.15.
Donald L., Lampman G.M., Kritz G.S., Engel R.G., “Introduction to Organic Laboratory Techniques (4th Ed.). Thomson Brooks/Cole, **2006**, 797–817, ISBN 978-0-495-28069-9.
Dong C., Zhang X., Cai H., “Green synthesis of monodisperse silver nanoparticles using hydroxy propyl methyl cellulose”, J. Alloys Compd., **2014**, 583, 267–271.

Dutrow B.L., Clark C.M., "X-ray Powder Diffraction (XRD)", retrived from http://serc.carleton.edu/research_education/geochemsheets/techniques/XRD.html.
Eustathopoulos N., Nicholas M.G., Drevet B., "Wettability at high temperatures", Oxford, UK: Pergamon, ISBN 0-08-042146-6, **1999**.
Fujishima A., Honda K., "Electrochemical Photolysis of Water at a Semiconductor Electrode", Nature, **1972**, 238, 37-38.
Fabris A., Biasioli F., Granitto P., "PTR-TOF-MS and data-mining methods for rapid characterization of agro-industrial samples: influence of milk storage conditions on the volatile compounds profile of Trentin grana cheese", J. Mass Spectrom. Ion Phys., **2010**, 45 1065–1074.
Gedanken A., "Doping nanoparticles into polymers and ceramics using ultrasound radiation", Ultrason. Sonochem., **2007**, 14, 418-430.
Goharshadi E.K., Azizi-Toupkanloo H., "Silver colloid nanoparticles: Ultrasound-assisted synthesis, electrical and rheological properties", Powder Technol., **2013**, 237, 97–101.
Griffiths P., De Hasseth J.A., "Fourier Transform Infrared Spectrometry", (2nd ed.), **2007**, Wiley-Blackwell, ISBN 0-471-19404-2.
Griffiths P.R., Holmes C., Handbook of Vibrational Spectroscopy, Vol 1. Chichester: John Wiley and Sons, **2002**.
Gupta S.M., Tripathi M., "A review on the synthesis of TiO_2 nanoparticles by solution route", Central European J. Chem., **2012**, 10, 279–294.
Haber J., Block J.H., Delmon B., "Manual of methods and procedures for catalyst characterization", Pure Appl. Chem., **1995**, 67, 1257-1306.
Hurum D.C, Agrios A.G., Gray K.A., Rajh T., Thurnauer M.C., "Explaining the Enhanced Photocatalytic Activity of Degussa P25 Mixed-Phase TiO_2 Using EPR", J. Phys. Chem. B, **2003**, 107(19), 4545–4549.
ISO - www.iso.org.
Jang J.S., Choi S.H., Kim H.G., Lee J.S., "Location and state of Pt in platinized CdS/TiO_2", J. Phys. Chem. C, **2008**, 112, 17200–17205.
Järn M., Xu Q., Lindén M., "Wetting studies of hydrophilic–hydrophobic TiO_2@SiO_2 nanopatterns prepared by photocatalytic decomposition", Langmuir, **2010**, 26(13), 11330–11336.
Jentoft F., "Diffuse reflectance IR and UV-vis Spectroscopy", Modern methods in heterogeneous catalysis, **2004**.
Jesus M., Neto J., Timò G., Paiva P., Dantas M.S., Ferreira A., "Superhydrophilic self-cleaning surfaces based on TiO_2 and TiO_2/SiO_2 composite films for photovoltaic module cover glass", App. Adh. Sci., **2015**, 3, 5.
Jordan A., Haidacher S., Hanel G., Hartungen E., Mark L., Seehauser H., Schottkowsky R., Sulzer P., Mark T. D., "A high resolution and high sensitivity proton-transfer-reaction time-of flight mass spectrometer (PTR-TOF-MS)", Int. J. Mass Spectrom., 2009, 286, 122.
Kamat P.V., Meisel D., "Nanoparticles in advanced oxidation processes", Curr. Opin. Colloid Interface Sci., **2002**, 7, 282–287.
Kerkez-Kuyumcu O., Kibar E., Dayloglu K., Gedik F., Akın A.N., Özkara-Aydınoglu S., "A comparative study for removal of different dyes over M/TiO_2 (M = Cu, Ni, Co, Fe, Mn and Cr) photocatalysts under visible light irradiation", J. Photochem. Photobiol. A: Chem., **2015**, 311, 176–185.

Khan Z., Hussain J.I., Kumar S., Hashmi A.A., "Silver nanoplates and nanowires by a simple chemical reduction method", Colloids Surf. B: Biointerfaces, **2011**, 86, 87–92.
Klosek S., Raftery D., "Visible light driven V-doped TiO_2 photocatalyst and its photooxidation of ethanol", J. Phys. Chem. B, **2001**, 105, 2815–2819.
Klug H.P., L.E. Alexander, "X-ray diffraction procedures for polycrystalline and amorphous materials", 2nd ed. Wiley, New York, **1974**.
Kortüm G., Reflectance Spectroscopy, Springer-Verlag, Berlin, **1969**.
Lemaitre J.L., Menon P.G., Delannay F., In: Delannay, F., "Characterization of Heterogeneous Catalysts", Marcel Dekker Inc., New York and Basel, **1984**.
Lien S.Y., Nautilyal A., Jhu J.H., Hsu J.K., Lee S.J., "Surface chemistry of super-hydrophilic SiO_2-doped TiO_2 photo-catalysts for self-cleaning glass", Asian J. Chem., **2013**, 25(11), 6071-6074.
Lindinger W., Hansel A., Jordan A., "On-line monitoring of volatile organic compounds at pptv levels by means of proton-transfer-reaction mass spectrometry (PTR-MS) medical applications, food control and environmental research", Int. J. Mass Spectrom., **1998**, 173 191–241.
Linsebigler A.L., Lu G., Yates J.T., "Photcatalysis on TiO_2surfaces: principles, mechanisms and selected results", Chem. Rev., **1995**, 95(3), 735–758.
Little L.H., "Infrared Spectra of Adsorbed Species", Academic Press, London, **1966**.
Liu Y., Chen S., Zhong L., Wu G., "Preparation of high-stable silver nanoparticle dispersion by using sodium alginate as a stabilizer under gamma radiation", Radiat. Phys. Chem., **2009**, 78, 251–255.
Lyman T., "The ozone layer protects humans from this", "Victor Schumann", Astrophysical J., **1914**, 38, 1–4.
Macwan D.P., Dave P.N., Chaturvedi S., "A review on nano-TiO_2 sol–gel type syntheses and its applications", J. Mater. Sci., **2011**, 46, 3669–3686.
Mei C.S., Zhong S.H., J. Inorg. Mater., **2005**, 20, 1396–1402.
Minella M., Faga M.G., Maurino V., Minero C., Pelizzeti E., Coluccia S., Martra G., "Effect of fluorination on the surface properties of titania P25", Langmuir, **2010**, 26, 2521–2527.
Minero C., "Kinetic analysis of photoinduced reactions at the water semiconductor interface", Cat. Today, **1999**, 54, 205-216.
Minero C., Vione D., "A quantitative evaluation of the photocatalytic performance of TiO_2 slurries", App. Cat. B Env., **2006**, 67, 257-269.
Moore D.M., R.C. Reynolds, "X-Ray diffraction and the identification and analysis of clay minerals", 2nd Ed. Oxford University Press, New York, **1997**.
Morterra C., "An infrared spectroscopic study of anatase properties. Surface hydration and strong Lewis acidity of pure and sulphate-doped preparations, Faraday Trans. 1, **1988**, 84, 1617–1637.
Morterra C., Bolis V., Fisicaro E., "The hydrated layer and the adsorption of carbon monoxide at the surface of titania (anatase)", Colloids Surf., **1989**, 4, 177–188.
Naldoni A., Bianchi C.L., Pirola C., Suslick K.S., "TiO_2 porous microsphere with tunable properties for air purification", Ultrason. Sonochem., **2013**, 20, 445–451.

Nelsen F.M., Eggertsen F.F., "Determination of surface area. Adsorption measurements by continuous flow method", Analytic. Chem., **1958**, 30, 1387-1390.
Nishimoto S., Othani B., Kajiwara H., Kagiya T., "Correlation of the crystal structure of titanium dioxide prepared from titanium tetra-2-propoxide with the photocatalytic activity for redox reactions in aqueous propan-2-ol and silver salt solutions", J. Chem. Soc., Faraday Trans. 1, **1985**, 81, 61-68.
Nobbs J.H., "Kubelka-Munk Theory and Prediction of Reflectance", Rev. Prog. Coloration, **1985**, 15(1), 66–75.
Nowotny J., Bak T., Nowotny M. K., Sheppard L. R., "TiO_2 Surface Active Sites for Water Splitting", J. Phys. Chem. B, **2006**, 110(37), 18492–18495.
Nye M.J., "The Cambridge History of Science: The Modern Physical and Mathematical Sciences", Cambridge University Press. p. 278, **2003**.
Ohno T., Sarukawa K., Tokieda K., Matsumura M., "Morphology of a TiO_2 Photocatalyst (Degussa, P-25) Consisting of Anatase and Rutile Crystalline Phases", J. Catal., **2001**, 203, 82-86.
Park H., Park Y., Kim W., Choi W., "Surface modification of TiO_2 photocatalyst for environmental applications", J. Photochem. Photobiol. C: Photochemistry Reviews, **2013**, 15, 1–20.
Pennycook S. J., Lupini A. R., Borisevich A., Varela M., Peng Y., Nellist P.D., Duscher G., Buczko R., Pantelides S.T., Transmission Electron Microscopy: Overview and Challenges.
Rao M.V., Rajeshwar K., Vernerker V.R., Kubow J., "Photosynthetic production of hydrogen and hydrogen peroxide on semiconducting oxide grains in aqueous solutions", J. Phys. Chem., **1980**, 84, 1987-1991.
Sakkas P.M., Schneider O., Sourkouni G., Argirusis C., "Sonochemistry in the Service of SOFC Research", Ultrason. Sonochem., **2014**, 21, 1939- 1947.
Sclafani A., Palmisano L., Schiavello M., "Influence of the preparation methods of titanium dioxide on the photocatalytic degradation of phenol in aqueous dispersion", J. Phys. Chem., **1990**, 94, 829-832.
Sharfrin E., William A., "Constitutive relations in the wetting of low energy surfaces and the theory of the retraction method of preparing monolayers", J. Phys. Chem., **1960**, 64(5), 519–524.
Shim I.K., Lee Y.I., Lee K.J., Joung J., "An organometallic route to highly monodispersed silver nanoparticles and their application to ink-jet printing", Mater. Chem. Phys., **2008**, 110, 316–321.
Skoog D.A., Holler F.J., Crouch S.R., "Principles of instrumental analysis", Thomas Brooks/Cole, **2006**.
Smith D.R., Morgan R.L., Loewenstein E.V., "Comparison of the Radiance of Far-Infrared Sources", J. Opt. Soc. Am., **1968**, 58(3), 433–434.
Stucchi M., Bianchi C.L., Pirola C., Vitali S., Cerrato G., Morandi S., Argirusis C., Sourkouni G., Sakkas P.M., Capucci V., "Surface decoration of commercial micro-sized TiO_2 by means of high energy ultrasound: a way to enhance its photocatalytic activity under visible light", Appl. Catal. B, **2015**, 178, 124-132.
Starr C., "Biology: Concepts and Applications", Thomson Brooks/Cole, **2005**.

Su C., Liu L., Zhang M., Zhang Y., Shao C., "Fabrication of Ag/TiO_2 nanoheterostructures with visible light photocatalytic function via a solvothermal approach", Cryst. Eng. Comm., **2012**, 14, 3989–3999.
Suttiponparnit K., Jiang J., Sahu M., Suvachittanont S., Charinpanitkul T., Biswas P., "Role of Surface Area, Primary Particle Size, and Crystal Phase on Titanium Dioxide Nanoparticle Dispersion Properties", Nanoscale Res. Lett., **2011**, 6-27; retrieved form http://www.nanoscalereslett.com/content/6/1/27.
Tao X., Zhao Y., "Sonochemical synthesis and characterization of disk-like copper microcrystals", Mater. Chem. Phys., **2011**, 125, 219–223.
Taurino R., Barbieri L., Bondioli F., "Surface properties of new green building material after TiO_2–SiO_2 coatings deposition", Ceram. Int., **2016**, 42, 4866–4874.
Thamaphat K., Limsuwan P. Ngotawornchai B., Kasetsart J., "Phase Characterization of TiO_2 powder by XRD and TEM", Nat. Sci., **2008**, 42, 357 – 361.
Tobaldi D.M., Severskapin A., Pullar R.C., Seabra M.P., Labrincha J.A., "Titanium dioxide modified with transition metals and rare earth elements: Phase composition, optical properties, and photocatalytic activity", Ceram. Int., **2013**, 39, 2619–2629.
Turchi C., Ollis D.F., "Photocatalytic Degradation of Organic Water Contaminants: Mechanisms Involving Hydroxyl Radical Attack", J. Catal., **1990**, 122, 178-192.
Vlasenko A., Macdonald A.M., Sjostedt S.J., Abbatt J.P.D, "Formaldehyde measurements by Proton transfer reaction – Mass Spectrometry (PTR-MS): correction for humidity effects", Atmos. Meas. Tech., **2010**, 3, 1055–1062.
Von Ardenne M., "Das Elektronen-Rastermikroskop. Theoretische Grundlagen", Zeitschrift für Physik, **1938**, 109, 553–572.
Von Ardenne M., "Improvements in electron microscopes", GB 511204, convention date (Germany), **1937**.
Wang X., Liu Y., Hu Z., Chen Y., Liu W., Zhao G., "Degradation of methyl orange by composite photocatalysts nano-TiO_2 immobilized on activated carbons of different porosities", J. Hazard. Mater., **2009**, 169, 1061–1067.
Wang R., Sakai N., Fujishima A., Watanabe T., Hashimoto K., "Studies of surface wettability conversion on TiO_2 single-crystal surfaces", J. Phys. Chem. B, **1999**, 103(12), 2188–2194.
Wang L., Zhang X., Zhang P., Cao Z., Hu J., "Photoelectric conversion performances of Mn doped TiO_2 under >420 nm visible light irradiation", J. Saudi Chem. Soc., **2015**, 19, 595–601.
Xia X.H., Lu L., Walton A.S., Ward M., Han X.P., Brydson R., Luo J.K., Shao G., "Origin of significant visible-light absorption properties of Mn-doped TiO_2 thin films", Acta Mater., **2012**, 60, 1974–1985.
Xina B., Wanga P., Dingb D., Liub J., Renb Z., Fub H., "Effect of surface species on Cu-TiO_2 photocatalytic activity", Appl. Surf. Sci., **2008**, 254, 2569–2574.
Xiong S., Tang Y., Sheena Ng H., Zhao X., Jiang Z., Chen Z., Woei Ng K., Loo S.C.J., "Specific surface area of titanium dioxide (TiO_2) particles influences cyto- and photo-toxicity", Toxicol., **2013**, 304, 132–140.

Yin B., Ma H., Wang S., Chen S., "Electrochemical synthesis of silver nanoparticles under protection of Poly(N-vinylpyrrolidone)", J. Phys. Chem. B, **2003**, 107, 8898-8904.
Zhao J., Yang X.D., "Photocatalytic oxidation for indoor air purification: a literature review", Build. Environ., **2003**, 38, 645–654.
Zhu J.F., Chen F., Zhang J.L., Chen H.J., Anpo M., "Fe^{3+}–TiO_2 photocatalysts prepared by combining sol–gel method with hydrothermal treatment and their characterization", J. Photochem. Photobiol. A: Chem., **2016**, 180, 196–204.

CHAPTER 3:
PHOTOCATALYTIC DEGRADATION OF VOCS

Abstract

VOCs molecules are present both in atmospheric air and in almost all the close environments where people pass the most part of their life. Pollution abatement, and the consequent studies of this kind of molecules are thus strongly connected, as well as important overall. Different kinds of organics have been selected to exploit the performances of different samples of TiO_2, able to degrade pollutants through photocatalytic reactions. Selected molecules are acetone, acetaldehyde, toluene, and formaldehyde respectively. Moreover photocatalytic tests using an aldehydes mixture, and a VOCs mixture also, have been performed in order to be as close as possible to real conditions. TiO_2 commercial samples in form of powder are obviously both nanometric and micrometric, in order to confirm the possibility to use micro-TiO_2 first. The photocatalytic active tiles have been obtained depositing just the micro-powder of TiO_2 on ceramic grés tiles, but by means of two different processes. The first is the classical airless spray deposition method; the second and newest is called Digital Printing. A complete set of characterization analysis has been performed on all the samples in order to investigate the TiO_2 main features, i.e. particles size, morphology, crystallographic phase composition, surface composition, presence of impurities, and wettability. Photocatalytic tests have been performed using two different method of organic molecules analytical monitoring, which are the classical gas chromatography for simpler systems, and the new proton transfer reaction mass spectrometry for more complex situations, such as the simultaneous presence of several molecules to follow. The results obtained and altogether collected data allows to confirm these general outcomes: i) micrometric TiO_2 can replace the nano-powders for photocatalytic reaction of organics degradation; ii) different organic molecules follow different degradation

reaction pathway even in connection with the particular catalyst features; iii) it is possible to calculate very interesting kinetic data and parameters; iv) it is possible to exploit the performances of both TiO_2 powders or photocatalytic TiO_2-based material in conditions close to reality, performing tests using simultaneously several VOCs molecules.

3.1 Introduction

3.1.1 VOCs and the problem of Indoor pollution

VOC molecules are constantly emitted in the troposphere by both anthropogenic and biogenic sources (R. Atkinson and J. Arey, 2003). For this reason they are present in either outdoor or indoor environments (J. Roberts and W. C. Nelson, 1995). However, contrary to what normally people tend to think, their concentration reaches more alarming values indoors. This is directly related to the sources of indoor pollution, which are mold and pollen, tobacco smoke, household products and pesticides, and materials usually used in the buildings. Volatile organic compounds (VOCs) include the most part of chemicals released from these sources, and they are frequently up to ten times higher indoors. Whereas especially in developed countries people spend most of their time in close environments, since they include homes, offices, public places, and vehicles, the problem is crucial. Each of us is constantly exposed to VOCs, and most of them are toxic or dangerous for human health. VOCs that have been detected and classified in indoor locations are both aromatic and aliphatic compounds (Institute for Environment and Health (IEH), 1996; NIOSH). Although the concentration values may still not be the real risk, health effects from indoor air pollutants depends particularly on the exposure period. There is still uncertainty

about the concentrations that can produce specific health problems but it is accepted that even low concentrations of some pollutants that are ubiquitous can be very dangerous (US Environmental Protection Agency, 2016).

3.1.1.1 Acetone, acetaldehyde and toluene

Acetone, acetaldehyde and toluene have been chosen as first reference molecules for indoor pollution. Acetone is the primary reference, having regard to its simplicity and being one of the most tested in literature, so it is useful for the first comparisons between the results. Moreover, acetone and acetaldehyde are each other's by-products; indeed acetaldehyde is the molecule corresponding to the first step of the acetone degradation (C.L. Bianchi et al., 2014). Toluene is a more cumbersome molecule, with the specific presence of the aromatic ring. Thus, contrary to acetone or acetaldehyde, toluene is interesting as molecule with a multi-step degradation pathway (S. Ardizzone et al., 2008), which makes possible the analysis of the influence of the formation of many by-products in a photocatalytic reaction, conducted on certain catalysts. For all these reasons, specifically in case of toluene, the various adsorbed species have been monitored by analyzing the samples surface by means of FT-IR spectroscopy.

3.1.1.2 Ethanol

Ethanol is another key molecule, generically wide studied in literature and used as reference. Furthermore, it is a rather important atmospheric pollutant. Indeed, ethanol is normally used as industrial solvent, as well as it is a common fuel additive. Its oxidation is of interest because it is

even emitted from many industrial processes such as breweries and bakeries. To give a general idea of its spread, ethanol emissions accounted for about 4% of the total VOC anthropogenic emissions in 1993 (R.G. Derwent et al., 1996). Afterwards, important is considering that the atmospheric concentration of this pollutant is rising as a consequence of the use of ethanol as a biofuel in the automotive sector. This issue besides implies an increase in the atmospheric levels of acetaldehyde, even more toxic and reactive in atmosphere (E.M. Martins et al., 2003; M. Colon et al., 2001). Acetaldehyde, included in the VOCs group selected for this research work, is present in the ethanol photodegradation pathway, as intermediate step between ethanol and the final CO_2 formation (C.L. Bianchi et al., 2015). Thus, from a kinetic point of view, the whole process can be simplified considering a first reaction on the catalyst surface, in which the adsorbed ethanol is converted to the adsorbed acetaldehyde, followed by a second reaction, in which the adsorbed acetaldehyde is mineralized to carbon dioxide and water, following a Langmuir-Hinshelwood mechanism. For this reason it has been possible to use the experimental data gathered for the regression of the characteristic kinetic parameters, assuming pseudo first order kinetic constants and obtaining very interesting results for the development of a kinetic model.

3.1.1.3 Formaldehyde

Formaldehyde is one of the major ubiquitous pollutants (EPA). The exposure to formaldehyde concerns almost the entire population of the industrialized countries. Indeed, formaldehyde is released from composite wood products usually used in buildings, resins, disinfectants, fixatives, and several products in which it is used as

preservative (EPA). Formaldehyde dangerousness for human health is a fact. IARC (International Agency for Research on Cancer) has classified formaldehyde as human carcinogen (Group 1) (T. Salthamer et al., 2013). TLV (Threshold Limit Value) is 0.1 mg/m^3, equivalent to 80 ppb (H. Dahnke et al., 2002). Samplings and studies, particularly conducted in indoor environments, showed that in the last period formaldehyde levels strongly increased, with a general concentration between 10 and 40 ppb in the most environs. However, values are higher in prefabricated houses and where there are chipboard furniture or carpets (D. Ryan and L. Bowles, US Department of Health and Human Service; A.P. Jones, 1999; K. Vaajasaari et al., 2004). The attention on formaldehyde is not a novelty and there are classical methods usually used to remove it: the first one uses impregnated potassium permanganate or organic amines as adsorbents but they are effective only for short periods; the second one is based on chemical reactions or catalytic oxidations that have a great potential but can be very expensive because they require high temperatures or noble metals as catalysts (B. Chen et al., 2013). In general, these methods are very difficult to use for the purification of indoor air. Still another crucial issue is the formaldehyde monitoring. The most accredited method is in fact based on the sampling by 2,4-dinitrophenylhydrazine (DNPH) cartridges, which are then analyzed by liquid chromatography. The sampling procedure requires 30 minutes at least and the complete analysis takes typically 30 h overall (M.N. Descamps et al., 2012). For this reason, an interesting alternative is the proton-transfer-reaction mass spectrometry (PTR-MS) that here we proposed to study the formaldehyde degradation kinetics (W. Lindinger et al., 1998; M. Graus et al., 2010).

3.1.1.4 Complex mixtures of organic molecules

In real conditions, indoor atmosphere contains a wide range of organics that are present simultaneously. More precisely, there are many different pollutant agents that it is possible to find indoors, both organic and inorganic. As already described, their concentration depends on the emissions from the various sources, on the environments dimensions in which these emissions occur, on the adsorption capacity of the materials and moreover they are linked to temperature and the environmental conditions that play a crucial role. Referring to organic compounds, which in real environments are more frequently detectable, they are formaldehyde and benzene. In addition to the several sources that increase their concentrations, it is important to consider also the semi-volatile organic compounds, which are most abundant specifically because they are deposited on surfaces, besides being dispersed in the air. They are phthalates, pesticides, alkilphenols and aromatic cyclic hydrocarbons. Overall, all the VOCs are present in the 80-100% of the environments. More specifically, aldehydes are the most prevalent compounds (observed in the 99,4% of the environments) with the highest concentrations: in the 50% of environments concentration of aldehydes exceeds the values of 1,1 $\mu g/m^3$ for acroleine and 19,6 $\mu g/m^3$ for formaldehyde, and in the 5% of environments the concentration of hexaldehyde is higher than 50,2 $\mu g/m^3$ (C. Duboudin, 2009). Among hydrocarbons the values go from a concentration of 1 $\mu g/m^3$ for styrene and trichloroethylene to 12,2 $\mu g/m^3$ for toluene, from 2,7 $\mu g/m^3$ for styrene to 150 $\mu g/m^3$ in case of 1,4-dichlorobenzene (S. Kirchner et al., 2009).

3.1.2 TiO_2 photocatalysts: the important challenge of micro-sized powders

TiO_2 photocatalysis is a well-established green technology for pollution abatement and environmental applications (J. Lyu et al., 2014). As direct consequence, TiO_2-based materials have attracted much attention of scientific research, even because of the advantageous main features of TiO_2, i.e. the fact that the catalyst is inexpensive, the reaction conditions are always mild-conditions, and because usually no other chemical reagent is needed (G. Cerrato et al., 2015). Considering that in a classical TiO_2 photocatalytic reaction higher is the sample surface area, higher are the performances, literature is full of synthesis routes to prepare tailored nano-TiO_2 (M. Gupta et al., 2012; X. Wang et al. 2009; D.P. Macwan et al., 2011). However this scientific run does not take into account the possibility that nano-sized materials could be dangerous for the human health. In the last period papers about nano-powders dangerousness increased (S.A. Love et al., 2012; S. Park et al., 2012; O. Creutzenberg, 2012; B.J. Panessa-Warren et al., 2006) and they often present increasingly more in detail new risks, effects of exposure and general adverse effects (E. Brun et al. 2012; C.J. Green et al., 2011). One of the goals of this work is to answer the question whether it is necessary to use nanoparticles. For this reason, the first test and studies we performed had intended to identify possible features of large-sized TiO_2 particles and a possible role for them in photocatalysis. As deeply described in the previous specific paragraphs, the commercial TiO_2 powders selected have a target market that is not photocatalysis, a part from P25 that is the nano-sized reference sample.

3.2 Materials

3.2.1 Organics

Acetone, acetaldehyde, toluene and ethanol are all Fluka products at high purity grade (99.9%). Formaldehyde was purchased from Sigma-Aldrich, precisely in two different solutions: formaldehyde 37% in water containing 10-15% methanol as stabilizer, and a second solution of formaldehyde, diluted in water and methanol free. Both were then diluted in water to obtain the requested final concentration. The polymerization of the un-stabilized aldehyde was avoided lowering the concentration of the molecule by dilution.

The gas cylinder containing a gaseous mixture of aldehydes (specific molecules listed in Table 3.1) was purchased from Apel-Riemer Environmental, Inc. Atmospheric Chemistry/Specialty gases. Standards are gravimetrically prepared in high-pressure aluminum cylinders that are cleaned and treated to eliminate contamination and ensure inertness.

Aldehyde	Concentration (ppb)
Formaldehyde	1119 ±5%
Acetaldehyde	1100 ±5%
Acrolein	933 ±5%
Propanal	986 ±5%
Butanal	1023 ±5%
Crotonaldehyde	1022 ±5%
Pentanal	968 ±5%
Hexanal	923 ±5%
Heptanal	952 ±5%
Octanal	965 ±5%
Nonanal	721 ±5%
Decanal	815 ±5%

Table 3.1 Aldehydes list and their concentration (ppb).

The gas cylinder containing a gaseous mixture of VOCs was purchased from IONICON Analytik Gesellschaft m.b.H. and the specific list of molecules is reported in Table 3.2.

Compound	Volume mixing ratio / ppmV	Uncertainty *I* %
Formaldehyde	1.10	± 7
Methanol	1.05	± 5
Acetonitrile	1.06	± 6
Acetaldehyde	1.04	± 5
Ethanol	1.10	± 5
Acrolein	0.91	± 5
Acetone	0.99	± 6
Isoprene	0.94	± 5
Crotonaldehyde	0.92	± 5
2-Butanone	0.97	± 5
Benzene	0.99	± 5
Toluene	0.93	± 5
o-Xylene	0.97	± 6
Chlorobenzene	0.98	± 6
a-Pinene	0.97	± 5
1,2-Dichlorobenzene	1.04	± 6
1,2,4-Trichlorobenzene	1.00	± 7

Table 3.2 VOCs list and their concentrations.

3.2.2 TiO_2 samples

3.2.2.1 Commercial powders

The following list reports the TiO_2 catalysts that have been tested and used in different photocatalytic reactions or studies. Then, during the experiments description each of them will be eventually recalled if necessary, referring to its specific characteristics or other properties.

TiO_2 Samples list:

- P25 – Evonik – reference material

- PC105 – Crystal
- AT-1 – Crystal
- 1077 – Kronos
- AH-R - Hunsdman

All the commercial powders have been purchased and used without further treatments.

3.2.2.2 Photoactive tiles

After various assessment tests, and after previous studies to find the best process for preparing TiO_2-coated ceramic grés tiles, for this work two main photoactive tiles samples have been selected. In this thesis the results about i) their main features, ii) their photocatalytic behavior, iii) photocatalytic activity in different conditions and in relation with different organic compounds, are described and compared, in order to give the final remarks about a new class of photocatalyitic TiO_2-based materials.

Photoactive grés tiles sample reference names are:

- Z23 – from the classical TiO_2 deposition industrial process
- S24 – from the Digital Printing process

3.2.3 Samples characterization

In Table 3.3 all the characterization techniques, exploited to collect information about the TiO_2 samples, have been listed and briefly described. The general experimental part (Chapter 2) reports more

details, and in the next sections, if necessary, each technique will be recalled and eventually deeply described.

Characterization technique	Features and properties	Instrument	Other information
BET	Surface area (m^2g^{-1})	◆Sorptometer instrument (Costech Mod. 1042)	*- Conventional N_2 adsorption at 77 K*
XPS	Surface characteristics	◆M-probe apparatus (Surface Science Instruments)	*- Source= monochromatic Al Kα radiation (1486.6 eV);* *- Accuracy of the reported BE = ±0.2 eV.*
XRD	Crystallographic phase composition and surface characteristics	◆PW3050/60 X' Pert PRO MPD diffractometer (from PAN analytical working Bragg-Brentano) ◆PW 3830/3020 X' Pert diffractometer (from PAN analytical working Bragg-Brentano) ◆Philips PW1710 diffractometer	*- Source = high power ceramic tube PW3373/10 LFF with a Cu anode equipped with Ni filter to attenuate Kβ.* *- Scattered photons collection by a RTMS (Real Time Multiple Strip) X'celerator detector.* *- Calculation of the crystallite size is given by the Scherrer equation.* *- CuKα radiation, operating at 40 kV and 20 mA, step scan 1 min^{-1}, and 1 s counting time in the 2–40° range at room temperature.*
SEM-EDX	Sample morphology TiO_2 distribution on supports elemental composition	◆Field Emission Gun Electron Scanning Microscopy LEO 1525 ◆Bruker Quantax	*- Acceleration voltage = 15 kV by inlens detector and with magnifications of 250,000 and 500,000.* *- Samples were*

	evaluation of the TiO2 amount in supports	EDS	*sputter-coated with chrome at 120 mA for 25 s.*
HR-TEM	Sample morphology particles size and size distribution	◆JEOL 3010-UHR instrument (acceleration potential: 300 kV; LaB_6 filament)	*- Samples "dry" dispersed on lacey carbon Cu grids.*
FT-IR	•OH free radicals population amount VOCs and by-products adsorption on TiO2 surface study	◆Bruker IFS28 spectrophotometer equipped with MCT cryo-detector ◆Perkin-Elmer FT-IR System 2000 spectrophotometer equipped with a Hg–Cd–Te cryo-detector	*- 4 cm^{-1} resolution.* *- All samples were examined in situ in the form of self-supporting pellets (~20 mg cm^{-2}) and mechanically protected with a pure gold frame.* *- Spectra obtained with the solid sample contained in a homemade quartz cell, equipped with KBr windows, connected to a conventional high-vacuum line (UHV).* *- Room temperature (RT).*
DRS	Light absorption features	◆UV–VIS scanning spectrophotometer PerkinElmer, Lambda 35 (equipped with a diffuse reflectance accessory)	*- Reference material = "total white" PerkinElmer.* *- Data elaborated using the Kubelka–Munk equation (L. Yang et al., 2004).*
Contact Angle	Wettability self-cleaning properties	◆OCA20 instrument (DataPhysics Co., Germany) equipped with a CCD camera and a 500μL-Hamilton syringe to dispense liquid droplets	*- Room temperature (~22◦C) by means of the sessile drop technique and replicated at least 15 times.*

Table 3.3: list of the characterization techniques used to study the main features of TiO_2 samples in form of powders or as ceramic tiles coated with TiO_2.

3.2.4 Photocatalytic setup

3.2.4.1 System connected to Micro-GC

This setup configuration operated in static condition. The Pyrex glass reactor has a diameter of 200 mm and an effective volume of 5 L. TiO_2 samples in form of powder have been deposited on flat glass slabs (10 x 10 cm^2) as thin film. Precisely, for each run 0.05 g of a TiO_2 different sample have been weighted and solved into a 2-propanol solution. Then, using a Pasteur pipette, the suspension has been layered on the glass surface, waiting that the solvent gradually evaporated and only the TiO_2 film remained (S. Ardizzone et al., 2008; C.L.Bianchi et al., 2012). In case of photoactive tiles, they were cut to the requested size (100cm^2), and they have been directly deposited at the bottom or reactor. The gaseous mixture in the reactor was obtained by mixing hot chromatographic air (f.i. 250°C for toluene), humidified at 40%, and a fixed amount of volatilized pollutant, in order to avoid condensation. The VOCs starting concentration in the reactor was set at 400ppmv for each molecule and relative kinetic reaction. As already mentioned, photon sources were provided by a 500 W iron halogenide lamp (Jelosil, model HG 500) emitting in the 315–400 nm wavelength range (UV-A) at 30Wm^{-2}. The duration of each photocatalytic run is different depending on the molecule. Acetone and acetaldehyde tests lasted for 2 h, while toluene photodegradations lasted for 6 h due to the presence of the aromatic ring. Tests on ethanol continued for 4 h, with the simultaneous monitoring of both ethanol and acetaldehyde (first by-product) by

micro-GC. The determination of CO_2 by gas chromatography was also performed, as well as photolysis tests under UV light in absence of photocatalysts, and adsorption tests in the dark. This last point was carried out in particular for ethanol, to perform the kinetic studies. Indeed, Adsorption tests were carried out by monitoring the concentration for 4 hours for both ethanol and acetaldehyde in the dark to obtain the adsorption constants (K) separately, in order to reduce the model parameters to be estimated. This approach has been already used in the literature for the independent determination of adsorption and kinetic constants, as reported by Popken et al. and by Song et al. (T. Popken et al., 2000; W. Song et al., 1998).

3.2.4.2 System connected to PTR-MS

The Pyrex glass reactor is the same that has been used to perform kinetic runs by Micro-GC. Formaldehyde has been loaded in the reactor by means of LCU (Liquid Calibration Unit, IONICON Analytik GmbH, Austria): LCU device mixes in a controlled manner the aqueous formaldehyde solution flow, with a flow of pure air. Formaldehyde solution has been vaporized at high temperature, then it has been diluted with the flow of pure air, and the final gaseous flow of the pollutant, at the desired concentration, is used for the reactor loading. In particular, reactor has 4 inputs; one is used to connect the reactor to the LCU and load formaldehyde, one is connected to the sampling instrument (i.e. PTR-MS), one is kept closed. The last is or connected to an outlet pipe, so the pollutant continuously flows during the reactor-loading step, or kept closed, in order to perform the kinetic test in batch mode. The gaseous mixtures, of aldehydes or VOCs respectively, were loaded by means of a GCU device (Gas Calibration Unit, IONICON

Analytik GmbH, Austria), because they are gaseous standards contained in classic pressurized cylinders. GCU controls the pollutants flow rate in order to obtain the wanted initial concentration. TiO_2 samples were deposited on a glass support with the same procedure use in case of GC sampling, as the photoactive tiles have been directly placed at the bottom of the reactor. Irradiation obtained by a UV got an irradiation power of 30 Wcm^{-2}. As already said, reactor is simultaneously connected to the injection tool (LCU or GCU) and to the PTR-MS instrument using two of the four reactor outlets. For pure formaldehyde, we operated at both 500 ppb and 5000 ppb, approximately ten or hundred times over a typical indoor concentration to verify photocatalyst efficiency under demanding conditions. The mixtures of aldehydes or VOCs were used at the concentrations provided by the supplier (see Tab. 3.1 and 3.2 respectively). When a stable value of the pollutant initial concentration was achieved, the photocatalytic reaction is initiated closing each reactor's outlets and by switching on the UV lamp. Photocatalytic test duration was set at 30 min.

3.3 Results and discussion

3.3.1 Commercial TiO_2 powders: characterization results and general considerations on their particles size.

The reference large-size commercial anatase samples are 1077 and AT-1 respectively (see TiO_2 samples list reported before). Anatase is the unique polymorph present for all samples, as shown by the XRD patterns. Only P25 exhibits the well-known phase composition 80:20 in anatase/rutile ratio.

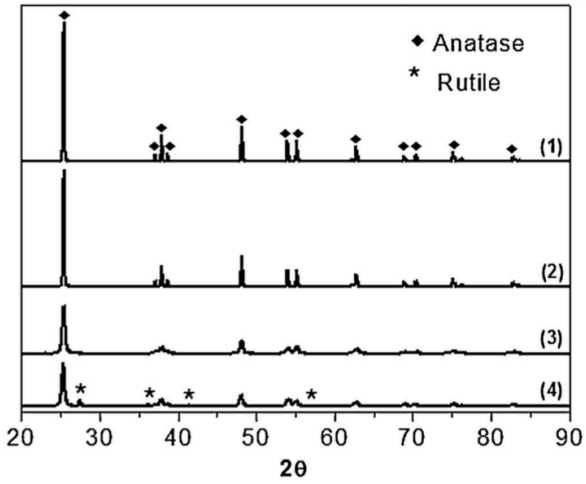

Fig. 3.1: XRD pattern of AT-1 (1), 1077 (2), PC105 (3) and P25 (4) (C.L. Bianchi et al., 2014)

The average crystallites size of various TiO_2 particles can be calculated by the crystallographic reflexes (1 0 1), (2 0 0) and (2 1 1), and results show that P25 and P105 have comparable crystallite size centered at around 25 nm, while the samples 1077 and AT-1 have values of 130 and 192 nm, respectively. These structural properties are reflected in the lower values of the BET surface area of micro-sized samples (1077 and AT-1), which have a surface area of 12 m^2g^{-1}, versus the vales calculated for nano-powders that instead are 50 m^2g^{-1} for P25 and 80 m^2g^{-1} for PC105, respectively. HR-TEM gives a perfect comparison between the different morphological features, as it is possible to see in the picture reported below (Fig. 3.2).

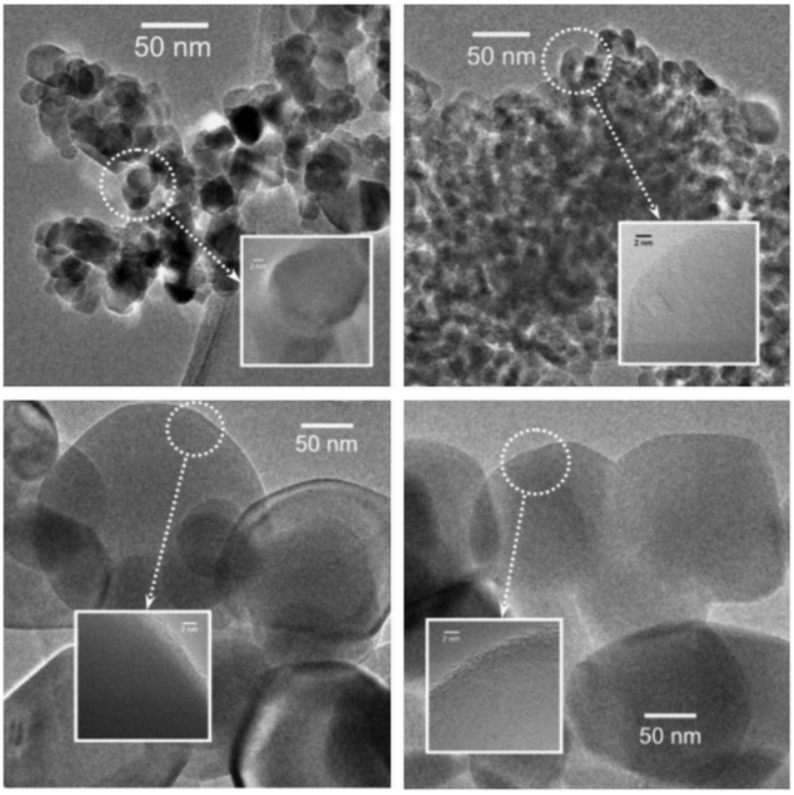

Fig. 3.2: Top sections: left-hand image refers to P25, right-hand image refers to PC105; Bottom section: left-hand refers to 1077, right-hand image refers to AT-1 (C.L. Bianchi et al., 2014).

Both TEM images (Fig. 3.2) and the average crystallites size extrapolated by XRD analysis exclude the presence of ultra-fine particles in 1077 or AT-1 samples. Especially for the nano-TiO_2 samples, also their highly crystalline nature is witnessed by the incidence of fringe patterns, generated by the superimposition of crystals belonging in particular to the TiO_2 anatase polymorph. For both nano-sized samples, the most frequently observed planes (d = 0.357 nm) are due to the (1 0 1) family (ICDD anatase file no. 21-1272).

The micro-sized materials are characterized by huge average dimensions of the particles as clear in the bottom sections of Fig. 3.2, in

total agreement with the indications coming from XRD analysis, which give for both 1077 and AT-1 samples an average dimensions in the 120–200 nm range. The (1 0 1) crystal planes belonging to the TiO_2 anatase polymorph are also in these cases the most frequently observed, with a consequent less defective nature of the particles themselves.

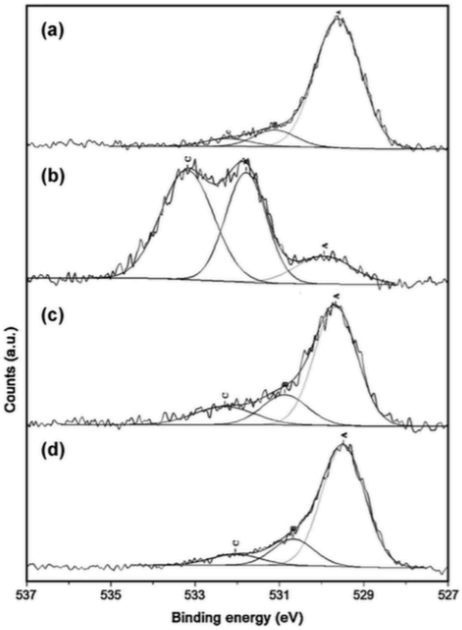

Fig. 3.3: O1s XPS spectra for P25 (a), PC105 (b), 1077 (c) and AT-1 (d).

By means of the XPS analysis, we performed the characterization of the TiO_2 surface state. The survey shows traces of K and P for AT-1 (5.3 and 3.4 at%, respectively), K for 1077 (3.3 at%) and S for AT-1 (1.4 at%) surely due to the starting reactants of the industrial process. No significant differences can be appreciated in the Ti 2p region among all the present samples concerning the binding energies (BE) and the full width at half-maximum (FWHM) values. The peak Ti $2p_{3/2}$ is always regular and the BE compares well with the data for Ti(IV) in TiO_2 materials (G. Cappelletti, C.L. Bianchi, S. Ardizzone, Applied Surface

Science 253 (2006) 519–524.). XPS gives even very important information about the oxygen peaks (Fig. 3.3): the presence of more than one component, which can be attributed to lattice oxygen in TiO_2 (529.9 eV) and to surface OH species (>531.5 eV), is clearly shown. In Fig. 3.3 is also possible to distinguish a particular O1s shape for PC105; indeed, the OH component is very intense probably due to a particular industrial synthesis in order to enhance the photocatalytic efficiency of the sample. Starting from the comparison between the different oxygen peaks, it is also possible to calculate the OH/O_{tot} surface ratio for each sample, a quantitative measure of the hydrophilicity/hydrophobicity of the TiO_2 surface (A. Naldoni et al., 2013). Results are reported in Tab. 3.4.

Sample	OH/O_{tot} surface ratio
P25	0.14
PC105	0.85
1077	0.32
AT-1	0.24

Tab. 3.4: OH/O_{tot} values for the selected TiO_2 samples (C.L. Bianchi et al., 2014).

The hydrophilicity/hydrophobicity character of photocatalysts surface plays a crucial role in determining the adsorption step and thus the photocatalytic activity (S. Ardizzone et al., 2008; A. Naldoni et al., 2013). P105 exhibits the highest concentration of OH that represent the 85% of the oxygen at the surface. It is noteworthy that the micro-sized samples present a higher atomic concentration of OH groups in comparison with P25, pointing out the higher hydrophilic character of their surface. Moreover, XPS gives even the information on the BE of a specific element (Fig. 3.4).

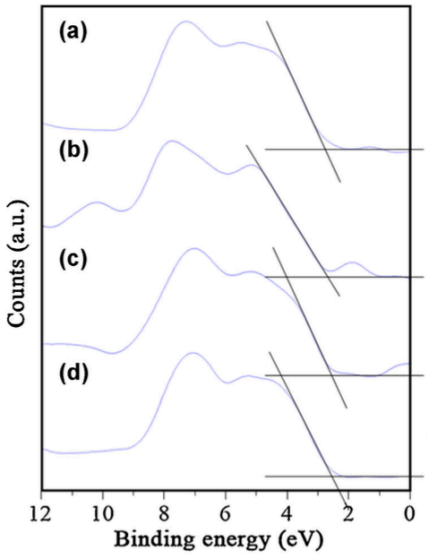

Fig. 3.4: VB XPS spectra along with VB maximum determining by the linear extrapolation method for a) P25; b) PC105; c) 1077; d) AT-1.

However, also the total density of states (DOS) of the valence band (VB) can be obtained (A.Naldoni et al., 2012), and exactly this measurement is useful to unravel the effect of TiO_2 structural modifications on the electronic properties of the material (X. Chen et al., 2008). The VB XPS spectra (Fig. 3.4) of both nano-sized (a,b) and micro-sized samples (c,d), allow to calculate the VB maximum position through linear extrapolation, and the same values around -2.6 eV (± 0.2 eV) were observed for all samples. This is the typical value for TiO_2 (X. Chen et al., 2008). Additionally, the absence of additional bands above the VB in the AT-1 spectra suggests that the impurity (i.e., S) revealed by survey analysis are not inserted in the TiO_2 lattice. Finally, it was possible to calculate the band-gap values starting from the experimental data of diffuse reflectance, elaborating them according to the Kubelka–Munk equation. There are no evident differences in the band-gap values, which are all around the typical anatase standard of 3.2 eV. Hydroxyl radicals (OH) groups are showed even in the FTIR spectra (see Fig.3.5)

in the region of absorption bands related to H-bonded and free hydroxyls (these last evidenced by grey box). Even if P25 material exhibits the lowest OH/O_{tot} ratio (Tab. 3.4), its better activity is surely related to the higher surface area, which ensures a bigger amount of surface OH groups, as demonstrated. The main difference between P25 and both the micro-sized TiO_2 samples is that the first has a larger amount with high heterogeneity of free hydroxyls.

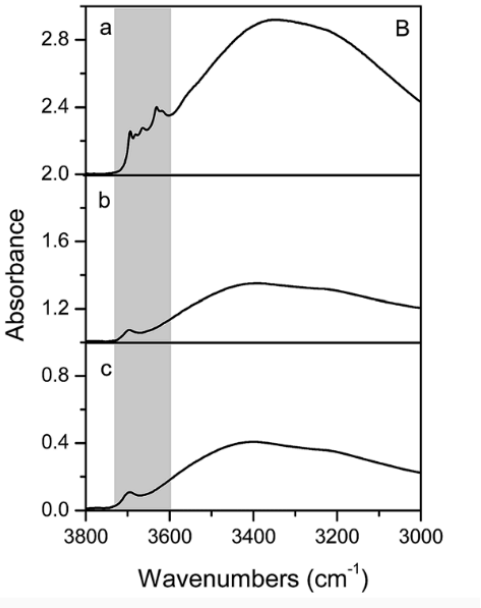

Fig. 3.5: FTIR spectra recorded at RT in air for P25 (a), A-HR (b), and 1077 (c).

3.3.2 Classical TiO_2 deposition method and Digital Printing: study on the photoactive tiles morphology in order to evaluate advantages and drawbacks.

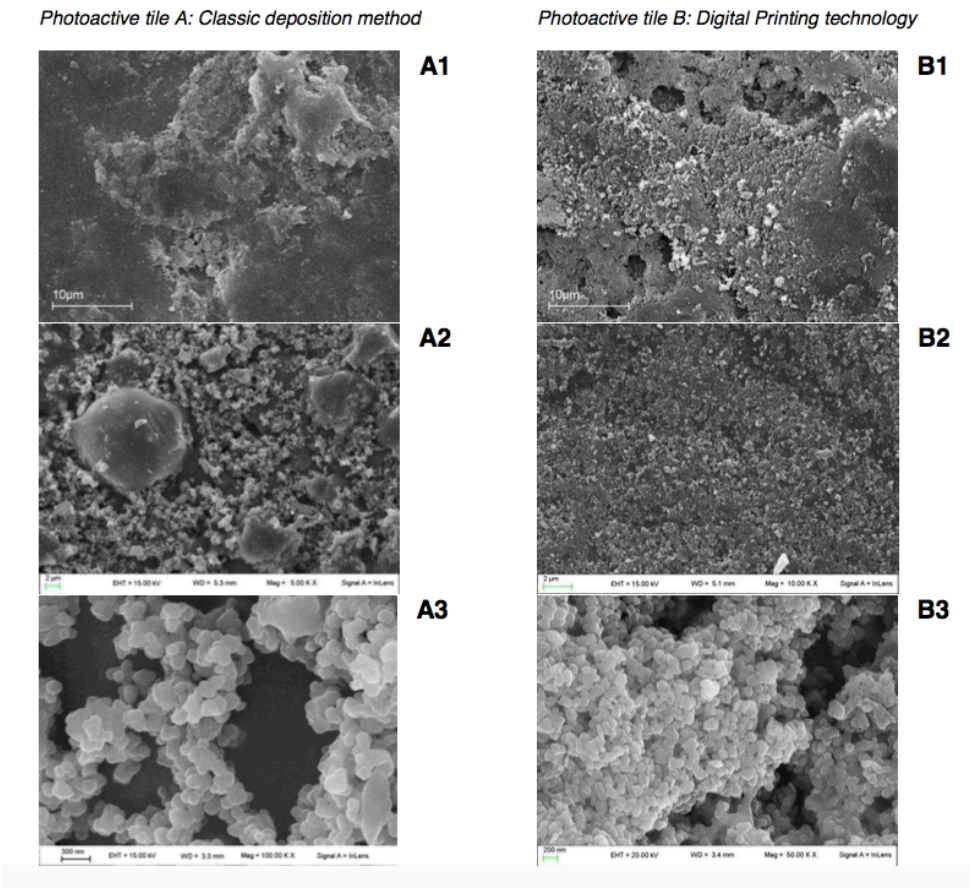

Fig. 3.6: SEM images of photoactive grés tiles prepared with two different methods: figures in the left column (A1; A2; A3) refer to the classical spray deposition method; figures in the right column (B1; B2; B3) refer to the new digital printing technology.

Three different magnifications (see Fig. 3.6) focus the main difference between the two different industrial preparation methods for the photoactive TiO_2-coated ceramic tiles: the crucial point is that depositing TiO_2 by digital printing it is possible to obtain a more uniform surface in term of powder distribution. Indeed, there are no empty areas, thus the entire tile surface works to degrade the pollutants (fig 3.6. magnification A3, B3). Wettability by the measurement of the contact angle values was evaluated on different areas of both samples of the photoactive grés

ceramic tiles. Even if the final values did not show significant differences, both the photoactive tiles show hydrophilic properties with an average angle around 23.0°. Hydrophilicity is a crucial parameter related to the photocatalytic activity, because of its close relation with the fact that a hydrophilic surface is more wettable. The water molecules are the key species from which, at the beginning of the photocatalytic process, the oxidizing radical species are generated. TiO_2 is the sole responsible for this behavior, indeed a classical tile without TiO_2 usually shows a higher contact angle value around 78.2°, denoting a completely hydrophobic surface (R. Wang et al., 1997; C.L. Bianchi et al., 2012). XRD analysis confirms both the TiO_2 size, which remains micrometric, and the presence of anatase as single crystallographic phase, with any phase transformation after the heat treatment. This feature is even demonstrated by the XRPD pattern collected at the high-resolution powder diffractometer at the ID31 beamline of the European Synchrotron Radiation Facility (ESRF), Grenoble, France and reported elsewhere (C.L. Bianchi et al., 2013).

3.3.3 Photocatalytic tests

In general, a crucial aspect to underline for this first part of results presentation, regards the pollutant level in the reacting chamber. While the major part of the literature results are related to concentrations of several hundred part per billion (ppb) or few parts per million (ppm) (C.H. Ao et al., 2003; J. Jeong et al., 2004; M. Addamo et al., 2006; G.Marcì et al., 2003), here higher VOCs levels (400 ppm) were adopted in order to precisely identify the nature of the reaction intermediates and also to evaluate the possible feasibility of a photocatalytic

degradation process even in severe pollution conditions on sample of different crystallite sizes.

3.3.3.1 Acetone, acetaldehyde and toluene: first group of photodegradation reactions to evaluate the performances of the commercial samples in form of powder.

Sample	**Acetone (reaction time 2h)**	**Acetaldehyde (reaction time 2h)**	**Toluene (reaction time 6h)**
P25	100% in 70 min	100% in 60 min	52%
PC105	100% in 60 min	100% in 50 min	50%
1077	100% in 90 min	100% in 70 min	46%
AT-1	49% after 120 min	46% after 120 min	46%

Table 3.5: Summary of the results obtained in the photocatalytic degradation of different VOCs with different TiO_2 samples.

The study of the photocatalytic activity of this first group of nano- and micro-sized samples allows to arrive at the preliminary conclusions about the possibility to use and improve the micrometer TiO_2 powders, assuming that they have been used as photocatalysts never before. Acetone, acetaldehyde and toluene photodegradation kinetics have been performed in order to arrive for the purpose. Acetone and acetaldehyde are hydrophilic and polar pollutants that usually are present in high concentration in indoor environment, and they have been firstly investigated. The acetone reaction pathway passes through the formation of acetaldehyde as by-product (Fig. 3.7).

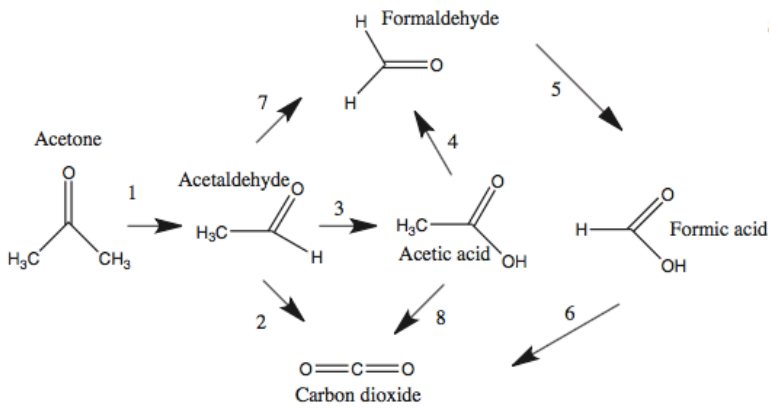

Fig. 3.7: Acetone oxidation reaction pathway (Stengl et al., 2010)

The fact that acetaldehyde reaction time is lower than acetone time in all cases is completely in agreement with this hypothesis (see the table 3.5, second and third column, in which the exact reaction time degradation are reported). Table 3.5 reports the summary of all the final results obtained in term of pollutant degradation time, or maximum percentage of degradation reached in the time available. The nano-sized samples exhibit high photocatalytic efficiency as expectation. They are able to give the complete degradation of the pollutants despite their high starting concentrations, in particular the complete degradation is reached after 60 min in the case of acetone and in 50 min for acetaldehyde. FTIR measurements on the sample surface after the kinetic runs confirm the absence of adsorbed by-products for P25, PC105 and 1077. Thus, the only by-product of reaction is CO_2 and this confirms the complete degradation of both acetone and acetaldehyde. However, the behavior of AT-1 sample is different, because it leads to an incomplete degradation of both the organic molecules. The most interesting result is that obtained with 1077 sample, because it shows an increased reaction time of only 15-30% compared to P25, despite to the low surface area. Another remarkable result is related to PC105, for

which it is possible to find a very strong correlation between the high photocatalytic activity and the high OH concentration at its surface revealed by XPS studies (Fig. 3.3). However, considering only OH/O_{tot} ratio, the catalytic results presents some disagreements. Indeed the micro-sized samples have higher hydrophilicity/hydrophobicity ratio than P25, while acetone and acetaldehyde photodegradation follows the classical trend that the smaller is the crystallite size the faster is the photocatalytic kinetic (tab. 3.5). In general, the photocatalytic behavior of a TiO_2 sample is influenced by the growth of its crystallites, because it is strongly related to the construction of the reactive sites at its surface. Nano-crystals have more numerous coordinately defects sites compared to micro-sized crystals, thus it is possible to conclude that the surface reactivity depends on the OH/O_{tot} ratio, as that the importance of OH groups might be determined by the TiO_2 crystallite size (i.e. different crystallite size is related to different kind of OH, more or less active for the photocatalytic reaction).

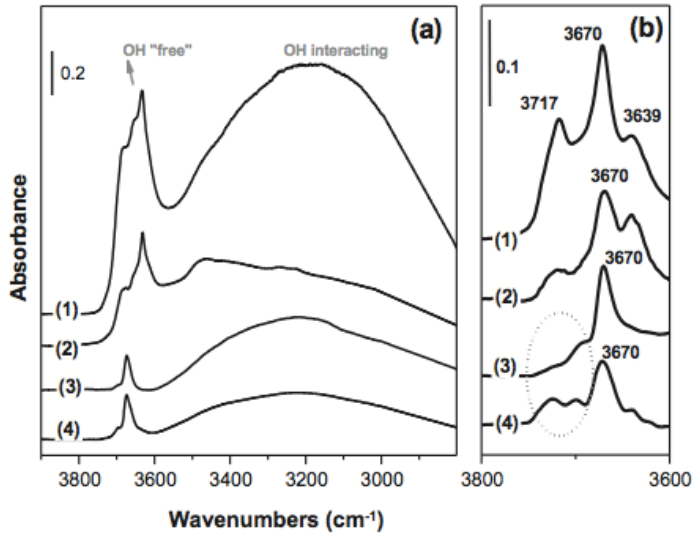

Fig. 3.8: Absorbance IR spectra relative to the O-H stretching spectral region of 1) PC105, 2) P25, 3) 1077, 4) AT-1; section a) samples outgassed at RT; section b) samples activated at 300°C.

The FTIR spectra already presented in Fig. 3.8 (OH spectral range 3900–2800 cm^{-1}) give more information about this kind of correlation. All the TiO_2 powders exhibit two complex absorption bands, respectively located in the 3000–3450 cm^{-1} range and at $\nu \geq 3600$ cm^{-1}. The first envelope refers to the ν_{OH} of all H-bonded OH groups present at the surface of the solid, according to the literature data, and the second one corresponds to the stretching mode (ν_{OH}) of all Ti-OH species free from hydrogen bonding interactions (L.H.Little, 1966; C. Morterra, 1988; C. Morterra, V. Bolis et al., 1989). Comparing the OH profiles of the different samples, it can be stated that the total amount of OH species (both free and H-bonded) present at the surface of PC105 is definitely higher than for all other TiO_2 (see curve 1), in agreement also with the XPS results, and the signals relative to the free OH species appear more complex in the case of the two nano-sized samples (see curve 1 and 2). Then, the activation of the samples in vacuum at 300°C (fig. 3.8, section b) allows to better identify the components present at higher ν, particularly because this treatment removes the specific ν_{OH} signals of the adsorbed water. The bands observed at $\nu \geq 3680$ cm^{-1} indicate the linear Ti-OH species, while the bands at lower frequencies can be related to Ti-OH-Ti bridged species. Overall, it is possible to point out a specific family of bridged OH groups (located at ~3670cm^{-1}), which is predominant. Particularly for nano-sized TiO_2 there is a clear presence of the signal around 3640 cm^{-1}, which highlights that the Ti-OH-Ti bridged species are located in different coordination environments, and the specific comparison between nano and micro-TiO_2 in the region at $\nu \geq$ 3680 cm^{-1}, still clearly shows that the nanometric samples are characterized by a significant higher amount of terminal Ti-OH species. The comparison between the micrometric samples only can better

explains their slight different photocatalytic performances. Indeed, there is a different ratio between the family of bridged-OH species at 3670 cm^{-1} and the families of terminal OH groups located at 3723 and 3700 cm^{-1}, which is definitely higher for the 1077 sample. Generally, the higher is the amount of Ti-OH-Ti bridged groups, the higher is the photocatalytic efficiency toward the degradation of acetone and acetaldehyde. However the linear Ti-OH species have a less relevant impact on the samples activity. Comparing to acetone or acetaldehyde, toluene is firstly a less polar and less hydrophilic molecule, and its degradation results more difficult because of the presence of the aromatic ring. Indeed, the molecule cannot be completely degraded even after 6h of reaction, both using nano or micro-TiO_2 (results reported in tab. 3.5). The most interesting point is that the degradation percentages fall more or less in the same range (46–52%) with a slightly higher value for the P25 system. Moreover, a general rather low amount of CO_2 formation verifies the fact that the degradation reaction is incomplete.

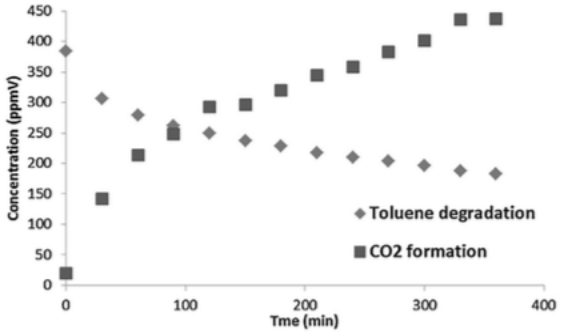

Fig. 3.9: Specific trend of toluene concentration (ppm) and CO_2 formation (ppm) over time.

The possible scheme of toluene oxidation has been already proposed by Ardizzone et al. (S. Ardizzone et al., 2008) and it is reported in fig. 3.10.

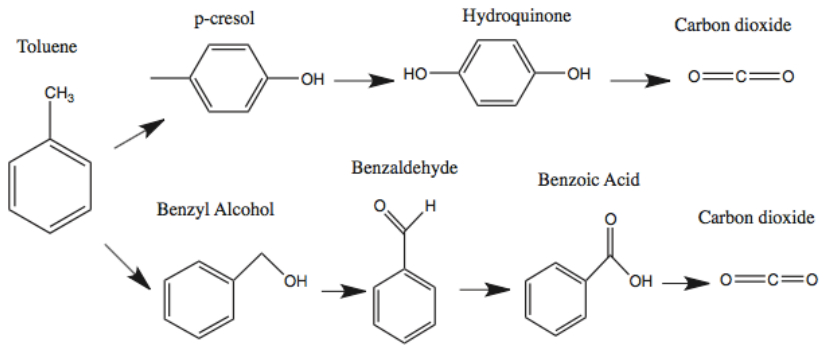

Fig. 3.10: Toluene oxidation reaction pathway.

The formation of the various by-products and their eventual adsorption on the TiO_2 sample surfaces has been deeply investigated by means of FTIR measurements. Fig. 3.11 reports the related spectra, particularly referred to PC105 as nano-reference and 1077 as micro-reference sample.

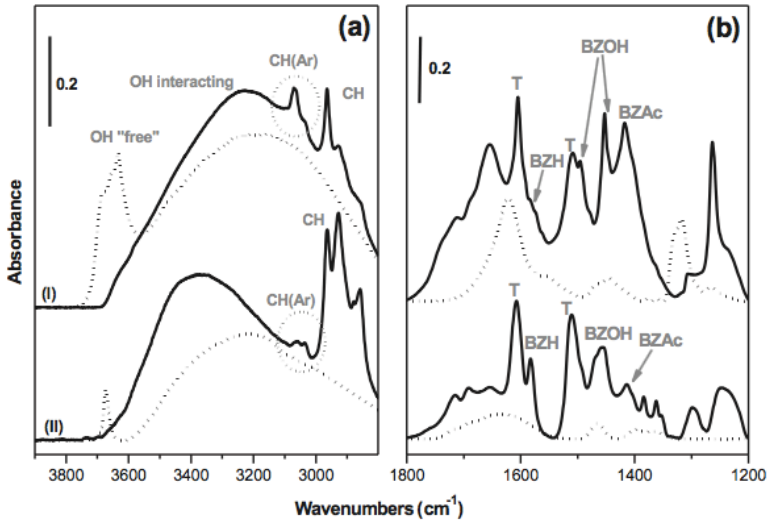

Fig. 3.11: Absorbance IR spectra in the 3900-2800 cm^{-1} (a) and 1800-1200 cm^{-1} (b) spectral regions; dotted lines refer to fresh samples and full lines refer to used samples; (I) nano-sized PC105; (II) micro-sized 1077. Abbreviations are explained in the text.

The spectra have been collected on both fresh and used TiO_2 samples in the 3900–2800 cm^{-1} and 1800–1200 cm^{-1} spectral ranges, reporting only

the spectra of PC105 and 1077 as references, being the behavior of the other two materials substantially coincident if the particles size is the same. Changes in the "before and after" spectra are evident and show firstly the total disappearance of the signals due to the stretching mode of Ti-OH species free from hydrogen bonding interactions with the parallel increase of the broad envelope generated by H-bonded OH groups, and secondly the formation of a new complex of bands located in the 3150–2850 cm^{-1} range, which is particularly related to the ν_{CH} stretching modes of CH-containing species of either aliphatic or aromatic nature (N.B. Colthup et al., 1975). At lower frequency (1800–1200 cm^{-1} range) new components appear in the spectrum and this underlines the formation of new adsorbed surface species generated during toluene degradation, according to the reaction profile (Fig. 3.10). In particular, the signals of unreacted toluene are indicated with (T), while it is possible to recognize the signals of benzyl alcohol (BZOH), benzoic acid (BZAc) and benzaldehyde (BZH) respectively (S. Ardizzone et al., 2008; N.B. Colthup et al., 1975). Considering all the results, it is possible to state that the catalysts surface undergoes irreversible changes after the employment in the photodegradation reaction of toluene. The photo-active "free" Ti-OH sites participate to the reaction and for this reason they are completely absent at the end, and this is the main cause on the incompleteness of the toluene degradation reaction. Moreover, it is possible to understand better why both micro-sized and nano-sized materials have almost the same photocatalytic activity for hydrophilic VOCs.

3.3.3.2 Ethanol: results and kinetic model description.

Ethanol photodegradation tests have been performed on three different commercial TiO_2 samples, which are respectively P25, 1077 and A-HR. P25 in the reference for nano-sized powders, while 1077 and A-HR have been selected as micro-powders to study their behavior and to obtain more detailed information about the kinetic parameters involved in the ethanol photocatalytic degradation reaction.

3.3.3.2.1 Kinetic parameters

The ethanol degradation reaction follows the pathway presented in the reactions (1) and (2), as reported in literature (M. A. Albrecht et al., 2006).

$$\begin{cases} (1)\ CH_3CH_2OH_{ads} \xrightarrow{k_1} CH_3COH_{ads} \\ (2)\ CH_3COH_{ads} \xrightarrow{k_2} 2CO_2 + H_2O \end{cases}$$

We considered two consecutive first order reactions to obtain the regression of the kinetic parameters, and here we report specifically the differential equation system.

$$\begin{cases} \dfrac{dn_e}{dt} = -k_1 \dfrac{K_e n_e}{1 + K_e n_e + K_a n_a} \\ \dfrac{dn_a}{dt} = +\dfrac{k_1 K_e n_e - k_2 K_a n_a}{1 + K_e n_e + K_a n_a} \\ \dfrac{dn_{CO_2}}{dt} = +2k_2 \dfrac{K_a n_a}{1 + K_e n_e + K_a n_a} \end{cases}$$

In detail, K_e and K_a (mol^{-1}) are the adsorption constant for ethanol (e) and acetaldehyde (a), and k_1 and k_2 (mol min^{-1}) are the first order kinetic constants. Considering reversible adsorption for both ethanol and acetaldehyde, the adsorption constant (K_i) was obtained, using the reported differential equation,

$$\frac{dn_i}{dt} = -k_{ads,\,i} n_i + k_{des,\,i}(n_{0,\,i} - n_i)$$

in which $n_{0,i}$ is the moles of the component charged in the reactor and n_i is the moles of the component at a certain time.

3.3.3.2.2 Photolysis, adsorption and photocatalytic degradation tests

In order to determine the real role of the photocatalytic process, both photolysis and simple ethanol absorption were investigated, concluding that the photolysis contribution is negligible. However, the role of absorption is different, as clear in Fig. 3.12.

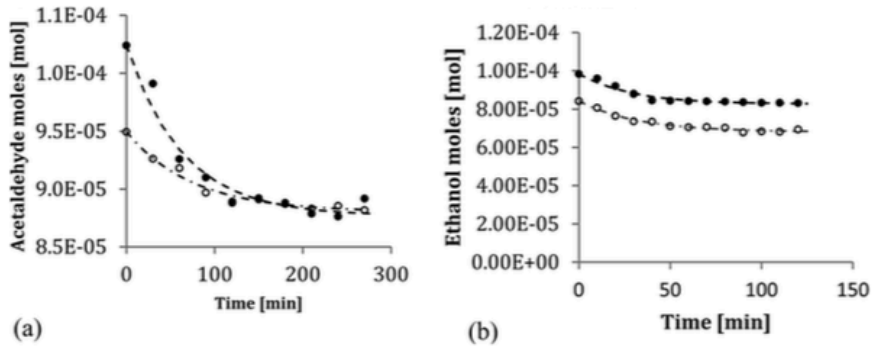

Fig. 3.12: Adsorption tests of acetaldehyde (a) and ethanol (b) using P25 (white dots) and 1077 (black dots).

In particular, as reported in table 3.6, the values of the calcualted adsorption constants are rather different.

Adsorption constant K (mol^{-1})			
Component	P25	1077	A-HR
Ethanol	0.2373	0.1891	0.1884
Acetaldehyde	0.0786	0.1680	0.1809

Tab. 3.6: Adsorption constants regressed from experimental data

P25 possesses a higher adsorption constant for ethanol if compared to that exhibited by both micrometric samples. On the contrary, acetaldehyde results show an opposite trend and the adsorption of these species seems to have no relation with the OH/O_{TOT} surface ratio of the catalyst.

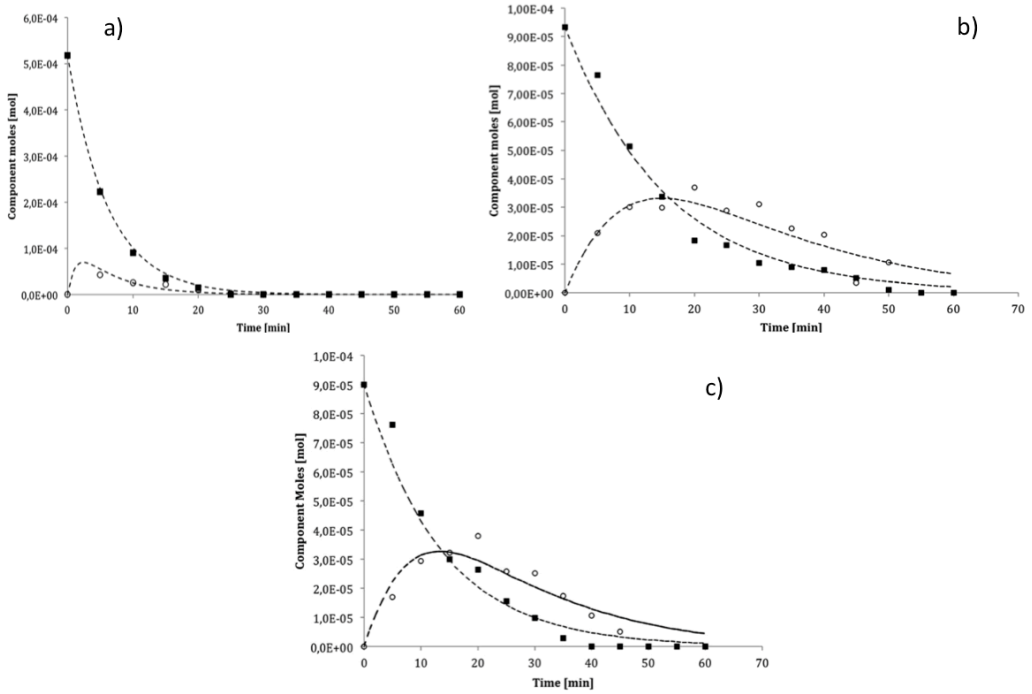

Fig. 3.13: Experimental ethanol photodegradation tests performed using a) P25, b) 1077, c) A-HR photocatalyst respectively. Empty points refer to

acetaldehyde and dotted lines are the simulated trends obtained using the regressed kinetic constants.

In Fig. 3.13 the experimental data obtained in the photocatalytic runs performed using the different catalysts (a,b,c for P25, 1077 and A-HR respectively) have been reported, together with the calculated trend using the optimized kinetic parameters (reported in tab. 3.7).

Sample	K_1 (mol min^{-1})	K_2 (mol min^{-1})	SSE
P25	0.68	10.41	3.91×10^{-9}
1077	0.34	0.42	1.69×10^{-9}
A-HR	0.39	0.42	6.88×10^{-9}

Table 3.7: Regressed kinetic constants for all photocatalysts

SSE refers to the sum of the squared errors, and values can be considered low for all samples. Thus, simulated results have a good fit for all the performed tests. The numerical values of the kinetic constants are clear higher for P25, in agreement with its better photoactivity. In particular, its k_2 value that is one order of magnitude larger than k_1, explains the reason why using nano-samples the degradation of acetaldehyde is absolutely faster than the ethanol conversion. Micrometric samples instead show a complete different behavior, indeed k_1 and k_2 values are rather similar. According to the general trend, even in case of ethanol the rate of the organic molecule degradation is increased using smaller TiO_2 particles, and this phenomenon is particularly significant for light compounds like acetaldehyde. Nevertheless, the catalytic properties of micrometric samples are confirmed from both the direct experimental conversion and this kinetic interpretation, with photocatalytic performances not so far from those reached using the classical nanometric TiO_2. FTIR

investigation has been performed in order to see eventual residues onto the support surfaces (spectra are reported in Fig. 3.14).

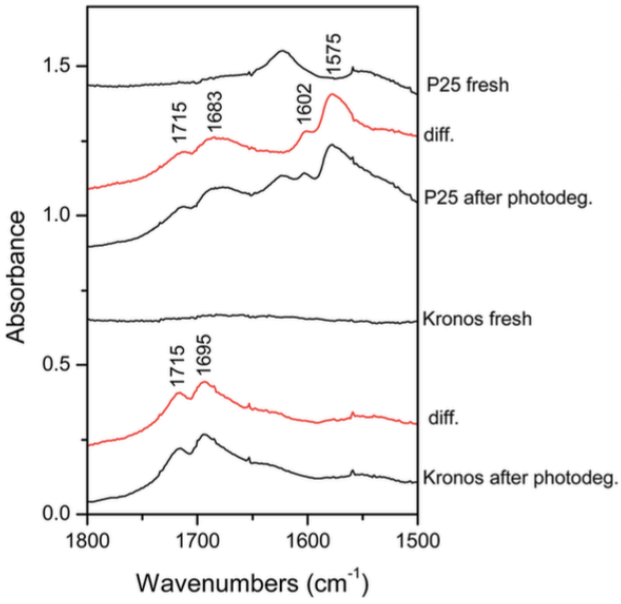

Fig. 3.14: Absorbance FTIR spectra relative to fresh and used P25 (top) and 1077 (bottom) for ethanol degradation reaction. Red lines refer particularly to the differences between spectra before and after the ethanol degradation. (A-HR is not reported because its behavior was similar to 1077).

The possible degradation products of ethanol (i.e. ketone/aldehyde) are normally located in the spectral range of 1800–1500 cm^{-1} (L. H. Little, 1966). Two net components are evident at ~1715 and ~1695.83 cm^{-1}, so traces of the degraded products are still present at the surface of the TiO_2 powders. Moreover, for the P25 material, other spectral components located at ~1602 and ~1575 cm^{-1}, reveal the presence of short chain carboxylate species (i.e. acetate or formate species) chemisorbed to the TiO_2 surface. This provides evidence of the formation of acetic acid as an intermediate in acetaldehyde degradation, particularly in case of P25.

3.3.3.3 Formaldehyde degradation reactions in gas phase

Formaldehyde has been selected because it presents several peculiarities that make it particularly interesting. As already said, formaldehyde is a pollutant really ubiquitous and it is maybe one of those with whom people really getting in contact, everyday, even unconsciously. Formaldehyde is harmful and this is a matter of fact (J.L. Shie et al., 2008), but because of the difficulty in monitoring there are very few strategies to analyze and remove it. From a photocatalytic point of view, formaldehyde is not a molecule that has already been deeply investigated, as well as there are still no publications about innovative materials (TiO_2-based, photocatalytically active materials) able to be effective for this pollutant. From the point of view of the setup and the analytic system to study the formaldehyde degradation kinetics, humidity and temperature are two key parameters. The relative humidity (RH) has been steadily controlled and kept constant, as well as for each kinetic the initial and final temperature has been measured. After 30 minutes of UV irradiation, temperature increased by 2 °C degrees and remains stable for the whole duration of the reaction.

3.3.3.3.1 Formaldehyde photolysis and degradation kinetics

In case of formaldehyde, 1077 by Kronos has been selected as reference for micrometer TiO_2-powders, and particularly it has been compared with P25 and PC105, which are two of the most nanosized photoactive TiO_2 samples.
The first investigation has been carried out on the formaldehyde photolysis reaction, evaluating the relative humidity (RH) inside the reactor as well; at the beginning of each test, the reactor was loaded with

a continuous and controlled flow of gaseous formaldehyde up to the set concentration. The contribution of the formaldehyde photolysis was negligible. After testing each commercial TiO_2 powders, using obviously the same conditions (see experimental part, chapt. 2, par. 2.4 and 2.4.1) in term of starting concentration, irradiation power, and reaction time, it is possible to conclude that and all samples are able to reach good values of formaldehyde conversion, in case of a starting concentration around 500 ppbv. In particular, figure 3.15 reports the trend of formaldehyde concentration over time during the UV irradiation, starting from the time of lamp ignition.

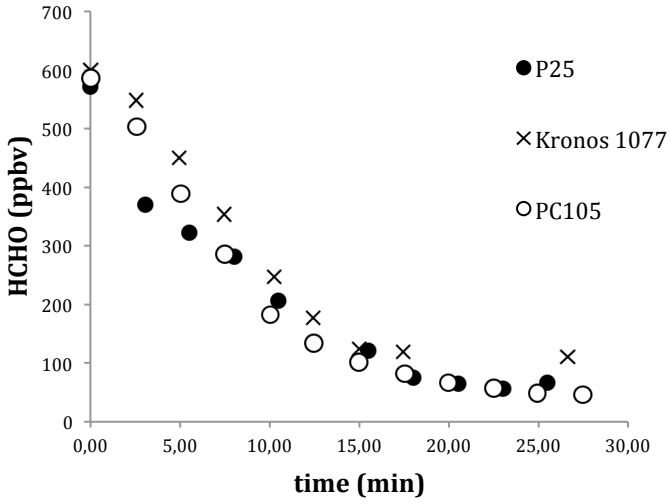

Fig. 3.15: HCHO (ppbv) concentration over time using P25 (black dots), 1077 (crosses) and PC105 (white dots) as photocatalysts. The reactor was irradiated by UV light (intensity 30Wm^{-2}) and the starting HCHO concentration was 500 ppbv.

As clear from the kinetics trend, for a formaldehyde concentration up to 500 ppbv, the morphological differences between the three TiO_2 catalysts do not almost affect the abatement of the pollutant, although the results are consistent with the respective values of surface area, because using

1077, the final value is slightly higher than the others. Degradation percentages reached after 30 min of photocatalysis using different TiO_2 samples are different. The micrometric sample is able to oxidized the 80% of formaldehyde, P25 reaches 89% of degradation, and using PC105 formaldehyde is almost completely degraded (90% of conversion). Therefore, preliminary tests on the commercial powders claim that the micrometric 1077 is effective and exploitable for this kind of application. The situation changes when the starting formaldehyde concentration rises to values of thousand of ppb, namely reaching the order of magnitude of part per million (ppm). Formaldehyde degradation kinetic reactions are showed in Fig. 3.16.

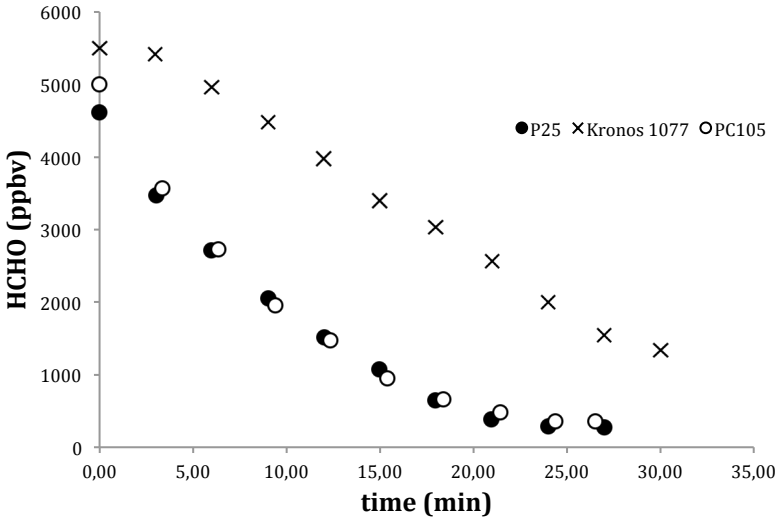

Fig. 3.16: HCHO (ppbv) concentration over time using P25 (black dots), 1077 (crosses) and PC105 (white dots) as photocatalysts. The reactor was irradiated by UV light (intensity $30Wm^{-2}$) and the starting HCHO concentration was 5000 ppbv.

Starting from higher formaldehyde concentrations, as in the kinetics show in fig. 3.16, morphological differences mainly affect the final result, and in particular the conversion reaches with the micrometric

sample is clearly lower. In case of high formaldehyde concentrations, the TiO_2 available surface area becomes crucial. Indeed, only a high TiO_2 surface area guarantees the sufficient number of active sites, in order to have a good level of adsorption pollutant, and a consequent good performance of the reaction. The adsorption of the organic molecule on the photocatalyst surface is always the first step of each photocatalytic reaction. If organics concentration is not overly high, the different surface area value of P25 and PC105, and 1077 respectively, does not imply the achievement of such changed final results. The effect is clear when concentrations are rather than high. As in case of the other organic molecules, working with a rather high starting pollutant concentration allows to more easily monitor the formation of by-products, being their concentration higher and thus detectable. Overall, this is an issue that the instrument here used, i.e. PTR-MS, completely solvers. Indeed one of the main advantage of this technique is the possibility i) to monitor several molecules simultaneously, as well as ii) monitor and detect low organics concentrations, until sub-ppb or ppt values. One of the main by-product of the formaldehyde oxidation to CO_2 is formic acid. Formic acid has been monitored during the formaldehyde degradation reaction at concentration of 5000 ppbv. Fig. 3.17 reports the formic acid trend over time.

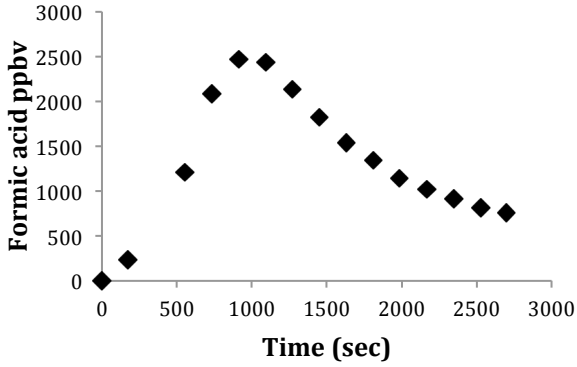

Fig. 3.17: Formic acid formation and degradation over time using 1077 as photocatalyst. The starting formaldehyde concentration is 5000 ppbv; UV irradiation with light intensity of 30Wm^{-2}.

Two are the main considerations important to underline. Firstly, the fact that formic acid is confirmed a by-product of formaldehyde oxidation; indeed, figure 3.17 clearly shows the increase of its concentration over time during the first part of reaction, when formaldehyde starts to convert into formic acid, increasing its concentration. Then, the degradation proceeds to the complete oxidation to CO_2 and even the formic acid is converted. Fig 3.17 reports in particular the formic acid trend using the micrometer powder of TiO_2, in order to demonstrate that even the bigger particles are able not only to convert formaldehyde, but they are able to degrade by-products as second step.

3.3.3.3.2 Reaction rate and kinetic constants evaluation

As the speed of a photocatalytic reaction depends on known parameters, i.e. such as catalyst surface area and particle dimensions, crystallographic phases and distribution of the OH free radical species on the surface, the results are consistent with the main features of the powders. Both P25 and PC105 systems reach the best results in less time if compared to the micrometer 1077 sample; however, even the micro-

sized powder shows good results also at higher concentration of formaldehyde, even if degradation process is slower. It is possible to better analyze the various reaction rates using the well-know Langmuir-Hinshelwood kinetic model (C.T. Campbell et al., 1922; J. Wintterlin et al., 1997; K. Vasanth Kumara et al., 2008). Reaction can be considered a first order reaction. The kinetic model provides that the rate of a heterogeneous reaction is controlled by the reaction of the adsorbed molecules, and that all adsorption and desorption pressure are in equilibrium. Langmuir–Hinshelwood (LH) kinetics is the most commonly used kinetic expression to explain the kinetics of the heterogeneous catalytic processes. The Langmuir–Hinshelwood expression that explains the kinetics of heterogeneous catalytic systems is given by eq. 3.1 here reported.

$$r = - dC/dt = (k_r K C) / (1+KC') \qquad (3.1)$$

"r" is the reaction rate, which becomes r_0 if related to the specific initial reaction rate as reported in eq. 3.2.

$$r_0 = k_r K C_0 / 1 + KC_0' \qquad (3.2)$$

The kinetic constants (k h^{-1}) have been calculated from data collected in formaldehyde photodegradation. The precise values obtained for each commercial sample are reported in table 3.8.

	P25	**PC105**	**1077**
Kinetic constant (h^{-1})	4.5427 h^{-1}	6.5115 h^{-1}	2.7298 h^{-1}

Tab. 3.8: kinetic constants values calculated from the experimental data

As expected, values related to the nanometric samples are higher, so the results can be considered consisted with the experimental tests.

3.3.3.4 Gas-mixtures of organic molecules: photocatalytic tests

The possibility to study the TiO_2 photocatalysts behavior, when they are subjected simultaneously to many molecules, is something absolutely understudied, as well as is maybe the closest context to real conditions. The same commercial samples exploited for formaldehyde degradation, i.e. P25 and PC105 for nano-, and 1077 for micro-sized respectively, are here tested in a specific atmospheric environment, in which a series of aldehydes or VOCs (see experimental part for the specific list, tables 3.1 and 3.2) are concurrently present.

3.3.3.4.1 Photocatalytic degradation of an aldehydes gaseous mixture using TiO_2 commercial samples in powder

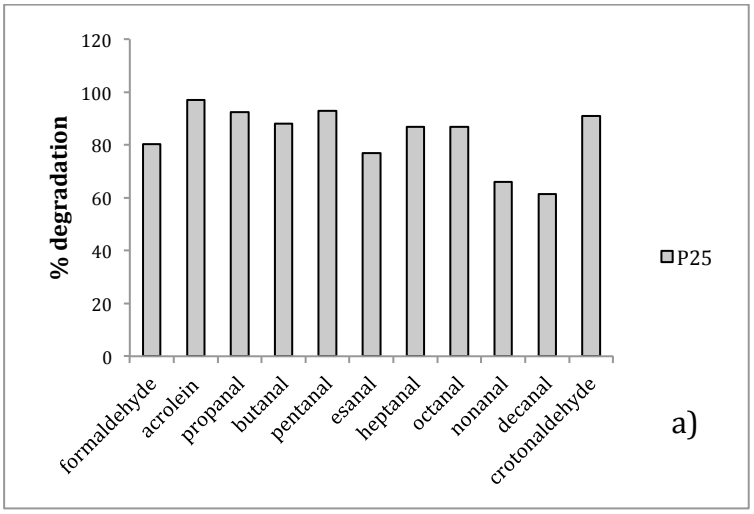

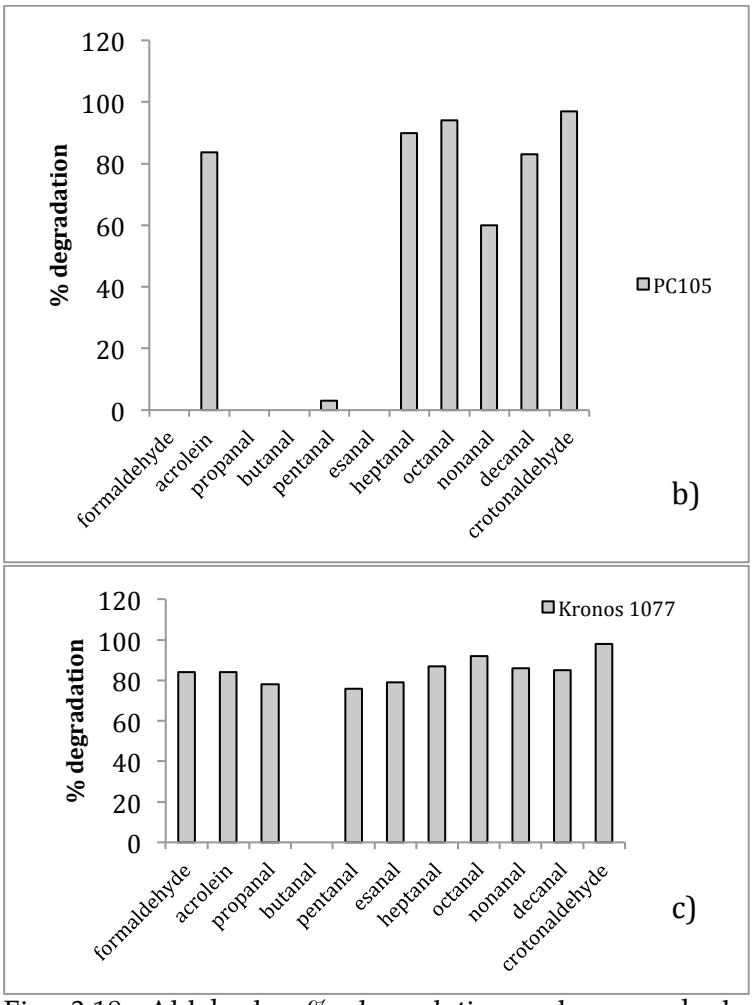

Fig. 3.18: Aldehydes % degradation values reached after 30 min of UV irradiation using a) P25, b) PC105, c) 1077; the empty columns refers to the aldehydes that are formed as by-products during the reaction process.

In an atmospheric environment characterized by the simultaneous presence of more than one molecule, in this case aldehydes, different TiO_2 powders lead to rather different final results. However, the really interesting outcome is that the overall performances of the catalysts are comparable, both for nano and micro-sized TiO_2. There are specific differences for specific molecules, which will be explained in the next lines. In general P25 is able to photodegrade all the aldehydes, reaching average conversion percentages higher than 70% for all the organics.

Using PC105 or 1077, the trend of the various aldehydes follows a different pathway: the crucial difference is that some molecules are formed in the first part of the kinetic and then degraded. Figure 3.19 shows the specific trend of propanal, butanal and hexanal, respectively.

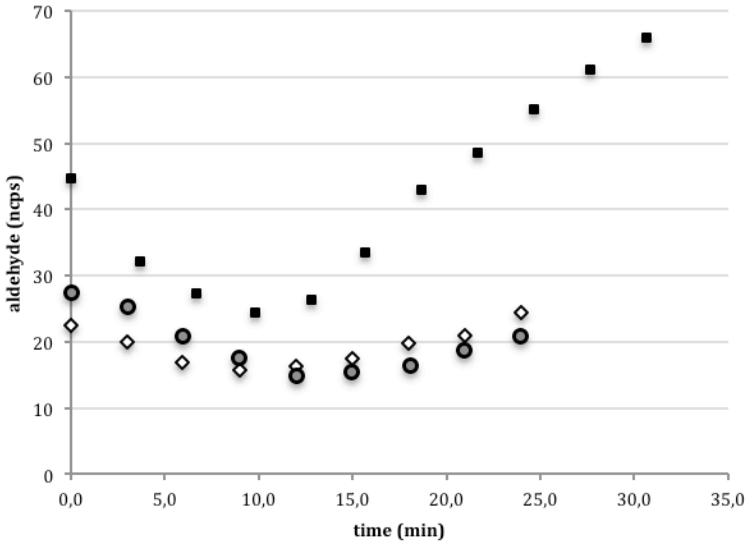

Fig. 3.19: Propanal (white rhombus), butanal (black squares) and hexanal (grey dots) trends over time, during the gaseous mixture of aldehydes photodegradation using PC105 as catalyst.

Figure 3.20 reports the specific trend of butanal, using 1077 as photocatalyst.

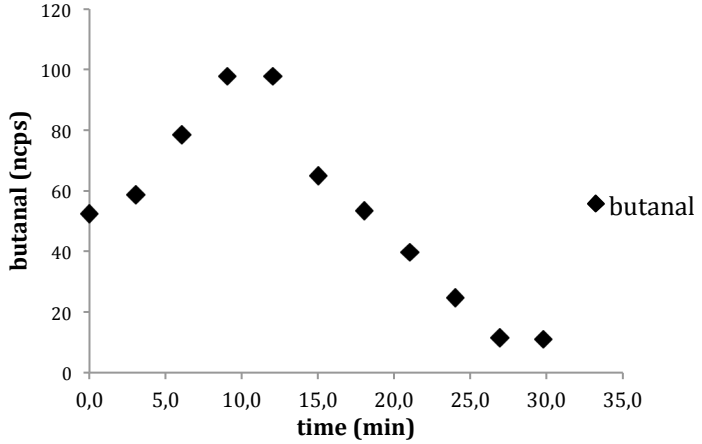

Fig. 3.20: Butanal trend over time during the photodegradation kinetic of the gaseous mixture of aldehydes, performed using 1077 by Kronos as TiO_2 catalyst.

PC105 differs from P25 both for particles size and crystallographic phase composition (C.L. Bianchi et al., 2015). The formaldehyde degradation process using this particular catalyst leads to the increase of butanal, propanal and hexanal respectively. Although its lower surface area, and even stressed with a mixture of pollutants, 1077 reaches lower degradation percentages in comparison with the nanometric samples on one hand, but it is able to degrade almost all of it in 30 minutes. Moreover, despite the initial increase of butanal as main by-product, 1077 is able to degrade it, is a sort of second-step of degradation. Therefore, considering the performances obtained overall, P25 is the more efficient photocatalyst, but considering price, particles dimension, and the possible dangerousness due to the presence of nanoparticles, performance obtained with the micrometric 1077 are absolutely more interesting.

From the point of view of the by-products formation, butanal increases both using PC105 and 1077, while it is degraded using P25. More in detail, the reason why using different photocatalysts we obtain different aldehydes degradation pathways, is to be found in the main features of

the different TiO_2 powders. First of all, the differences obtained comparing P25 and PC105, which are both nano-sized samples, come from the different OH radicals population on their surfaces. The OH free radicals on the catalyst surface are the key species that control the organic molecules adsorption, which is in turn closely related to the degradation reaction pathway. A huge number of active sites leads to a better adsorption, but consider also the interaction force between the organic species and the OH radicals is crucial. The starting very high activity of a sample as PC105 leads to the easy formation of several by-products, thus the next reabsorption to instantaneously convert also these species to CO_2 is more difficult. The final result is thus worse. This kind of competition between by-products is less significant using a 1077, maybe because of its low surface area, which in this specific case is not a drawback.

3.3.3.4.2 Photocatalytic degradation of aldehydes using photoactive tiles

Two different type of photoactive tiles have been selected and tested on the formaldehyde degradation first, and then on organic mixtures. As presented in the experimental part, the photoactive tile prepared by the classical TiO_2 deposition method is the sample Z23, while S24 refers to the TiO_2-photoactive ceramic tile obtained by Digital Printing deposition process.

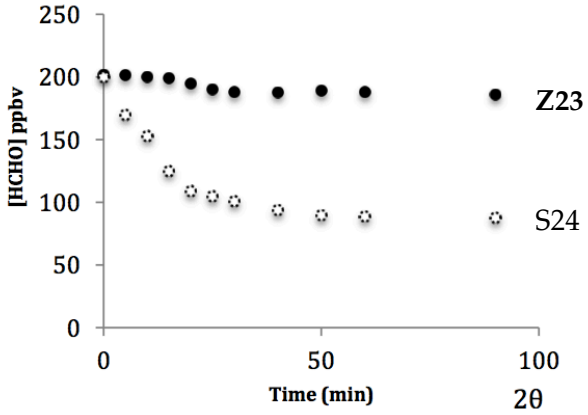

Fig. 3.21: Formaldehyde concentration (ppbv) over time using photoactive tiles as photocatalysts; Z23 (black dots); S24 (white dashed points); photocatalytic degradation reaction was performed under UV irradiation, the starting formaldehyde concentration is 200 ppbv and kinetic duration is 1 hour.

Figure 3.21 shows the first comparison in the formaldehyde photodegradation, obtained performing the photocatalytic tests firstly used the active tile prepared by spray method (Z23) and then using digital printing tile (S24). The clear different tiles behavior confirms the importance of the TiO_2 deposition method. In particular, the results prove that a more homogeneous surface in term of TiO_2 distribution is crucial to have a better performance in a short time. As a matter of fact the TiO_2 deposition by means of the classical method leads to an ineffective final material for the formaldehyde abatement. Digital printing photoactive tile degrades more than half of the formaldehyde loaded in the reactor, equal to 110 ppb (corresponding to 0.1 ppm) in 60 min. The Threshold Limit Value (TLV) is actually set at 0.3 ppm (0.37 mg/m^3), however a European proposal (SCOEL) aims to lower it to 0.2 ppm at least. Furthermore, considering that the average concentration of formaldehyde measured in most environments is 0.1 ppm, results attest that the digital printing photoactive tiles can be efficient to improve air quality. In general, even higher levels of formaldehyde can be easily

reached, that is the reason why each test was performed starting from a quite high formaldehyde concentration as already explained in other previous paragraphs. Starting from the preliminary conclusion that sample S24, obtained by digital printing, might be a good base development for photoactive materials able to improve the indoor air quality, the second step was testing it under conditions closer to reality. Thus, S24 was further tested on the photodegradation of a gaseous mixture of aldehydes. The mixture has been loaded in the reactor by means of a GCU (Gas Calibration Unit), and single-aldehydes concentrations have been followed simultaneously over time by PTR-MS instrument.

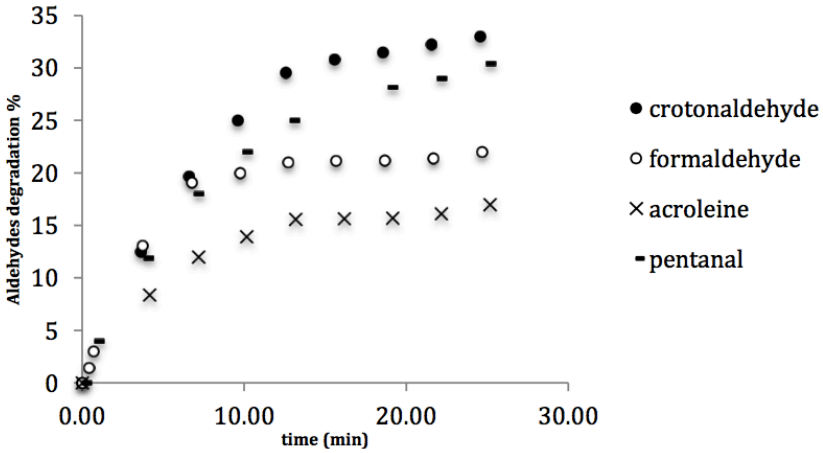

Fig. 3.22: Trend of the degradation percentages of randomly chosen aldehydes contained in the gas-mixture; photocatalytic degradation performed using Digital Printing S24 sample under UV irradiation.

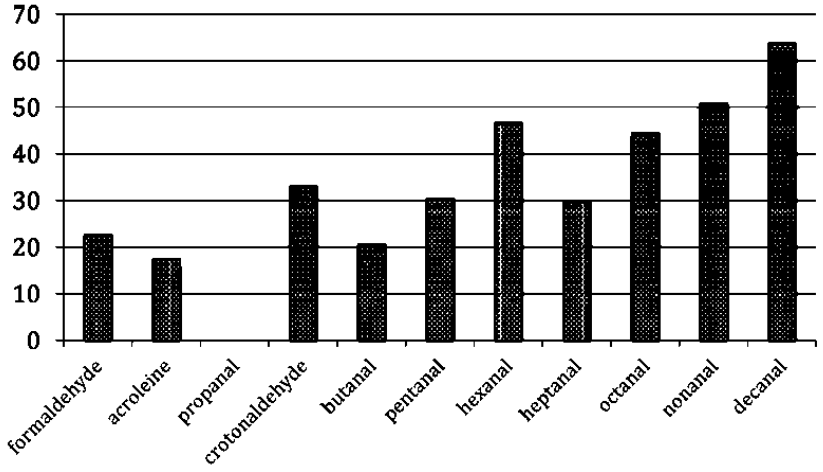

Fig. 3.23: Final degradation (%) of each aldehyde contained in the gas-mixture, after 30 min of UV irradiation in presence of Digital Printing tile S24 as photocatalyst.

In figures 3.22 and 3.23 we reported the results, summarized in particular in the second bar chart, with all the final degradation percentages obtained for each single aldehyde in the mixture.

3.3.3.4.3 Aldehydes degradation pathway and reaction mechanism

The photodegradation pathway of formaldehyde has been deeply studied (T. Noguchi et al., 1998), however the other molecules, particularly if they are simultaneously present in a gaseous mixture, have not been investigated truly in depth. Formaldehyde oxidation follows the already described pathway, in which formic acid is formed at the first step before being converted to carbon dioxide. Observing the results obtained in case of the aldehydes in which the carbon chain is longer and longer (fig. 3.22 and 3.23), the trend of the degradation percentages follow the length of the carbon chains, i.e. C10>C9>C8>C7, with a slight anomaly only for hexanal (C6). This is rather consistent with the radicalic photocatalytic degradation mechanism, in which the

terminal CH_3-CH_2 bonds are broken step by step. Thus, the shorter carbon chain aldehydes are the intermediate species of the longer aldehydes degradation (T.Shi et al., 2015), and they are simultaneously both degraded and generated. The fact that propanal is not degraded is only apparent. Indeed, it is well degraded but it is also a by-product of the degradation pathway of the upper aldehydes as shown in Fig. 3.24. The short duration of the reaction (stopped at 30 min to compare the results with tests performed on powdered TiO_2), in the present case allows better observing the accumulation of the by-products and appreciating the degradation pathway of the mixture.

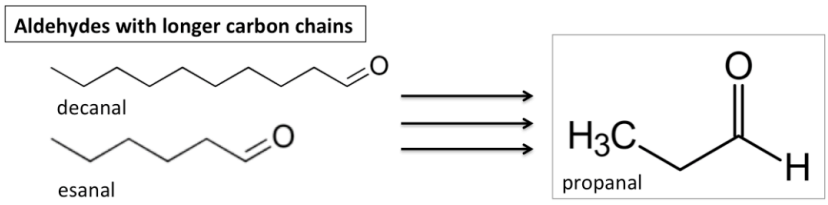

Fig. 3.24: degradation of aldehydes with long carbon chains.

Overall, starting from decanal, that progressively breaks in the shorter carbon chain aldehydes, it is possible to explain why decanal reaches the highest degradation percentage first, and then find a linear correlation with the results obtained for the other aldehydes, which are respectively by-products one of the other. Finally, interesting are also the chrotonaldehyde and acrolein, in particular because they are the only two aldehydes in the mixture that contain the double bond in the carbon chain, reason why they might be degraded less easily. However, their behavior respects the rule of the carbon chain length, with the degradation percentage of acrolein that is lower than chrotonaldehyde (C4>C3). See also fig. 3.25 in which chrotonaldehyde first degradation step is reported.

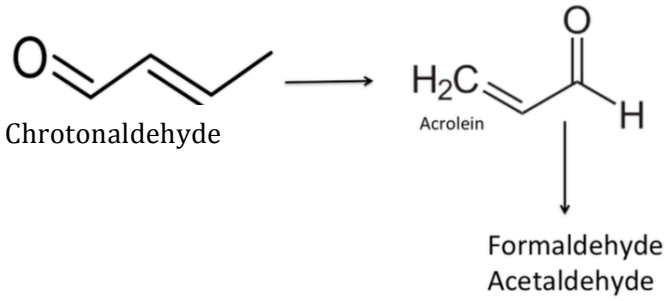

Fig. 3.25: Degradation pathway of chrotonaldehyde

In summary, the chain length and complexity of the molecule, its relative adsorption on TiO_2, the degradation pathway of the more complex aldehydes, and the by-products of their degradation, are the crucial points to explain the obtained results, which thus are consistent. Overall, the photoactivity of the Digital Printing photoactive porcelain grés tile is confirmed even when a mixture of molecules is simultaneously present highlighting the efficiency of this product to improve air quality in real life environments.

3.3.3.4.4 Photocatalytic degradation of a VOCs gaseous mixture

The degradation of a gaseous mixture of VOCs is very interesting because indoors are full of organics, as well as it completely exploits the ability of an instrument as the PTR-MS to detect a huge number of different molecule simultaneously. Moreover, this kind of tests completes the study about the general photocatalytic possibilities of S24 samples. VOCs mixture list was reported in table 3.2 (see experimental part).
Reaction kinetic has been followed monitoring the concentration of each volatile compound over time. Figure 3.21 shows the % degradation

reached over time for the most interesting VOCs molecules contained in mixture.

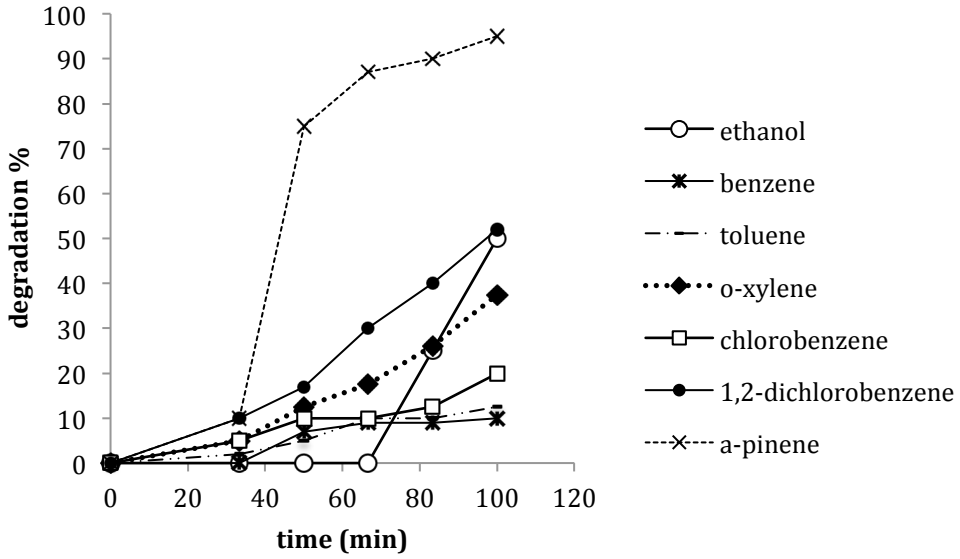

Fig. 3.21: degradation % over time of VOCs gaseous mixture. Kinetic reaction performed using the digital printing photoactive grés tile. Reactor has been irradiated by UV light.

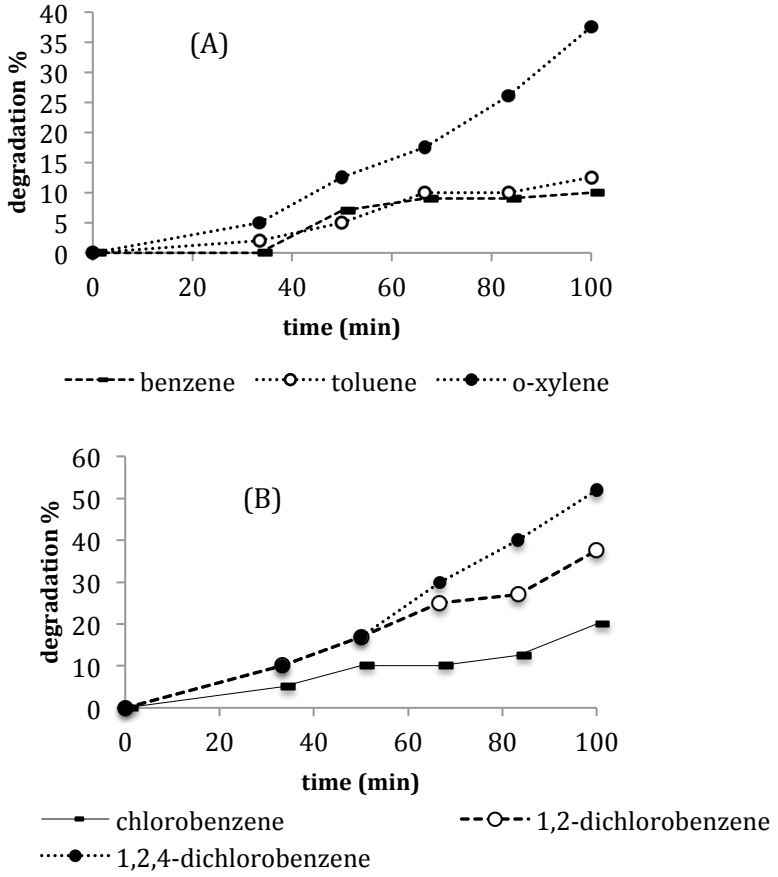

Fig. 3.22: Aromatic compounds degradation in the mixture (A); chlorinated compounds degradation in the mixture (B).

In fig. 3.22 (A), on the left, aromatic compounds degradation % over time is highlighted, as the specific kinetic of chlorinated compounds degradation is showed in fig. 3.22 (B), on the right. The behavior of these molecules in mixture is very interesting, and it is a preliminary result on which further tests could give very important information in term of photocatalytic activity of ceramic materials and reaction kinetic as well.

Additional considerations

As it clear from the results just now presented, the photocatalytic studies on the photodegradation of the VOCs mixture are preliminary and yet to be explored or more deeply investigated. Surely, they open the way for new specific photocatalytic studies on organic pollutants on one hand, as new studies of development even more efficient materials on the other.

3.4 conclusions

The present chapter compares first of all the photocatalytic performance of four commercial TiO_2 powders, two nano-sized and two-micro- sized materials, in the degradation of three important VOCs, representative of the indoor pollution. The primary conclusion we can reach is that the adsorption of the pollutant molecule at the semi-conductor surface promotes the photocatalytic reaction, and particularly for acetone/acetaldehyde or toluene, their adsorption on TiO_2 surface has been demonstrated to be a crucial point in affecting the subsequent photocatalytic activity. Strongly connected with the adsorption is the presence of the OH species on the TiO_2 surface. FTIR analysis of the •OH stretching region demonstrated that the Ti-OH-Ti bridged species play a key role in driving the photocatalytic activity of all the TiO_2 samples. Overall, the higher is the amount of Ti-OH-Ti bridged groups, the higher is the photocatalytic efficiency toward the degradation of acetone and acetaldehyde. The best photocatalyst for acetone and acetaldehyde is PC105, and nanometric samples are in general better than the micrometric ones. For toluene, which is less hydrophilic, the differences in particles size are not so important and the photocatalytic behavior is very similar for all samples. In particular, after the contact with toluene,

the photoactive "free" Ti-OH sites totally disappear, as a result of their participation to the reaction, explaining why toluene degradation appears incomplete even after 6 h of reaction for all the samples, regardless of the morphological features of the materials. Finally, these first tests allowed to demonstrate that micro-sized TiO_2 are efficient and they can replace the most used nano-TiO_2 powders.

The photodegradation of ethanol was performed using a commercial nanometric sample and two different micrometric powders. In this case, also the rate of reaction and the kinetic constants have been calculated starting from the experimental data. In particular, the good fitting between the experimental and simulated results confirms the assumption that ethanol photodegradation is a consecutive first order reaction, as well as the degradation is not influenced by the TiO_2 crystallite dimension.

The final aim of this work always refers to the possibility to use photocatalysis as a way to improve the air quality of the indoor environments, in particular against molecules that are ubiquitous and very dangerous for human health. This is the main reason why, after reference VOCs molecules such as acetone, toluene or ethanol, formaldehyde photocatalytic degradation was investigated. Moreover, photocatalytic tests on mixture of aldehydes or VOCs respectively have been performed, particularly because in these conditions there is the possibility to evaluate the real photocatalysts performance, as it was used in a real-life environment. Indeed, in a real environment TiO_2 is never in contact with just a single molecule. Furthermore, the behavior of each TiO_2 powder may be different when more than one molecules is present. From the point of view of the semiconductor, the use of TiO_2 photocatalysts, even in the form of micro-sized particles, seems very promising: formaldehyde is removed rapidly and efficiently even if the

initial concentration is far above the values expected in any practical application. Finally, when a mixture of pollutants is present, we observe that: i) in the case of the PC105 sample (which exhibits the highest SSA) different by-products are formed; ii) 1077, even if micrometric and with a much lower SSA, is the only one that leads to a linear degradation of all the organic molecules present in the gaseous mixture. This outcome allows to conclude that the micro-sized TiO_2 sample is able to reach very good results, despite its much lower SSA, because is precisely the lower surface area that leads to a more linear pollutants abatement.

The second part of the chapter regards the results obtained in case of TiO_2-based ceramic grés tiles. Digital printing technology has been exploited to cover the ceramic tile surface with a micrometric powder of TiO_2, obtaining a very homogeneous surface, a very good TiO_2 distribution and an even better photocatalytic performance. The photoactive tiles have been tested on formaldehyde as reference VOCs molecule first, but also on a gaseous mixture of aldehydes first, and then VOCs. This is important to simulate a real indoor environment. Even when exposed to a mixture of organics compounds, the digital printing photoactive grés ceramic tiles is effective and able to degrade them, breaking the more complex molecules in the relative by-products up to their complete oxidation to CO_2. Moreover, following the photocatalytic reaction kinetic of the gaseous mixture of aldehydes by means of PTR-MS instrument, it is possible to understand the real degradation pathways of the various pollutants even when they are mixed. In particular, aldehydes are destroyed in accordance to clear and linear sequences, in which the long-chain molecules are broken before. Also the preliminary results obtained for VOCs mixture allows to conclude that by digital printing technology is possible to get a material with a higher photocatalytic activity, as well as TiO_2 digital printing tiles are

able to work in an environment in which manifold organic molecules are concurrently present.

References

Addamo M., Augugliaro V., Coluccia S., Di Paola A., Garcia-Lopez E., Loddo V., Marcì G., Martra G., Palmisano L., "The role of water in the photocatalytic degradation of acetonitrile and toluene in gas-solid and liquid-solid regimes", Int. J. Photoenergy, **2006**, 1–12.

Albrecht M.A., Evans C.W., Raston C.L., "Green chemistry and the health implications of nanoparticles", Green Chem., **2006**, 8, 417–432.

Ao C.H., Lee S.C., Mak C.L., Chan L.Y., "Photodegradation of volatile organic compounds (VOCs) and NO for indoor air purification using TiO_2: promotion versus inhibition effect of NO", Appl. Catal. B, **2003**, 42, 119–129.

Ardizzone S., Bianchi C.L., Cappelletti G., Naldoni A., Pirola C., "Photocatalytic degradation of toluene in the gas phase: relationship between surface species and catalyst features", Environ. Sci. Technol., **2008**, 42, 6671–6676.

Atkinson R., Arey J., "Atmospheric degradation of volatile organic compounds", Chem. Rev., **2003**, 103, 4605-4638.

Bianchi C.L., Gatto S., Pirola C., Naldoni A., Di Michele A., Cerrato G., Crocellà V., Capucci V., "Photocatalytic degradation of acetone, acetaldehyde and toluene in gas-phase: Comparison between nano and micro-sized TiO_2", App. Cat. B: Envir., **2014**, 146 123–130.

Bianchi C.L., Pirola C., Galli F., Cerrato G., Morandi S., Capucci V., "Pigmentary TiO_2: A challenge for its use as photocatalyst in NOx air purification", Chem. Eng. J., **2015**, 261, 76-82.

Bianchi C.L., Gatto S., Pirola C., Scavini M., Vitali S., Capucci V., "Micro-TiO_2 as a starting material for new photocatalytic tiles", Cem. Concr. Compos., **2013**, 36, 116–120.

Bianchi C.L., Pirola C., Galli F., Stucchi M., Morandi S., Cerrato G., Capucci V., "Nano and micro-TiO_2 for the photodegradation of ethanol: experimental data and kinetic modeling", RSC Adv., **2015**, 5, 53419.

Bianchi C.L., Pirola C., Gatto S., Nucci S., Minguzzi A., Cerrato G., Biella S., Capucci V., "New surface properties in porcelain gres tiles with a look to human and environmental safety", Adv. Mater. Sci. Eng., **2012**, 8 pp.

Bianchi C.L., Pirola C., Selli E., Biella S., "Photocatalytic NOx abatement: the role of the material supporting the TiO_2 active layer", J. Haz. Materials, **2012**, 211-212, 203-207.

Brun E., Carriere M., Mabondzo A., "In vitro evidence of dysregulation of blood-brain barrier function after acute and repeated/long-term exposure to TiO_2 nanoparticles", Biomater., **2012**, 33, 886–896.

Campbell C.T., Ertl G., Kuipers H., Segner J., "A molecular beam study of the catalytic oxidation of CO on a Pt(111) surface", J. chem. Phys. (II) Langmuir, Trans. Faraday Soc., **1922**, 17, 621-672.

Cappelletti G., Bianchi C.L., Ardizzone S., "XPS study of the surfactant film adsorbed onto growing titania nanoparticles", Appl. Surf. Sci., **2006**, 253, 519–524.

Cerrato G., Bianchi C.L., Morandi S., Pirola C., Stucchi M., Diamanti M.V., Pedeferri M.P., Capucci V., "The role of the nano/microstructure in the case of

the photodegradation of two Model VOC pollutants using commercial TiO_2", En. Environ. Focus, **2015**, 4, 226–231.
Chen X., Burda C., "The electronic origin of the visible-light absorption properties of C-, N- and S-Doped TiO_2 nanomaterials", J. Am. Chem. Soc., **2008**, 130, 5018–5019.
Chen B., Shi C., Crocker M., Wang Y., Zhu A., "Catalytic removal of formaldehyde at room temperature over supported gold catalysts", App. Cat. B, **2013**, 132-133, 245-255.
Colon M., Pleil J.D., Hartlage T.A., Guardani M.L., Martins M.H., "Survey of volatile organic compounds associated with automotive emissions in the urban airshed of Sao Paulo, Brazil", Atmos. Environ., **2001**, 35, 4017–4403.
Colthup N.B., Daly L.H., Wiberley S.E., "Introduction to Infrared and Raman Spectroscopy", 2nd ed., Academic Press, New York, **1975**.
Creutzenberg O., "Biological interactions and toxicity of nanomaterials in the respiratory tract and various approaches of aerosol generation for toxicity testing", Inorg. Comp., **2012**, 86, 1117–1122.
Dahnke H., Vonbasum G., Kleinermanns K., Hering, P., Murtz, M., "Rapid formaldehyde monitoring in ambient air by means of mid-infrared cavity leak-out spectroscopy", Appl. Phys. B, **2002**, 75, 311-316.
Descamps M.N., Bordy T., Hue J., Mariano S., Nonglaton G., Schultz E., Tran-Thi T.H., Vignoud-Despond S., "Real-time detection of formaldehyde by a sensor", Sens. Actuators B, **2012**, 170, 104-108.
Derwent R.G., Jenkin M.E., Saunders S.M., "Photochemical ozone creation potentials for a large number of reactive hydrocarbons under European conditions", Atmos. Environ., **1996**, 30, 181–199.
Duboudin C., "Pollution inside the home: descriptive analyses. Part I: Analysis of the statistical correlations between pollutants inside homes", Environnement, risques & Santé, pp. 485-496, **2009**.
EPA, US Environmental Protection Agency, "Volatile organic compounds impact indoor air quality", retrieved from https://www.epa.gov/indoor-air-quality-iaq/volatile-organic-compounds-impact-indoor-air-quality.
EPA, US Environmental Protection Agency, "Formaldehyde standards for Composite Wood Products", retrieved from http://www.epa.gov/formaldehyde.
Gupta M., Tripathi M., "A review on the synthesis of TiO_2 nanoparticles by solution route", CE J.: Chem., **2012**, 10, 279–294.
Green C.J., Ndegwa S., "Nanotechnology: A review of exposure, health risks and recent regulatory developments", National Collaborating Centre for Environmental Health, **2011**.
IEH, Institute for Environment and Health, "IEH assessment on indoor air quality in the home", Institute for Environment and Health, Leicester, UK, **1996**.
Jones A.P., "Indoor air quality and health", Atmosph. Env., **1999**, 33, 4535-4564.
Jeong J., Sekiguchi K., Sakamoto K., "Photochemical and photocatalytic degradation of gaseous toluene using short-wavelength UV irradiation with TiO_2 catalyst: comparison of three UV sources", Chemosphere, **2004**, 57, 663–671.

Kirchner S., Derbez M., Duboudin C., Elias P., Grégoire A., Jédor B., Lucas J.P., Pasquier N., Ramalho O., Weiss N., "Indoor air quality in French dwellings", AIVC Contributed Report, 30p, **2009**.
Little L.H., Infrared Spectra of adsorbed Species ,AcademicPress ,London, **1966**.
Love S.A., Maurer-Jones M.A., Thompson J.W., Lin Y-S., "Assessing nanoparticle toxicity", Annual Review of Analytical Chemistry, **2012**, 5, 181–205
Lyu J., Zhu L., Burda C., "Considerations to improve adsorption and photocatalysis of low concentration air pollutants on TiO_2", Catal. Today, **2014**, 225, 24–33.
Macwan D.P., Dave P.N., Chaturvedi S., "A review on nano-TiO_2 sol–gel type syntheses and its applications", J. Mater. Sci., **2011**, 46, 3669–3686.
Marcì G., Addamo M., Agugliaro V., Coluccia S., Garcia-Lopez E., Loddo V., Marra G., Palmisano L., Schiavello M., "Photocatalytic oxidation of toluene on irradiated TiO_2: comparison of degradation performance in humidified air, in water and in water containing a zwitterionic surfactant", J. Photochem. Photobiol. A, **2003**, 160, 105–114.
Martins E.M., Correa S.M., Arbilla G., "Formaldehyde and acetaldehyde in a high traffic street of Rio de Janeiro, Brazil", Atmos. Environ., **2003**, 37, 23–29.
Morterra C., "An infrared spectroscopic study of anatase properties. Part 6. Surface hydration and strong Lewis acidity of pure and sulphate-doped preparations", Faraday Trans., **1988**, 84(5), 1617-1637.
Morterra C., Bolis V., Fisicaro E., "The hydrated layer and the adsorption of CO at the surface of TiO_2 (anatase)", Colloids Surf., **1989**, 41, 177–188.
Naldoni A., Allieta M., Santangelo S., Marelli M., Fabbri F., Cappelli S., Bianchi C.L., Psaro R., Dal Santo V., "Effect of nature and location of defects on bandgap narrowing in black TiO_2 nanoparticles", J. Am. Chem. Soc., **2012**, 134, 7600–7603.
Naldoni A., Bianchi C.L., Pirola C., Suslick K.S., "TiO_2 porous microsphere with tunable properties for air purification", Ultrason. Sonochem., **2013**, 20, 445–451.
Noguchi T., Fujishima A., Sawaunyama P., Hashimoto K., "Photocatalytic degradation of gaseous formaldehyde using TiO_2 film", Environ. Sci. Technol., **1998**, 32, 3831–3833.
Panessa-Warren B.J., Warren J.B., Wong S.S., Misewich J.A., "Biological cellular response to carbon nanoparticle toxicity", J. Phys.: Cond. Mat., **2006**.
Park S., Lee S., Kim B., Lee S., Lee J., Sim S., Gu M., Yi J., Lee J., "Toxic effects of titanium dioxide nanoparticles on microbial activity and metabolic flux", Biotechnol. Bioproc. Eng., **2012**, 17(2), 276–282.
Popken T., Gotze L. , Gmehling J., "Reaction Kinetics and Chemical Equilibrium of Homogeneously and Heterogeneously Catalyzed Acetic Acid Esterification with Methanol and Methyl Acetate Hydrolysis", Ind. Eng. Chem. Res., **2000**, 39, 2601–2611.
Roberts J., Nelson W.C., "National Human Activity Pattern Survey Data Base", United States Environmental Protection Agency (USEPA), Research Triangle Park, NC, **1995**.
Ryan D., Bowles L., "Safety and health in manufactured structures", US Department of Health and Human Service, retrieved from http://www.cdc.gov/healthyhomes/manufactured_structures.pdf.

Salthamer T., "Formaldehyde in the ambient atmosphere: from an indoor pollutant to an outdoor pollutant?", Angew. Chem. Int. Ed. Engl., **2013**, 52, 3320-3327.
Shi T., Chang W., Zhang H., Ji H., Ma W., Chen C., Zhao J., "H_2O-involved two-electron pathway for photooxidation of aldehydes on TiO_2: an isotope labeling study", Environ. Sci. Technol., **2015**, 49, 3024–3031.
Shie J.L., Lee C.H., Chiou C.S., Chang C.T., Chang C.C., Chang C.Y., "Photodegradation kinetics of formaldehyde using light sources of UVA, UVC and UVLED in the presence of composed silver titanium oxide photocatalyst", Journal of Hazardous Materials 155 (2008) 164–172
Song W., Venimadhavan G., Manning J. M., Malone M.F., Doherty M.F., "Measurment of residue curve maps and heterogeneous kinetics in methyl acetate synthesis", Ind. Eng. Chem. Res., **1998**, 37, 1917.
Stengl V., Houskova V., Bakardjieva S., Murafa N., "Photocatalytic degradation of acetone and butane on mesoporous titania layers", New J. Chem., **2010**, 34, 1999–2005.
US Environmental Protection Agency (EPA), "Indoor Air Quality", retrieved from https://www.epa.gov/indoor-air-quality-iaq, **2016**.
Vaajasaari K., Kulovaara M., Jouiti A., Schultz E., Soljamo K., "Hazardous properties of paint residues from the furniture industry", J. Hazard. Mater., **2004**, 106(A), 71-79.
Vasanth Kumara K., Porkodib K., Rocha F., "Langmuir–Hinshelwood kinetics – A theoretical study", Catal. Commun., *2008*, 9, 82–84.
Wang R., Hashimoto K., Fujishima A., "Photogeneration of highly amphiphilic TiO_2 surfaces", Nature, **1997**, 388, 431–432.
Wang X., Liu Y., Hu Z., Chen Y., Liu W., Zhao G., "Degradation of methyl orange by composite photocatalysts nano-TiO_2 immobilized on activated carbons of different porosities", J. Hazar. Mater., **2009**, 169, 1061–1067.
Wintterlin J., Volkening S., Janssens T.V.W., Zambelli T., Ertl G., "Atomic and macroscopic reaction rates of a surface-catalyzed reaction", Science, **1997**, 278.
Yang L., Kruse B.J., "Revised Kubelka–Munk theory. I. Theory and application", Opt. Soc. Am. A, **2004**, 21, 1933–1941.

CHAPTER 4:
PHOTOCATALYTIC DEGRADATION OF NITROGEN OXIDES

Abstract

Nitrogen oxides (NO_x) are the mains responsible for outdoor pollution with a rather important impact on human health, considering the more or less serious diseases that they can cause. Moreover, NO_x do not concern only people well being, but also the health of our planet, because of their well-known negative effects on vegetation. For all these reasons, EU defined specific Limit Values for NO_x, and can take action against any Member State if the air quality does not meet the Limit Values throughout its territory. It explains the importance of finding strategies to remove them. Heterogeneous photocatalytic oxidation easily converts NO_x in urban environments to nitrates, using TiO_2 as photocatalyst. This chapter is focused on the use of TiO_2 as a photocatalyst for removing NO_x gases from the atmosphere, with particular attention to TiO_2 particles size as presented for VOCs in the previous chapter. Although prove the efficiency of TiO_2 is nothing new, it was important to assess the properties of each individual commercial catalyst, especially because some of them were not produced for photocatalytic purpose. Secondly, the same tests were performed on the photocatalytic tiles prepared as described in the previous chapter, in order to study and evaluate their potential for the specific NO_x photodegradation. Photocatalytic tests were executed both in static condition and in continuous, taking the first step toward studies to test the TiO_2-modified materials in real condition. Moreover, tests were performed at two different and especially chosen NO_x concentrations, i.e. 1000 ppb, that is the specific concentration requested by ISO 22197-1 rules, and 200 ppb, very close to the alert threshold set by the EU Directive 2008/50/CE for NO_2. For the photodegration tests in continuous, reactions were conducted firstly according to UNI

11484:2013 rules, in order to confirm the photoactivity of the photoactive ceramic tiles. A comparison between the two different starting pollutant concentrations was presented, coming first of all to the conclusion that the pigmentary TiO_2 samples show a good catalytic performances for the NO_x degradation, and it can be used to replace P25. 1077 by Kronos was selected as starting power to produce photoactive ceramic tiles, which as in case of VOCs, were tested on NO_x photodegradation, comparing two different industrial processes to produce them. The first important outcome is that by Digital Printing process the improvement of the material is evident, and to conclude the photoactivity of the Digital Printing TiO_2-tile (S24) was confirmed by means of UNI 11484:2013 rule, testing it even in continuous.

4.1 Introduction

4.1.1 NO_x and outdoor (air) pollution

Nitrogen oxides (NO_x) come from the reaction of nitrogen and oxygen in air during combustion, i.e. whenever combustion occurs in the presence of nitrogen, as in car engines. Thus, in all the areas of high motor vehicle traffic the amount of NO_x emitted in the atmosphere as air pollution is huge. Overall, NO_x derive naturally from volcanic activity and from decoposition of organic matter by microbial and solar action (J. Ângelo et al., 2013), while the most relevant anthropogenic sources are the combustion processes in stationary and mobile units as already mentioned.

Three basic mechanisms lead to the formation of three different types of NO_x, identified as prompt NO_x(from the hydrocarbon radical reactions with N_2 species), fuel NO_x (from the oxidation of nitrogen compounds

present in the fuel; it depends on the nitrogen content in the fuel) and thermal NO_x (high-temperature >1600°C reactions between nitrogen and oxygen) (Charles, 2005; Roy et al., 2009). They are the mains responsible for outdoor pollution, as well as they have a strong impact on human health. NO_x mainly influences on respiratory conditions causing inflammation of the airways at high levels. Moreover, long-term exposure can decrease lung function, increase the risk of respiratory conditions and increases the response to allergens. The negative effects caused by high levels of NO_x do not concern only people well-being, but also the health of our planet. Indeed, they can have a negative effect on vegetation, including leaf damage and reduced growth, which consequently can make vegetation more susceptible to disease and frost damage. Many studies state that pollution is likely to be significantly influencing ecosystem health in forests and habitats. Particular critical levels for vegetation and nature were established after several studies in the past. In detail, Critical Level is the threshold level for the atmospheric concentration of a pollutant above which harmful direct effects can be shown on a habitat or species. Critical Load is the threshold level for the deposition of a pollutant above which harmful indirect effects can be shown on a habitat or species.

The critical level for the protection of vegetation is 30 $\mu g/m^3$ of NO_x, measured as an annual average. Starting from this point, it was also demonstrated that the actual volume of local traffic emissions contributes substantially to exceeding the Critical Level and the Critical Load. Another problem related to NO_x emissions is that they can also reacts with other pollutants in the presence of sunlight to form ozone, which as known can damage vegetation as well. Twelve European Member States exceeded one or more of the emission limits set by the EU National Emission Ceilings (NEC) Directive, according to recent

official data reported to the European Environment Agency (EEA). The European Union sets Limit Values for a range of pollutants that are considered to be harmful to health and the environment. The European Commission can take action against any Member State if the air quality does not meet the Limit Values throughout its territory. The health based objectives that have been set for NO_x are basically two: concentrations shall not exceed 200 μg m^{-3} for more than 18 hours per year, and the annual average must not be greater than 40
μg m^{-3}.
Another critical issue is the NO_x relation with the degradation to many inner city buildings (Allen et al., 2000).

4.1.2 TiO_2 photocatalysis for NO_x abatement

Despite attempts to lower these emissions from cars, it is crucial to find a way of removing such pollutants once in the atmosphere. As already said and deeply explained, titanium dioxide photocatalysis is a relatively cheap and effective way of removing organic poison compounds and pollutant gases from both air and aqueous environments (Bilmes et al., 2000; Chen et al., 1997; Hashimoto et al., 2000; Nakamura et al., 2000; Ohtani et al., 1997; Wu et al., 2000). Even though earlier works focused mainly on the wastewater treatment, heterogeneous photocatalytic oxidation easily converts NO_x in urban environments to nitrates, and it received increasingly attention regarding removal of air pollutants in the last years. In fact, the NO_x gases oxidation to nitrates by UV irradiation to activate TiO_2 has been extensively studied and demonstrated, as well as it has been shown that the photocatalytic effect of TiO_2 is dependent on crystal structure,

particle size and surface area also for this reaction (J.S. Dalton et al., 2002).

This chapter is focused on the use of TiO_2 as a photocatalyst for removing NO_x gases from the atmosphere, with particular attention to TiO_2 particles size as presented for VOCs in the previous chapter. Thus, the commercial samples of TiO_2, both nanometric and micrometric, were tested and investigated and relative results and conclusions will be presented here. The photocatalytic properties and their relation with the sample characteristics must be considered as starting point. Moreover, crucial parameters are the operational conditions on the photocatalysis process, the experimental details, and the main photoreactors used for that purpose. Although prove the efficiency of TiO_2 is nothing new, it was important to assess the properties of each individual commercial catalyst, especially because some of them were not produced for photocatalytic purpose.

4.2 Materials and methods

4.2.1 TiO_2 samples briefly presentation and list

P25 by Evonik was used as first photocatalytic reference material. In order to obtain the fullest possible range of results, five commercial and pigmentary TiO_2 powders were chosen with the following features: pure anatase, uncoated surface, un-doped material, not sold as photocatalytic material. For practical reasons samples will be labeled in this chapter as A*, B, C, D, E.

Industrial porcelain grés tiles were classified mainly on the basis of the preparation method. The basic product is not photocatalytic active; to make it photoactive, it was covered at the surface with a mixture of

micro-TiO_2 (1077) and a commercial SiO_2-based compound by the airless spray classical deposition method; the last one was obtained by Digital Printing.

Sample	Main properties and characteristic		
P25	Powder	Anatase:rutile (75:25)	Nano-sized reference
A (1077)	Powder	Anatase	Micro-sized reference
B	Powder	Anatase	(95 nm)
C	Powder	Anatase	(40 nm)
D	Powder	Anatase	(Micro-sized+ ultrafine)
E	Powder	Anatase	(180 nm)
Orosei	Ceramic tile	Without TiO_2	Manufactured under high pressure by dry-pressing fine processed ceramic raw materials with large proportions of quartz, feldspar, and other fluxes and finally fired at high temperatures (1200–1300°C) in a kiln.
Z23	Ceramic tile	Anatase	Classical TiO2 deposition method.
S24	Ceramic tile	Anatase	Digital Printing

Table 4.1: List of all the samples tested in photocatalytic degradation of NOx. For details see Chapter 2, General experimental part.

4.2.2 Operating conditions

TiO_2 powders

TiO_2 powder samples were tested in NO_x degradation operating in static condition. A previous work (C.L. Bianchi et al., 2013) reports the photodegradation test on the references P25 and 1077 in flowing condition, according to the ISO 22197-1. Since all the details are provided in chapter 2 (General Experimental Part), Table 4.2 sums up the overall operating conditions.

General condition	STATIC
Reactor	PIREX glass cylindrical, volume 20 L
Pollutant	NO_x: NO+NO_2 from NO_2 (0.6% Nitrogen) + air (humidity 40%)
[C_0]	200 ppb 1000 ppb (ISO 22197-1)
TiO_2 amount	0.05 g (dissolved in 2-Propanol)
Catalyst preparation	TiO_2 deposited as film on flat glass plate 20x2 cm^2
Photon source	500 W Iron halogenide lamp (Jelosil model HG 500) 320-400nm UV-A
Irradiation power	10 Wm^{-2}
Temperature	30°C
Kinetic duration	4 h
Analytical techniques	Chemiluminescence (Serinus40, Ecotech, ID Serial N° : 14 - 0325)

Table 4.2: Operating conditions for photocatalytic test on commercial TiO_2 powers, performing in static conditions.

Specific NO_x starting concentrations were set according to the concentration requested by the ISO 22197-1 rules (www.iso.org), and because 200 ppb is very close to the alert threshold set by the EU Directive 2008/50/CE for NO_2 (http://eur-lex.europa.eu/LexUriServ/LexUriServ.do?uri=OJ:L:2008:152:0001:0044:EN:PDF.)

Tiles

Photoactive grés tiles were tested in NO_x degradation operating in both static and flowing conditions, in order to make all the necessary comparisons with the starting powders. Static conditions totally reflect the set up used for powders. Photoactive tiles were specifically prepared with the same dimension of the glass plate (20x2 cm) and they were placed at the bottom of reactor alike to TiO_2 powder samples. Tests in flowing conditions were performed according to UNI 11484:2013 rules. Details of the specific photocatalytic tests that will be reported in this chapter are summarized in table 4.3.

Test	**Sample and SA**	**C_0 [NO_x]**	**Reactor**	**UV power**	**Time duration**
STATIC	Z23 (2x20 cm)	1000 ppb	Cylinder 20L	20 Wm^{-2}	360 min.
STATIC	S24 (2x20 cm)	1000 ppb	Cylinder 20L	20 Wm^{-2}	360 min.
CONTINUOUS	S24 (10x10 cm)	500 ppb	CSTR (UNI) - *see par. 2.3.3.3, general experimental part*	10 Wm^{-2}	200 min.

Table 4.3: Conditions and details of NO_x degradation using photoactive tiles.

4.2.3 Photocatalytic tests

Ceramic photoactive tiles were placed at the bottom of the cylindrical reactor (20 L) and NO_x mixture were loaded directly inside the reactor up to reach the set concentration (1000 ppb for tests in static conditions). All the reactor outlets were closed, including the one connected to the chemiluminescence. The sampling was done manually at regular intervals by opening the connecting valve (open/closed) between reactor and instrument.

The starting concentrations (C_0, ppb) of NO, NO_2 and NO_x respectively, were monitored until values are constant. The photodegradation starts when the UV lamp is switched on.

For the specific tests in continuous each tile sample (10x10 cm) were conditioned under UV irradiation according to the standard (see UNI 11484:2013 rules, www.uni.com). The rector (3.5 L, see general experimental part – reactors) is equipped with a fan (EBMPAPST – 612JH; Nominal power: 12V; Nominal speed: 11700 rpm). Starting NO concentration was set at 500 ppb (see table 4.3, second column) using a gas flow rate of 1.6 dm^3min^{-1}.

4.3 Results and discussion

4.3.1 TiO_2 powders: morphological characterization and photocatalytic activity in NO_x degradation

Table 4.4 sums up the specific structural and morphological features of the powders.

Sample	Particles size (nm)	SSA (m^2g^{-1})	Bang gap (eV)
A*	110	12	3.15
B	95	11	3.25
C	40	23	3.28
D	Micro-sized + ultrafine	11	3.25
E	180	11	3.17

Table 4.4: Main differences in TiO_2 powders structure and morphology.

All data, spectra and information, were collected by means of the characterization methods already explained in the previous chapters. The trend that has been followed is using TiO_2 samples that consist of bigger particles size in comparison to P25. In this way it was possible to

study the more or less negative effect of a lower specific surface area (SSA) (see tab. 4.4, third column). Concerning the bang gap values, they do not show particular differences. Thus, the average size of the TiO_2 particles is the key point in order to better understand the results.
Two initial concentrations of NO_x in the reactor were tested: 1000 ppb and 200 ppb. For reason of brevity, results are summarized in the following tables (Tab. 4.5 and Tab. 4.6).

Sample	Conv. NO_x % (30′)	Conv. NO_x % (60′)	Conv. NO_x % (120′)
P25	72	90	**99**
A	29	89	**92**
B	52	70	**84**
C	62	81	**93**
D	62	83	**92**
E	67	83	**97**

Table 4.5: Photocatalytic activity of the powder samples for the degradation of NOx starting from a concentration of 1000 ppb. Conversion values reported are after 30 min. (first column), 60 min. (second column) and 2 hours (third column, final value in bold).

From an overall point of view, all samples show a good activity in NO_x photodegradation. They are able to reach the complete abatement of almost all the pollutant in the reactor in two hours. The slight difference between P25 and the other samples is consistent considering that it is the only nano-sized sample, however, having regard to the final conversion, results clearly show that micro-TiO_2 is photoactive and suitable for photocatalytic application, even in case of nitrogen oxides. Ordering samples in increasing order in term of average crystallites size (P25<C<B<A<E; D is a mix so it was considered separately), there is only an inconsistency relating to the sample E, which seems to have the higher activity despite the higher particles dimension as well as the very low surface area. A part from this, C e B samples confirm the relevance of the surface area, particularly for higher concentration of starting

pollutant. Indeed, sample B shows the worse result (see in table 4.4 the low surface area combined with the high particles dimension), as well as sample C reaches a final conversion higher than 90% (lower particles size, higher SSA).

Lowering the NO_x starting concentration to 200 ppb, nano-sized and micro-sized powders reach the complete NO_x degradation within 50 min. Therefore, the amount of surface OH species on the TiO_2, -micro or -nano, is enough to guarantee good performance.

4.3.2 Photoactive tiles for the photodegradation of NO_x: results and comparison between different working conditions

4.3.2.1 Tests at 1000 ppb: classical TiO_2 deposition vs. Digital Printing

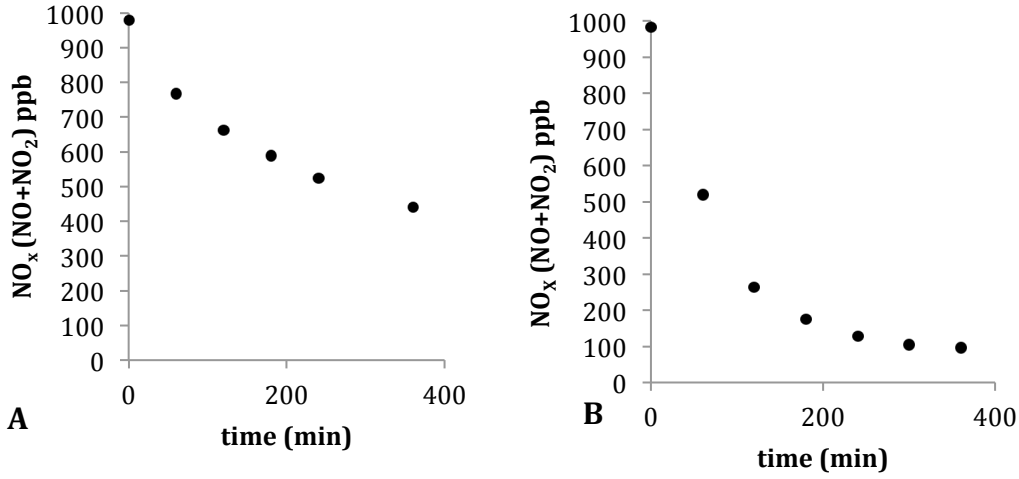

Fig. 4.1: NO_x photodegradation over time (starting concentration of 1000 ppb) using A) tile sample Z23 (classical TiO_2 deposition), in the top left; B) tile sample S24 (Digital Printing), in the top right.

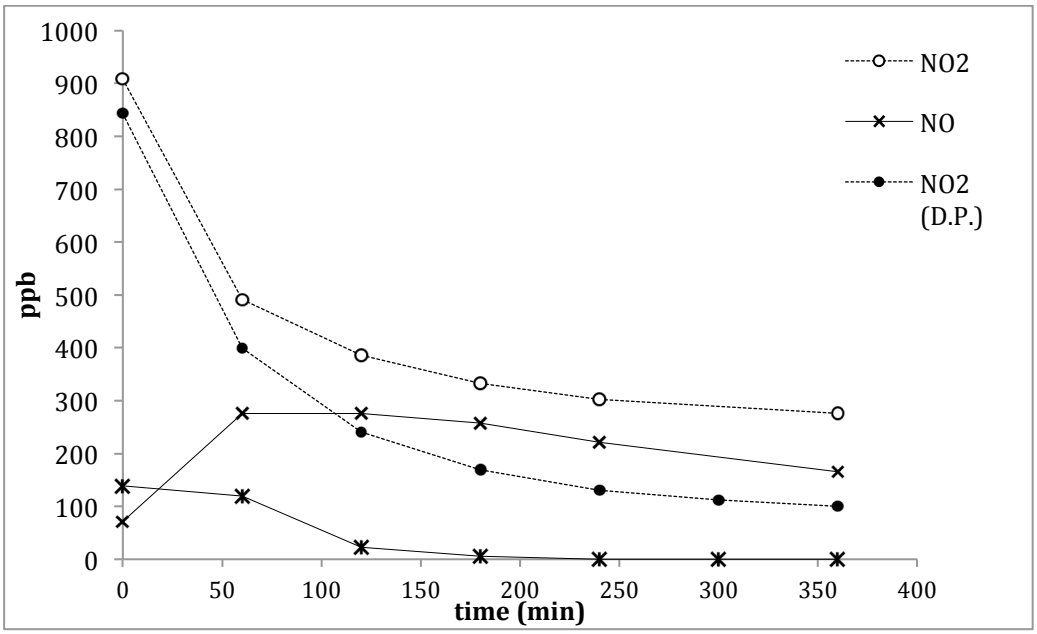

Fig. 4.2: Concentration (ppb) over time of NO_2 and NO respectively. Comparison between Z23 (white dots for NO_2, black crosses for NO) and S24 - Digital Printing (D.P.) (black dots for NO_2, six-pointed crosses for NO).

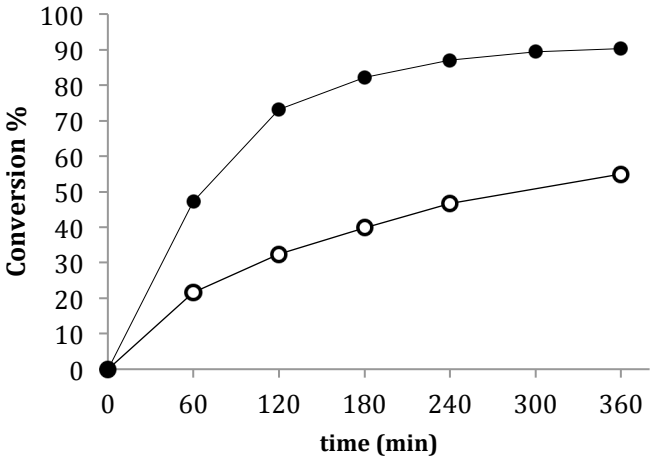

Fig. 4.3: NO_x conversion % over time using S24 (black dots) or Z23 (white dots). Photodegradation performed under UV irradiation, total duration is 6 h.

Digital Printing deposition method allows obtaining a more homogeneous distribution of the TiO_2 on the ceramic tile surface, as well

as it results in a lower loss of TiO_2 powder during the process. The advantages are consistent with the results, even for the NO_x photodegradation. The improvement in terms of photoactivity and effectiveness is evident. In particular, in case of high NO_x concentration (1000 ppb), sample Z23 (classic TiO_2 deposition) is not able to convert the entire amount of the pollutant. The final NO_x concentration after 6 hours of UV irradiation was still above 400 ppb. The final concentration reached using sample S24 (Digital Printing) was lower than 100 ppb (precise value 96 ppb, see fig. 4.1B), which is four times lower and especially below a value for which nitrogen oxides pollution is not dangerous. Figure 4.2 shows the NO_2 and NO concentrations separately. According to the degradation pathway, NO molecules were first formed and than degraded (see crosses points in fig. 4.2). The higher activity of the digital printing tile (S24) (black dots and six-pointed crosses in fig. 4.2), due to the improved availability of the active sites distributed on TiO_2 particles, produced a lower number of NO molecules, and it was able to completely degrade them after 6 h. Situation is completely different using sample Z23; the accumulation of formed NO is higher because the kinetic is slower, thus their concentration reached higher values, and as final result NO molecules were not completely converted. To conclude, at the end of 6 hours of UV irradiation of sample Z23, concentrations of NO_2 and NO are about 300 ppb and 100 ppb respectively (see curves with white dots and black crosses, fig. 4.2).

4.3.2.2 NO_x photodegradation in the continuous flow reactor: test on Digital Printing active tile

The specific test stated in the standard UNI 11484:2013 “Determination of photocatalytic activity by the tangential continuous flow method –

Nitric Oxide abatement", was performed in order to check and study the photocatalytic performance of sample S24 (Digital Printing), considering the good results obtained in static condition. Working in continuous is important to have a better assessment of the material possibilities in a real environment. The rule requires three different tests, at different flow rate (F, m^3h^{-1}), obtained changing the power of the fan fixed inside the reactor. For reason of brevity, fig. 4.4 reported here shows the specific trend of NO_2, NO and the total flow of NO_x (NO_2+NO) for the test performed with a flow rate of 70 m^3h^{-1}. Starting NO_x concentration was set at 500 ppb.

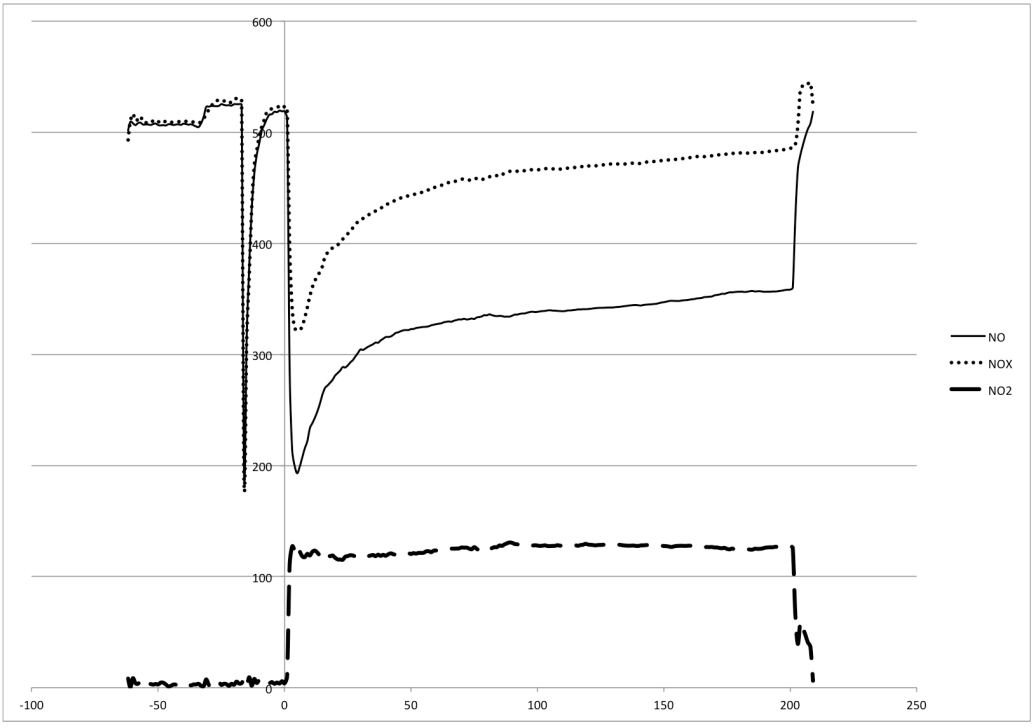

Fig. 4.4: NO_x (dotted curve) (NO_2+NO) (continuous line and dashed curve, respectively) photodegradation in a continuous flow reactor, using S24 sample (Digital Printing photoactive tile). Starting NO_x concentration is 500 ppb, and the flow rate is 70 m^3h^{-1}. Before time zero (0), curves refer to NO_x concentration darkroom. UV lamp was turned on at time 0. NO_x trend was followed for 200 minutes as required. Then, UV was switched off.

Table 4.6 reports the experimental data collected from the three different tests (1,2,3 listed in table). F is the flow rate (first column), η in the conversion and r is the degradation rate over time.

	$F_{V,i}$ (m^3h^{-1})	$\eta^{totale}_{NO,i}$	$\eta^{totale}_{NO2,i}$	$r^{foto}_{NO,i}$ ($\mu g\ m^{-2}h^{-1}$)	$r^{foto}_{NOx,i}$ ($\mu g\ m^{-2}h^{-1}$)
test 1	70	0.41	0.27	5211.5	3887.8
test 2	55	0.40	0.25	4939.3	3786.9
test 3	40	0.29	0.25	3105.2	1121.4

Table 4.6: Experimental data from NO_x photodegradation kinetics performed in the continuous flow reactor.

According to the rule (www.uni.com) we calculated the final NO degradation rate (r_{NO}, $\mu g\ m^{-2}\ h^{-1}$), which is the specific photocatalytic activity identifier value. The precise number calculated for S24 is 50.000 $\mu g\ m^{-2}\ h^{-1}$, which confirms its photoactivity for NO_x degradation.

Because of the very hard conditions, very far from reality, this test is not suitable to give a good overall evaluation of the real photocatalytic performance of the tile in continuous. For a better evaluation of the tiles photoactivity for NO_x degradation, specifically in continuous, another part of this research was dedicated to the development of new reactors, specific for building materials. Results and discussion will be presented in the dedicated chapter.

4.3.3 From powder samples to ceramic photocatalytic materials: comparison and general consideration

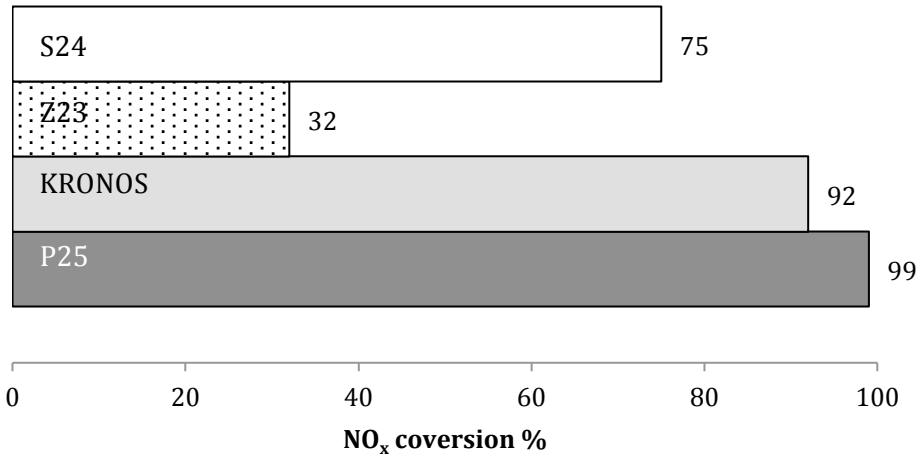

Fig. 4.4: Overall comparison between TiO_2 powder samples (P25, 1077) and photoactive tiles, prepared starting from micro-TiO_2, using the classical deposition method (Z23) or Digital Printing technology (S24). NO_x conversion % was estimated after 2 h of UV irradiation.

One of the main problems concerning the production of building material using TiO_2 is the photocatalytic activity loss, more or less accentuated and due firstly to physical and structural features of the materials. Obviously TiO_2 cannot be available as if it is used in powder, even because its surface is more contaminated by other products or molecules, which can cover the active sites. However, apart from what it depends on some intrinsic features, the TiO_2 deposition process can be changed and improved, in order to improve the final material photocatalytic activity. Overall results presented in Fig. 4.4 show both the aspects. Values reported in the graph refer to the NO_x average conversion percentages reached after 2 hours of UV irradiation. Samples S24 and Z23 are both not able to reach values comparable with the

powder samples. However, sample S24 (from digital printing) shows doubled conversion values compared to the classic TiO_2-tile (Z23). Performances of Z23 are not comparable with the powders, while the conversion value obtained with S24 is absolutely promising. The TiO_2 deposition process in this case, not only leads to a general improvement, but also strongly affects the final conclusion. Indeed, only S24 can be considered an effective ceramic material activated by TiO_2, which can be effective, efficient and interesting for the next developments.

4.4 Conclusions

Firstly, five commercial pigmentary-powdered TiO_2 were characterized and their photocatalytic performances in NO_x degradation were compared to that of P25 nano-powder. All the selected samples were similar for specific features, such as the band gap and the crystallographic phase composition. In particular band gap values fall in the classical range (3.15–3.28 eV) of the anatase polymorph. Particles average size was different from sample to sample, with ranges from 40 (or even less in sample D) to 180 nm. The photocatalytic activity in NO_x degradation was tested with a concentration of 1000 ppb (to follow the 22197-1 ISO rules) and 200 ppb (2008/50/CE threshold alert). The second part of the chapter presents the photocatalytic performances in NO_x degradation of the TiO_2-modified ceramic tiles (samples Z23 and S24), in order to compare powder samples and building materials and give an overview. As expected, at 1000 ppb P25 shows the highest efficiency, reaching the complete pollutant degradation only after 120 min; however, pigmentary powders exhibit very good efficiency, reaching conversion percentages higher than 90%. At 200 ppb of NO_x nano-sized and micro-sized powders show quite the same photocatalytic activity. The presence of surface OH groups is the key

factor for the TiO_2 activity against nitrogen oxides. P25 is characterized by a significant higher amount of hydroxyl species (details presented in chapter 2 – General experimental part), in agreement with the best performances in NO_x abatement at 1000 ppb. However, also the pigmentary TiO_2 samples show appreciable amounts of OH groups and this justifies their good catalytic performances.

As first conclusion, results testify that the gap of activity between nano and micro-sized samples allows replacing nanopowders with micro-ones without a significant loss of activity. Moreover, the low activity tends to disappear when the starting NO_x concentration was reduced and fixed from 1000 to 200 ppb, closer to the real pollution level in our cities. Therefore, 1077 by Kronos was selected as starting power to produce photoactive ceramic tiles. As in case of VOCs, two tiles samples were tested on NO_x photodegradation, comparing two different industrial processes to produce them. Moreover, results are useful to give a comparison even between TiO_2 in form of powder and TiO_2 supported on building materials, to give an overview about possibilities and problems. The first important outcome is that by Digital Printing process (sample S24), the improvement of the material is evident, in comparison to Z23 (classical procedure). The increase of the photocatalytic performance in term of NO_x degradation is testified by the results, as well as the photoactivity of the Digital Printing TiO_2-tile (S24) was confirmed by means of UNI 11484:2013 rule, testing it even in continuous.

References

Allen G.C., El-Turki A., Hallam K.R., McLaughlin D., Stacey M., "Role of NO_2 and SO_2 in degradation of limestone", Br. Corros. J., **2000**, 35, 35–48.

Ângelo J., Andrade L., Madeira L.M., Mendes A., "An overview of photocatalysis phenomena applied to NO_x abatement", J. Environ. Manage., **2013**, 129, 522-539.

Bianchi C.L., Gatto S., Pirola C., Scavini M., Vitali S., Capucci V., "Micro-TiO_2 as a starting material for new photocatalytic tiles", Cem. Concr. Compos., **2013**, 36, 116–120.

Bilmes S.A., Mandelbaum P., Alvarez F., Victoria N.M., "Surface and electronic structure of titanium dioxide photocatalysts", J. Phys. Chem. B., **2000**, 104, 9851–9858.

Charles B., "Everything you need to know about NO_x: controlling and minimizing pollutant emissions is critical for meeting air quality regulations", Met. Finishing, **2005**, 103, 18-24.

Chen L.X., Rajh T., Wang Z., Thurnauer M.C., "XAFS studies of surface structures of TiO_2 nanoparticles and photocatalytic reduction of metal ions", J. Phys. Chem. B., **1997**, 101, 10688–10697.

Dalton J.S., Janes P.A., Jones N.G., Nicholson J.A., Hallam K.R., Allen G.C., "Photocatalytic oxidation of NO_x gases using TiO_2: a surface spectroscopic approach", Environ. Pollut., **2002**, 120, 415–422.

Hashimoto K., Wasada K., Toukai N., Kominami H., Kera Y., " Photocatalytic oxidation of nitrogen monoxide over titanium (VI) oxide nanocrystals large size areas" J. Photochem and Photobiol. A: Chemistry, **2000**, 136, 103–109.

Nakamura I., Negishi N., Kutsuna S., Ihara T., Sugihara S., Takeuchi K., " Role of oxygen vacancy in the plasma treated TiO_2 photocatalyst with visible light activity for NO removal", J. Molecular Catalysis A: Chemical, **2000**, 161, 205–212.

Ohtani B., Okugawa Y., Nishimoto S., Kagiya T., "Photo- catalytic activity of TiO_2 powders suspended in aqueous silver nitrate solution—correlation with pH dependent surface structures", J. Phys. Chem., **1987**, 91, 3550–3555.

Ohtani B., Ogawa Y., Nishimoto S., "Photocatalytic activity of amorphous-anatase mixture of titanium (VI) oxide particles suspended in aqueous solutions", J. Phys. Chem. B, **1997**, 101, 3746–3752.

Oosawa Y., Graetzel M., "Effect of surface hydroxyl density on photocatalytic oxygen generation in aqueous TiO_2 suspensions", J. Chem. Soc. Faraday Trans, **1988**, 1, 84. 197-205.

Roy S., Hegde M.S., Madras G., "Catalysis for NO_x abatement", Applied Energy, **2009**, 86, 2283-2297.

Wu W.C., Chuang C.C., Lin J.L., "Bonding geometry and reactivity of methoxy and ethoxy groups adsorbed on powdered TiO_2", J. Phys. Chem. B, **2000**, 104, 8719–8724.

CHAPTER 5:

VISIBLE LIGHT PHOTOCATALYSIS: TiO_2 MODIFICATION BY ULTRASOUND

Abstract

A crucial issue in photocatalysis is that the light of energy should be greater than the band gap of the semiconductor to excite its electrons from the valence band to the conduction band. With its band gap of 3.2 eV, TiO_2 requires UV light to be photocatalytically effective. Considering that in real indoor environments the source of light is the artificial lighting, almost completely given by LED lamps, UV wavelengths are not compatible. Here the main reasons why several modification methods were developed to make TiO_2 active in visible. Metal nanoparticles (NPs) affect the photochemical properties of TiO_2, leading to many advantages among which the specific activation even in the visible wavelengths. To modify TiO_2 with metals, Ultrasound (US) can be used. The specific procedure on which this part of the work is based on is the decoration of TiO_2 as substrate with metal or metal-oxide NPs, specifically by means of ultra-sounds (US). US play a crucial role in the synthesis procedure. The advantages of decorated TiO_2 are mainly due to the presence of the metal oxides and one the so-called "antenna effect". W, Cu, Re and Mo were selected as first specific metals to decorated 1077 micro-TiO_2, both for reasons of previous published works (Cu, W respectively) and for new investigations (Re and Mo). Each sample was characterized with the basic techniques, i.e. BET, XRD, XPS, ans absorption/transmission IR spectroscopy. Samples were tested on toluene and acetone photodegradation, in order to investigate both the improvement of the photocatalytic activity under UV light or visible light. Firstly, characterization tests put in evidence the successful decoration of TiO_2. Indeed, the presence of the various metals was verified in all cases. Photodegradation tests confirmed the enhancement of the photocatalytic activity and the characterization results were

consistent, particularly in term of structural and chemical features of the samples. Thus, sonochemistry can be applied to the synthesis of metal and metal-oxides nanoparticles, and together with TiO_2 support it was possible to obtain its surface decoration. This is the first step to produce new TiO_2 photocatalysts active under visible light.

5.1 Introduction

Titanium dioxide is typically an n-type semiconductor and its band gap is 3.2 eV as already said, specifically when it consists mainly of anatase. As known and explained in details in the previous chapters, in photocatalysis the light of energy should be greater than the band gap of the semiconductor to excite its electrons from the valence band to the conduction band (e_{CB}^-), generating a positive hole in the valence band (h_{VB}^+). The crucial issue is: because of the 3.2 eV band gap, UV light is required (Nakata and Fujishima, 2012). In order to make TiO_2 usable to reduce air pollution, the problem must be solved, and the reasons are mainly two. For all the applications in outdoor environments, the source of irradiation is solar light. Sunlight is a portion of the electromagnetic radiation, and it consists of infrared, visible and ultraviolet light. Thus, UV radiation is a portion of the entire spectrum; besides, part of it is screened by the atmosphere. As final consequence, solar light emission spectrum contains only about 5% of UV radiation, with values that can rise up to 10% in particular period or in specific areas of our planet (World Meteorological Organization, 2008). For every possible application in real indoor environments, the only source of light is the artificial lighting. In particular, the current great attention given to energy savings induced to an increasingly use of LED lamps, which are

completely UV-free. Considering that more than 300 species of VOCs molecule were detected in the indoor atmosphere, with a concentration from 2 to 10 times higher than in the outdoor one, strategies to improve the air quality are necessary (Curtis et al., 2006; Heinrich, 2011).

TiO_2-photocatalysis is able to oxidize and degrade organic molecules (Ochiai and Fujishima, 2012) as amply proved and described in the previous chapters. In this section methods to modify TiO_2 will be presented; in particular, high-energy ultrasound were used to synthesize new samples of TiO_2 in order to study their behavior under UV or visible spectrum.

Overall, TiO_2 has very good features and many advantages. However, in addition to the wide band gap there are issues that should be considered, such as the quite fast recombination of photogenerated charge carriers, which is one of the main limitations in semiconductor photocatalysis, even using UV light. Here the main reasons why several modification methods were developed. The principal purposes are accelerating the photoconversion, enable the absorption of visible light, and alter the reaction mechanism or control products and intermediates (Lyu et al., 2014). One of the most applied strategy was the surface deposition of metal or metal oxide nano-particles (NPs), which can be useful because of many factors: firstly, it was shown that metals onto the TiO_2 surface can enhance the electron transfer or the charge separation. Secondly, they improve the formation of the free hydroxyl radicals. Particularly metal oxide particles have a positive effect because they support the charge separation and prevent their recombination (Park et al., 2013.; Tobaldi et al., 2013). Metal nanoparticles (NPs) affect the photochemical properties of TiO_2 for three specific reasons: i) the UV radiation leads to a Fermi level shift, indicating an electron transfer at the interface that promote the photocatalytic reactions, ii) also, in metal

species there are more free electrons that can be excited by light; iii) finally, metals can act as electron sink promoting also in this case the charge separation. Ultrasound (US) is used for many chemical applications, from compounds synthesis, to specific chemical reactions, or combined with other techniques in many scientific fields. The specific procedure on which this part of the work is based on is the decoration of ceramics or polymer substrate powders with metal or metal-oxide NPs, by means of ultra-sounds (US), as reported first by Gedanken (Gedanken, 2007). Sakkas et al. performed the decoration of anode materials for Solid Oxide Fuel Cells (SOFC) (Sakkas et al. 2014). Thus, starting from micrometric TiO_2 as substrate, the same method was applied in order to deposit M- and M-Ox NPs on its surface. This particular modification can not be called "doping", because nanoparticles do not modify the intrinsic structure of TiO_2; so we decided to call it "decoration", as well as the modified TiO_2 was identified as "decorated-TiO_2". Molybdenum, copper, tungsten oxide and rhenium oxide were respectively selected as metals species to decorate TiO_2.

5.1.1 Molybdenum, copper, tungsten and rhenium

The advantages of decorated TiO_2 are mainly due to the presence of the metal oxides and one of their main properties, which causes the so-called "antenna effect" (Wang et al., 2006). In particular, the species deposited on the TiO_2 are able to capture the electrons of the visible light, making them usable in the redox reactions that occur upon the surface. Moreover, both metal and metal-oxide species act as electron trap, holding the electrons both from visible light and those derived from charge separation that moved from the valence band to the

conduction band. As consequence, the electron-hole recombination rate is slower (Park et al., 2013; Kubacka et al., 2013). The overall photo-energy transfer from the location of light absorption to the local of reaction plays a significant role in all types of photocatalytic system. The electrons transfer is guaranteed by the differences between the valence and conduction bands of the elements (Rawal et al., 2012; Rawal et al., 2013), which must be anchored to each other. In particular, according to relative energy band positions between TiO_2 and visible-light-absorbing semiconductors, it is possible to distinguish three different types of heterojunction, i.e. i) Type-A, when the sensitizer conduction band (CB) more negative than that of TiO_2, ii) Type-B, when the sensitizer valence band (VB) is more positive than that of TiO_2, and iii) Type-C, when the sensitizer energy level is located between the CB and VB of TiO_2 (Rawal et al., 2013). Accordingly, various coupled systems were investigated, checking both previous publications and metal species that are poorly studied. In this sense, molybdenum and rhenium were selected first, because they are classified as potential antenna sensitizer (Bignozzi et al., 1995). Many papers were published about copper; in particular, like Ag or Zn, Cu and Cu-Oxides are able to separate charge carrier upon both UV and visible light (Yang et al., 2012, Kubacka et al., 2013). WO_3 is a semiconductor with known photocatalytic activity (Liu et al., 2011; Carcel et al., 2012), as well as TiO_2-WO_3 catalyst is classified as a type-b system (Rawal et al., 2013). In particular, there is a synergistic effect that can strengthen the separation of electron-hole pairs in both TiO_2 and WO_3.

In this chapter, the first experiments, results and conclusions about the TiO_2 decoration by US will be presented. Then, a separate chapter will focus on more specific results on copper and silver.

5.2 Materials and methods

5.2.1 Samples synthesis with US

1077 TiO_2 was selected as micrometer sample reference, and it was used as basic substrate. The precursor materials used to decorate TiO_2 were purchased and used without further purification; they are respectively $Mo(CO)_6$ (≥99,9% Sigma Aldrich), $Re_2(CO)_{10}$ (98% Aldrich), $W(CO)_6$ (99,99% Sigma Aldrich), and $CuCl_2$*$2H_2O$ (≥99% Sigma Aldrich). The specific instrument used to generate US is a Bandelin SONOPLUS HD 3200, equipped with a 200W U/S generator and a sonication extension horn of 13mm diameter. The specific procedure steps are described below.

$W(CO)_6$, $Mo(CO)_6$ or $Re_2(CO)_{10}$ (0.25 g for each synthesis) was mixed with 1077 TiO_2, directly in a 100 ml glass flask. 1077 weight was 2 g for tungsten and molybdenum, only 1 g for rhenium (to have a higher metal relative percentage). Then 100 ml of diphenylmethane were added and the solution was sonicated at a constant temperature of 80°C for 3 h, with 33.0% amplitude and a 50 Wcm^{-2} intensity. After US treatment, the solution is centrifuged many times to remove the starting solvent. Then the powder is washed again, three times with n-pentane, and one time with pentane. Solvent was always removed firstly by centrifugation, then by evaporation at 100°C overnight. Sample calcination was performed at 480°C for 40 h; in this way all the organic scents were removed. Procedure was slightly different for copper decoration. Specifically, two solution were prepared: the first one contained 3 g of L-ascorbic acid, 5g of CTAB, 72 ml of H_2O and 2 g of TiO_2. The second one consisted of 1.5 g of $CuCl_2$•$2H_2O$, 6 ml of NH_3 and 15 ml of H_2O. After mixing, solution was treated with US at a set temperature of 62°C for 2.5

h, with a 55,0% amplitude, and US intensity of 100 W/cm^2. The final steps of centrifugation and washing are the same, but in this case we worked only with pure water. Calcination of copper-decorated TiO_2 samples were performed at 480°C for 40 h.

Each sample was characterized with the basic techniques, described in chapter 2 (General experimental part). To summarize, BET analysis was performed with a Sorptometer Instrument (Costech mod. 1042); the XRD spectra were collected using a PW 3830/3020 X' Pert Diffractometer from PANalytical working Bragg-Brentano, using the Cu Kα1 radiation (λ = 1.5406 Å); TEM images were collected using the JEOL 3010-UHR Instrument (acceleration potential 300kV; LaB6 filament); the XPS characterizations were performed with a M-probe apparatus (Surface Science Instruments); and finally absorption/transmission IR spectra were obtained on a Perkin-Elmer FT-IR System 2000 spectrophotometer.

Sample name	Metal species
A	W
B	Re
C	Mo
D	Cu

Table 5.1 Samples list

5.2.2 Photocatalytic tests

The photodegradation kinetics was performed using both a UV lamp (Jelosil – Model HG-500, 500 W, λ = 315-400 nm) and a LED lamp (MW mean well, 350mA rated current, 9-48V DC voltage range, 16.8W rated power) with an emission between 400 and 700 nm. The pollutants concentration was monitored using a gas chromatography (Agilent 3000

A microGC). (Details are reported in chapter 2, General Experimental Part).

5.3 Results and discussion

5.3.1 Structural and morphological characterization of TiO_2-decorated samples

Surface decoration had no effect on the surface area of the samples. Sample n. 4 (TiO_2+Cu) showed a marked reduction of the surface area (BET SSA was 4 m^2g^{-1}) in comparison with 1077, which has a specific surface area of 12 m^2g^{-1}.

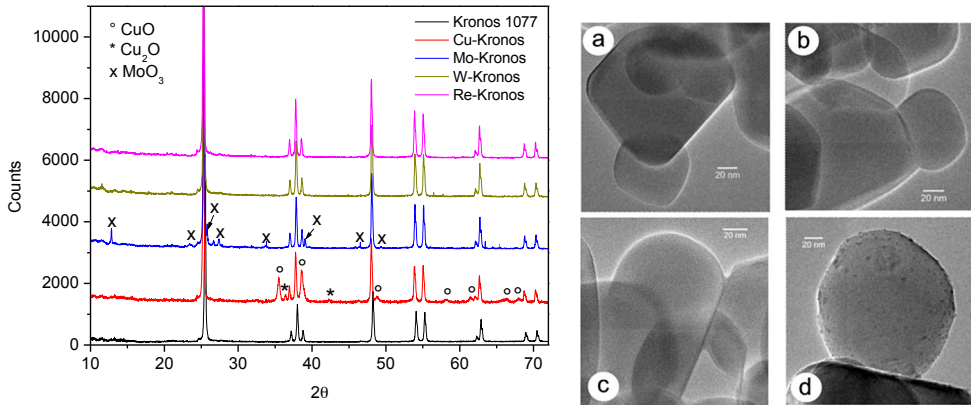

Fig. 5.1: XRD patterns of bare and decorated 1077 TiO_2 on the left, and low magnification TEM images of all decorated systems on the right: specifically, a) Mo decorated Kronos; b) Re decorated Kronos; c) W decorated Kronos; d) Cu decorated Kronos.

XRD patterns reported in Figure 5.1 show that even the structural properties of 1077 powder were not affected by the US surface

decoration. Particularly, the peaks characteristic of the anatase phase [ICDD anatase file no. 21-1272] appear in each spectrum. In more detail, for W- and Re-containing samples XRD analysis puts in evidence that only the peaks related to anatase are present, while the XRD patterns of Cu- and Mo- containing samples show the presence of peaks related to CuO [spatial group C2/c, monoclinic phase, ICDD tenorite file no. 01-072-0629], Cu_2O [spatial group Pn3m, cubic phase, ICDD cuprite file no. 01-075-1531] and MoO_3 [spatial group Pbnm, orthorhombic phase, ICDD molybdite file no. 01-075-0912] phases, respectively. The presence of copper oxide phases is reasonably related to the loss of surface area observed for Cu-containing sample. Low magnification TEM analysis (see fig. 5.1, right-side) show all decorated samples exhibit the main morphological features typical of the parent 1077 system, i.e. well ordered TiO_2 crystallites with almost unchanged average dimensions, in agreement with XRD results. However, a few peculiarities can be put into evidence for the Cu decorated TiO_2 (fig. 5.1, right-side, image D). In particular, a huge amount of small (nano) particles are present on top of the parent 1077-TiO_2 surface, which instead it was not verified for the other three samples. Thus, EDX analyses were performed for all samples. The presence of the extra species has been confirmed for all samples (data not reported of the sake of brevity). A detailed inspection in high-resolution transmission electron microscopy was performed as well, as reported in Fig. 5.2.

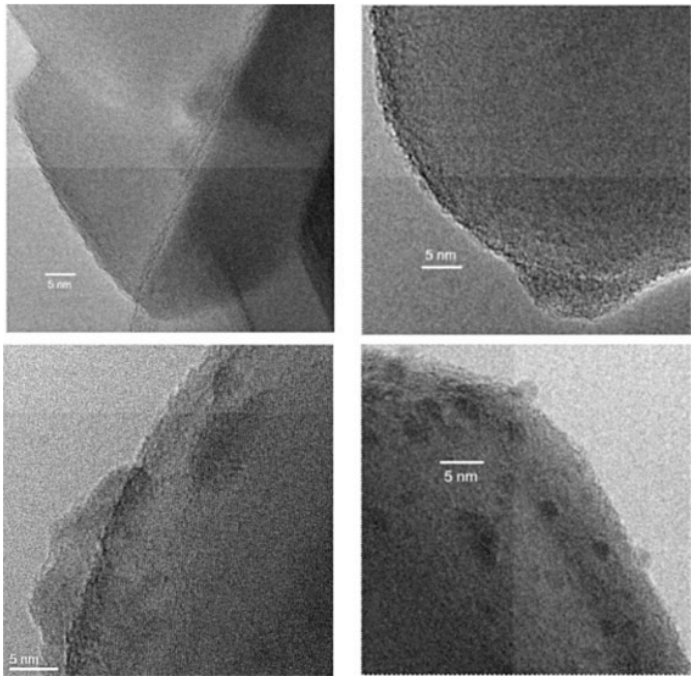

Fig: 5.2: High magnification TEM images of W (top images) and Cu (bottom images) decorated systems.

High magnification images show that, while for Re decoration the features typical of the micrometer TiO_2 remain almost unchanged, in the case of Mo, W and Cu there are notable changes that need to be explained. In Fig. 5.2 the specific images of 1077 decorated with W (top images) and 1077 decorated with Cu (bottom images) are reported. In case of W decoration, a general loss of definition of the crystallinity of the TiO_2 particles was observed, and it was the same for Mo- containing sample (not reported). The main reason is the presence of either W or Mo in the form of oxide (or sub-oxide), which cover the support particles as a thin "coating", and not in the form of metal, as the typical features of metallic W or Mo have been never evidenced. This is in agreement with XRD results obtained for Mo-Kronos that put well in evidence the presence of the MoO_3 phase. Otherwise, no W-phases were

visible by XRD, reasonably either due to the amount under the detection limit of the technique or because in the form of an amorphous coating.
Different the considerations that it is possible to sum up in case of copper. Indeed, for all decorations carried out using Cu, its presence is well evident. In fact, many particles (1nm or less in diameter) with the contrast typical of a metal are observed, as evident in the bottom images of fig. 5.2. The fringes patterns described for the 1077 TiO_2 are still observable. XPS spectra firstly confirmed the presence of the metal species on the 1077 surface.

Cu	$2p_{3/2}$ = 933.6 eV Δ = 19.9 eV
W	$4f_{7/2}$ = 31.4 eV Δ = 2.2 eV
Re	$4f_{7/2}$ = 40.3 eV Δ = 2.4 eV
Mo	$3d_{5/2}$ = 228 eV Δ = 3.1 eV

Tab. 5.2: XPS Binding Energy (eV) of the metal species from Handbook

Sample	Composition	Oxidation state	Binding energy (eV)	%(M^+)	M^+/Ti	OH/O_{tot}
A	TiO_2-W	Oxides (WO_3) Tungstate	35.7 eV 35.7 eV	4.7%	0.3	0.51
B	TiO_2-Re	Re^{6+} (ReO_3)	48.6 eV	0.5%	0.01	0.26
C	TiO_2-Mo	Mo^{6+} (MoO_3)	232.4 eV 235.5 eV	4.5%	0.1	0.09
D	TiO_2-Cu	Cu^+ (Cu_2S) Cu^{2+} (CuO)	932.2 eV 934.2 eV	3.4%	0.1	0.24

Tab. 5.3: Summary data XPS spectra of all the synthetized samples

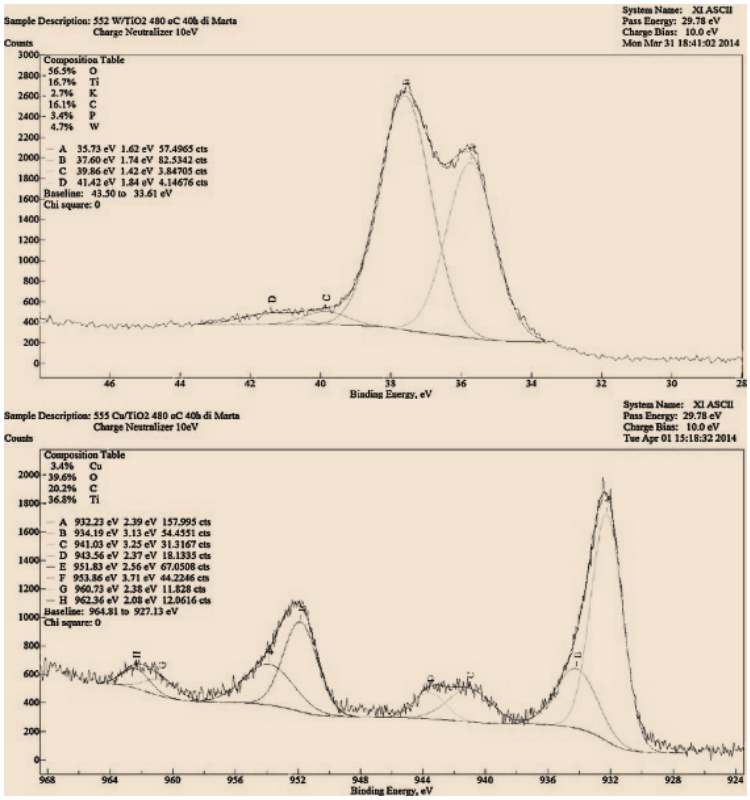

Fig. 5.3: XPS high-resolution spectra of W (above) and Cu (below).

XPS high-resolution spectrum reported in Fig. 5.3 (left-hand) shows the distribution of the tungsten peaks and in particular the most important is the peak "A" that refers to the WO_3 species (Tab. 5.3, first line), in agreement with the results obtained by TEM analysis.

On the righ-side of Fig. 5.3, the specific spectrum of Cu-decorated TiO_2 shows the main peaks related to the species Cu, CuO and Cu_2S (see specific peak values in table 5.3, fourth line) and the presence of Cu in metal form is demonstrated, in agreement with the results obtained with XRD and TEM analysis. Another important parameter strongly related to the final photocatalytic activity of the samples is the OH/O_{tot} ratio, as already discussed by Bianchi et al. (Bianchi et al., 2014). This particular value was calculated from the XPS oxygen high-resolution spectra. Precise values are listed in table 5.3, in the seventh column. FT-IR spectra allowed having a more detail description of the surface hydroxyl groups present on the surface of each sample (Fig. 5.4).

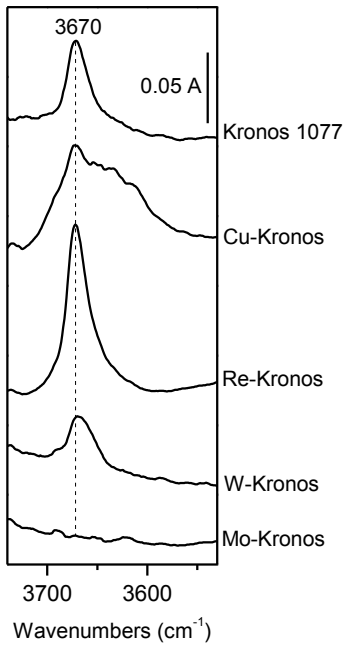

Fig. 5.4: FT-IR spectra.

The analysis was performed after prolonged outgassing at room temperature in order to remove physisorbed molecular water. The typical peak related to the stretching mode of free hydroxyl radical groups of 1077-TiO_2 at 3670 cm^{-1} (Panayotov et al., 2005) was present in all decorated samples (Cu, Re, and W), but it disappeared in case of Mo. This last finding is related to the complete coverage of Kronos surface by a widely spread MoO_3 phase, whose presence has been put into evidence by XRD, TEM and XPS analysis. Another important consideration to underline is that TiO_2 decorated by copper is characterized by other families of free hydroxyl groups reasonably related to CuO and Cu_2O phases, whose presence was already put into evidence by XRD and XPS analysis.

5.3.2 Photocatalytic test and photoactivity evaluation

5.3.2.1 Toluene photodegradation under UV light and CO_2 formation

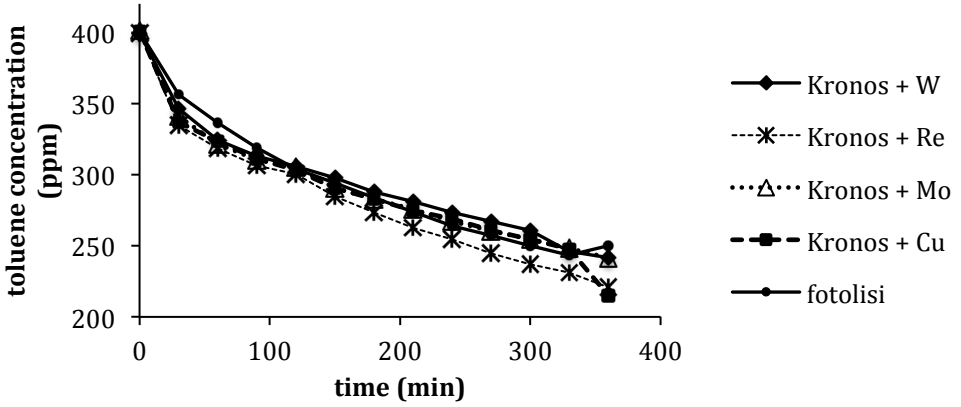

Fig. 5.5: Toluene photodegradation in gas-phase under UV radiations.

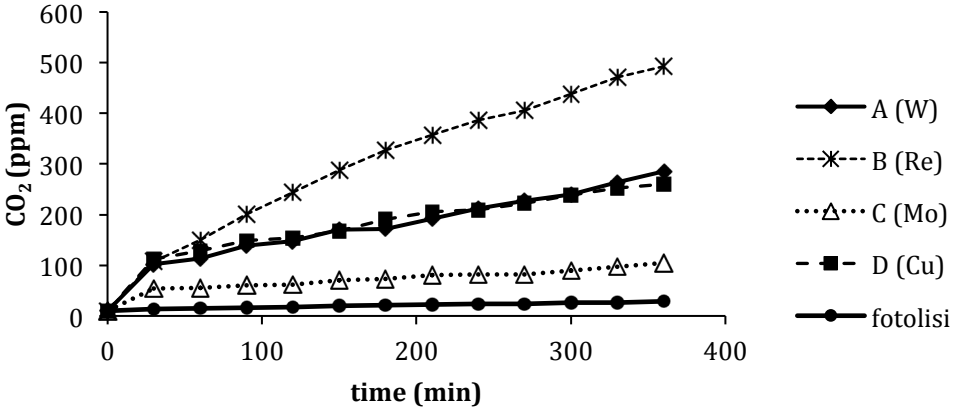

Fig. 5.6: CO_2 formation

Photodegradation tests on toluene were performed following the ordinary procedure for VOCs. Setup, rector, and the plant scheme are described in the general experimental part (see paragraph 2.3, Reactors). Starting toluene concentration was set at 400 ppm, and reaction kinetics

was conducted using a UV lamp as first irradiation source. The degradation reaction of toluene follows a multi-step path, with the formation of different byproducts before getting to the complete oxidation to CO_2 and water (Bianchi et al., 2014; Di Paola et al., 2014; Du et al., 2008; Augugliaro et al., 1999). This is the crucial point, from which it was possible to discriminate the different activities of the decorated-samples. Indeed, in case of the toluene degradation, apparently the species put on the surface by the decoration do not increase the photocatalytic activity of the material (fig. 5.5); however, they affect the byproducts' conversion into CO_2, so the surface decoration profitably acts on the byproducts, showing its concrete help in the degradation of the pollutant. In particular, the Re-containing sample shows the highest CO_2 formation (fig. 5.6).

5.3.2.2 Test on acetone under UV and visible light

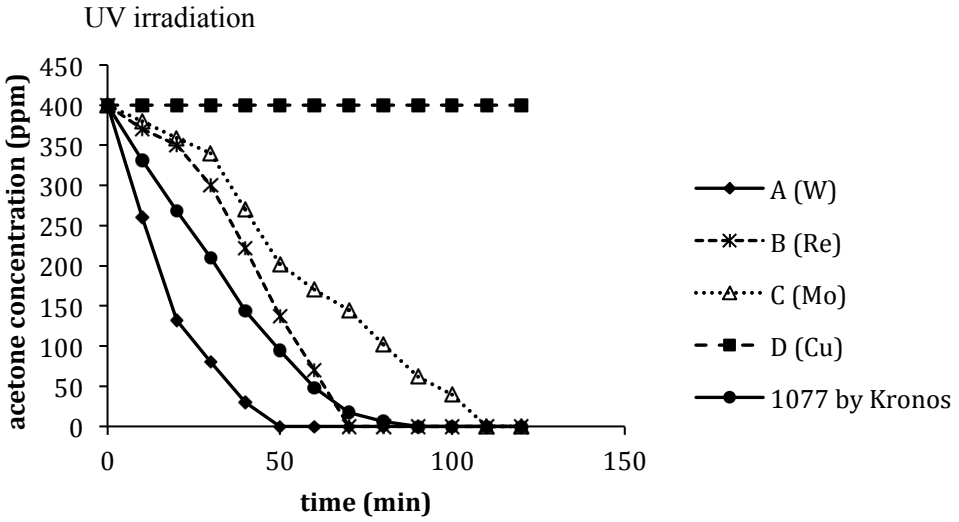

Fig. 5.7: Acetone photodegradation in gas-phase under UV irradiation.

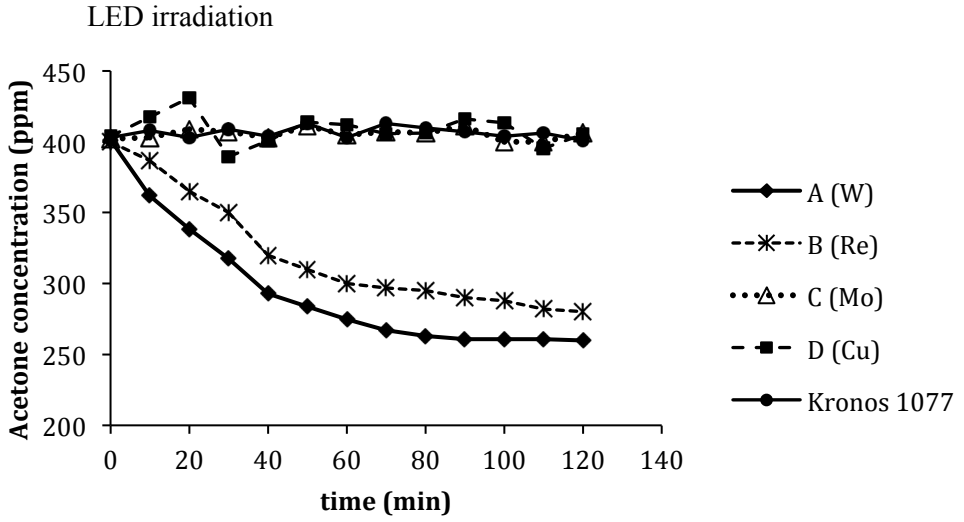

Fig. 5.8: Acetone photodegradation in gas-phase under visible light (performed by LED lamp).

Tests on toluene confirmed the improvement given by the metal presence on the TiO_2 surface, even in case of UV irradiation. If irradiated by UV light, 1077 TiO_2 is effective in toluene degradation, but it was not able to reach the complete conversion to CO_2, mainly because of the several intermediates. Re and W in particular showed a substantial increase of the CO_2 % formation, confirming the increase in the complete oxidation of toluene. The action mechanism is different.

In case of Re, the presence of a higher number of OH free groups is the main reason, while in case of W, WO_3 maybe works simultaneously with TiO_2, increasing the total activity. Tests on the acetone photodegradation were performed both with the UV lamp and the LED lamp. In case of acetone degradation, 1077-TiO_2 is already completely effective. However, the metals presence improved the kinetics in terms of degradation rate. In particular, for W-containing sample the complete acetone oxidation was reached in 50 minutes (fig. 5.7, see the line with black rhombus related to W), less than 90 minutes required by 1077. The

presence of the tungsten oxide (WO_3) is confirmed in particular by the XPS analysis; moreover, in the TEM images it is possible to see that a thin film covers the 1077 surface, and it is tungsten oxide. Also the IR spectrum complies with this last information because the lower OH peak compared to not-decorated micrometer TiO_2 is maybe due to the coating effect of tungsten oxide. All these hypotheses support the results in the photodegradation tests, even because WO_3 is a semiconductor with known photocatalytic activity (Liu et al., 2011; Carcel et al., 2012).
Opposite was the result obtained with Cu-decorated TiO_2, with which a complete loss of activity is observed. This point must be related to the rather high covering of the TiO_2 surface, and it will be better explained in the next chapter, specific for copper and silver.
The use of LED light sources avoided any contribution of UV irradiation. Bare-TiO_2 would not be active in this particular condition, because energy is not appropriate for the band gap (3.2 eV). Thus, testes performed by LED irradiation gave a clear indication of the TiO_2 samples under visible-light. Acetone degradation tests in the visible clearly showed that W and Re play a crucial role in the activation of the catalyst under the visible light. As already mentioned before, the most apparent characteristic that could be related to the good activity of Re-decorating sample is the presence of a significant amount of free hydroxyl radicals, confirmed by the peak in the IR spectrum.
In general, if we take into consideration the chemical activity of the metal oxides themselves, first of all their presence increases the "antenna effect", because they are able to capture the electrons of the visible light, making them usable in the redox reactions that occur upon the surface; secondly, overall it was shown that species like metal or metal oxides are able to act as an electron trap, reducing the electron-hole recombination rate (Park et al., 2013; Kubacka et al., 2013).

Wang et al. explained the so-called "antenna mechanism" as the electrons or holes transfer between some particles in contact. When the particle is on a semiconductor surface can act as much as electrons trap as holes trap, and the immediate effect is a better electron-hole separation (Wang et al., 2006). Moreover it has to be considered that the electrons transfer assumed in the M-TiO_2 systems takes place even thanks to the differences between the valence and conduction bands of the respective elements, as reported by Rawal et al. (Rawal et al., 2012; Rawal et al., 2013). Overall, samples prepared with Tungsten or Rhenium showed the best photocatalytic activity improvement of the micrometer TiO_2: WO_3 has a specific band gap of 2.8 eV, and it is able to absorb some portion of the visible light (Shamaila et al., 2011); considering instead the sample containing Rhenium, the latter is also regarded as an "antenna-sensitizer" (Bignozzi et al. 1995).

5.4 Conclusions

Sonochemistry can be applied to the synthesis of metal and metal-oxides nanoparticles, and together with TiO2 support it was possible to obtain its surface decoration. Surface-decoration of TiO2 with appropriate metals improves the photocatalytic activity of anatase TiO2, both under UV light and LED (visible wavelengths). Specifically, bare TiO_2 is not active under visible wavelengths because of the higher band gap. Starting from the first results, to conclude this part it was shown that: the most effective species loaded on the TiO_2 surface are the tungsten oxide and the rhenium oxide because they have the best performances in terms of degradation of VOC's. Although the results obtained using the samples prepared with copper NPs are absolutely not good, it is

highly likely that this is due to the to the amount of copper. For this reason, specific copper properties were investigated and the relative results are reported in the next chapter.

References

Augugliaro V., Coluccia S., Loddo V., Marchese L., Martra G., Palmisano L., Schiavello M., "Photocatalytic oxidation of gaseous toluene on anatase TiO_2 catalyst: mechanistic aspects and FT-IR investigation", Appl. Catal. B: Env., **1999**, 20, 15–27.

Bianchi C.L., Pirola C., Crocella V., Cerrato P., Di Michele A., Naldoni A., Capucci V., "Photocatalytic degradation of acetone, acetaldehyde and toluene in gas-phase: comparison between nano and micro-sized TiO_2", Appl. Catal. B: Env., **2014**, 146, 123-130.

Bignozzi C.A., Argazzi R., Schoonover J.R., Meyer G.J., Scandala F., "Photosensitization of wide bandgap semiconductors with antenna molecules", Sol. Energy Mater. Sol. Cells, **1995**, 38, 187-198.

Carcel R.A., Andronic L., Duta A., "Photocatalytic activity and stability of TiO_2 and WO_3 thin films", Mater. Charact., **2012**, 70, 68-73.

Curtis L., Rea W., Smith-Willis P., Fenyves E., Pan Y., " Adverse health effects of outdoor air pollutants", Environ. Int., **2006**, 32, 815-830.

Di Paola A., Bellardita M., Palmisano L., Barbieriková Z., Brezová V., "Influence of crystallinity and OH surface density on the photocatalytic activity of TiO_2 powders", J. Photochem. Photobiol. A: Chem., **2014**, 273, 59–67.

Du P., Bueno-López A., Verbaas M., Almeida A.R., Makkee M., Moulijn J.A., Mul G., "The effect of surface OH-population on the photocatalytic activity of rare earth-doped P25-TiO_2 in methylene blue degradation", J. Catal., **2008**, 260, 75–80.

Gedanken A., "Doping nanoparticles into polymers and ceramics using ultrasound radiation", Ultrason. Sonochem., **2007**, 14, 418-430.

Heinrich J., "Influence of indoor factors in dwellings on the development of childhood asthma", Int. J. Hygiene Environ. Health, **2011**, 214, 1–25.

Kubacka A., Munoz-Batista M.J., Ferrer M., Fernández-García M., "UV and visible light optimization of anatase TiO_2 antimicrobial properties: Surface deposition of metal and oxide (Cu, Zn, Ag) species", Appl. Catal. B: Env., **2013**, 140–141, 680–690.

Liu Y., Xie C., Li H., Chen H., Zou T., Zeng D., "Improvement of gaseous pollutant photocatalysis with WO_3/TiO_2 heterojunctional-electrical layered system", J. Hazard. Mater., **2011**, 196, 52–58.

Lyu J., Zhu L., Burda C., "Considerations to improve adsorption and photocatalysis of low concentration air pollutants on TiO_2", Catal. Today, **2014**, 225, 24–33.

Nakata K., Fujishima A., "TiO_2 photocatalysis: Design and applications", J. Photochem. Photobiol., C: Photochemistry, **2012**, 13, 169–189.

Ochiai T., Fujishima A., "Photoelectrochemical properties of TiO2 photocatalyst and its applications for environmental purification", J. Photochem. Photobiol. C: Photochemistry **2012**, 13, 247–262.

Panayotov D.A., Yates Jr. J.T., "Depletion of conduction band electrons in TiO_2 by water chemisorption-IR spectroscopic studies of the independence of Ti-

OH frequencies on electron concentration", Chem. Phys. Lett., **2005**, 410, 11-17.
Park H., Park Y., Kim W., Choi W., " Surface modification of TiO_2 photocatalyst for environmental applications", J. Photochem. Photobiol. C: Photochemistry, **2013**, 15, 1–20.
Rawal S.B., Bera S., Lee D., Jang D., In Lee W., "Design of visible-light photocatalysts by coupling of narrow bandgap semiconductors and TiO_2: effect of their relative energy band positions on the photocatalytic efficiency", Catal. Sci. Technol., **2013**, 3, 1822.
Rawal S.B., Chakraborty A.K., Kim Y.J., Kim H.J., In Lee W., "Double-heterojunction structure of SbxSn1-xO_2/TiO_2/CdSe for efficient decomposition of gaseous 2-propanol under visible-light irradiation", RSC Adv., **2012**, 2, 622–630.
Sakkas P.M., Schneider O., Sourkouni G., Argirusis C., "Sonochemistry in the Service of SOFC Research", Ultrason. Sonochem., **2014**, 21, 1939-1947.
Shamaila S., Sajjad A.K.L., Chen F., Zhang J., "WO_3/BiOCl, a novel heterojunction as visible light photocatalyst", J. Colloid Interface Sci., **2011**, 356, 465–472.
Tobaldi D.M., Severskapin A., Pullar R.C., Seabra M.P., Labrincha J.A., "Titanium dioxide modified with transition metals and rare earth elements: Phase composition, optical properties, and photocatalytic activity, Ceramics Int., **2013**, 39, 2619–2629.
Wang C., Pagel R., Dohrmann J.K., Bahnemann D.W., "Antenna mechanism and deaggregation concept: novel mechanistic principles for photocatalysis", Chimie, **2006**, 9, 761–773.
World Meteorological Organization, "Chapter 8 – Measurement of sunshine duration", CIMO Guide, **2008**, retrieved from hhtp://public.wmo.
Yang X., Zhou C., Gao X., Gao W., "ZnO/TiO2 core–brush nanostructure: processing, microstructure and enhanced photocatalytic activity", J. Mater. Chemistry, **2012**, 22, 5629.

CHAPTER 6:
COPPER AND SILVER NPs DECORATED TITANIA

Abstract

The surface modification of commercial micro-sized TiO_2 by means of high-energy ultrasound (US), employing $CuCl_2$ or $AgNO_3$ as precursor molecules, to obtain both metallic copper/silver as well as copper/silver oxides species at the TiO_2 surface, is here presented. We have prepared samples with different copper or silver content, in order to evaluate the impact on the photocatalytic performances of the semiconductor, and studied in particular the photodegradation in the gas phase of some volatile organic molecules (VOCs), namely acetone and acetaldehyde. We used a LED lamp in order to completely eliminate the ultraviolet light and exploit the contribution of the visible wavelengths only. We employed several techniques (i.e., HR-TEM, XRD, FT-IR and UV–Vis) in order to characterize the prepared samples, thus evidencing different sample morphologies as a function of the various copper or silver content. Through the study of UV-VIS absorption spectra, it was possible to calculate even the band gap values. Also, we performed ICP analysis to observe the definite amount of silver on the TiO_2 surface. We also compared the US-assisted M/Mox-TiO_2 synthesis with the classical impregnation method. Both copper and silver nanoparticles affected the photoactivity of TiO_2 under visible light, making this semiconductor effective in volatile organic compounds (VOC) oxidation even in the absence of UV-A. Contribution of US is also crucial to obtain defined size and shape of the nanoparticles, as well as a better distribution of the metal species on the surface of TiO_2.

6.1 Introduction

The combination between TiO_2 and metal nanostructures has shown very promising results for enhancing the semiconductor's visible light absorption and promotes the charge separation (Banerjee et al., 2014; Linic et al., 2011; Awazu et al., 2008). As known, ultrasonic irradiation can act on shape and size of the inorganic metal nanoparticles, thanks to the extreme conditions attained during bubble collapse, and for this reason it was exploited to produce nanoscale metals, metal oxides, and nanocomposites (Suslick et al., 1999). Gutierrez et al. published the first report on the use of ultrasound for noble metals synthesis. The specific procedure presented in this research work and already described in chapter 5 draws on the work of Tao et al. (Gutierrez et al., 1987; Tao et al., 2011; Stucchi et al., 2015). Considering the very promising possibilities to use US to obtain metal nanoparticles and substrates decoration as well, sonochemistry were exploited to decorate the surface decoration of TiO_2. This specific chapter is dedicated to copper and silver, for all the reasons that will be explained in the next lines.

6.1.1 Copper NPs and photocatalytic properties: state of art

To modify TiO_2, the most investigated species are noble metals, such as gold or platinum. One of the main drawbacks to consider is their rather high cost. This one of the reason why species like copper has recently attracted much attention. Copper is firstly less expensive and more abundant that silver, gold or platinum (Chiang et al., 2014). Many researches confirmed that Cu affects the properties of TiO_2 particularly decreasing the electron-hole recombination and thus improving the photocatalytic activity (Xina et al., 2008). More specifically, copper in

metal form, as well as its oxidized species can serve as electron mediators. Cu(I) and Cu(II) species, i.e. Cu_2O and CuO, are able to extend the adsorption to the long wavelength region, in particular because of the formation of an heterojunction with TiO_2 that is the principal cause of the charge separation promotion (Chiang et al., 2014). As described in chapter 5, sonochemistry can be a new, economical and green method for the synthesis and decoration of metallic particles on various ceramic substrates, and micrometer TiO_2 can be easily used as support. In particular, we performed the TiO_2 decoration with copper, and we found that the amount of copper deposited on TiO_2 surface could be a decisive factor for the photocatalytic activity (Stucchi et al., 2015). Furthermore, there are several publications in which the very good and promising properties of copper were proven and described, in particular under solar or visible light (Zhao et al., 2016; Zhang et al., 2015).

6.1.2 Silver NPs and photocatalytic properties: state of art

Studies on transition metals that easily make heteronanostructures with other semiconductors were deeply performed. Ag, Pd or Pt atoms were greatly investigated and even the Ag specific properties are very well known (Podasca et al., 2016). In particular when Ag is combined with TiO_2, results in terms of activity in visible light were promising, and this is the reason why silver is one of the metals that in the recent years attracted more and more attention (Kochuveedu et al., 2013; Wang et al., 2014). Silver nanoparticles (AgNPs), promote charge separation, and enhance light absorption mainly because of its plasmon resonance (SPR) phenomena. Indeed, they are classified as plasmonic noble metal nanostructures (Ansari et al., 2015; Su et al., 2012). Firstly, AgNPs

interact with the radiation in the visible range, improving the photocatalytic responses obtained for metal-metal oxide photocatalytic materials, and, specifically when they are anchored on TiO_2 surface, cause the slowdown of the electron-hole pairs recombination (Ansari et al., 2013). Silver nanoparticles synthesis can be carried out by various methods, deeply described in the literature: M. Darroudi et al. presented a laser ablation method of preparation (Darroudi et al., 2011), Y. Liu et al. described a procedure in which they successfully employed the UV irradiation reduction of Ag precursor (Liu et al., 2009). Other methods are microwave processing (Wani et al., 2011), electrolysis method (Dong et al., 2014), thermal decomposition or chemical reduction (Shim et al., 2008; Khan et al., 2011). One of the crucial drawbacks of the chemical method are the specific chemicals used in in the reduction step that in most cases are toxic (Tahira et al., 2015). This is the first reason why the exploitation of the Ag-TiO_2 surface decoration by means of US has to be considered as useful.

6.1.3 Copper and silver decorated titania

From all the consideration presented above, this chapter presents the investigation of the influence of copper loading on the photocatalytic activity of TiO_2 catalysts first. Then, the same procedure was applied to obtain the TiO_2 surface decoration by silver nanoparticles, exploring the US properties both for depositing the particles on the TiO_2 and for metal nanoparticles synthesis. For both, we studied the distribution and morphology of metal and metal-oxides NPs present on the TiO_2 surface with the appropriate characterization techniques. Specifically, the different amount of metal precursor used during the synthesis procedure was the crucial point on which we focused on. Indeed,

samples of Cu-metal and metal-oxides decorated titania, were prepared considering copper amounts in the range 1–75 wt.%. Following the same way, Ag-TiO_2 samples were synthesized starting from different metal amounts.

The evaluation of the photocatalytic activity of TiO_2 modified samples, only under visible light, is a very little explored field; thus, properties of TiO_2 decorated with copper or silver were investigated for the abatement of VOCs molecules (acetone or acetaldehyde respectively) in gas phase. For copper, both the impact of the copper amount and the importance of the power of the irradiation were considered.

6.2 Materials and methods

TiO_2 (1077 by Kronos), copper precursor ($CuCl_2 \cdot 2H_2O$) and silver precursor ($AgNO_3$), and all the other reagents were purchased and used without further purification. As already mentioned, acetaldehyde (ACS Reagent, P99.5% Sigma–Aldrich) or acetone (Chromasolv plus, for HPLC, P99.9% Sigma–Aldrich) were selected as reference pollutant molecules.

6.2.1 Synthesis of copper NPs-decorated TiO_2

Starting from the procedure proposed by Tao et al. (X. Tao, Y. Zhao, Sonochemical synthesis and characterization of disk-like copper microcrystals, Mater. Chem. Phys. 125 (2011) 219–223.), titanium dioxide substrate were decorated with some necessary adjustments and small changes in the synthesis. For the preparation of copper NPs and their

consequent deposition on TiO_2, the procedure is the same already described in chapter 5, in the experimental part. Here some crucial points to remind the main steps.

Two different solutions were prepared.

- Solution (A): L-ascorbic acid, CTAB, H_2O and 1077 TiO_2
- Solution (B): $CuCl_2 \bullet 2H_2O$, NH_3, water.

Specifically, L-ascorbic is the reductant, while CTAB acts as surfactant and plays a crucial role on the morphology and size of the final product. It was shown that a low concentration of CTAB leads to particles characterized by a less regular morphology and a broader size distribution. The final solution (A+B) was treated by US. Table 6.1 summarizes the main settings.

US Device	**Bandelin SONOPLUS HD 3200**
US Generator	200 W
US Frequency	20 KHz
Horn diameter	13 mm
US Power	50 Wcm^{-2}
Temperature (°C)	62 °C
Time	2.5 h

Table 6.1 Work settings

The role of ultrasound is very important as regards the formation of nanoparticles from the precursor, and for a good distribution of them on the TiO_2 support surface. In particular, ultrasonic irradiation speeds up the diffusion of solute in the reaction system, as well as it influences the selective adsorption of the surfactant on copper, inducing elongation or compression in defined directions, affecting the particles morphology. Another advantage is that the use of US allows working in conditions that do not require extreme settings (high temperature for instance) in order to make the reaction faster or to obtain the expected nanoparticles formation.

Six samples with different copper content were prepared. Table 6.2 reports the composition details of the synthesis for each one.

Sample name	**TiO_2 (1077-Kronos)**	**$CuCl_2 \cdot 2H_2O$**
K_1	2 g	0.02 g
K_5	2 g	0.1 g
K_10	2 g	0.2 g
K_10	2 g	0.4 g
K_40	2 g	0.8 g
K_75	2 g	1.5 g

Table 6.2 Composition of the samples

Specific number indicated in the names of the samples refers to the different percentages of copper, which were calculated comparing the weight of TiO_2 and copper chloride. Instruments and techniques used for the characterizations tests were described in detail in the general experimental part, and they are not reported here for brevity. Photodegradation kinetics parameters are summarized in table 6.3.

Reactor	PIREX Glass reactor 5 L
Lamps	▪ UV: Jelosil, Model HG-500, 500 W, k=315-400 nm; ▪ LED: MW Mean-Well, 350 mA rated current, 9-48 V DC voltage range, 16.8 W rated power, emission 400-700nm.
Irradiation distance (*specific for LED*)	20 cm = 15.000 lux 40 cm = 2000 lux 60 cm = 1100 lux
Pollutants monitoring	Micro-GC Agilent 3000

Table 6.3 Tools and setup used to perform photodegradation kinetics

In case of visible light irradiation, obtained by LED, the specific amount of emitted light depended on the distance, however it is not linearly depended from it. Emitted light was measured in Lux. Lux is the SI unit of illuminance and luminous emittance per unit area. It is equal to lumen per square meter. Three different distances were set to study the influence of the light power on the photocatalyst activation.

6.2.2 Synthesis of silver NPs-decorated-TiO_2

TiO_2 surface decoration assisted by US were performed on the basis of the ultrasound-assisted synthesis of silver colloid nanoparticles described by Goharshadi et al. (Goharshad et al., 2013). Details are summarized in the following lines.

- Solution (A): $AgNO_3$, PVP40, 1077 TiO_2 and water
- Solution (B): $NaBH_4$ in water

Ultrasound settings and setup are the same described for copper. Precisely, the solution (A) was first of all treated by US for 10 minutes, then solution (B) was added, continuing sonication for other 60 minutes. Six different samples were synthesized with an increasing silver amount in the range 1-20 % w/w (also in this case calculated from $AgNO_3$ and TiO_2 specific weights). Table 6.4 reports the samples list.

Sample name	**TiO_2 (1077-Kronos)**	**$AgNO_3$**
K_Ag(1a)	2 g	0.02 g
K_ Ag(1b)	2 g	0.02 g
K_ Ag(5a)	2 g	0.1 g
K_ Ag(5b)	2 g	0.1 g
K_ Ag(10a)	2 g	0.2 g
K_ Ag(20a)	2 g	0.4 g

Table 6.4 Samples list with TiO_2 and $AgNO_3$ contents

Polyvinylpyrrolidone (PVP) amount plays an important role in the final shape and size of silver metal nanoparticles. In particular its content was calculated according to the constant ratio mol($AgNO_3$):g(PVP)/1:40. This value is the result of literature searches and tests we performed and do not report here for reason of brevity. Samples indicated by "a" or "b" letter differ because of the power of the US applied during their synthesis. In particular we used 30 Wcm^{-2} in case of samples indicated with "a" or 50 Wcm^{-2} in case of samples "b". Finally, the reaction temperature was controlled, being 30±1 °C, for all samples. Instruments and techniques used for the characterizations tests were described in detail in the general experimental part, and they are not reported here for brevity. Specifically, the precise silver content was evaluated by ICP analysis. Silver NPs decorated TiO_2 were tested for the photodegradation of acetone in gas-phase under visible light only, selecting a distance between reactor and light of 20 cm.

6.3 Results and discussion

6.3.1 Copper-decorated TiO_2: characterization results and photocatalytic tests

6.3.1.1 XRD spectra and HR-TEM analysis

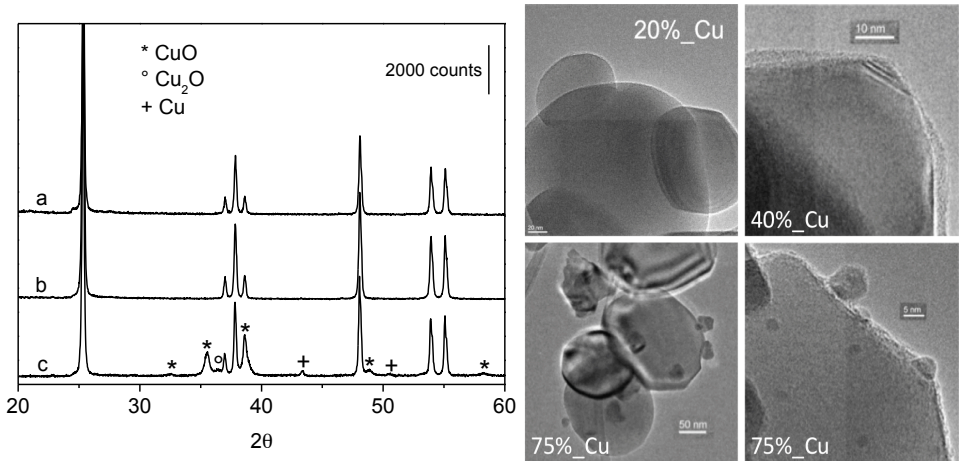

Fig. 6.1: XRD patterns of 1077 TiO_2 (curve a), K_40 (curve b) and K_75 (curve c) samples, on the left; TEM images for K_20, K_40, and K_75, on the right.

1077 bare TiO_2 XRD diffractogram (curve a, left side of fig. 6.1) primarily confirms the presence of the anatase crystallographic phase, indeed all the peaks reported in this 2θ range are typical of that specific TiO_2 polymorph [ICDD Anatase file No. 21-1272]. The first comparison between 1077 and decorated samples verifies that after the US treatment the support maintains the typical structure of micrometer anatase. Particularly for Cu-containing materials up to 40%, no additional XRD peaks were observed (curve b, left side fig. 6.1). Otherwise, for the highest Cu-wt% (curve c, left side fig. 6.1) the typical peaks related to the metallic Cu [ICDD file No. 4- 0836], CuO [ICDD file No. 48-1548] and Cu_2O [ICDD file No. 5- 0667] are evident. At the right side of fig. 6.1 TEM images were reported. This investigation confirms the particles size dimensions, as well as definitely defines that US treatment does not affect to any extent the external habit of the TiO_2 micro-particles. Even through this kind of analysis, a loading less than 40% is not enough to see changes in the sample. Moreover, from 40% to 75% some differences need to be considered: indeed, for K_40 sample (Fig. 6.1, right side,

square in the upper right), the presence of the Cu species is confirmed by the amorphous edges; for K_75 sample (Fig. 6.1, right side, squares at the bottom), Cu–NPs are very evident both in the form of single particles and of aggregates.

6.3.1.2 High-resolution XPS

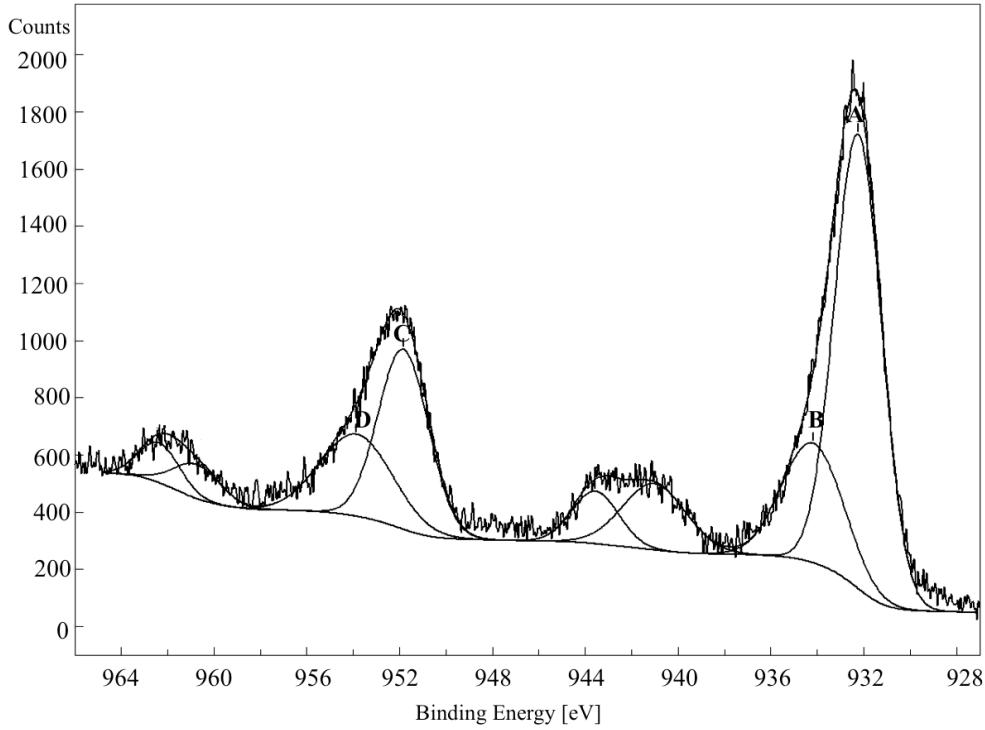

Fig. 6.2: XPS Cu High resolution spectrum for the sample K_75.

High resolution XPS spectrum was performed with a M-probe apparatus (Surface Science Instruments). Mainly the analysis of copper 2p confirms the presence of both the oxidation state of copper (Fig. 6.1), i.e. Cu_2O (corresponding to peak A: 932.2 eV) and CuO (corresponding to peak B: 934.2 eV) (Moulder et al., 1992).

6.3.1.3 Absorption/transmission IR spectra and band gap evaluation

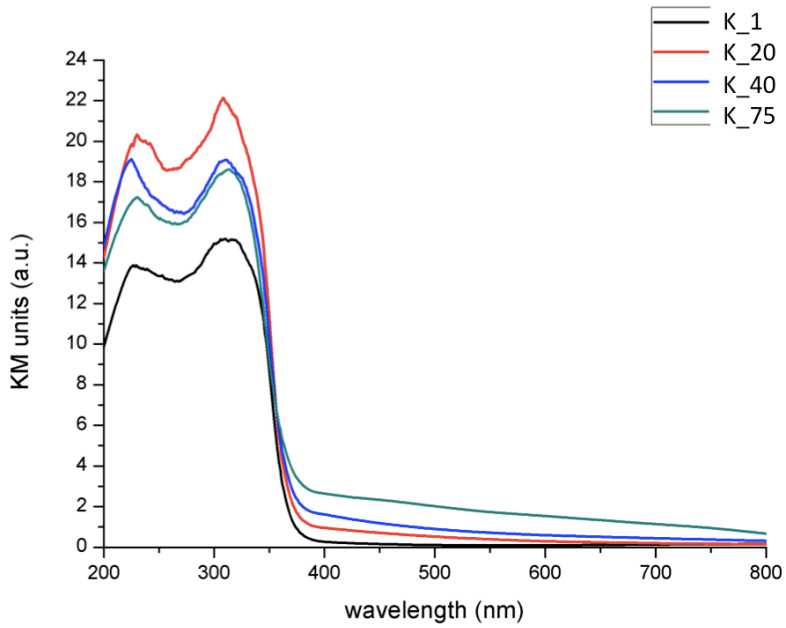

Fig. 6.3: Absorbance spectra in UV-VIS region of samples K_1, K_20, K_40, and K_75.

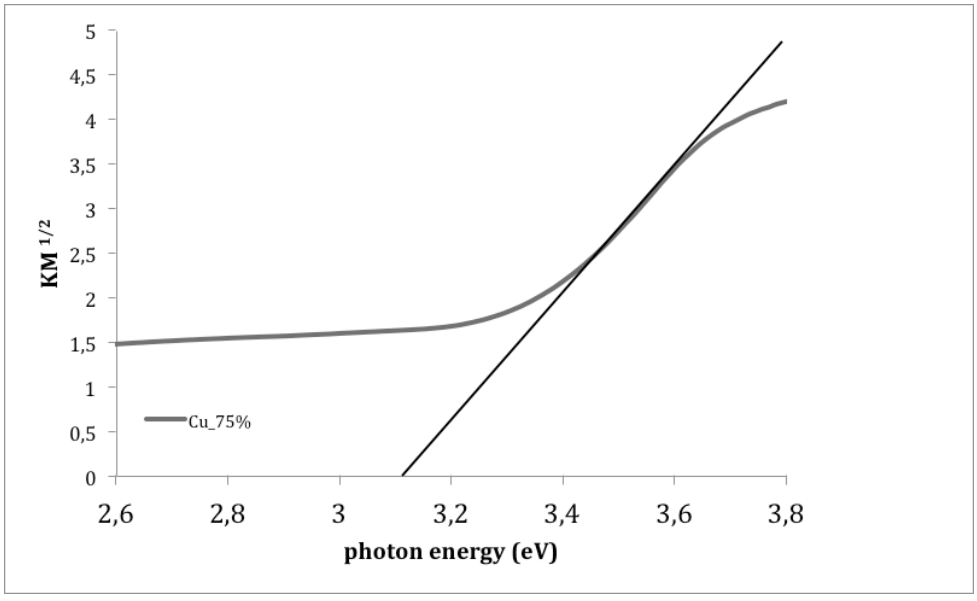

Fig. 6.4: $KM^{1/2}$ vs. photon energy (eV) for the sample K_75.

Fig. 6.3 reports the absorbance spectra in UV–VIS region and clearly shows the linear correlation between the copper amount and the width of the absorption peak in the visible wavelengths (>400 nm). Precisely, spectra reported in fig. 6.3 show the increasing of typical band of CuO (k > 420 nm). When present in high amounts, copper can affect the values of the band gap, as confirms by the graph presented in fig. 6.4. It was possible to calculate the value according to the Kubelka–Munk function to plot the $KM^{1/2}$ value versus eV first, and then drawing the tangent line to the curve. Reasons principally depend on the nature of cupric oxide. Indeed cupric oxide is an important p-type semiconductor metal oxide with a narrow band gap of 1.21–1.51 eV (Yang et al., 2014); thus, firstly, greater the amount of copper greater is the increasing of the visible light absorption, which slightly affects the band gap reducing it. Furthermore, both particles in metal form and oxidized form have to be considered, differently. As already explained, metal NPs are able to capture the electrons of the visible light and they can act as electron traps, reducing the electrons-holes recombination rate, thus the immediate effect on TiO_2 is the better electron-hole separation (Kubacka et al., 2013; Wang et al. 2006). Else metal oxides species, i.e. CuO and Cu_2O form a heterojunction with TiO_2 (Wang et al., 2015; Babu et al., 2015), forming the system Cu_2O–CuO, which is precisely a p-type semiconductor. The specific presence of TiO_2 promotes electron transfer from Cu_2O to CuO. Finally, in particular as regards the reduction of the band gap, Cu is considered to be one of the most important transition metals, thus it shifts the absorption spectra by decreasing the band gap of TiO_2, as reported by several studies. Specifically, when Ti^{4+} is replaced

by Cu^{2+}, CuO is formed; as known, it is able to absorb light with longer wavelength (Munir et al., 2016; Zhang et al. 2015).

6.3.1.4 Photocatalytic tests using copper-decorated TiO_2 as photocatalyst

Acetone and acetaldehyde were chosen to investigate the activity of the Cu-decorated-TiO_2 in terms of pollutants degradation in the gas-phase. Several photodegradation tests were performed changing some important parameters.

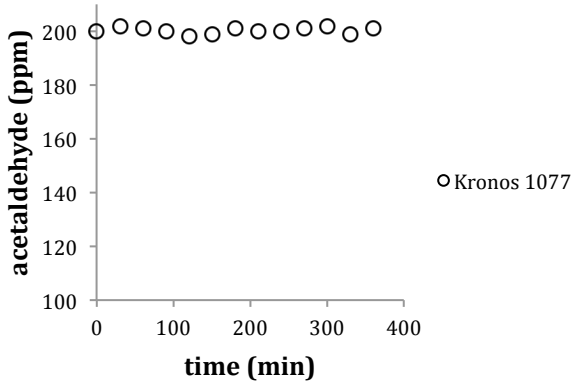

Fig. 6.5: Acetaldehyde photodegradation vs. time for bare 1077 TiO_2 – LED lightning.

Bare TiO_2 has no photoactivity (Fig. 6.5). Thus, it was the presence of surface copper to make it active. Especially, the photoefficiency of TiO_2 increased changing the copper amount, with a maximum for K_40 both for acetone and acetaldehyde degradation (Fig. 6.6). Then, exceeded the point of maximum activity, the concentration started to cover too much the TiO_2 surface inhibiting to the photocatalytic process.

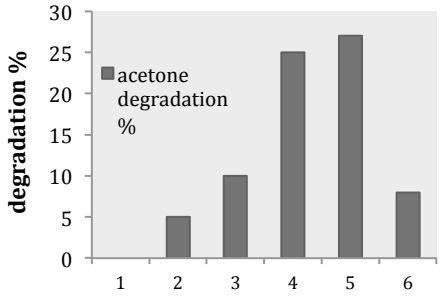

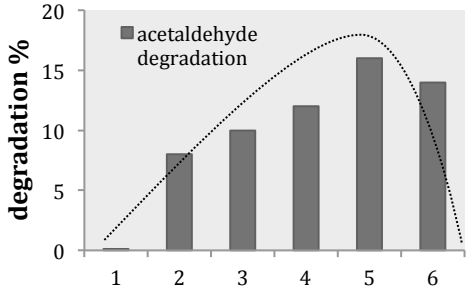

Fig. 6.6 (on the left): Acetone degradation % reached in 6 h increasing the amount of copper on the TiO_2 surface. 1) 1077 TiO_2; 2) K_5; 3) K_10; 4) K_20; 5) K_40; 6) K_75. – LED lightning.
Fig. 6.7 (on the right): Acetaldehyde degradation % reached in 6 h increasing the amount of copper on the TiO_2 surface. 1) 1077 TiO_2; 2) K_5; 3) K_10; 4) K_20; 5) K_40; 6) K_75. – LED lightning.

TEM images showed that copper is distributed with different morphologies and in form of different chemical species (either metallic or oxide) on the TiO_2 surface, but this aspect is not to be relevant to the final efficiency of the material. The strong correlation was instead between the amounts of the metal species deposited onto the support and the TiO_2 different abilities to degrade pollutants. Indeed, as explained even before, first metal and metal oxides species can positively act on the photoactivity of TiO_2 (Chiang et al., 2014; Xina et al., 2008; Zhang et al., 2015): greater was the quantity of them, greater were the photons captured from visible light; finally, being them available for the formation of more electron-hole couples (e^-/h^+), they can better act as electrons traps, improving the e^-/h^+ separation (Zhang et al., 2015). Beyond a certain amount of copper the decorated-TiO_2 performances start to decrease, because there is a point at which decoration do not bring more advantages. The main reason is the decrease of the number of available active TiO_2 surface sites (Fig. 6.7).

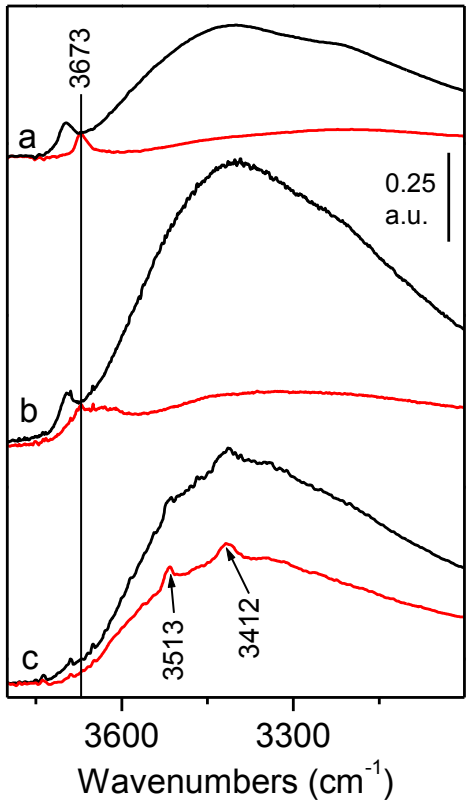

Fig. 6.8: FT-IR Spectra collected for Kronos 1077 (curves a), K_40 (curves b) and K_75 (curves c) in air (black lines) and after prolonged outgassing at RT (red lines).

The FT-IR spectra of bare 1077 TiO_2, K_40, and K_75 samples were performed both in air and after prolonged outgassing at RT. In the 4000–2500 cm^{-1} spectral range (see Fig. 6.8) different absorptions are present both in the absence and in the presence of Cu species. In particular, there are two absorption bands, located in the 3000–3600 cm^{-1} range and at 3620 cm^{-1} respectively. The former envelope is related to the stretching mode of all H-bonded OH groups present at the surface, according with literature data and precisely corresponds to the stretching mode of all

Ti–OH species free from hydrogen bonding interactions (Little, 1966; Morterra, 1988; Morterra et al., 1989). After prolonged out- gassing at RT, the peak due to free OH groups is now the only evident. In this specific case, other spectral components were evident at low wavenumbers for samples that contain a Cu content up to 40% (Fig. 6.8). This is reasonably related to the presence of Cu species, even though not confirmed by XRD (as they are most probably amorphous) but only observed by HR-TEM. Moreover, for the K_75 sample, the typical features observed for 1077 are upset. In particular there are no traces of free Ti-OH species are evident, as well as a much higher resistance upon outgassing of the H-bonded hydroxyls is observed, revealing a higher hydrophilic character with respect to the samples with lower Cu amount; finally, on top of the huge envelope due to H-bonded OH species two spectral components at 3513 and 3412 cm^{-1} are observable and reasonably ascribable to CuO and Cu_2O phases, whose presence is confirmed by both XRD and HR-TEM measurements. Because of the different amount of Cu, it was possible to observe that for the K_75 sample the OH related to Cu phases are evident at much lower wavenumbers than those observed for the K_40 sample. Specifically because of the lower Cu content, OH groups can be located in a bridged position between Ti and Cu cations, putting into evidence the almost complete coverage of TiO_2 surface by Cu phases. Thus, the loss in photo-catalytic activity passing from K_40 to K_75 sample can be related to the absence of accessible TiO_2 sites and, in particular, of Ti–OH species.

6.3.2 Silver-decorated TiO_2: characterization results and photocatalytic tests

6.3.2.1 Role of $NaBH_4$ and PVP in Ag-NPs synthesis

$NaBH_4$ is a common reducing agent and it is usually used for synthesis of metallic silver, starting from silver nitrate ($AgNO_3$) as precursor. PVP (Polyvinylpyrrolidone) is an anionic surfactant, and it is mainly used to control the particle size distribution (Yin et al., 2003). The presence of PVP influences the silver formation rate, and even it acts protecting particles during their growth. Thus, particle size and particle aggregation decrease with the PVP/$AgNO_3$ mole ratio. Mechanism of PVP protection acts in three steps: i) PVP donates loan pair electrons of oxygen and nitrogen atoms to sp orbitals of silver ions, and this first step leads to the formation of the coordinative complex of Ag ions and PVP; ii) on one hand, PVP promotes the nucleation of the metallic silver, because the Ag ions-PVP complex is more easily reduce than the pure Ag ions; iii) on the other hand, PVP prohibits silver particle aggregation, because particles growth as a result of its steric effect (Zhang et al., 1996; Pastoriza-Santos et al., 1999; Carotenuto et al., 2000). The long poly-vinyl chains of PVP that enclose silver particles have a classical steric affect and regulate the final silver NPs average dimension. A higher amount of PVP prevents more the growth of the nanoparticles, leading to a smaller average dimension.

6.3.2.2 Absorption/transmission UV-VIS spectra and band gap evaluation

Starting from the Kubelka-Munk equation that creates a linear relationship for spectral intensity relative to concentration, it was possible to evaluate the UV-vis absorbance spectra, finding specifically a linear correlation between the amounts of silver and the width of the absorption peak in the visible wavelengths (>400 nm). Figure 6.9 reports the curves related to samples containing 10% and 20% of silver respectively. Considering the visible-light wavelengths, from 400 nm to 700 nm, the red curve (20% Ag) is slightly above the black one, showing an increase of absorption increasing the silver amount.

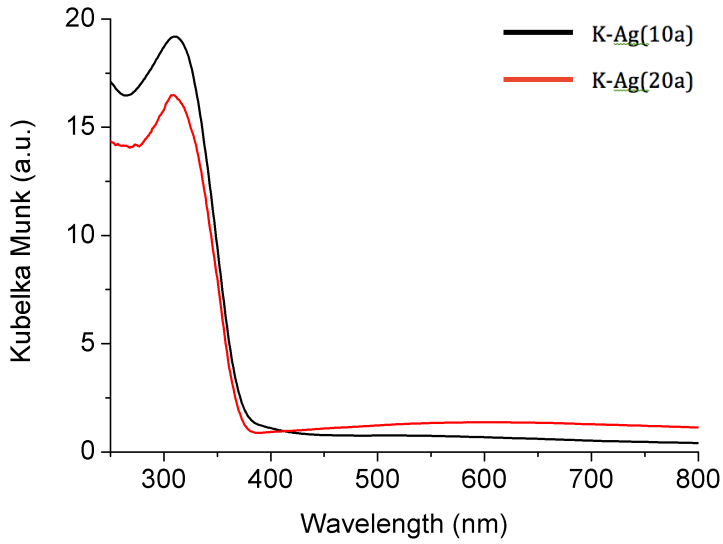

Fig. 6.9: Absorbance spectra in UV–VIS region of samples K-Ag(10a) (black line) and K-Ag(20a) (light-blue line). Samples contains 10%w/w and 20%w/w of silver respectively.

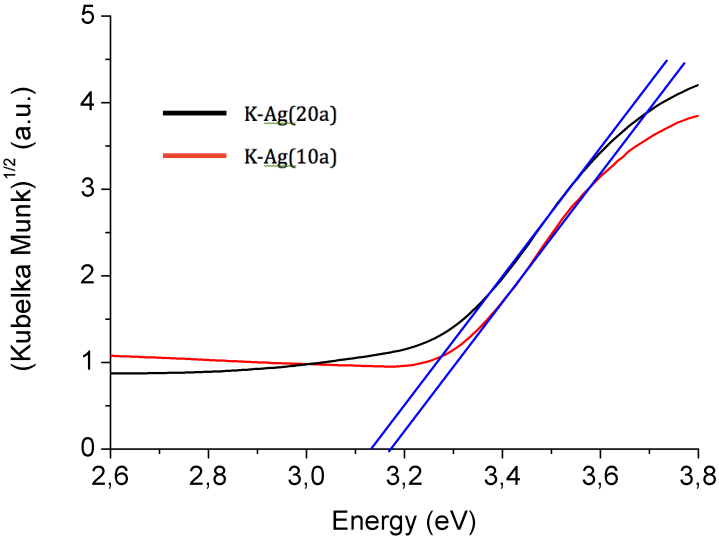

Fig. 6.10: $KM^{1/2}$ vs. photon energy (eV) for the sample K-Ag(10a) and sample K-Ag(20a).

Band gap values can be calculated plotting $R^{1/2}$ values as a function of energy (eV), as reported in fig. 6.10. Higher amount of silver caused a slightly decrease from the standard band gap value of TiO_2; however, the effect was not predominant and it is mainly attributable to the strong light absorption behavior typical of noble metal nanostructure, mostly due to surface plasmon resonance (SPR) deriving from the collective oscillation of surface electrons (Gao et al., 2016). Concerning this, both previous and more recent studies that investigated the effect of Ag NPs on the absorbance enhancement in thin film C-Si solar cells (Pillai et al., 2007), showed that localized plasmonic resonances can be used as an efficient light trapping part of Ag-TiO_2 (Sheng et al., 2012; Faramarzi Nezhad et al., 2016).

6.3.2.3 HR- TEM investigation: Ag particles size and distribution

HR-TEM analysis gave crucial information about the different distribution or dimension of silver nanoparticles of TiO_2 commercial samples surface (clearly micrometer in the figures). Firstly, US treatment has effect on the external habit of the TiO_2 micro-particles. Moreover, the role of US is now clear. Figure 6.11, A and B respectively, reports a first comparison, then discussed.

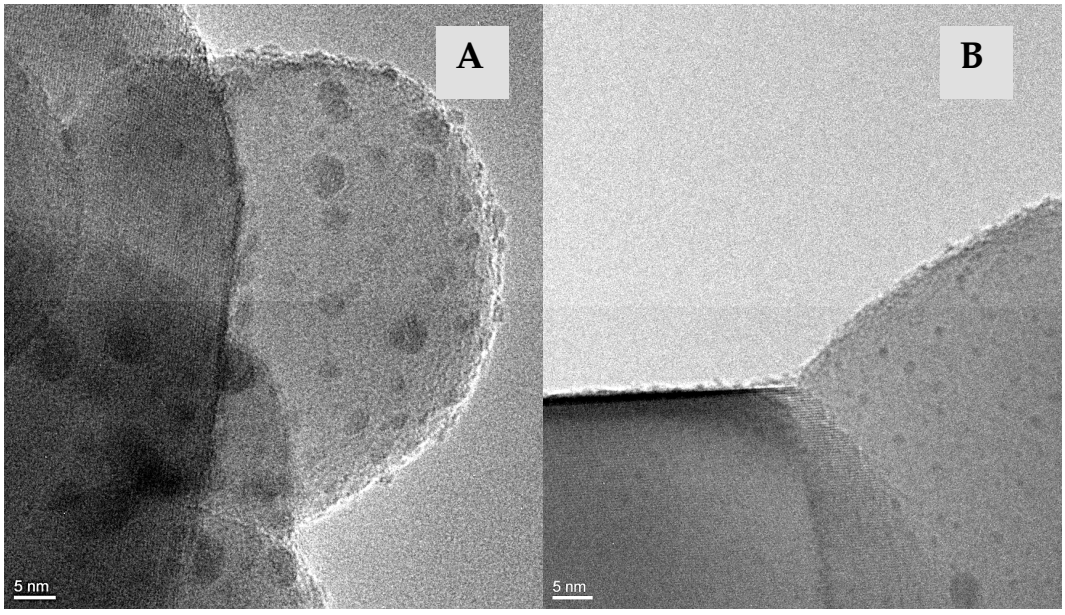

Fig. 6.11: Silver-decorated TiO_2 by means of high energy ultrasound (A) and without US application (B). Amount of silver (%w/w) is the same for both, exactly 10% of silver.

First of all, silver nanoparticles are bigger and they have a clear spherical shape. Indeed, PVP has a good influence of their growth. Furthermore, ultrasound is essential for their formation, because speeds up the diffusion of the solute, influences the contact between PVP and silver, and finally shapes the adsorption of Ag NPs on the surface of TiO_2 (Goharshadi et al., 2013). However, the total final effect depends on the simultaneous presence of both PVP and sonication. On one side, US

could reduce the nanoparticles dimension as expected, however, the concurrent presence of PVP give a sort of double effect, which as final results give the specific kind of silver nanoparticles, clearly visible in TEM images. Ag-NPs synthesized using $NaBH_4$, PVP as surfactant, and US, are distributed very homogeneously on the TiO_2 surface, and they have an average size between 2-8 nm (see also fig. 6.12).

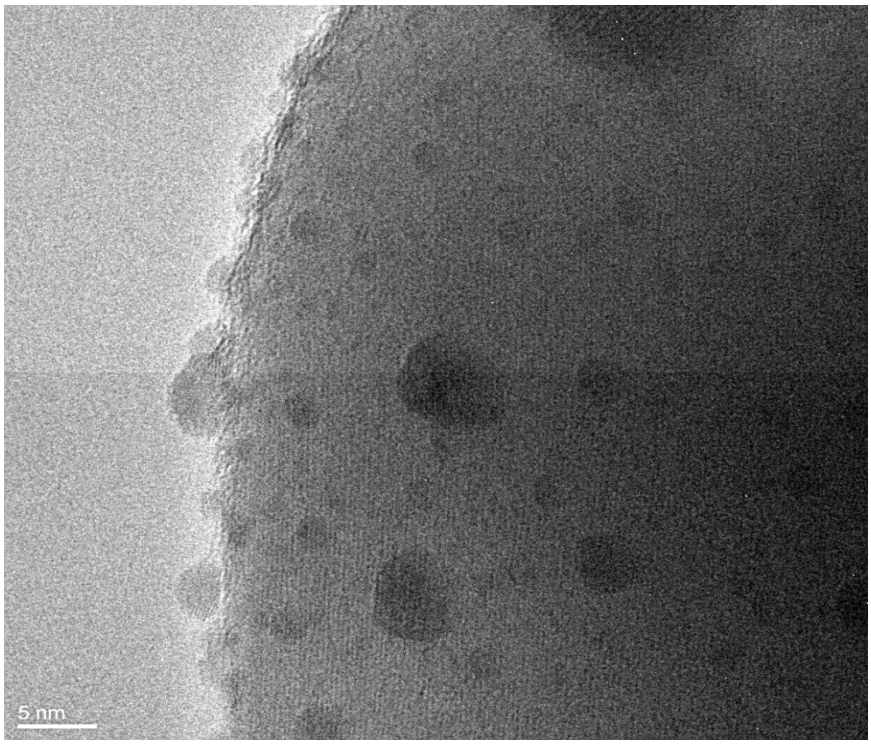

Fig. 6.12: TiO_2 decorated with silver nanoparticles (10%); synthesis procedure from $AgNO_3$ as precursor, 1077 TiO_2 as support, $NaBH_4$, PVP and ultrasound.

6.3.2.4 XRD, XPS analysis and ICP

All samples maintain the crystallographic phase composition typical of the 1077 starting material, which completely consists of anatase. Figure 6.13 reported below shows the XRD pattern. It exhibits strong diffraction peaks at 25° and 48° 2 theta, indicating TiO_2 in the anatase

phase. Overall, all peaks are in good agreement with the standard spectrum (JCPDS no.: 88-1175 and 84-1286). Peaks at 65°, 78°, 45° and 38° 2 theta values refer for the presence of a portion of Ag_2O, confirming even the presence of metallic silver. The simultaneous presence of oxide species depends particularly on the calcination step, because it was carried out in air, thus an oxidizing process occurred unavoidably. However, each peak related to silver is in good agreement with the standard spectrum (ICDD Database).

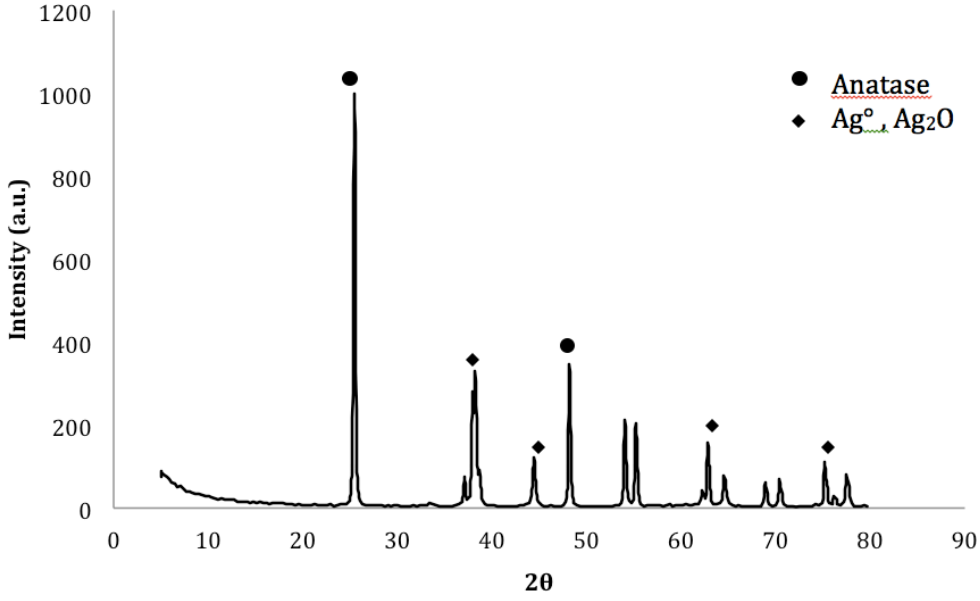

Fig. 6.13: X-ray diffraction of K-Ag(20a)-TiO_2 decorated by Ag (20% w/w) by means of US

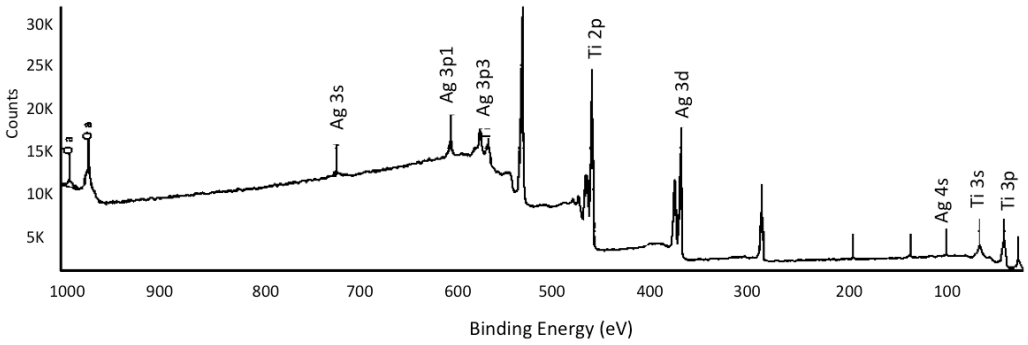

Fig. 6.14: XPS Survey analysis.

The analysis of the silver region first evaluated by XPS survey analysis (fig. 6.14) confirms the presence of Ag. Nevertheless, it was not possible to quantify the ratio between metal and oxidic species, because these binding energies are too close. Figure 6.15 reports the high-resolution spectrum of Ag.

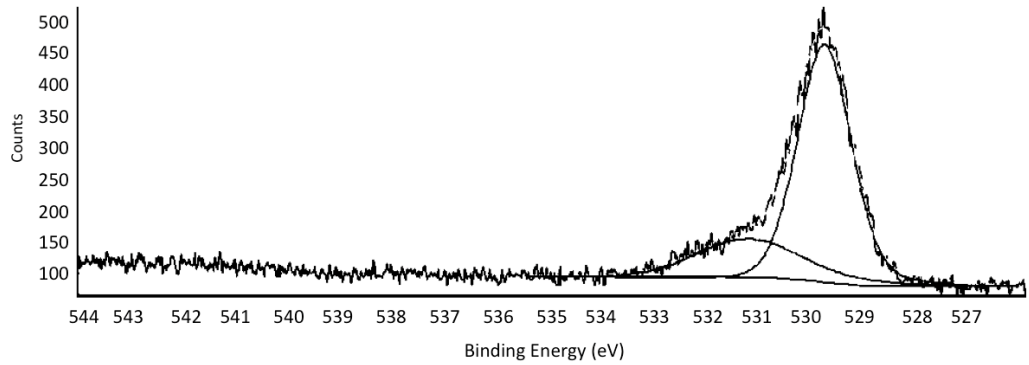

Fig. 6.15: XPS High-resolution spectrum of Ag.

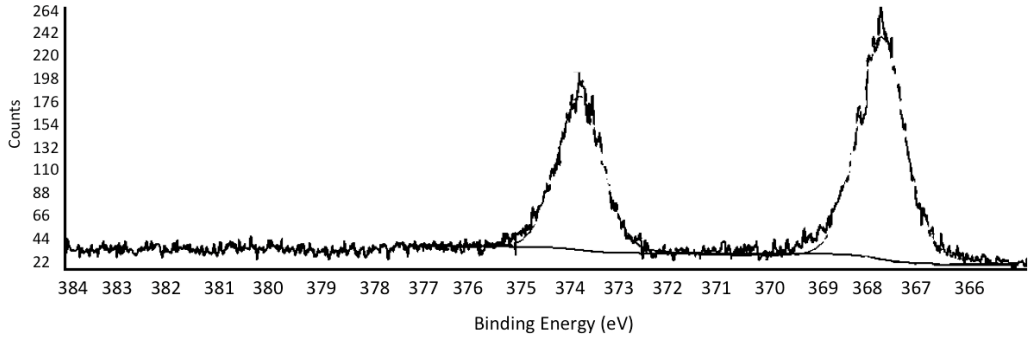

Fig. 6.16: XPS High-resolution spectrum of O.

Oxygen high-resolution spectrum (fig. 6.16) distinguishes the peaks ascribable to Ti-O bonds at 529.6 eV and surface hydroxyl groups at 531.0 eV. The ratio between these peak areas gives useful information about the hydroxyl species (OH) located at the surface of the photocatalyst. The OH/O ratio calculated for Ag-20(a) is 0.35, slightly higher than the value already measured for plain 1077 (0.32) (Bianchi et al., 2014). To confirm the precise value of silver amount deposited on TiO2 particles surface, ICP analysis were performed. For all samples, the theoretical silver percentage was confirmed by ICP, with a maximum variation detected in terms of silver lost around – 0.5% from the theoretical estimate. Thus, TiO_2 surface decoration with silver NPs using high-energy ultrasound leads to the complete deposition of silver on TiO_2 surface.

6.3.2.5 Photocatalytic degradation of acetone in gas phase by silver-decorated TiO_2 under visible light

In order to investigate the activity of the Ag-decorated-TiO2 in terms of pollutants degradation in the gas-phase, acetone was chosen as a reference molecule. Figure 6.17 shows the acetone concentration (ppm)

versus time during each single photocatalytic test, performed using the same setup described in the previous chapters, as well as in the experimental part.

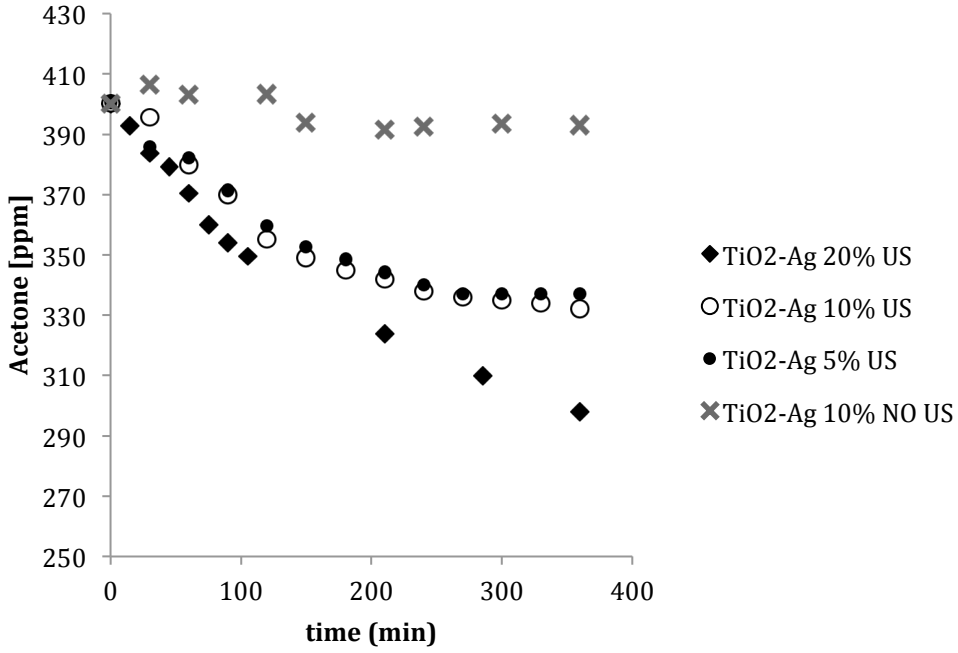

Fig. 6.17: Acetone concentration vs time under LED irradiation: comparison between samples prepared with US at different Ag %w/w (black rhombus, white dots and black dots respectively) and without US by means of classical impregnation method (grey crosses).

While undecorated TiO_2 exhibited no photoactivity if irradiated only with visible wavelengths, the presence of silver nanoparticles at the surface of TiO_2 activates the photoefficiency of TiO_2. In particular, the photocatalytic performance is clearly higher in case of TiO_2-Ag(20a), which the highest percentage of silver NPs distributed on the surface (precisely, 19.50% calculated by ICP analysis). Figure 6.18 clearly shows the increase of activity corresponding to the increase of silver amount.

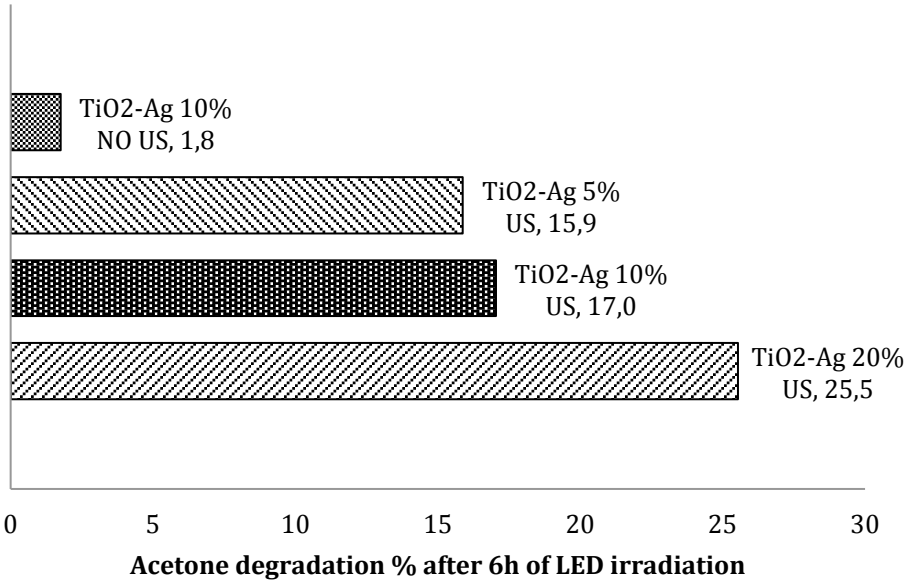

Fig. 6.18: Final acetone degradation % reached after 6 hours of irradiation by LED. Comparison between samples with or without US, different Ag %w/w

6.4 Conclusions

1077 TiO_2 was confirmed not photoactive if irradiated by visible light wavelengths, and thus not effective for the photodegradation of organic pollutants in gas phase. Modification of TiO_2 surface by depositing metal or metal oxide species, positively affected the TiO_2 absorption of light. In particular, copper or silver species can be synthesized and then deposited on TiO_2 by means of US. US acted both on the nanoparticles formation, as well as on their deposition and distribution on TiO_2 micro-particles. Moreover, US do not change the morphology of TiO_2. The amount of copper deposited on the surface is crucial for the important correlation existing between its presence and the number of available active sites on the TiO_2 surface, on which the pollutants must be

adsorbed to start the oxidation process. Hence, a higher amount of copper both increases the absorption of the visible light and improves the electron-hole separation, with better photocatalytic results, but over a certain amount of metal the performance decreases, because of the excessive coverage of the active sites of TiO_2. Equally, TiO_2 decorated with silver NPs is effective in photodegradation of acetone under visible light. Even in this case, the number of silver nanoparticles distributed onto TiO_2 surface affect the final photoactivity, and the correlation is linear, because an higher number of NPs leads to a better caption of the visible light electrons first, as well as they reduce the electron-hole recombination, acting as electron traps. In particular for silver nanoparticles synthesis, we found that PVP plays an important role in their formation, and influence their final shape, dimension and distribution on TiO_2 surface as well.

References

Ansari S.A., Khan M.M., Ansari M.O., Cho M.H., "Silver nanoparticles and defect-induced visible light photocatalytic and photoelectrochemical performance of Ag@m-TiO_2 nanocomposite", Sol. Energy Mater. Sol. Cells, **2015**, 141, 162–170.

Ansari S.A., Khan M.M., Ansari M.O., Lee J., Cho M.H., "Biogenic synthesis, photocatalytic, and photoelectrochemical performance of Ag–ZnO nanocomposite", J. Phys. Chem. C, **2013**, 117, 27023– 27030.

Awazu K., Fujimaki M., Rockstuhl C., Tominaga J., Murakami H., Ohki Y., Yoshida N., Watanabe T.A., "Plasmonic photocatalyst consisting of silver nanoparticles embedded in titanium dioxide", J. Am. Chem. Soc., **2008**, 130, 1676–1680.

Banerjee S., Pillai S.C., Falaras P., O' Shea K.E., Byrne J.A., Dionysiou D.D., "New insights into the mechanism of visible light photocatalysis", Phys. Chem. Lett., **2014**, 5, 2543–2554.

Bianchi C.L., Gatto S., Pirola C., Naldoni A., Di Michele A., Cerrato G., Crocellà V., Capucci V., "Photocatalytic degradation of acetone, acetaldehyde and toluene in gas-phase: Comparison between nano and micro-sized TiO_2", Appl. Catal. B: Env., **2014**, 146, 123–130.

Carotenuto G., Pepe G.P., Nicolais L., "Preparation and characterization of nano-sized Ag/PVP composites for optical applications", L. Eur. Phys. J. B, **2000**, 16, 11-17.

Chiang L.F., Doong R., "Cu–TiO_2 nanorods with enhanced ultraviolet and visible- light photoactivity for bisphenol A degradation", J. Hazard. Mater., **2014**, 277, 84–92.

Darroudi M., Ahmad M.B., Zamiri R., Abdullah A.H., Ibrahim N.A., Shameli K., Husin M.S., "Preparation and characterization of gelatin mediated silver nanoparticles by laser ablation", J. Alloys Compd., **2011**, 509, 1301–1304.

Dong C., Zhang X., Cai H., "Green synthesis of monodisperse silver nanoparticles using hydroxyl- propyl-methyl-cellulose", J. Alloys Compd., **2014**, 583, 267–271.

Faramarzi Nezhad M., Shahtahmassebi N., Behdani M., "Improvement efficiency of thin-film solar cell by plasmonic properties of silver", Optik, **2016**, 127, 8419–8422.

Gao S., Zhang Z., Liu K., Dong B., "Direct evidence of plasmonic enhancement on catalytic reduction of 4-nitrophenol over silver nanoparticles supported on flexible fibrous networks", Appl. Catal. B: Env., **2016**, 188, 245–252..

Goharshadi E.K., Azizi-Toupkanloo H., "Silver colloid nanoparticles: Ultrasound-assisted synthesis, electrical and rheological properties", Powder Technol., **2013**, 237, 97–101.

Gutierrez M., Henglein A., Dohrmann J.K., "Hydrogen atom reactions in the sonolysis of aqueous solutions", J. Phys. Chem., **1987**, 91, 6687–6690.
Khan Z., Hussain J.I., Kumar S., Hashmi A.A., "Silver nanoplates and nanowires by a simple chemical reduction method", Colloids Surf. B: Biointerfaces, **2011**, 86, 87–92.
Kochuveedu S.T., Jang Y.H., Kim D.H., "A study on the mechanism for the interaction of light with noble metal–metal oxide semiconductor nanostructures for various photophysical applications", Chem. Soc. Rev., **2013**, 42, 8467-8493.
Kubacka A., Munoz-Batista M.J., Ferrer M., Fernandez-Garcia M., "UV and visible light optimization of anatase TiO_2 antimicrobial properties: Surface deposition of metal and oxide (Cu, Zn, Ag) species", Appl. Cat B., **2013**, 140-141, 680-690.
Morterra C., "An infrared spectroscopic study of anatase properties - Surface hydratation and strong Lewis acidity of pure and sulfate-doped preparations", Faraday Trans., **1988**, 1(84), 1617–1637.
Morterra C., Bolis V., Fisicaro E., "The hydrated layer and the adsorption of carbon monoxide at the surface of titania (anatase)", Colloids Surf., **1989**, 41, 177–188.
Moulder J., Stickle W., Sobol P., Bomben K., "Handbook of X-ray photoelectron spectroscopy", J. Chastainc, Ed., United States of America: Perkin-Elmer Corporation Publication, **1992**.
Munir S., Mujtaba Shah S., Hussain H., Ali Khan R., "Effect of carrier concentration on the optical band gap of TiO_2 nanoparticles", Mater. Des., **2016**, 92, 64–72.
Linic S., Christopher P., Ingram D.B., "Plasmonic-metal nanostructures for efficient conversion of solar to chemical energy", Nat. Mater., **2011**, 10, 911– 921.
Little L.H., "Infrared spectra of adsorbed species", Academic Press, London, **1966**.
Liu Y., Chen S., Zhong L., Wu G., "Preparation of high-stable silver nanoparticle dispersion by using sodium alginate as a stabilizer under gamma radiation", Radiat. Phys. Chem., **2009**, 78, 251–255.
Pastoriza-Santos I., Liz-Marzan L.M., "Formation and stabilization of silver nanoparticles through reduction by N, N-dimethylformamide", Langmuir, **1999**, 15, 948-951.
Pillai S., Catchpole K.R., Trupke T., Green M.A., "Surface plasmon enhanced silicon solar cells", J. Appl. Phys., **2007**, 101, 93105-93108.
Podasca V.E., Buruiana T., Buruiana E.C., "UV-cured polymeric films containing ZnO and silver nanoparticles with UV–vis light-assisted photocatalytic activity", Appl. Surf. Sci., **2016**, 377, 262–273.
Sheng X., Hu J., Michel J., Kimerling L.C., "Light trapping limits in plasmonic solar cells: an analytical investigation", Opt. Express, **2012**,

20, 496–501.
Shim I.K., Lee Y.I., Lee K.J., Joung J., "An organometallic route to highly monodispersed silver nanoparticles and their application to ink-jet printing", Mater. Chem. Phys., **2008**, 110, 316–321.
Stucchi M., Bianchi C.L., Pirola C., Vitali S., Cerrato G., Morandi S., Argirusis C., Sourkouni G., Sakkas P.M., Capucci V., "Surface decoration of commercial micro-sized TiO_2 by means of high energy ultrasound: a way to enhance its photocatalytic activity under visible light", App. Catal. B, **2015**, 178, 124–132.
Su C., Liu L., Zhang M., Zhang Y., Shao C., "Fabrication of Ag/TiO_2 nanoheterostructures with visible light photocatalytic function via a solvothermal approach", Cryst. Eng. Comm., **2012**, 14, 3989–3999.
Suslick K.S., Fang M.M., Hyeon T., Mdleleni M.M., "Applications of sonochemistry to materials synthesis", Sonochem. Sonolum., **1999**, 291–320.
Tahira K., Nazir S., Li B., Khan A.U., Khan Z.U.H., Ahmad A., Khan Q.U., Zhao Y., "Enhanced visible light photocatalytic inactivation of Escherichia coli using silver nanoparticles as photocatalyst", J. Photochem. Photobiol. B: Biology, **2015**, 153, 261–266.
Tao X., Zhao Y., "Sonochemical synthesis and characterization of disk-like copper microcrystals", Mater. Chem. Phys., **2011**, 125, 219–223.
Wani I.A., Ganguly A., Ahmed J., Ahmad T., "Silver nanoparticles: ultrasonic wave assisted synthesis, optical characterization and surface area studies", Mater. Lett., **2011**, 65, 520–522.
Wang H., Zhang L., Chen Z., Hu J., Li S., Wang Z., Liu J., Wang X., "Semiconductor heterojunction photocatalysts: design, construction, and photocatalytic performances", Chem. Soc. Rev., **2014**, 43, 5234–5244.
Wang C., Pagel R., Dohrmann J.K., Bahnemann D.W., "Antenna mechanism and deaggregation concept: novel mechanistic principles for photocatalysis", C.R. Chimie, **2006**, 9, 761-773.
Wang P., Wen X., Amal R., Hau Y., "Introducing a protective interlayer of TiO_2 in Cu_2O–CuO heterojuction thin film as a highly stable visible light photocathode", RCS Adv., **2015**, 5, 5231–5236.
Xin B., Wang P., Ding D., Liu J., Ren Z., Fu H., "Effect of surface species on Cu-TiO_2 photocatalytic activity", Appl. Surf. Sci., **2008**, 254, 2569–2574.
Yang C., Wang J., Xiao F., Su X., "Microwave hydrothermal disassembly for evolution from CuO dendrites to nanosheets and their applications in catalysis and photo-catalysis", Powder Technol., **2014**, 264, 36–42.
Yin B., Ma H., Wang S., Chen S., "Electrochemical synthesis of silver nanoparticles under protection of Poly(N-vinylpyrrolidone)", J. Phys. Chem. B, **2003**, 17, 8898-8904.

Zhao J., Li Y., Zhu Y., Wang Y., Wang C., "Enhanced CO_2 photoreduction activity of black TiO_2-coated Cu nanoparticles under visible light irradiation: role of metallic Cu", Appl. Catal. A, **2016**, 510, 34–41.
Zhang W., Liu Y., Yu B., Zhang J., Lian W., "Effects of silver substrates on the visible light photocatalytic activities of copper-doped titanium dioxide thin films", Mater. Sci. Semicond. Process., **2015**, 30, 527–534.
Zhang S., Peng B., Yang S., Wang H., Yu H., Y. Fang Y., Peng F., "Non-noble metal copper nanoparticles-decorated TiO_2 nanotube arrays with plasmon-enhanced photocatalytic hydrogen evolution under visible light", Int. J. Hydrogen Energy, **2015**, 40, 303–310.
Zhang Z., Zhao B., Hu L., "PVP protective mechanism of ultrafine silver powder synthesized by chemical reduction processes", J. Solid State Chem., **1996**, 121, 105-110.

CHAPTER 7:
BUILDING MATERIALS

Abstract

The development of new strategies and new materials to clean the environment is definitely imperative, and this is one of the first reasons why TiO_2-coated materials with interesting photocatalytic properties have been deeply studied and developed. As known, the deposition of anatase TiO_2 confers special properties and architectural features, and the traditional ceramic easily become photocatalytic eco-active materials able to reduce polluting molecules. While at the beginning of the industrial productions tiles were considered as just a technical material, market demands are now geared towards product with specific properties and beauty. The production of large ceramic slabs is one of the newest frontiers. Thus, first we need a suitable technology to depose TiO_2 on these "new-sized" tiles. Digital Printing was exploited as a new tool to manufacture photocatalytic tiles even of very large size. Secondly, it is important to find a serious and reproducible way to confirm their photo-efficiency, because although in literature different reactors were presented, working conditions are always far from reality. This chapter presents a new kind of gas-flow reactor able to test photocatalytic building materials of large size, whose the right design was confirmed by 3D simulations. It was then exploited to test and compare the two different methods (previously presented) to obtained photocatalytic active ceramic tiles, and the effectiveness of the materials was demonstrated in real conditions. This setup for testing material on the NO_x degradation in gas phase gave us information about the real capacity of a material in term of pollution abatement, as well as it allows to conduct tests even under direct sunlight.

7.1 Introduction

The application of TiO_2 in different materials has been studied, applied and even exploited in many different ways. Especially in this field, the use of micrometer TiO_2, on building materials and paintings, may bring many benefits, as already told, particularly because compared with nanometric TiO_2, does not entail problems in handling, storage and it is known to be much less expensive (Bianchi et al., 2014). The coating of TiO_2 allows conferring the material surfaces all the properties of TiO_2 as semiconductor (Taurino et al., 2106). Overall, TiO_2 is widely used on different materials and for different applications, such as for exterior construction materials (Graziani et al., 2014; Chen et al., 2009) or for water and air purification (Zhao et al., 2003; Fujishima et al., 1972) for the preparation of self-cleaning and antibacterial cements (Diamanti et al., 2013), on tiles (Sciancalepore et al., 2015; Bianchi et al., 2012), on glass (Zhaoet al., 2008), and, recently, for the protection of the cultural heritage (Quagliarini et al., 2012). In general, the most exploited strategy to prepare photocatalytic materials containing or supporting TiO_2, is coating. Indeed, there are different techniques by means of which it is possible to prepare and coat TiO_2 on solid supports, such as glass, metals or ceramics. Dip-coating, spin-coating and spray-coating, are the most used to spread the TiO_2 mixture over the support. Also, the addition of silica as a suspension improves both adhesion and hydrophilicity of coating. As many deposition techniques were exploited, there are also many different supports or materials that can be used. Concerning TiO_2-coated materials with interesting photocatalytic properties, and that can be employed in both outdoor and indoor environments, specifically for the pollution abatement, porcelain grés tiles are among the most attractive. When the industrial production began in the 1970s, porcelain

grés tiles were aesthetically not very attractive and considered as just a technical material characterized by lack of porosity and strong resistance to both abrasion and acid attack. However, in the last decades, porcelain grés tiles underwent significant transformations in terms of appearance, mainly in size. The advanced and innovative industrial production methods allow obtaining both useful structural and aesthetic properties. One of the last progresses was the increasingly easier production of slabs of large sizes (such as 300×150 cm). In general, this is the new frontier of building materials (Bianchi et al., 2012). The deposition of anatase TiO_2 confers special properties and architectural features, as well as converts the traditional ceramic into a photocatalytic eco-active material with the ability to reduce polluting molecules present in both air and water, to eliminate bacteria and to reduce the surface dirt thanks to the self-cleaning properties (Bianchi et al., 2013). Self-cleaning properties are more linked to the different behavior of TiO_2 towards water, indeed they depend on TiO_2-based material's hydrophobicity or hydrophilicity (Ragesh et al., 2014). TiO_2 presence can be exploited from two different points of view. In the first case TiO_2 nanoparticles are introduced inside a polymeric matrix in order to create nano-roughness on the surfaces and make them hydrophobic and superhydrophobic (Cappelletti et al., 2015; La Russa et al., 2012): superhydrophobic surfaces have high roughness, which implies low adhesion forces between contaminating particles and the surface, so water droplets roll off very quickly, as well as dirt can be very efficiently removed (Furstner et al., 2005). On the contrary, TiO_2 becomes superhydrophilic when exposed under UV light. In this other case, water is able to create a uniform film on the treated surfaces, preventing contact between external dirt and surfaces themselves (Quagliarini et al., 2012). Finally, TiO_2 confers an increasing of the antibacterial properties, making

ceramic surfaces strongly active for bacteria destruction, just in presence of light and humidity (Matsunaga et al., 1985; Scuderi et al., 2016).

7.1.1 Large slabs production: Digital Printing to eco-activate porcelain grés large slabs using micro-TiO_2 as photocatalyst

New industrially produced photocatalytic slabs provide very good photocatalytic performance, but also meet standard requirements with respect to hardness, lack of porosity, vitrified surface, durability: these are key features required of porcelain floor and wall tiles, which best representing innovation in today's surfaces. A very interesting product of technological progress, which increasingly asks for sophisticated products with beautiful aesthetic effects, is a maxi floor and wall tile system, which combines the traditional qualities of porcelain with the new features of ultra-high performance. As already mentioned, mostly at the beginning of the industrial productions, porcelain grés tiles were considered as just a technical material. On the contrary, today, market demands are also geared towards product both with specific properties and beauty. The last frontier of building materials, particularly in term of aesthetic features, is the preparation of slabs of large sizes. Not only they have strength, light weight, flexibility, and ductility: these sophisticated products offer amazing aesthetic effects, as maxi floors and wall tile systems, which combines the traditional qualities of porcelain with the new features of ultra-high performance and a milestone in design and technology: the largest size currently available. However, if the final goal is the realization of photoactive materials, we need a suitable technology to depose TiO_2 on these "new-sized" tiles. The digital printing technology, already presented in this work, was thus exploited as a new tool to manufacture photocatalytic tiles even of

very large size (150x300 cm). Photocatalytic materials are capable of reacting with the most common pollutants, as explained and showed even in the previous chapters of this work. Also their distinctiveness antibacterial and self-cleaning properties were fully demonstrated through the specific tests (internationally approved). The ceramic surface digitally printed with a TiO_2-based ink, present on their surface a stable photocatalytic film, with all the properties of a photocatalytic material. As presented more in detail in the previous dedicated paragraphs, positive results are obtained in the photodegradation of either nitrogen oxides or organics, single or in mixture. Also self-cleaning action and antibacterial property were confirmed.

7.1.2 From laboratory to reality: are they real effective?

The development of new strategies and new materials to clean the environment is definitely imperative. Moreover, year-by-year laws and regulations become stricter. Nitrogen oxides are continuously monitored all over the world, and more carefully. The preparation of TiO_2-based materials is well known and definitely it was approved that it is a workable anti-pollution system. However, one of the main problems regarding tests on construction materials (paints, cements, tiles, concretes, etc.) is finding a serious and reproducible way to confirm their photo-efficiency. In literature, different reactors with different configurations were presented (Minero et al., 2013; Matsuda and Hatano, 2005; Signoretto et al., 2010). In addition, ISO 22197-1 rule presents the reference photocatalytic reactor (ISO 22197-1, 2007). The most described and used reactors, particularly for NO_x degradation, are the following: i) a gas-tight acrylic flow reactor equipped with a Pyrex window containing the pressed photocatalyst (Menéndez-Flores et al.,

2011), ii) a photoactive sample coated on a glass plate placed in a quartz reactor (Kim et al., 2010), iii) a fixed-bed reactor (Signoretto et al., 2010), iv) a glass holder plate set in the center of a reactor (Zhan et al., 2009), and v) a glass substrate coated with the film placed in the center of an acrylic container (Lee et al., 2009). Moreover, Minero et al. (Minero et al., 2013) investigated specifically different gas/solid reactors, such as batch or flow-through either a continuous stirred-tank reactor (CSTR) or a plug flow reactor (PFR). The crucial problem concerns the conditions, which are almost always far from reality. Indeed, the main parameters are very good for the laboratory photocatalytic tests concerning the NO_x analysis, but using them there is no way to verify the real performance of a photocatalytic material in a true realistic context. The main issues go from the small sizes requested for testing samples, very far from the dimension of the actual final material used, to too high pollutants concentrations, as well as UV irradiation levels impossible to obtain on earth. As example the values of the NO_x collected by the monitoring stations in Milan (Italy) in the last year, the average value does not get over 100 ppb even during the less windy days (*http://itaarpalombardiait/ita/indexasp*). In general, air of good quality has to have NO_x concentrations lower than 20 ppb (*http://www.who.int/en.*) and 200 ppb is the second and last alert threshold.

Therefore, compared to all that was just described, another goal of this research project was the development and the study of a new kind of gas-flow reactor able to test photocatalytic building materials of large size. Reaction conditions were optimized in order to work both under artificial conditions of irradiation (UV-A lamp) and under direct sunshine. Particularly in the latter case, the test can predict the real efficiency of the material. The reactor was designed to simulate on laboratory bench-scale equipment the actual environment in which a

photocatalytic tile works. It is clear that outdoor, pollutants have no a defined flow and concentration, thus the situation is in general very different from which that is created inside a normal chemical reactor. Moreover, the weather conditions should be considered, because both the concentration of the reactants and the way in which these reactants come in contact with the tile are strongly dependent on them. For example, in the absence of wind, the contact time between pollutant molecules and the tile surface can be very high; on the other hand, under conditions of strong wind, the same parameter can be very low. These considerations explain the reason why this reactor is not based on a traditional engineering approach, with the aim of reproducing the real working environment of the photocatalytic product. Reactor dimensions were specifically established so that it contained the industrial tile (600 mm x 600 mm), as well as the height was calculated in order to obtain residence times in the range of 0.25-0.35 h, considering the flow rate between 140 and 180 NL h^{-1}. Using such dimensions and such flow rates, the simulation study performed by using the COMSOL software indicates good homogeneity in the reactor and residence times suitable for the reproduction of the real working conditions.

7.2 Materials and methods

7.2.1 General conditions

NO_x degradation was reported using 140 NL h^{-1} or 180 NL h^{-1} of gas stream polluted either with 100 ± 10 or 200 ± 10 ppb NO_x. NO and NO_2 in a mixture were constantly monitored individually as well. For the kinetics performed under sunlight, the amount of UV-A was monitored by using a radiometer. As testing samples, different kinds of

photocatalytic porcelain-grés tile by GranitiFiandre SpA were chosen. In general, as described more in detail in the previous chapters, these tiles are all industrially produced by making use 1077 micro-sized TiO_2, according with the purpose to completely replace nanopowders (Trouiller et al., 2009; Kuhlbusch et al., 2011; Quigg et al. 2013). Calcination temperature was set at 600°C, showing no changes in the TiO_2 crystallographic phase from anatase to rutile (Bianchi et al., 2013). This mainly because the presence of SiO_2 together with TiO_2 inhibits the crystal growth this latter, allowing the preservation of the anatase (Anderson and Bard, 1997; Xie and Lin, 2007).

7.2.2 Catalytic tile preparation

For reasons of brevity, because of the process have already been described in the general experimental part, only the key steps are here summarized.
Industrial grés tile were manufactured under high pressure, by dry-pressing of raw materials (mainly quartz, feldspar and other fluxes). Firing was done at temperatures between 1200-1300 °C. The covering process by TiO_2 can be obtained by classical spray method or by Digital Printing as already presented. TiO_2 was fixed by firing at 680°C.

7.2.3 Photocatalytic performances: from shorter to longer photocatalytic tests, from 24h24 testing to multiple-days testing.

Table 7.1 resumes all the different work conditions, used to perform the photodegradation kinetics.

General work conditions	
Irradiation	▪ UV-A 20 Wm^{-2} ▪ Sunlight (from July to September)
NO_x starting concentration	100 ± 10 ppb 200 ± 10 ppb ** 106 ppb = limit value (Directive 2008/50/EC); 213 ppb = alert treshold*
Gas flow rate	140 NL h^{-1} 180 NL h^{-1}
Duration of tests	6h 12h 24h Multiple-days

Table 7.1 Work conditions summary.

The final design of the reactor was selected among many possibilities, mainly considering the results of simulation studies. Overall, size and the inlet/outlet position assure good homogeneity of the reactant in the gas phase and a contact between the reactant and the photocatalytic tiles that effectively reproduce the real working conditions.

7.2.4 Simulations

Fluid dynamics simulations and kinetic simulations were performed. Firstly, the fluid dynamics simulations (performed using COMSOL Multiphysics® 4.0a) allow to study the reactor configuration under flowing conditions, coupling the laminar flow with the species transport in a 3D space; each geometry was similar to the relevant reactor dimensions. Results verified the homogeneous distribution of the gas flow over the tile surface, and allow visualizing the eventually formed concentration gradients. The initial NO_x concentration value (equivalent to 100 ppb) was 4.132×10^{-6} mol m^{-3}, and the diffusion coefficient of NO_x

in air (D) at 21.1 °C was precisely 1.54 × 10^{-5} m^2 s^{-1} (Massman, 1998). Simulations were performed considering air as the medium (using the relevant constant provided by the software) and two inlet fluxes: 5.0 × 10^{-5} m^3 s^{-1} (equivalent to 180 NL h^{-1}) or 3.8 × 10^{-5} m^3 s^{-1} (equivalent to 140 NL h^{-1}). Equation 7.1 refers to the integration of the reactor mass balance.

$$F_{out} = F_{in} + r_{NOx} \quad (7.1)$$

F refers to the molar fluxes expressed in mol min^{-1}, while *r* is the rate of the photocatalytic reaction, expressed using the Langmuir–Hinshelwood model. Complete expression for *r* is reported below (eq. 7.2).

$$r_{NOx} = -dNO_x/dt = -k_{NOx}(A \times W \times K_{NOx} \times n_{NOx})/(1+K_{NO} \times n_{NO} \times K_{NO2} \times n_{NO2} \times K_{NO3} \times n_{NO3}) \quad (7.2)$$

k (lowercase) represents the kinetic constants, while K (uppercase) represents the adsorption constants. A and W are the catalytic surface and the specific lamp power measured on the tile surface, respectively. NO_3 is related to reaction products and their concentration is calculated by molar balance, i.e. summing the reacted moles of NO and NO_2. The kinetic parameters were regressed in a previous study by Bianchi et al. (Bianchi et al., 2015) and are resumed in Table 7.2.

NO_2 adsorption constant, K_{NO2} (mol-1)	NO_2 kinetic constant, K_{NO2} (mol-1 W-1)	NO adsorption constant, K_{NO} (mol-1)	NO adsorption constant, K_{NO} (mol-1 W-1)
194.7	8.00	77.3	3.20

Table 7.2 NO_x degradation kinetic parameters

Concerning to the method reported by Bianchi et al. (Bianchi et al., 2015), similarly 106 mol^{-1} was used as specific value of adsorption constant of the species irreversibly adsorbed. Equations were integrated by MatLab version R2015a software by The MathWorks, Inc.

7.3 Results and discussion

7.3.1 Reactor fluid dynamics and kinetic simulations

Fig. 7.1 shows the x–y and y–z views of the reactor and the red lines represent the gas flow streams in the reactor volume.

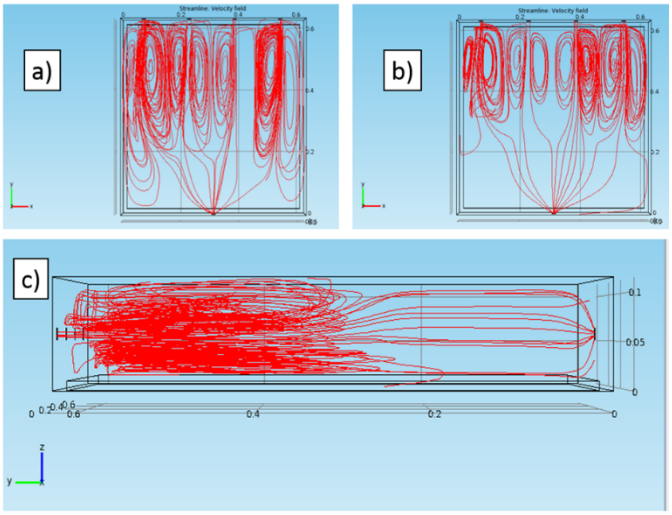

Fig. 7.1: Flow lines of the gas stream in the reactor in the 3D simulation for a) 180 NLh^{-1} and b), c) 140 NLh^{-1}. Views of the a), b) x-y and of the c) y-z planes.

The gas flux is high and leads to turbulence, especially for the region closer to the reactor inlet. Thus, first of all simulations confirm that the presence of four inlets and one outlet is an ideal choice to allow a good

gas stream and an adequate distribution of the gas on the photoactive tile.

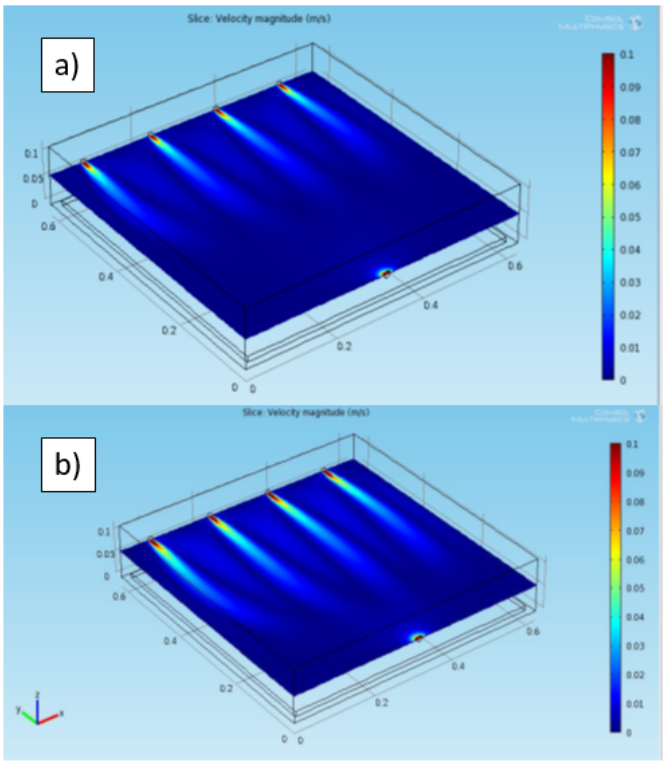

Fig. 7.2: Local velocity as x-y sections (at z=57.5 mm, i.e. in correspondence of the inlets centre height of the gas stream in the reactor) in the 3D simulation for (a) 140 NL h^{-1} and (b) for 180 NL h^{-1}. The maximum range was limited to 0.1 m s^{-1}.

Because the highest local velocities are located close to the inlet and the outlet (see fig. 7.2), the maximum value of the visualized range was limited to 0.1 m s^{-1}; the simulated maximum speeds are 0.3 m s^{-1} for 140 NL h^{-1}, and 0.4 m s^{-1} for 180 NL h^{-1}, respectively. The important point to underline is that, overall, the dead zone can be considered as negligible in this configuration.

The kinetic simulation was performed primarily through a 1D simulation (MatLab), considering both the average distribution of the pollutants and the average activity of the photocatalytic tile.

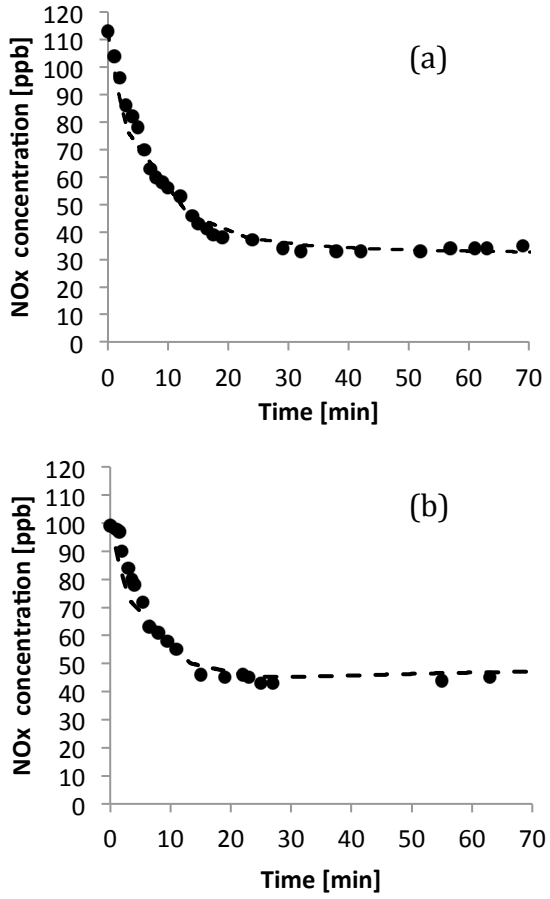

Fig. 7.3: NO_x photodegradation under 20 W m^{-2} of UV-A light. a) total flow rate 140 NL h^{-1}; b) total flow rate 180 NL h^{-1}.

As evident in fig. 7.3, pollutants are successfully degraded and that the maximum conversion is reached after about 40 minutes for both flows. Using a reactant flow of 140 NL h^{-1}, a minimum level of NO_x concentration was reached (Fig. 7.3 (a)) because of the higher residence time in the reactor. Overall, the simulation agrees with the experimental

data, confirming the validity of this model. The degradation kinetic performed starting with a double concentration (i.e. 200 ppb) was reported in Fig. 7.4, together with the simulations. Duration is this case was longer and prolonged up to 24 h.

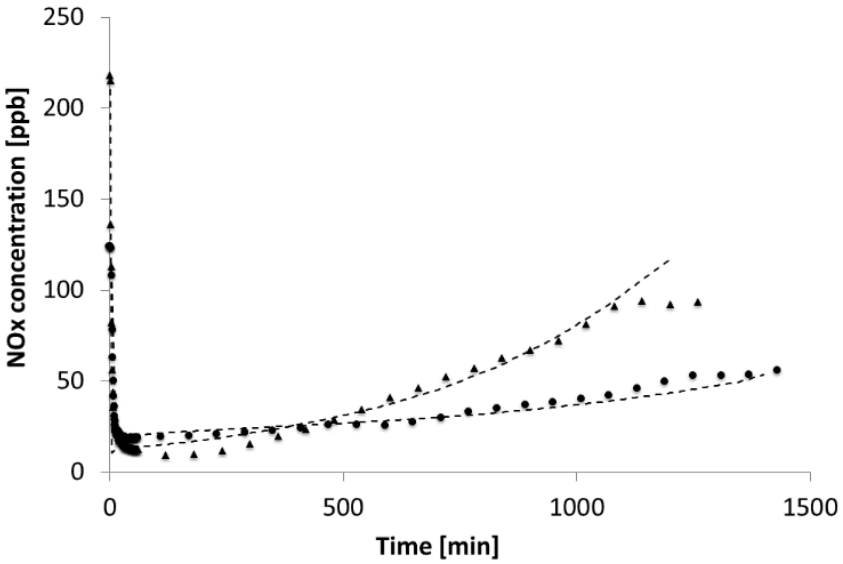

Fig. 7.4: NO_x photodegradation, light power: 20 W m^{-2}, total flow rate of 140 NL h^{-1}, NO_x concentrations of 124 ppb (circles), 217 ppb (triangles). Dotted lines stand for the simulated trends.

The longer experiment time permits to see better the formation of the adsorbed species, because after several hours it becomes more important and it affects the tile performance. In particular, the formation of NO^{3-} onto the catalyst surface causes a decrease in the reaction rate. The value chosen for the irreversible adsorbed species is well estimated, as the model reproduces quite well the experimental data.

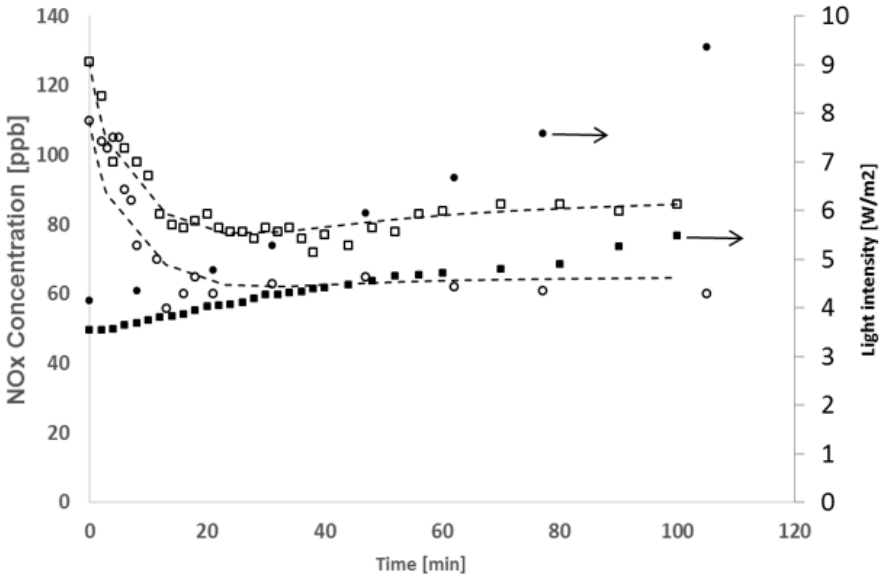

Fig. 7.5: NO_x photodegradation under sunlight, feed flow of 140 NL h^{-1}, circles stand for the experiment performed during July, squares for the one performed in September. Full points indicate the light intensity (UV fraction) while empty points the NO_x concentration exiting the reactor.

The results of the runs conducted under sunlight are reported in Fig. 7.5. The first important consideration is that the dependence of the light intensity on time was approximated as linear, since the experiments were conducted in a rather short time (2 h). Even the experimental data confirm that the photoactivity is actually dependent on the light intensity, and precisely the sunlight power is greater during July. And, the calculated values fit the experimental ones. Thus, consider the kinetic constant as proportional to the UV light intensity was the right choice.

7.3.2 Comparison between different tiles and multiple-days testing

7.3.2.1 Classical deposition method ceramic tiles: evaluation of the photocatalytic performance in different situations

After confirming the actual activity of the photocatalytic ceramic materials, first prepared by means of classical deposition of micrometer TiO_2, small steps in the industrial process were changed. Thus, different tiles slightly modified from each other were tested on NO_x photodegradation. This latter just to confirm first they operate in the proper way. Fig. 7.6 reports specifically five degradation tests. Samples are the so-called "series-24" (i.e. A-B-C-D) and Z23, which is the reference one for classical TiO_2 deposition method (already presented and reported in the previous chapters).

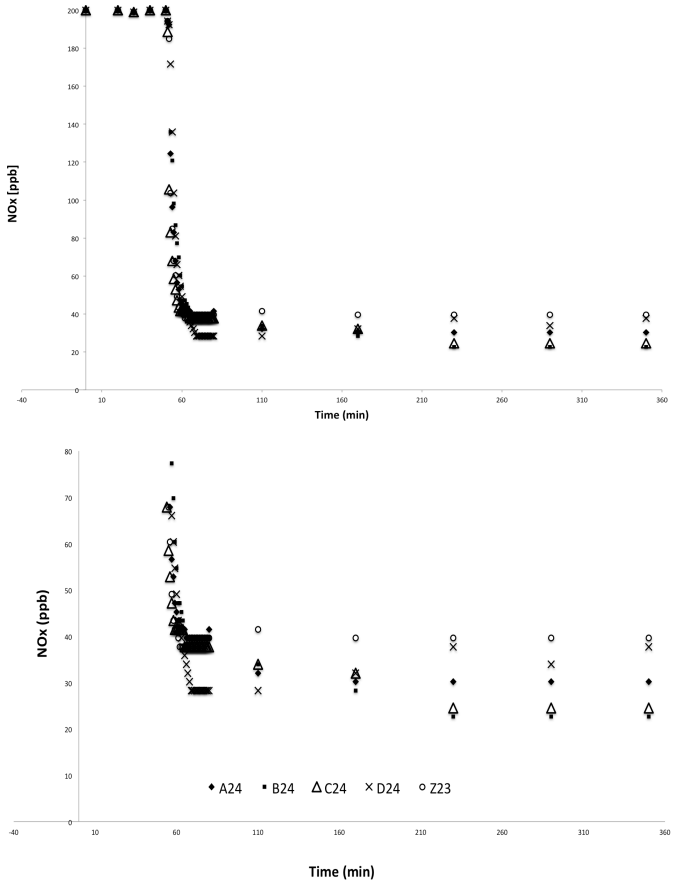

Fig. 7.6: Tests on a series of tiles prepared by classical TiO_2 deposition method; NO_x starting concentration set at 200 ppb, photodegradation duration time = 6 hours.

The second graph of fig. 7.6 is just a magnification of the first one, in order to see clearly the differences between a tile and another one. In general, not so important steps in the procedure, such as little changes in the TiO_2 amount, more or less intense final brushing, or different kinds of washings, do not change the final result. Indeed, classical deposition TiO_2 on ceramic tiles is confirmed as good method to obtain photocatalytic materials.

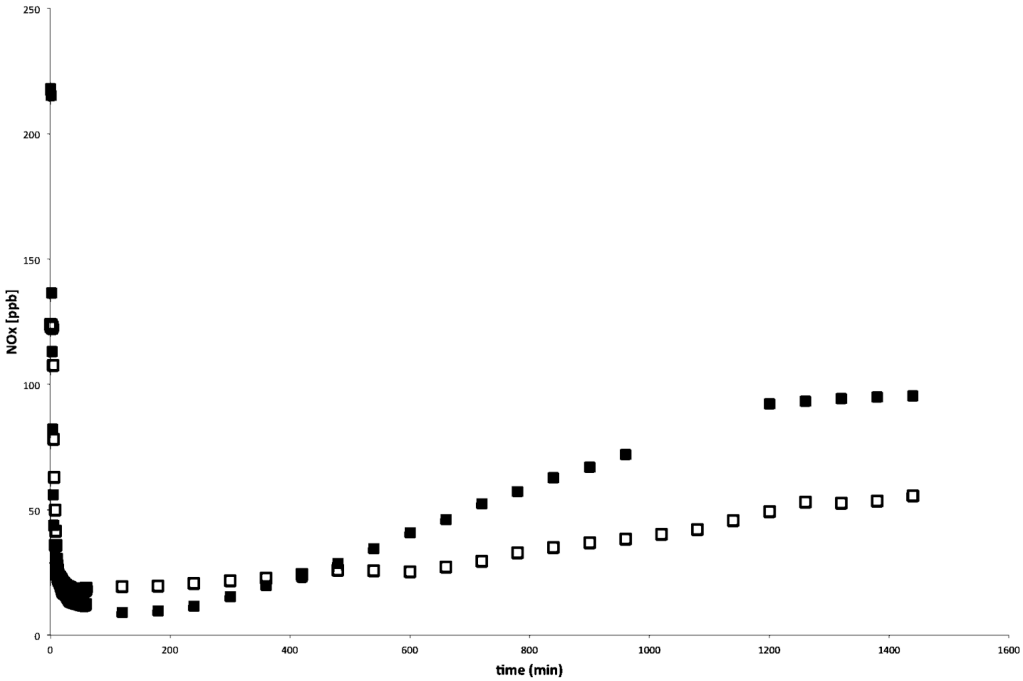

Fig. 7.7: Sample C24 tested for 24 hours at 100 ppb or 200 ppb NO_x starting concentration.

24 h tests at two different concentrations were performed in order to evaluate the specific impact of the NO_x flow concentration after a long time exposure (fig. 7.7). This latter is a rather extreme condition, which expose the material to a very high stress. Although the NO_x

concentration usually present in atmosphere is lower, this kind of kinetics can be useful to evaluate the maximum capacity of the material. After a 24 h continuous passage of a constant flow of nitrogen oxides, concentrations in both cases were halved, 50 ppb or 100 ppb respectively (see specifically fig. 7.7, black squares for the kinetic started at 200 ppb, white squares for 100 ppb as initial concentration).

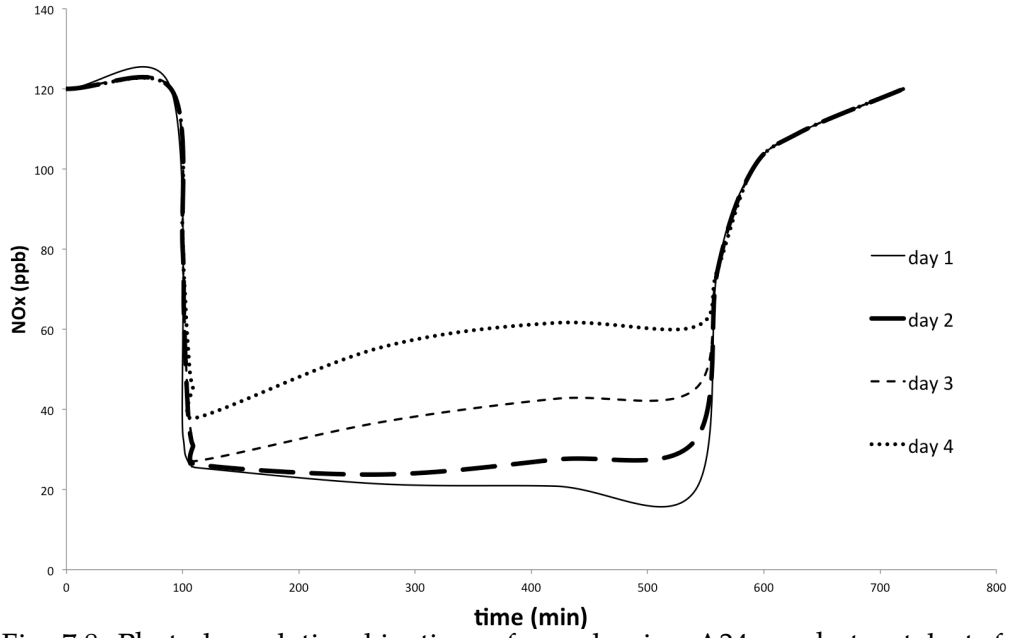

Fig. 7.8: Photodegradation kinetic performed using A24 as photocatalyst, for four days long.

Fig. 7.8 shows a particular test, performed continuously for 4 days long. We tried to simulate a real day, in which there was also the alternation of light and dark. Thus, after setting the initial concentration around 100 ppb, UV light was switched on starting the pseudo-first day (see fig. 7.8, black and continuous line). UV was switched off exactly after 8 hours. NO_x flow was kept constant, in order to simulate the pollution overnight. The procedure was repeated keeping the reactor close and maintaining the system in the standard conditions. The black line with

large hatches refers to the pseudo-second day, then the next one with smaller hatches refers to the third day, and finally the pointed line reports the kinetic performed at the fourth day. Results are consistent with the expectations. Indeed, more are the days passed more is the lost of the photocatalytic activity of the tile. This obviously because the nitrogen oxides flow which passes over the tile was constant and continuous. However, even after 4 days, tile is effective. More then 50% of nitrogen oxides were degraded constantly.

7.3.2.2 Digital Printing deposition method: an overview on the photocatalytic properties of this new material

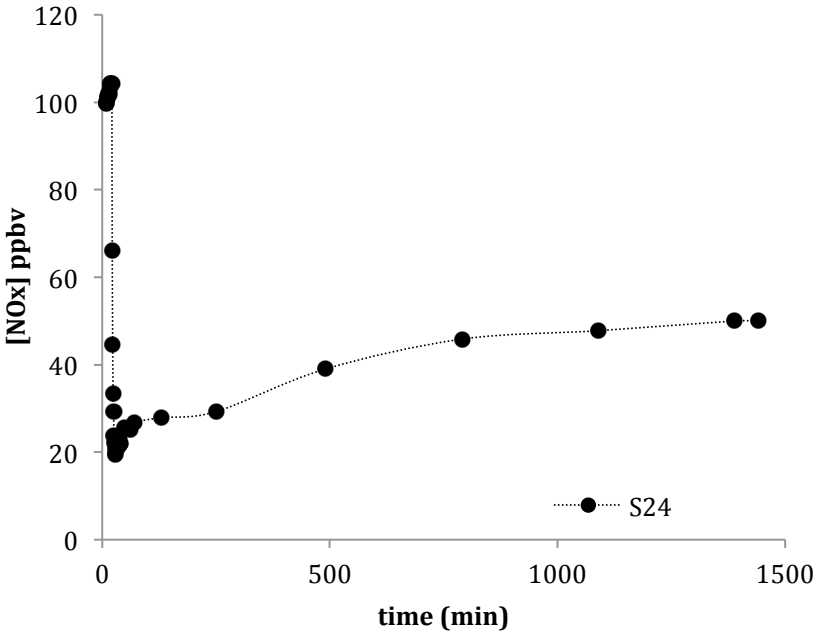

Fig. 7.9: 24 h test on NO_x degradation using tile S24 (obtained by digital printing). NO_x starting concentration is 100 ppb, irradiation is obtained by UV lamp (setting parameters) and flow rate is 140 Lh^{-1}.

After 24 h working (fig. 7.9), tile S24 was able to maintain the NO_x flow at a constant concentration of 50 ppb, corresponding to 50%

degradation. The lowest value was reached at the beginning of the reactor, after 30 minutes, and corresponded to 19 ppb, with a maximum degradation percentage of 80%.

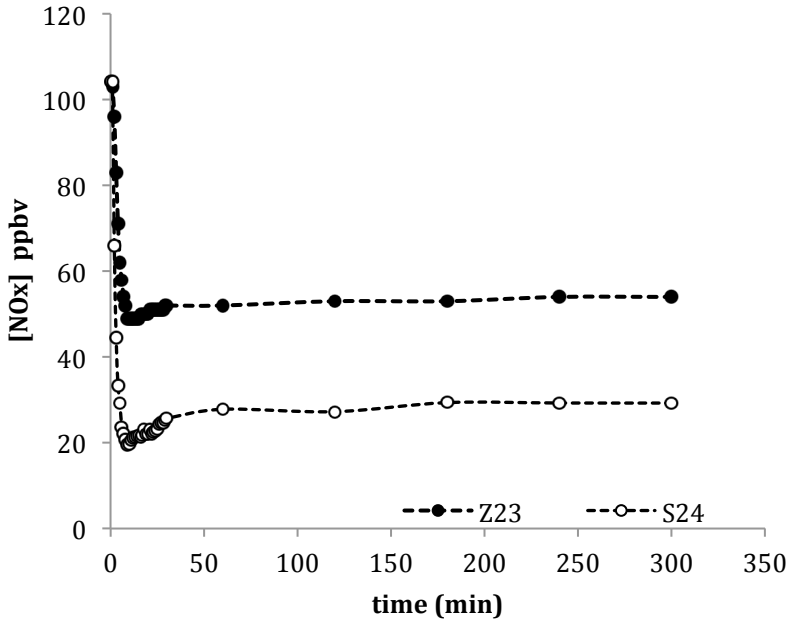

Fig. 7.10: 24 h tests on NO_x degradation with the comparison between tile S24 (white dots) and Z23 (black dots), respectively obtained by digital printing or classical TiO_2 deposition method; NO_x starting concentration is 100 ppb, irradiation is obtained by UV lamp (setting parameters) and flow rate is 140 Lh^{-1} for both kinetics.

The specific comparison between digital printing method and the classical one is reported in Fig. 7.10. The best-achieved performances among the all conducted tests were selected as reference. The relative curves reported in the graph clearly put in evidence the improvement obtained with digital printing, also for big size photocatalyst, also under a continuous flow of nitrogen oxides. Particularly, there is a difference between the minimum values of NO_x achieved, from 20 ppb in case of digital printing tile to 50 ppb using Z23 tile sample (classical method). Secondly, concentration values of NO_x that tiles were able to keep after

24 hours working differ from each other from 30 ppb (best kinetics performance) to 50 ppb. Therefore the improving was over than 20%.

7.4 Conclusions

This chapter focuses on a series of photodegradation tests performed in order to evaluate the performance of the final photocatalysts, consisting of ceramic tiles with TiO_2 deposited onto surface. These specific types of testing differed from the traditional ones, particularly because the working conditions try to be as much as possible close to reality. The main parameters to take into account are the pollutants concentration values, as well as the reactor and photocatalyst materials size. Therefore NO_x photodegradation was studied here using a continuous bench-scale reactor, specifically suitable for entire (600 × 600 mm^2) photocatalytic tiles. Firstly, 3D simulations showed that the design allows good reactant dispersion inside the reactor, confirming the right design of it. Then, different conditions in terms of reactant flow, pollutant concentration and test duration were used. Some tests were performed even under sunlight. The first aim was verifying from a kinetic point of view the efficiency and the operation of the new designed reactor. By means of suitable kinetic simulators, the reactor functionality was confirmed. Subsequently, the second key point was the comparison of the two different methods (previously presented) to obtained photocatalytic active ceramic tiles: the effectiveness of the materials was demonstrated in real conditions; moreover, the concrete increase in performance due to the new exploited production method was evaluated. Both ceramic tiles obtained with the classical deposition method and digital printing tiles were produced in large size (60 cm x 60

cm) and then tested. Results are perfectly fittable with the expectations. This setup for testing material on the NO_x degradation in gas phase gave us information about the real capacity of a material in term of pollution abatement, particularly when tests were conducted under solar light. Finally, active ceramic tiles were confirmed photocatalytically active materials, with a strong improvement gave by the new digital printing process.

Addition consideration about Digital Printing technology

ACTIVE® ceramic tiles production by Digital Printing technology has many other advantages in addition to the improvement of the ceramic materials. The first contribution concern the energy saving and the consequent money saving. The process achieves the same production amount at a total lower price, first of all for the total energy savings. However, the economics benefits are related also to the general waste reduction. Precisely, they are water saving and TiO_2 saving. Digital printing process completely avoids the wet-deposition of the aqueous solution of TiO_2 by airbrushing. In this latter case, all the water evaporated during the next steps of drying or firing. The TiO_2 application, through the ink deposition by means of a digital printer, does not deposit excess water on the tile surface. Moreover, there is not any dispersion of TiO_2 powder in the air. TiO_2 wastes are unavoidable during its application by an airbrush. The exact savings are stated in the table 7.3 here reported.

Energy saving	+ 12%
Water saving	+ 100%
TiO_2 saving	+ 50 %
Environment	ECO-friendly
Photoactivity	Active against pollution
Health	Antibacterial

Table 7.3 Advantages of the digital printing technology

References

Anderson C., Bard A., "Improved Photocatalytic Activity and Characterization of Mixed TiO_2/SiO_2 and TiO_2/Al_2O_3 Materials", J. Phys. Chem. B, **1997**, 101, 2611–2616.

Bianchi C.L., Gatto S., Nucci S., Cerrato G., Capucci V., "Self-cleaning measurements on tiles manufactured with micro-sized photoactive TiO_2", Adv. Mater. Res., An Interntional Journal, **2013**, 2(1), 65-75.

Bianchi C.L., Pirola C., Galli F., Cerrato G., Morandi S., Capucci V., "Pigmentary TiO_2: a challenge for its use as photocatalyst in NOx air purification", Chem. Eng. J., **2014**, 261, 76-82.

Bianchi C.L., Pirola C., Gatto S., Nucci S., Minguzzi A., Cerrato G., Biella S., Capucci V. "New surface properties in porcelain grés tiles with a look to human and environmental safety", Adv. Mater. Sci. Eng., **2012**, 2012, 1-8.

Bianchi C.L., Gatto S., Pirola C., Scavini M., Capucci V., "Micro-TiO_2 as a starting material for new photocatalytic tiles", CCC, **2013**, 36, 116–120.

Cappelletti G., Fermo P., Camiloni M., "Smart hybrid coatings for natural stones conservation", Progress Org. Coatings, **2015**, 78, 511–516.

Chen J., Poon C.S., "Photocatalytic construction and building materials: from fundamentals to applications", Build. Environ., **2009**, 44, 1899–1906.

Diamanti M.V., Del Curto B., Ormellese M., Pedeferri M.P., "Photo-catalytic and self-cleaning activity of colored mortars containing TiO_2", Construction Build. Mater., **2013**, 46, 167–174.

Fujishima A., Honda K., "Electrochemical photolysis of water at a semiconductor electrode", Nature, **1972**, 238, 37-38.

Furstner R., Barthlott W., Neinhuis C., Walzel P., "Wetting and self-cleaning properties of artificial superhydrophobic surfaces", Langmuir, **2005**, 21, 956–961.

Graziani L., Quagliarini E., Bondioli F., D'Orazio M., "Durability of self-cleaning TiO_2 coatings on fired clay brick facades: effects of UV exposure and wet & dry cycles", Build. Environ., **2014**, 71, 193-203.

ISO 22197-1: Fine ceramics advanced ceramics, advanced technical ceramics – Test method for air-purification performance of semiconducting photocatalytic materials – Part 1:Removal of nitric oxide, Geneva, Switzerland, **2007**.

Kim J.Y., Kim C.S., Chang H.K., Kim T.O., "Effects of ZrO_2 addition on phase stability and photocatalytic activity of ZrO_2/TiO_2 nanoparticles",Adv. Powder Technol., **2010**, 21, 141–144.

Kuhlbusch T.A.J., Asbach C., Fissan H., Göhler D., Stintz M., "Nanoparticle exposure at nanotechnology workplaces: A review", Part. Fibre Toxicol., **2011**, 8, 1–22.

La Russa M.F., Ruffolo S.A., Rovella N., Belfiore C.M., Palermo A.M., Guzzi M.T., Crisci G.M., "Multifunctional TiO_2 coatings for cultural heritage", Progress Org. Coatings, **2012** 74, 186–191.

Lee S.H., Yamasue E., Okumura H., Ishihara K.N., "Effect of oxygen and nitrogen concentration of nitrogen doped TiO_x film as photocatalyst prepared by reactive sputtering", Appl. Catal., A, **2009**, 371, 179–190.
Massman W.J., "A review of the molecular diffusivities of H_2O, CO_2, CH_4, CO, O_3, SO_2, NH_3, N_2O, NO, and NO_2 in air, O_2 and N_2 near STP", Atmos. Environ., **1998**, 32, 1111–1127.
Matsuda S., Hatano H., "Photocatalytic removal of NO_x in a circulating fluidized bed system", Powder. Technol., **2005**, 151, 61–67.
Matsunaga T., Tomoda T., Nakajima T., Wake H., "Photoelectrochemical sterilization of microbial cells by semiconductor powders", FEMS Microbiology Letters, **1985**, 29, 211–214.
Minero C., Bedini A., Minella M.," On the standardization of the photocatalytic gas/solid tests", Int. J. Chem. React. Eng., **2013**, 11, 717–732.
Menéndez-Flores V.M., Bahnemann D.W., Ohno T., "Visible light photocatalytic activities of S-doped TiO_2-Fe^{3+} in aqueous and gas phase", Appl. Catal. B: Environ., **2011**, 103, 99-108.
Quagliarini E., Bondioli F., Goffredo G.B., Cordoni C., Munafò P., "Self-cleaning and de-polluting stone surfaces: TiO_2 nanoparticles for limestone", Constr. Build. Mater., **2012**, 37, 51–57.
Quagliarini E., Bondioli F., Goffredo G.B., Licciulli A., Munafo P., "Smart surfaces for architectural heritage: preliminary results about the application of TiO_2-based coatings on travertine", J. Cultural Heritage, **2012**, 13, 204–209.
Quigg A., Chin W.C., Chen C.S., Zhang S., Jiang Y., Miao A.J., "Direct and indirect toxic effects of engineered nanoparticles on algae: role of natural organic matter", ACS Sustainable Chem. Eng., **2013**, 1, 686–702.
Ragesh P., Ganesh V.A., Naira S.V., "A review on self-cleaning and multifunctional materials", Mater. Chem. A, **2014**, 2, 14773.
Sciancalepore C., Bondioli F., "Durability of SiO_2–TiO_2 photocatalytic coatings on ceramic tiles", Int, J, Appl. Ceramic Technol., **2015**, 12, 679–684.
Scuderi V., Buccheri M.A., Impellizzeri G., Di Mauro A., Rappazzo G., Bergum K., Svensson B.G., Privitera V., "Photocatalytic and antibacterial properties of titanium dioxide flat film", Mater. Sci. Semicond. Process., **2016**, 42, 32–35.
Signoretto M., Ghedini E., Trevisan V., Bianchi C.L., Ongaro M., Cruciani G., "TiO_2 -MCM-41 for the photocatalytic abatement of NO_x in gas phase", Appl. Cat. B: Environ., **2010**, 95, 130-136.
Taurino R., Barbieri L., Bondioli F., "Surface properties of new green building material after TiO_2–SiO_2 coatings deposition", Ceramics Int., **2016**, 42, 4866–4874.
Trouiller B., Reliene R., Westbrook A., Solaimani P., Schiestl R.H., "Titanium dioxide nanoparticles induce DNA damage and genetic instability in vivo in mice", Cancer Res., **2009**, 69, 8784–8789.
Xie T.H., Lin J., "Origin of Photocatalytic Deactivation of TiO2 Film Coated on Ceramic Substrate", J. Phys. Chem. C, **2007**, 111, 9968–9974.
Zhang P., Liu X., Yin S., Sato T., "Enhanced visible-light photocatalytic activity in $K_{0.81}Ti_{1.73}Li_{0.27}O_4$/$TiO_2$−xNy sandwich-like composite", Appl. Catal., B, **2010**, 93, 299–303.

Zhao J., Yang X.D., "Photocatalytic oxidation for indoor air purification: a literature review", Build. Environ., **2003**, 38, 645–654.
Zhao X.J., Zhao Q.N., Yu J.G., Liu B.S., "Development of multifunctional photoactive self-cleaning glasses", J. Non-Crystal Solids, **2008**, 354, 1424–1430.

Final Remarks and Conclusions

Besides the conclusions reported at the end of each single chapter, as final remark it can be stated that the original objectives have been achieved. In particular:

- The potential of micrometer TiO_2 was established. Among several commercial samples the best candidate was selected, confirming anatase as the most photoactive crystallographic phase. Micro-TiO_2 efficiency was proven against NOx, single molecules of VOCs, and organics in mixture as something never studied before. The benefits associated with the use of micrometric powders are mainly economic and, even more important, related to safety and health of each of us.
- The traditional methods ordinarily used to produce photocatalytic materials were studied, modified and thus improved successfully. A new technology to deposit micro-TiO_2 on ceramic grés tiles was developed and here finally presented. It is called Digital Printing and it is based on the use of a special digital printer to cover tiles with TiO_2. The goals are first the improvement of the photocatalytic activity, secondly the waste reduction, finally the energy and water saving. This technology improves the environment and does not harm the environment.
- TiO_2 is not active or efficient under visible light. By means of ultrasound as new technique, the starting micro-TiO_2 was successfully modified with metals, finally getting a new material actually active in the visible. Copper and silver were deeply studied as reference noble metals; technique, synthesis methods and testing methods were enhanced.
- Eco-active materials in every day life: as final goal, a new method

to test materials in real conditions was studied, improved and finally presented as workable.

Future work should also be devoted to the optimization of the digital printing technology to applied not only the starting micro-TiO_2, but also the new modified one, in order to obtain real materials, usable in houses, public places and more for a better quality of air and a thus better quality of life.

List of publications

Papers in peer-reviewed journals

C.L. Bianchi, E. Colombo, S. Gatto, **M. Stucchi**, G. Cerrato, S. Morandi, V. Capucci, "Photocatalytic degradation of dyes in water with micro-sized TiO_2 as powder or coated on porcelain-grès tiles", Journal of Photochemistry and Photobiology A: Chemistry, vol. 280, (2014), pp. 27–31.

C.L. Bianchi, C. Pirola, F. Galli, **M. Stucchi**, S. Morandi, G. Cerrato, V. Capucci, "Photodegradation of ethanol as model for VOC's: experimental data and kinetic modelling using nanosized and microsized TiO_2", RSC Advances, vol. 5, (2015), pp. 53419-53425.

C.L. Bianchi, C. Pirola, F. Galli, S. Vitali, A. Minguzzi, **M. Stucchi**, F. Manenti, V. Capucci, "NOx degradation in a continuous large-scale reactor using full-size industrial photocatalytic tiles", Catal. Sci. Technol., vol. 6, **2016**, pp. 2261-2267.

G. Cerrato, C.L. Bianchi, S. Morandi, C.Pirola, **M. Stucchi**, M.V. Diamanti, M.P. Pedeferri, V. Capucci, "The role of the nano/microstructure in the case of the photodegradation of two model VOC pollutants using commercial TiO_2", Energy and Environment Focus vol. 4 (**2015**), pp. 226-231.

M. Stucchi, C.L. Bianchi, C. Pirola, S. Vitali, G. Cerrato, S. Morandi, C. Argirusis, G. Sourkouni, P.M. Sakkas, V. Capucci, "Surface Decoration of Commercial Micro-sized TiO_2 by means of High Energy Ultrasound: a Way to Enhance its Photocatalytic Activity Under Visible Light", Applied Catalysis B: Environmental,

vol.178 (2015), pp. 124-132.

M. Stucchi, C.L. Bianchi, C. Pirola, G. Cerrato, S. Morandi, C. Argirusis, G. Sourkouni, A. Naldoni, V. Capucci, "Copper NPs decorated titania: A novel synthesis by high energy US with a study of the photocatalytic activity under visible light", Ultrasonics Sonochemistry, vol. 31, (2016), pp. 295–301.

C.L. Bianchi, **M. Stucchi**, C. Pirola, G. Cerrato, F. Biasioli, M. Lanza, A.Di Michele, F. Demartin, V. Capucci, "TiO_2-Porcelain Grés tiles coatings: new strategies for the removal of the main indoor pollutants", Building and Environment, *under review*.

C.L. Bianchi, M. Stucchi, C. Pirola, M. Lanza, G. Cerrato, L. Cappellin, F. Biasioli, V. Capucci, "TiO_2-Photocatalysis for Ubiquitous Indoor Pollutants Abatement: Study of the Simultaneous Degradation of Aldehydes", Trends in Photochemistry & Photobiology, *under review*.

Book Chapters

C.L. Bianchi, C. Pirola, **M. Stucchi**, B. Sacchi, G. Cerrato, S. Morandi, A. Di Michele, A. Carletti, V. Capucci, "A New Frontier of Photocatalysis Employing Micro-Sized TiO_2: Air/Water Pollution Abatement and Self-Cleaning/Antibacterial Applications", in Cao W. (ed.): Photocatalysis, InTech Europe, ISBN 978-953-51-4661-2

Publications in Conference Proceedings (peer reviewed)

C.L. Bianchi, C. Pirola, **M. Stucchi**, F. Minozzi, V. Capucci, "Digital printing to ecoactivate porcelain gres large slabs using micro-TiO_2 as photocatalyst" - In: Proceedings of the Annual International Conference on Architecture and Civil Engineering, First Edition, 2016, pp. 490-494.

Communications at congresses

Micro-Sized TiO_2 for Toluene Photodegradation in Gas Phase: catalyst preparation and role of doped metal to increase the photo-activity

Marta Stucchi[1], Claudia L. Bianchi[1],

[1] *Chemistry Department – University of Milan, Via Golgi 19, 20133 Milano, Italy*

1st Workshop of Catalysis, 22-23 November 2013, Clausthal, Germany

Surface Decorated Photocatalytic TiO_2: A Sonochemical Method to Improve its Activity

Marta Stucchi[1], Claudia L. Bianchi[1], Carlo Pirola[1], Christos Argirusis[2], Georgia Sourkouni[3], Petros M. Sakkas[2], Dimitra Kanellopoulou[2], Giuseppina Cerrato[4], Sara Morandi[4],

[1] *Chemistry Department – University of Milan, Via Golgi 19, 20133 Milano, Italy*

[2] *School of Chemical Engineering – National Technical University of Athens, 9 Heroon Polytechniou St., Zographos, Athens GR-157 80, Greece*

[3] *Technische Universität Clausthal, Leibnizstr. 28, 38678 Clausthal-Zellerfeld, Germany*

[4] *Dip. Chimica & NIS Centre, University of Torino, via Pietro Giuria 7, 10125 Torino, Italy*

Workshop of the Greek Ceramic Society, 3-4 April 2014, Athens, Greece

Surface Decorated Photocatalytic TiO_2: A Sonochemical Method to

Improve its Activity

Marta Stucchi[1], Claudia L. Bianchi[1], Carlo Pirola[1], Christos Argirusis[2], Georgia Sourkouni[3], Petros M. Sakkas[2], Dimitra Kanellopoulou[2], Giuseppina Cerrato[4], Sara Morandi[4],

[1]*Chemistry Department – University of Milan, Via Golgi 19, 20133 Milano, Italy*

[2]*School of Chemical Engineering – National Technical University of Athens, 9 Heroon Polytechniou St., Zographos, Athens GR-157 80, Greece*

[3]*Technische Universität Clausthal, Leibnizstr. 28, 38678 Clausthal-Zellerfeld, Germany*

[4]*Dip. Chimica & NIS Centre, University of Torino, via Pietro Giuria 7, 10125 Torino, Italy*

14th Meeting of the European Society of Sonochemistry, 2-6 June 2014, Avignon, France

Surface decoration of photocatalytic TiO_2 with metal nanoparticles by means of high-energy ultrasound to improve its photocatalytic activity

Marta Stucchi[1], Claudia L. Bianchi[1], Carlo Pirola[1], Christos Argirusis[2], Georgia Sourkouni[3], Petros M. Sakkas[2], Dimitra Kanellopoulou[2], Giuseppina Cerrato[4], Sara Morandi[4],

[1]*Chemistry Department – University of Milan, Via Golgi 19, 20133 Milano, Italy*

[2]*School of Chemical Engineering – National Technical University of Athens, 9 Heroon Polytechniou St., Zographos, Athens GR-157 80, Greece*

[3]*Technische Universität Clausthal, Leibnizstr. 28, 38678 Clausthal-Zellerfeld, Germany*

[4]*Dip. Chimica & NIS Centre, University of Torino, via Pietro Giuria 7, 10125*

Torino, Italy

SPEA8 – 8th European meeting on Solar Chemistry and Photocatalysis: Environmental Application, 25-28 June 2014, Thessaloniki, Greece

Entire photocatalytic tiles (60x60cm) evaluation in NOx degradation in a continuous bench-scale reactor

Marta Stucchi[1], Claudia L. Bianchi[1], Carlo Pirola[1], Stefania Vitali[1], Valentino Capucci[2]

[1]*Chemistry Department – University of Milan, Via Golgi 19, 20133 Milano, Italy*

[2]*GranitiFiandre SpA, Castellarano (MO), Italy*

X Convegno Nazionale INSTM sulla scienza e tecnologia dei materiali, 28 June – 1 July 2015, Favignana, Italy

Copper NPs Decorated Titania: a Novel Synthesis by High Energy US with a Study of the Photocatalytic Activity under Visible Light

Marta Stucchi[1], Claudia L. Bianchi[1], Carlo Pirola[1], Giuseppina Cerrato[2], Sara Morandi[2], Christos Argirusis[3], Georgia Sourkouni[4], Alberto Naldoni[5], Stefania Vitali[1], Valentino Capucci[6],

[1]*Chemistry Department – University of Milan, Via Golgi 19, 20133 Milano, Italy*

[2]*Dip. Chimica & NIS Centre, University of Torino, via Pietro Giuria 7, 10125 Torino, Italy*

[3]*School of Chemical Engineering – National Technical University of Athens, 9 Heroon Polytechniou St., Zographos, Athens GR-157 80, Greece*

[4]*Technische Universität Clausthal, Leibnizstr. 28, 38678 Clausthal-Zellerfeld, Germany*
[5]*CNR, Istituto di Scienze e Tecnologie Molecolari, Via C. Golgi 19, Milano 20133, Italy*
[6]*GranitiFiandre SpA, Castellarano (MO), Italy*

2nd Asia-Oceania Sonochemical Society Conference, 25-28 July 2015, Kuala Lumpur, Malaysia

Copper NPs Decorated Titania to Improve the Photoactivity Under Visible Light: a Novel Synthesis by High Energy US

Marta Stucchi[1], Claudia L. Bianchi[1], Carlo Pirola[1], Giuseppina Cerrato[2], Sara Morandi[2], Christos Argirusis[3], Georgia Sourkouni[4], Alberto Naldoni[5], Stefania Vitali[1], Valentino Capucci[6],
[1]*Chemistry Department – University of Milan, Via Golgi 19, 20133 Milano, Italy*
[2]*Dip. Chimica & NIS Centre, University of Torino, via Pietro Giuria 7, 10125 Torino, Italy*
[3]*School of Chemical Engineering – National Technical University of Athens, 9 Heroon Polytechniou St., Zographos, Athens GR-157 80, Greece*
[4]*Technische Universität Clausthal, Leibnizstr. 28, 38678 Clausthal-Zellerfeld, Germany*
[5]*CNR, Istituto di Scienze e Tecnologie Molecolari, Via C. Golgi 19, Milano 20133, Italy*
[6]*GranitiFiandre SpA, Castellarano (MO), Italy*

4th European Conference on Environmental Applications of advanced oxidation processes, 21-24 October 2015, Athens, Greece

Formaldehyde Abatement by Photocatalysis: Fast Detection by PTR-MS

Marta Stucchi[1], Matteo Lanza[2], Claudia L. Bianchi[1], Giuseppina Cerrato[3], Luca Cappellin[4], Valentino Capucci[5], Franco Biasioli[4],

[1]*Chemistry Department – University of Milan, Via Golgi 19, 20133 Milano, Italy*

[2]*IONICON Analytik GmbH, Eduard-Boem-Gasse 3, 6020 Innsbruck, Austria*

[3]*Dip. Chimica & NIS Centre, University of Torino, via Pietro Giuria 7, 10125 Torino, Italy*

[4]*Research and Innovation Centre, Fondazione Edmund Mach, Via E. Mach 1, 38010 San Michele a/A, Italy*

[5]*GranitiFiandre SpA, Castellarano (MO), Italy*

EMEC 16, The European meeting on Environnmental Chemistry, 30 November – 3 December 2015, Torino, Italy

Micro-TiO_2 as Photocatalyst For New Ceramic Surfaces Activated Via Digital Printing

Marta Stucchi[1], Claudia L. Bianchi[1], Carlo Pirola[1], Giuseppina Cerrato[2], Alessandro Di Michele[3], Valentino Capucci[4],

[1]*Chemistry Department – University of Milan, Via Golgi 19, 20133 Milano, Italy*

[2]*Dip. Chimica & NIS Centre, University of Torino, via Pietro Giuria 7, 10125 Torino, Italy*

[3]*Department of Physics and Geology, Università degli studi di Perugia, Perugia, Italy*

[4]*GranitiFiandre SpA, Castellarano (MO), Italy*

CIMTEC 2016, 5th International Conference "Smart and Multifunctional Materials, Structures and Systems", 5-9 June 2016, Perugia, Italy

Formaldehyde abatement: Micro-TiO_2 and Innovative Photoactive Grés Tiles as Very Promising Allies to Improve Air Quality

Marta Stucchi[1], Claudia Bianchi[1], Carlo Pirola[1], Giuseppina Cerrato[2], Sara Morandi[2], Franco Biasioli[3], Valentino Capucci[4],

[1]*Chemistry Department – University of Milan, Via Golgi 19, 20133 Milano, Italy*

[2]*Dip. Chimica & NIS Centre, University of Torino, via Pietro Giuria 7, 10125 Torino, Italy*

[3]*Research and Innovation Centre, Fondazione Edmund Mach, Via E. Mach 1, 38010 San Michele a/A, Italy*

[4]*GranitiFiandre SpA, Castellarano (MO), Italy*

SPEA 9, 9th European Meeting on Solar Chemistry and Photocatalysis: Environmental Applications, 13-17 July 2016, Strasburgo, France

Digital Printing: a new tool to activate Ceramic Surfaces using Micro-TiO_2 as Photocatalyst

Marta Stucchi[1], Claudia L. Bianchi[1], Carlo Pirola[1], Giuseppina Cerrato[2], Sara Morandi[2], Valentino Capucci[3],

[1]*Chemistry Department – University of Milan, Via Golgi 19, 20133 Milano, Italy*

[2]*Dip. Chimica & NIS Centre, University of Torino, via Pietro Giuria 7, 10125*

Torino, Italy
[3]*GranitiFiandre SpA, Castellarano (MO), Italy*

JUNIOR EUROMAT 2016, 10-14 July 2017, Lausanne, Switzerland

Acknowledgements

This research was financially supported by the LIFE+ Environment Policy and Governance project Digitalife LIFE13 ENV/IT/000140.
My thanks go also to the company Graniti Fiandre SPA for the supply of all the ceramic supports and building materials, in particular thanks to Mr. Valentino Capucci and Mr. Roberto Pellini.
I would like also to thank:

- Ministero dell'Istruzione, dell'Università e della Ricerca for having paid my scholarship for three years;
- The National Technical University of Athens for having me in the laboratories of the Chemical Engineering Departemnt and for the possibility of using tools and equipments;
- The Edmund Mach Research Centre for the possibility of using the PTR-MS Instrument.

Ringraziamenti

(segue versione in Inglese)

Il mio dottorato è iniziato soprattutto grazie alla fiducia che mi hanno dato Claudia e Christos. Scegliere di continuare dopo la laurea magistrale è sempre una scelta che comporta qualche paura. La loro insistenza è stata fondamentale, e ora non posso che ringraziarli per aver insistito un po'. Sono stati tre anni di crescita scientifica, personale, culturale e ricchi di esperienze. Sono stati tre anni di traguardi, di errori, di momenti più faticosi premiati da obiettivi raggiunti, e anche di qualche sconfitta da cui ripartire con ancora più impegno.
Siamo al traguardo? Forse ancora non del tutto, ma questo è il bello.
Al principale mio punto di riferimento, la Prof. Claudia Bianchi, vorrei dire grazie per tutto il lavoro fatto insieme, dall'inizio con la tesi magistrale a oggi; grazie per avermi trasmesso la passione che lei per prima mette in tutte le cose che affronta, per avermi dato i consigli giusti, per avermi ripreso quando serviva, per esserci stata, sempre, nel lavoro come nella mia vita. Questi tre anni mi hanno cambiato, formato, e fatto crescere. Non sarebbe stato così senza di lei.
A Christos, grazie per avermi regalato moltissima della sua esperienza scientifica e lavorativa. Per il tempo dedicato alla mia formazione iniziale quando sono arrivata per la prima volta nei suoi laboratori dell'università di Atene; grazie per i preziosi consigli scientifici, per le correzioni, e per il suo contributo e la sua collaborazione tanto al mio progetto di dottorato, quanto a molti dei progetti che insieme, tra Milano e Atene, abbiamo portato a termine.
E a entrambi, anche, vorrei dire grazie per non essere stati soltanto "quelli che.. al lavoro si chiamano capi", ma per essere davvero persone che hanno fatto parte, e anche ora fanno parte, della mia vita, tutta intera. Grazie per tutto quello che abbiamo condiviso anche fuori dalle università, che siano pericolose barche malesi o ancor più pericolosi piatti greci a base di aglio.

Per chiudere questo primo cerchio magico, ora vorrei ringraziare Stefania, la persona con cui ho condiviso molti dei momenti veri in laboratorio. È stata un aiuto fondamentale, e soprattutto collaborare con lei per me è stata una fortuna perché ho potuto, grazie alla sua esperienza, incrementare la mia. Non è stata solo una collaboratrice e un'insegnante, ma anche una compagnia piacevole, ed è grazie a lei se i momenti difficili sono passati in modo migliore. Anzi, affrontarli insieme è stato ciò per cui ricorderò tutto in modo positivo.

Grazie mille anche a Carlo, che è stato uno tra i migliori esercitatori incontrati ai tempi della mia laurea, e che oggi oltre ad essere un super Prof. è un braccio destro, un aiuto, e un collega di cui non potremmo fare a meno.

Un progetto di ricerca di successo è chiaramente frutto di un lavoro di squadra. Nella mia ci sono state anche due donne e scienziate di primo livello, Pinuccia e Sara, che lavorano con me, o meglio con noi, e insieme a noi hanno raccolto e continuano a raccogliere risultati, vittorie, ansie, fatiche, e soddisfazioni. Per me, per la mia tesi, e per il mio progetto sono state più che importanti, tanto che forse dire semplicemente grazie non basta. Io spero di poterci lavorare ancora, e dedico il mio traguardo raggiunto anche a loro.

Ricordare il mio dottorato riporta sicuramente ad Atene. E Atene per me significa un gruppo di ragazzi molto importante e che non voglio dimenticare di ringraziare. Petros per primo, che quando sono arrivata era un esperto PhD al termine del suo percorso, e che mi ha affiancato come un maestro e un fratello maggiore, e poi Dimitra, ancora più esperta, che ha contribuito in modo diretto a buona parte del lavoro ed è stata anche la mia guida ufficiale per il primo periodo. Infine i ragazzi, Anthi, Avra, Iannis, Kostas e Pavlos, e tutti quelli che per un po' sono stati in laboratorio con me; ciascuno ha lasciato qualcosa di sè che non dimenticherò facilmente, e tutti mi hanno aiutata e accolta come poche volte mi era accaduto.

Un passo avanti, e ancora un altro scenario: l'istituto di ricerca Edmund Mach, a San Michele all'Adige. Grazie a Franco per la disponibilità e la collaborazione

prima di tutto, e grazie a chi ha lavorato con me, ancora una volta, arrivando da collega, rimanendo da amico: parlo di Matteo e Iulia, di Luca, Kos, Sine, e Brian.

La complessa e divertente vita di laboratorio, qui a Milano invece, significa Capannone Impianti Pilota: e capanno per noi vuol dire un gruppo di ricerca che durante il dottorato ho visto cambiare, aumentare, rimpicciolirsi, ma sempre vivere con entusiasmo il meraviglioso mondo della chimica. Quindi, un grazie va a tutti i tesisti e tirocinanti che hanno lavorato qui, più o meno direttamente con me. Ai miei tesisti e tirocinanti "personali" invece, che hanno vissuto da vicino il mondo (più o meno fantastico) della fotocatalisi, un doppio grazie, perché tutto quello che ha riempito le righe di questa tesi esiste anche e soprattutto grazie a loro. Quindi, Stefano, Alessandro, Mattia, Arianna, Vanessa, Valentina, Michele, Davide, Marco, Ivan, Gianmaria, Edoardo, e Cristina, grazie.

Loro sono passati, e adesso in mille modi diversi continuano come me a barcamenarsi tra dispense di chimica industriale che pesano quintali, professori più o meno simpatici, ansie da esame, e vacanze sui libri e pomeriggi infiniti in laboratorio.

Qualcuno però era qui con me ad aspettarli, e a vivere le trasformazioni del gruppo impianti. Non posso non ringraziare, e abbracciare anche se con le parole, i miei compagni di dottorato: Valeria per prima, che ho guardato spesso come un riferimento, e che grazie alla sua esperienza in più è stata una guida essenziale per me; una delle persone più disponibili e efficienti che mi sia capitato di incontrare, anche se i nostri progetti erano diversi, lei c'era, sempre. E poi insieme abbiamo avuto Atene, perché li abbiamo lavorato fianco a fianco per un po', condividendo la bellezza di un paese nuovo, e scoprendo anche di avere molto in comune. Quindi, di nuovo un grazie per essere entrata nella mia vita, portando tutto quello che è, e cioè un genio, ma anche una ragazza fantastica! Alberto, con me dal primo giorno di corso quando andavamo fieri del

nostro bel numero di matricola, fino alla laurea, e poi con il dottorato: si perché Alberto si è laureato con me, quindi abbiamo condiviso insieme tutto il travagliato percorso, e poi insieme abbiamo fatto il concorso fino ad aver saputo di essere stati presi ufficialmente come PhD di Unimi. Grazie per la disponibilità, perché anche lui è, ed è stato, un collega tuttofare e sempre presente, e grazie per tutto il resto, che è un'amicizia che spero di non perdere in futuro.

Poi ci sono stati Federico, che osservavo cercando di imparare, perché qui è sempre stato il riferimento di tutti, e che mi ha aiutato tante volte per affrontare problemi con le sue idee geniali, Sara, la mia dottoranda di riferimento quando ero ancora in tesi, che mi ha introdotto al mondo del TiO_2, e la ultime arrivate, Sofia, che in un anno è già diventata un pilastro del gruppo e senza il quale non potremmo vivere, e Benedetta, una "titania", come dicono i ragazzi, che ha condiviso con me il progetto fotocatalisi, e che quindi mi è stata vicinissima soprattutto nell'ultima parte di questo percorso. È stata capace di darmi ottimi consigli, di aiutarmi nel lavoro e anche come una vera amica, e per questo la ringrazio davvero, oltre che per tutto il tempo condiviso insieme tra viaggi, congressi e imprese … da titani.

I corridoi di Unimi nascondono spesso piacevoli sorprese, che si incontrano per lavoro o per caso o perché si è più o meno nella stessa situazione nello stesso momento. Un grazie a Valentina, collega, ricercatrice di primo livello, e persona fantastica; grazie a Gianluca, che spesso mi ha dato consigli molto utili; grazie a Alessandro, che alla chimica mette davanti la parola Ing., che oltre a condividere con me un pezzetto di vita da dottorandi mi ha fatto scoprire Venezia, e che mi è stato d'aiuto per affrontare l'ultimissima salita.

L'inizio della salita, invece, mi porta a ricordare una persona particolare, che voglio ringraziare pubblicamente qui. Parlo di Raffaele, figlio di Giacomo Bonaiuti, grazie al quale, ogni anno, vengono consegnate agli studenti di chimica e ingegneria chimica della Lombardia due borse di studio. Giacomo

Bonaiuti era un ingegnere chimico, che ha amato questa materia e il suo lavoro tanto da aiutare con una borsa di studio a suo nome chi come lui ha scelto di studiarla, facendo un po' di fatica, a volte anche economica; i suoi figli continuano a farlo tutt'ora. Io questa borsa l'ho vinta, e quei soldi sono stati davvero un evento particolare che mi ha fatto avere meno paura. Quindi se sono arrivata qui è anche un po' grazie a loro. Il mio grazie a Raffaele, in realtà, è doppio anche per la vicinanza dimostrata in tutti questi anni, perché non dimentica mai un avvenimento importante del mio percorso, perché so che il suo interesse è sincero, e quanto valgono le sue congratulazioni. Quindi grazie Raffaele, un grazie profondo e sincero.

E vedere avvicinarsi il traguardo, infine, porta inevitabilmente a ricordare e a voler lasciare un grazie anche a tutti quelli che sono stati con te, semplicemente vicino, fondamentali magari anche senza aver mai visto un laboratorio di chimica.

Grazie ai miei ragazzi di ripetizioni, tutti, perché le soddisfazioni che mi hanno dato in questi anni sono state uno slancio per affrontare anche il mio dottorato, anche se loro non lo sanno.

Grazie ai miei amici, di sempre o appena arrivati. Grazie a Gas, Laura, Ermanno, Fabri, Elio, Erica, Simona, Lucia, Miki, Andrea, Manuel, Marco e Loris.

Grazie a chi è stato fondamentale per la mia preparazione scientifica, cioè la mia prima Prof. di matematica e scienze, Alessandra. Tutto, in fondo, è iniziato con lei, per come è stata capace di insegnare la scienza, e per come, lei forse non sa, mi ha fatto innamorare della biologia, della chimica, delle provette e dei microscopi.

Grazie alla mia famiglia, tutta intera, inclusi zie, cugini e piccole principesse arrivate da non molto. Non c'è bisogno di dire perché. Loro ci sono, sempre. Di questi tre anni hanno raccolto tutto; i sorrisi per i successi, i pianti per le sconfitte, la Marta che lotta, la Marta che si arrende, quella che ha tempo, quella

che non ne ha, che rompe le palle raccontando della sua vita da dottoranda, che rompe le palle perché ha duemila ore di ripetizioni, che generalmente rompe le palle, e che a volte invece no, porta solo un po' di se, che ogni tanto non è poi così male.
Ah, la new entry si chiama Martino, è il numero 6 del nucleo base, e ogni tanto il numero 1. È tutto nero, abbastanza casinista, ruba le scarpe ma non le mangia, pensa che io sia molto severa, ma sa che può dormire nel mio letto. Da quando è arrivato, ha partecipato attivamente e scodinzolando alla mia vita da ricercatrice in erba. Più o meno, è una delle cose più belle che ci sia mai capitata tra le zampe, cioè, tra i piedi…le zampe sono le sue.

Martedì 20 dicembre 2016, h. 16.22

Postazione: ufficio del capanno
Meteo: Freddo
Giorni a Natale: 5
Marta sei felice? Si, la risposta nelle righe precedenti.

English version:

I truly decide to start a PhD because Claudia and Christos really trust in me. The choice of keep studying after the master degree is rather difficult, and implies a bit of fear. Their insistence was crucial, and now I strongly want to thank them. These three years have been three years of scientific and personal growth, as well as culturally significant and full of experiences. They are three years of achievements, mistakes, goals and some little defeats from which start again with more effort. Are we at the finish line? Maybe not, but that's the beauty.

To my most important reference point, the Prof. Claudia Bianchi, I would like to say thank you for all the work done together, from the beginning and up to now; thank you for conveying to me all your passion, for the right and important tips, for the recommendations, and thank you for being here, always, in my work and in my life. These three years change me, train me, and make me grow, and it would not be the same without you.

To Chris, thank you for giving me so much of your scientific and work experience. Thank you for all the time that you gave me for my training when I came the first time in your laboratories, in Athens. Thank you for the scientific tips, for the corrections and the advices, for your direct contribution and collaboration to my project, as well as to many projects that we did together, Milan and Athens.

And to both of them, I would say thank you for being not just "the boss", but for being persons that are in my life, overall. Thank you for what we shared even outside the university, from the very dangerous Malaysian boats, to the even more dangerous Greek dishes made with garlic.

To conclude this first part, I would like to thank Stefania, the woman with I shared several moments in the lab. She is a crucial help, and the collaboration with her was a real fortune for me because I could, thanks to her experience,

increase mine. She was not only a collaborator and a teacher, but also a very nice friend, and thanks to her some more difficult moments passed by easily.

Also thanks very much to Carlo, one of the best teaching assistant that I have met during my studies; at present he is first of all a super Professor, but also a real right-hand man, and a colleague of which we can not do without.

A successful research project is clearly the result of a team work. In my team there were also two women and first level scientists, Pinuccia and Sara, which work with me and with us, and with us achieved results, goals, worries, labors and satisfactions. They were fundamental for my PhD work. Maybe say just thank you is not enough. I truly hope to work again with them and I dedicate this goal even to them.

Thinking about my PhD brings me also in Athens. Athens means a very important group of guys, which I don't want to forget. Petros, firstly, which stay with me in the lab as a teacher and as an older brother, and then Dimitra, even more expert, which contributes directly to my work and was even my personal guide when I was in Athens for the first time. Finally all the guys, Anthi, Avra, Iannis, Kostas and Pavlos, and everyone who stayed a little bit there with me.

Another step, another place: the Researches institute Edmund Mach, at Trento. Thank you Franco for the availability and for the collaboration, and thank to everyone worked with me, as a colleague and then also as friend: I mean, Matteo and Iulia, Luca, Kos, Sine and Brian as well.

The complicated and funny laboratory-life, here at Milan, means Capannone Impianti Pilota: and for us, "shed" means a research group, which I've seen change and grow and shrink, but it was always excited about the world of chemistry. Thus, thanks to all the students that worked here. In particular, to my personal master and bachelor degree's students, a double thanks because this thesis is the result of their commitment as well. So thank you Stefano,

Alessandro, Mattia, Arianna, Vanessa, Valentina, Michele, Davide, Marco, Ivan, Gianmaria, Edoardo, and Cristina.

And even more important are my doctoral fellows: firstly, Valeria, which I often saw as a reference; she was an essential guide for me and one of the most helpful people I've been met, she worked on a different project but she was always here. Together we stayed in Athens for a brief period, and we found we have a lot in common. Thus, thank you Valeria for coming in my life as you are, a genius and a wonderful girl! Alberto was with me since the beginning, up to the master degree, and finally during the PhD: we went together throughout the long path, and we knew that we had won the scholarship for the PhD at the same time. Thank you Alberto for your kindness, for your presence and for everything, in particular thank you for your friendship.

Then there was Federico, which I often saw for learning, because he was a real reference; he helped me many times and he solved several problems thanks to his brilliant ideas. And then Sara, my reference when I was just a master thesis student; she introduced me in the world of photocatalysis and TiO_2 and she was great. Finally there are Sofia and Benedetta, the newcomers; Sofia has become a pillar of our group in less than one year and she is crucial, and Benedetta worked with me on photocatalysis and she was very close to me in particular during this last part; she gave me very helpful tips and she was also a true friend, thus thank you very much, for everything.

Through the university halls you can find beautiful surprises: you can meet people because of the work or simply by chance. Thanks to Valentina, a fellow, a first level researcher and a wonderful girl; thanks to Gianluca, which gave me very useful tips thanks to his long experience; thanks to Alessandro, which shared with me a little piece of our PhD-life and helped me in this last climb.

The beginning of this climb, instead, brings me memories of a special man, Raffaele Bonaiuti; he was the son of Giacomo Bonaiuti, a chemical engineer, to whom a scholarship is dedicated. This scholarship is in particular for chemistry

and chemical engineering students, and I won it some years ago. That money was very important for me and for the final decision about the PhD. Moreover, Raffaele is also a very kind person, and he was strongly present in my life during these years, so thank you so much, really.

Finally, seeing the finish line brings also memories about all people who are close to you, even if not involved with your work.

They are all very important.

Thanks to my younger students, because of all the rewards they gave me were so important to meet the challenges of my life.

Thanks to my friends, the oldest and the newest. Thank you Gas, Laura, Ermanno, Fabri, Elio, Erica, Simona, Lucia, Miki, Andrea, Manuel, Marco e Loris.

Thanks to the people that was fundamental for my scientific knowledge, and in particular I would say thank you to my first professor of science and math, Alessandra. Everything started thanks to her, because of her passion in teaching and because thanks to her I fell in love with science.

Thanks to my family, overall. No matter to say why. They are here, always. They took everything from these three years: smiles, cries, the fighter-Marta, the looser-Marta, Marta with time, Marta that has no time, Marta as a pain in the neck because she's a PhD, Marta as pain in the neck because she has a lot of work to do, Marta as a pain in the neck overall, or Marta that is not, because she brings just a little piece of her, which sometimes is not so bad.

The new entry is called Martino, the number 6 of the family, but sometimes he's the number one. He's black, he's rowdy, he steals my shoes but he doesn't eat them, he thinks I'm very stern, but he knows that he can sleep in my bed. Since he came, he actively participates at my life of a budding researcher, wagging his tail. More or less, it is one of the best things that ever happened.

Tuesday, 20th December 2016, 4.22 pm.

Location: my office
Weather: cold
Days at Christmas: 5
Marta, are you happy? Yes, the answer is reported above.